ASSESSMENT OF PATHOPHYSIOLOGICAL MECHANISMS IN OBESITY-RELATED DISEASES THROUGH METABOLOMICS, TRANSCRIPTOMICS AND MOUSE MODELS OF DISEASE

Marta Riera Borrull

UNIVERSITAT ROVIRA i VIRGILI

ASSESSMENT OF PATHOPHYSIOLOGICAL MECHANISMS IN OBESITY-RELATED DISEASES THROUGH METABOLOMICS, TRANSCRIPTOMICS AND MOUSE MODELS OF DISEASE

MARTA RIERA BORRULL

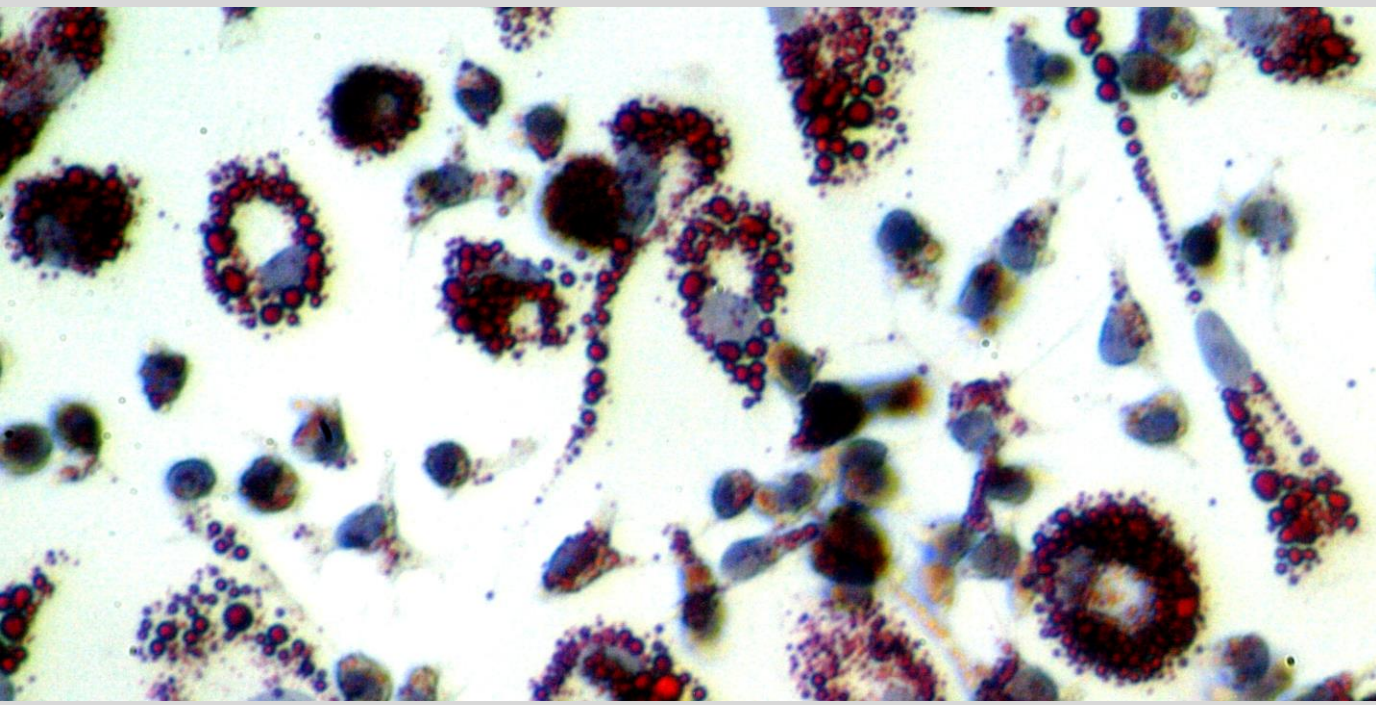

DOCTORAL THESIS
2017

Marta Riera Borrull

ASSESSMENT OF PATHOPHYSIOLOGICAL MECHANISMS IN OBESITY-RELATED DISEASES THROUGH METABOLOMICS, TRANSCRIPTOMICS AND MOUSE MODELS OF DISEASE

PhD Thesis Dissertation

Supervised by

Dr. Jorge Joven Maried

Dr. Ángel Luis Corbí López

Department of Medicine and Surgery

UNIVERSITAT ROVIRA I VIRGILI

Reus

2017

UNIVERSITAT ROVIRA i VIRGILI

FACULTAT DE MEDICINA I CIÈNCIES DE LA SALUT

DEPARTAMENT DE MEDICINA Y CIRUGIA

Carrer Sant Llorenç, 21
43201 Reus
Tel. 977 759 306
Fax. 977 759 352

I STATE that the present study, entitled **"Assessment of pathophysiological mechanisms in obesity-related diseases through metabolomics, transcriptomics and mouse models of disease"**, presented by **Marta Riera Borrull** for the award of the degree of Doctor, has been carried out under my supervision at the **Department of Medicine and Surgery** of this University.

Reus, 4th May 2017

Doctoral Thesis Supervisor/s

Dr. Jorge Joven Maried

Dr. Ángel Luis Corbí López

A la meva família,

Acknowledgments

Després de cinc anys m'agradaria agrair a tots els que heu compartit moments amb mi per ensenyar-me, aconsellar-me, escoltar-me i estar al meu costat en els mals i bons moments. No tot ha estat fàcil, però la vostra ajuda ha estat imprescindible per tirar endavant, gràcies!

Me gustaría agradecer a mis dos directores de tesis todo lo que he aprendido de ellos. Al Dr. Joven por darme la oportunidad de empezar en el mundo de la investigación y por enseñarme otra manera de ver la vida. Al Dr. Corbí por aceptarme en su laboratorio como a una más y darme la oportunidad de conocer el mundo de los macrófagos. Gracias por tu disponibilidad y tu ayuda.

Al Dr. Jordi Camps per l'ajuda tot el temps que vaig estar al CRB.

Al personal del l'estabulari, especialment a l'Amparo. A la Fàtima per totes les hores, tot l'esforç i per no dir mai que no. Gràcies Fàtima!

A la gent del CRB, a l'Anna, el Raúl i el Gerard per ensenyar-me a treballar al laboratori i sobretot per la paciència quan vaig començar les pràctiques.

A l'Esther pels moments compartits i a l'Anna per estar sempre disposada a ajudar en tot, gràcies! A la Fedra i a la Noemí per les hores amb els ratolins, ànims amb el que us queda! A la Isa per totes les tardes compartides al CRB, al final lo hemos conseguido! Al Lisard i a l'Aran, que van patir les meves qualitats docents, per tot el que em vau ensenyar, sou genials! A Salva por todo lo que me has ayudado (que no es poco) hasta el último día! Sé que aún no hay suficientes cervezas para compensarte... pero llegarán! Gracias! Y por último a Anabel, por estar siempre, en el CRB y fuera, por las llamadas y los cafés, por ser un gran apoyo en muchos momentos y por todos tus buenos consejos (que a veces intento aplicar...) mil gracias!!

En 2014, surgió una colaboración de tres meses en Madrid, que acabó alargándose tres años y la mitad de la tesis. Gracias a toda la gente del laboratorio del Dr. Corbí, he compartido muy buenos momentos con vosotros. A Ángeles por sus consejos y por saber siempre dónde está todo. A Miguel Vega por su interés y ayuda con la bioinformática. A "Conch" por todos sus buenos consejos, de mayor quiero ser como tú! A Víctor, por enseñarme ciencia y música a partes iguales, gracias chiqui!! A Igni, por

hacerme los #oscaralamáspringada más originales... y ánimo que sé que puedes!

A Jelen, por ayudarme tanto en el laboratorio y en todo lo demás, y aunque la distancia entre Bohn y Madrid nos ha impedido muchos planes, nuestros audios de 5 minutos hacen como si casi estuvieras aquí al lado, gracias Jelen! Y a mi Berb, trabajar contigo lo hace todo mucho más fácil, no sabes lo que echaré de menos nuestros desayunos, conversaciones y a ti!

Mil gracias por todo chiquis! Por las fiestas de primavera, las comidas al sol, la diversidad de opiniones en la música del labo, las acumulaciones en cultivos y las reparticiones de células en los buffys, os echaré mucho de menos!

Als biotecs, Erica, Amaia, Alba, Noe, David, Mateu i Martu, per tots els bons moments de la carrera i tots els que en queden encara! Tot i que no ens puguem veure tant com ens agradaria sempre hi serem. Sou el millor Ranchito!

A Aurora, Víctor y Alfredo, por apuntarme siempre a vuestros planes como una química más! Y a Javi! Por tener el mejor sentido del humor del mundo, espero que seas un buen vecino!

A les meves amigues de sempre, a la Myriam que m'agradaria que estigués més a prop, a l'Anna per proposar sempre els plans, a la Maria per la seva naturalitat i els seus consells, a la Núria per acollir-me a Vielha i fer-me sentir com si fos casa meva, i per tot el que m'ajudes sempre, t'estimo molt! A la Laura, encara que crec que no tinc prou espai. Per ser la millor companya de pis i perquè casi 25 anys d'amistat no els canviaria per res. Per ser-hi sempre i perquè seguim compartint tant. "En las buenas por estar y en las malas por no irte", gràcies Lau!

A la meva família, als meus avis, tiets i cosins per interessar-vos sempre tant, per tot el que us heu preocupat i tot el que us heu alegrat per mi. A la meva germana Maria, per ser també una gran amiga i per estar sempre al meu costat, ja saps que sempre anirem juntes. I als meus pares, perquè sense el vostre recolzament ni aquesta tesi ni moltes altres coses no haguessin estat possibles. Gràcies per tot el que m'heu donat, per creure tant en mi i per estimar-me tant, aquestes pàgines també són vostres.

Moltes gràcies a tots!

CONTENTS

ABBREVIATIONS

Abbreviations

Ahr: Aryl hydrocarbon receptor

AMPK: Adenosine monophosphate activated protein kinase

AP-1: Activator protein 1

ATM: Adipose tissue macrophage

BCAA: Branched chain amino acid

BMI: Body mass index

BSA: Bovine serum albumin

C/EBP: CCAAT/enhancer-binding protein

CAC: Citric acid cycle

CCL: C-C Motif chemokine ligand

CCR: C-C chemokine receptor

CD: Chow diet

DAMP: Danger-associated molecular pattern

DMSO: Dimethyl sulfoxide

ECM: Extra-cellular matrix

EI: Electron ionization

ELISA: Enzyme-linked immunosorbent assay

ER: Endoplasmic reticulum

ERK: Extracellular signal-regulated kinases

GC: Gas chromatography

GM-CSF: Granulocyte-macrophage colony-stimulating factor

GM-MØ: GM-CSF-polarized macrophage

GSK3: Glycogen synthase kinase 3

HFD: High-fat diet

HTR: 5-hydroxytryptamine receptor

IFN: Interferon

IKK: IκB kinase

IL: Interleukin

IRAK: IL-1 receptor-associated kinase

IRF3: Interferon regulatory factor 3

IRS: Insulin receptor substrate

IκB: Inhibitor of nuclear factor κB

JNK: Jun N-terminal kinase

KC: Kupffer cell

LC: Liquid chromatography

LDL: Low density lipoprotein

LPS: Lipopolysaccharide

MAPK: Mitogen-activated protein kinase

MCP-1: Monocyte chemoattractant protein 1

M-CSF: Macrophage colony-stimulating factor

M-MØ: M-CSF-polarized macrophage

MS: Mass spectrometry

Abbreviations

mTOR: Mammalian target of rapamycin

MyD88: Myeloid differentiation factor 88

NAFLD: Non-alcoholic fatty liver disease

NASH: Non-alcoholic steatohepatitis

NEFA: Non-esterified fatty acids

NFκB: Nuclear factor κB

NK: Natural killer

NLR: NOD-like receptor

p38: p38 mitogen-activated protein kinase

PAD: Peripheral artery disease

PAMP: Pathogen-associated molecular pattern

PKR: Protein kinase R

PPAR: Peroxisome proliferator-activated receptor

PRR: Pattern recognition receptor

QTOF: Quadrupole-time of flight

ROS: Reactive oxygen species

SFA: Saturated fatty acids

STAT: Signal transducer and activator of transcription

T2D: Type 2 diabetes

TG: Triglycerides

TGF: Transforming growth factor

TIR: Toll-interleukin 1 receptor

TLR: Toll-like receptor

TNF: Tumor necrosis factor

TRAM: TRIF-related adaptor molecule

TRIB3: Tribbles homolog 3

TRIF: TIR domain-containing adaptor protein inducing interferon-β

TZD: Thiazolidinedione

UPR: Unfolded protein response

WAT: White adipose tissue

ABSTRACT

Abstract

Nutrient management and energy balance are involved in maintenance of metabolic homeostasis systems. Current lifestyle patterns, like exposure to excessive amounts of nutrients and lack of physical activity, promote the disruption of homeostatic mechanisms and are the basis for the development of numerous pathologies. In the case of obesity, chronic over nutrition and reduced energy expenditure exceed the storage capacity of metabolic tissues and activate several metabolic pathways involved in the development of inflammatory responses and insulin resistance. Thus, as a contributor to disruption of homeostasis, low-grade chronic inflammation has a crucial role in the development of metabolic diseases, such as obesity, type 2 diabetes, cardiovascular diseases and non-alcoholic fatty liver disease. Moreover, maintenance and reinforcement of an inflammatory state results in the development of chronic metabolic diseases.

A close link exists between the function of metabolic tissues and the presence of immune cells. Specifically, macrophages are considered as triggers of the inflammatory responses underlying metabolic diseases like obesity. By virtue of their huge plasticity to adapt to different microenvironments, macrophages can display a wide spectrum of functional "polarization" states. In lean adipose tissue, macrophages exhibit an anti-inflammatory phenotype that contributes to insulin sensitivity. Conversely, an excessive amount of fat induces a macrophage polarization switch that leads to the acquisition of pro-inflammatory effector functions, best exemplified by the release of pro-inflammatory cytokines, and the ability to recruit other immune cells that impair insulin sensitivity and further exacerbate the obesity-associated inflammation state.

In the **first study**, we addressed the consequences of excessive nutrient intake in energy metabolism. Since mitochondrial dysfunction is a common feature in metabolic disorders, we develop a method to identify and quantify

metabolites in biological samples as a mean to predict mitochondrial alterations. Specifically, we developed a GC-EI-QTOF-MS method to measure a wide range of intermediate metabolites from energy metabolism. The method was validated in cell-culture lysates, plasma from patients and tissues from mice models of disease, and was confirmed as a valid analytical platform to assess the energy metabolism in biological samples.

The **second study** focused on the identification of therapeutic strategies to ameliorate the metabolic disturbances induced by high-fat diet (HFD) in low density lipoprotein receptor-deficient mice (*Ldlr*$^{-/-}$). Specifically, the effects of metformin in HFD- or chow diet-fed mice, as well as the effect of "diet reversal" with or without metformin in HFD-fed mice, were assessed on liver and adipose tissue through the use of biochemical, histological and metabolomics analysis. Our findings reveal that the combination of metformin and caloric restraint provides a better alternative against metabolic damage and might be a therapeutic strategy to ameliorate the metabolic dysfunction induced by excessive nutrient intake.

The effects of the saturated fatty acid (SFA) palmitate on human macrophage polarization are reported in the **third study**. We observed that exposure of M-CSF-dependent monocyte-derived human macrophages to palmitate (200μM) lowers the expression of transcription factors that drive "anti-inflammatory gene set" expression (MAFB, AhR) and simultaneously promote the acquisition of a pro-inflammatory transcriptional and functional profile via JNK activation. Besides, palmitate was found to prime macrophages for exacerbated inflammatory responses towards a pathogenic stimulus like LPS, a process also mediated by JNK activation. Importantly, we report that the transcriptional and functional effects of palmitate differ from those triggered by LPS, with stimuli oppositely regulating the expression of

CCL19 and *TRIB3*. These results have established that palmitate induces a specific pro-inflammatory polarization state in human macrophages.

INTRODUCTION

1. Obesity: an epidemic disease

The prevalence of obesity has increased drastically during recent decades and constitutes a serious threat to the future of all populations. At the present time, obesity and the associated metabolic pathologies are the most common and detrimental metabolic diseases, and are considered one of the greatest public health challenges of the century [1], [2].

The World Health Organization (WHO) postulates that obesity has reached epidemic proportions globally, with at least 2.8 million people dying each year as a result of this disease. Moreover, the WHO reports that, in 2014, more than 1.9 billion adults worldwide were overweight and over 600 million of them were obese. Overall, about 39% of the world population is overweight and 13% is obese and, without intervention, these numbers are expected to rise in the future. Particularly, there is also an alarming increase in the global prevalence rate of overweight and obesity among children, leading to serious health problems in this susceptible population [3], [4].

The most common used index used in guidelines for classifying underweight, overweight and obesity in adults is a simple index of weight-for-height. Additionally, body mass index (BMI) is defined as the body weight in kilograms divided by height in meters squared (kg/m^2), and it is assumed that individuals with a BMI ≥30 kg/m^2 are obese [2].

Although obesity is considered as a single disease entity, it actually encompasses multiple diseases and related disorders with different phenotypes, causes and clinical characteristics. The regulation of body fat store and energy balance involves multiple central and peripheral, metabolic and biochemical signaling pathways [5]. The physiologic regulation of body's fat mass is influenced by developmental, environmental and genetic factors. The relative contribution of behavioral and environmental factors, such as

excess of energy intake combined with sedentary lifestyles is responsible for the increasing prevalence of obesity. The combination of all these factors promotes the development and maintenance of an "obesogenic" environment that overwhelms the physiological maintenance of energy balance [6], [7].

Obesity-related morbidity and mortality

Obesity is considered to be a central feature that increases the risk for a vast array of health problems, with significant morbidity and mortality [8]. This cluster of associated pathologies can be classified in different obesity-related disease categories: metabolic, structural, inflammatory, degenerative, neoplastic and psychological.

Metabolic complications include non-alcoholic fatty liver disease (NAFLD), diabetes mellitus and dyslipidemia, among others. Structural effects of obesity as arthritis in weight-bearing joints or obstructive sleep apnea. Obesity-associated inflammatory and autoimmune diseases include asthma, pancreatitis and non-alcoholic steatohepatitis (NASH). Degenerative disorders are considered as long-term sequelae of severe manifestations such as atherosclerosis, complications of type 2 diabetes (T2D) and NASH-associated cirrhosis. Obesity also promotes the development of several types of cancer, including all the common reproductive tumors and several gastrointestinal cancers. Finally, obesity has also a psychological impact as it leads to depression, eating and anxiety disorders. All these comorbidities substantiate the relation of obesity with an increased risk of death [5]. In any event, although obesity-induced metabolic diseases promote pathology through a wide range of specific mechanisms, most disorders emerge from the characteristic milieu of chronic low-grade inflammation [9].

1.1 Non-alcoholic fatty liver disease (NAFLD)

Dramatic changes in diet and lifestyle of the worldwide population are triggering a global epidemic of obesity. Furthermore, the prevalence of obesity-related NAFLD has also certainly increased, becoming the most common cause of chronic liver disease in adults and children. Moreover, fatty liver itself is associated with increased cardiovascular risk and associated biomarkers and is considered a marker of insulin resistance and diabetes in obese patients [10]–[12]. By definition, NAFLD is characterized histologically by ≥5% of intracytoplasmic triglycerides (TG) accumulation -steatosis- and other parenchymal changes ranging from inflammation, apoptosis, necrosis and hepatic fibrosis. The diagnosis of this disease requires exclusion of patients with excessive alcohol and/or drugs consumption and viral-induced steatosis.

The prevalence of NAFLD in America is estimated to range from 20-40%, but in certain subpopulations this prevalence is significantly higher. In Europe, the prevalence of NAFLD is estimated to be about 24% of the general population [13, 14]. Many of the risk factors for NAFLD are known but the underlying pathogenesis is still not fully understood.

As shown in Figure 1, the spectrum of NAFLD ranges from simple steatosis with no symptoms, to non-alcoholic steatohepatitis (NASH) and, in some patients, progressive fibrosis leading to cirrhosis, which can result in hepatocellular carcinoma and liver failure [15], [16]. Why some patients with NAFLD progress to fibrosis and cirrhosis and other patients have a stable disease without clinical progression or histological sequelae is not clear.

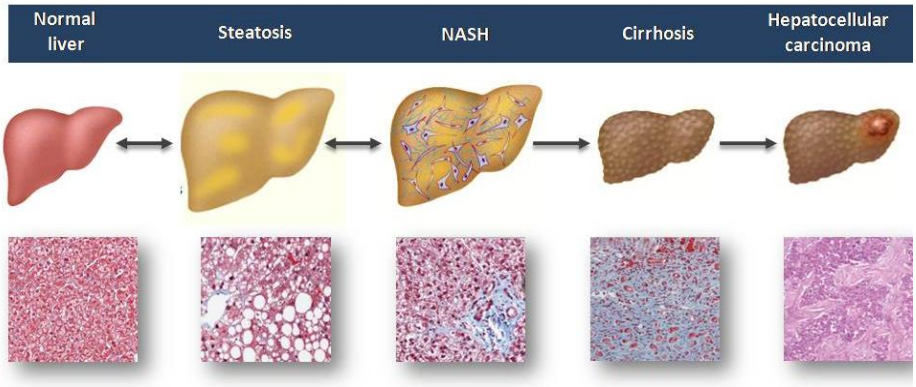

Figure 1. Schematic progression and histological sections of NAFLD. This chronic liver disease is characterized by a wide spectrum of pathogenic states. From simple steatosis, NASH and progression to fibrosis (15-20% of patients over the next 10 years), cirrhosis and hepatocarcinoma. Adapted from *J.C. Cohen et al.* [17].

Hepatic steatosis arises from an imbalance between TG uptake and removal. This earliest stage is characterized by the deposition of TG as lipid droplets in the cytoplasm of hepatocytes leading to the development of macrovesicular steatosis. The accumulation of hepatic fat can be due to increased hepatic lipogenesis, reduced oxidation of free fatty acids and decreased output of hepatic lipid stores [10], [13], [17], [18].

The initiation of necroinflammation suggest a process that involves excessive lipid accumulation in the liver cells, inflammation and oxidative stress, steps that result in the release of lipid peroxidation products such as malondialdehyde and 4-hydroxynonenal [19] that are involved in stimulation of collagen production and fibrosis [20].The main features of NASH include hepatocyte injury manifested as hepatocyte ballooning and cell death [21], inflammatory cell infiltration, lipotoxicity, mitochondrial injury and collagen deposition. It has been described that lipotoxicity leads to cell death through

apoptotic or necrotic processes [22], and is the main driver of inflammation and fibrosis in this pathology [23].

Hepatic fibrosis is the consequence of chronic injury that is usually mediated by inflammation. The myofibroblastic cells, derived from the hepatic stellate cells or Ito cells [24], are responsible for collagen production. Once activated, these cells proliferate into the sites of tissue damage and secrete large amounts of extra-cellular matrix (ECM), and are also able to produce cytokines and chemokines that further promote inflammation and fibrogenesis [23], [25]. This advanced stage of injury involves a cluster of alterations within hepatocytes and the surrounding parenchyma.

The hepatic inflammatory response is mediated by immune cells, including neutrophils, natural killer (NK) cells, natural killer T (NKT) cells and macrophages (Kupffer cells, KC). Activated KCs produce IL-6 and TNF-α [26], which induce insulin resistance leading to hepatic steatosis, and also generate reactive oxygen species (ROS) that causes lipid peroxidation products resulting in hepatocyte injury. The activated KCs also secrete transforming growth factor-β (TGF-β) [27], [28], one of the key fibrogenic factors [29], [30]. Chronic inflammatory infiltrate characterizes patients with an advanced liver diseases with a high risk of progression to cirrhosis and related complications such as liver failure or hepatocarcinoma.

A critical contribution for the onset on these pathologies is the presence of pro-inflammatory cytokines such as tumor necrosis factor α (TNF-α), interleukin 1β (IL-1β) and interleukin 6 (IL-6), whose levels are elevated in blood and liver of patients with this disease. A second relevant mechanism is the endoplasmic reticulum (ER) stress, which results from the accumulation of incorrectly folded proteins eliciting the unfolded protein response (UPR). This response activates numerous pathways related to oxidative stress and

inflammation, and implicated in the progression and development of the disease [10], [13], [17]. In any event, some evidences suggest a genetic contribution from patatin-like phospholipase-3 (*PNPLA3*) rs738409 polymorphism, that encodes for the isoleucine-to-methionine substitution at residue 148 (I148M), with an increase in hepatic fat content but not in alterations in glucose metabolism [31]. The *PNPLA3*-I148M allele is highly associated with the presence of NAFLD and with the expression of genes involved in liver damage including Fas ligand. Importantly, this genetic variant is also associated with the progression of hepatic steatosis to necroinflammation and fibrosis [32].

NALFD is a complex disease with variation in severity amongst individuals. Hepatic steatosis can be diagnosed by non-invasive techniques, but determining the presence of fibrosis or hepatic inflammation requires invasive methods like hepatic biopsy, the gold standard for the diagnosis of this disease. A better understanding of the mechanisms responsible for the pathophysiology of NAFLD and NASH will potentially identify targets for therapeutic intervention and it might promote the development of novel non-invasive biomarkers, improved detection methods and more effective treatment strategies [13], [18].

1.2. Diabetes and insulin resistance

Diabetes is a chronic disease that arises when pancreatic β-cells does not produce enough insulin to maintain blood glucose levels or when the organism cannot effectively use the insulin and fails to compensate for the peripheral insulin resistance. In 2014, diabetes affected over 422 million people worldwide. Because complex tests are needed to distinguish between type 1 diabetes and type 2 diabetes (T2D), no separate estimates of the prevalence of each pathology currently exist [33].

In type 1 diabetes or the monogenic maturity onset diabetes of youth (MODY), an impairment in insulin production exists that severely affects health, particularly in children [34]. However, more than 90% of diabetic patients are affected by T2D, which has become the most common endocrine disorder [35]. The rising prevalence of obesity and T2D is dramatically increasing in our societies and insulin resistance is gaining a prominent role [36].

The development of T2D is a pathophysiological process that involves genetic and environmental influences. Insulin lowers blood glucose levels in order to promote glucose uptake into skeletal muscle and adipose tissue and to inhibit glucose production by the liver. In the insulin-resistant state, the target tissues do not correctly respond to insulin, leading to hyperglycemia and a high increase in insulin secretion. The increased levels of insulin can compensate for the low insulin response for a limited time, but it eventually becomes detrimental and results in insulin resistance. This loop between peripheral insulin resistance and pancreatic β-cells function promotes the clinical manifestation of T2D and associated disturbances [35].

Inflammatory pathways are critical in this pathology. Specifically, the inflammatory response is triggered in obesity and maintained as a low-grade state, what results in a deteriorated metabolic homeostasis that primarily affects glucose metabolism [37].

Obesity-induced insulin resistance

Insulin resistance is the principal metabolic abnormality in the majority of patients with T2D and an unequivocal condition in the pathogenesis for many of modern diseases. The action of insulin provides a set of signals that balance nutrient availability and requests. After nutrient intake, insulin

promotes carbohydrate uptake at key storage organs and stimulate the conversion to lipids and proteins, an efficient reservoir for calories [36].

With chronic over-nutrition and reduced energy expenditure, the storage capacity of the white adipose tissue, skeletal muscle or liver is exceeded. These metabolic tissues and the surrounding milieu are exposed to high-physiological levels of metabolic substrates, resulting in cell dysfunction [9] (Figure 2). These alterations activate several metabolic pathways implicated in the development of insulin resistance. Different cell-extrinsic and cell-intrinsic mechanisms are the causal factors that correlate overfeeding and weight gain with peripheral insulin resistance. The main cell-extrinsic mechanisms include alterations in the levels of circulating fatty acids and adipokines and the contribution of metabolic tissue inflammation whereas the cell-intrinsic pathways include oxidative stress, development of ER stress, mitochondrial dysfunction and ectopic lipid accumulation [38]–[40].

The dysregulation of cell-intrinsic and cell-extrinsic mechanisms activates a set of signaling pathways related with stress-response, including the activation of Jun N-terminal kinases (JNK), inhibitor of nuclear factor κB (IκB), IκB kinase β (IKKβ), mammalian target of rapamycin (mTOR), extracellular signal-regulated kinases (ERKs), endoplasmic reticulum-to-nucleus signaling I (IRE-1) and protein kinase Cθ (PKCθ), among other. These pathways cooperate to produce two metabolical effects [9].

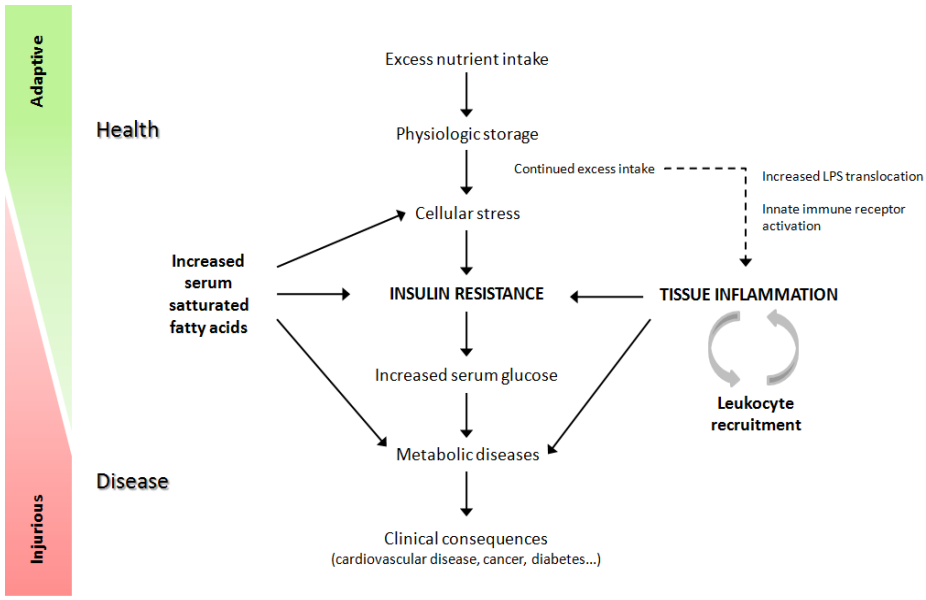

Figure 2. Inflammation and insulin resistance are the key players in obesity-induced metabolic alterations. With a chronic nutrient intake, the imbalance between intake and expenditure exceed the capacity of metabolic tissues for caloric storage. This long-term nutrient excess is manifested through heterogeneous mechanisms as the activation of cellular stress signaling pathways, the inhibition of insulin signaling and triggers the inflammatory activation through different pathways. Furthermore, these alterations might lead to a chronic inflammation and insulin resistance, which might progress to pathological consequences as cardiovascular disease, diabetes or cancer. Adapted from *J. Odeegard et al.* [9].

First, in a normal situation, the presence of insulin at the cell surface is transduced to cytoplasmic and nuclear responses by tyrosine phosphorylation of insulin receptor substrate (IRS)-1 and (IRS-2) [34]. Conversely, a number of hormones, circulating free-fatty acids, ceramides, glucose, diverse metabolites and cytokines promote serine/threonine phosphorylation of IRS proteins, reducing the ability of these molecules to activate phosphatidylinositol 3-kinase (PI3K) [41]. Subsequently, the downstream signaling of insulin receptor is inhibited, inducing insulin resistance in affected tissues. While serine/threonine phosphorylation is considered a short-term mechanism, the degradation of IRS proteins in a regulated manner might promote long-term insulin resistance [9], [41].

Second, all these signals converse on JNK and IKKβ, two of the most important inflammatory signaling pathways, which increase and potentiate the inflammatory response in the specific tissues and provide a potential link between inflammation and insulin resistance [9]. Moreover, increased concentrations of non-esterified fatty acids (NEFA) and inflammatory mediators as TNF-α, released by expanded adipose tissue, activate signal transduction cascades to impair insulin action by increasing serine phosphorylation of IRS and reducing the downstream IRS signaling [8].

In fact, the activation of JNK and IKKβ triggers the release of inflammatory cytokines that activate these pathways in an autocrine and paracrine manner, thus initiating a feed-forward loop. These activated and upregulated serine kinases phosphorylate the transcription factor targets activator protein 1 (AP-1) (c-Jun/Fos) and nuclear factor-kappa B (NF-κB), which both intensify insulin resistance through the transcriptional activation of the pro-inflammatory gene set [41], [42].

1.3 The link between metabolic diseases and inflammation

Homeostasis and disease

The development of non-communicable and chronic diseases in our modern societies results when normal physiologic control is disrupted and maintenance of homeostasis fail. A broad spectrum of human modern diseases has the common feature of being closely associated to chronic inflammation, as they imply the disruption of physiological homeostasis. Inflammation has a protective role on the response to challenges to homeostasis, such as infection or tissue injury. The release of inflammatory signals as cytokines and chemokines causes alterations and changes in

numerous biological processes as an attempt to restore physiological functions when homeostatic mechanisms are not sufficient [43].

The inflammatory response promotes the suppression of non-compatible homeostatic processes and activates mechanisms for the restoration of homeostasis. However, in persistent inflammation, these changes may be damaging and can result in a chronic pathologic state. For example, hyperglycemia can lead to the development of glucose toxicity and tissue dysfunction and consequently to inflammation. In this scenario, inflammation is not necessary for the initial process of insulin resistance, but the homeostatic perturbations promote the development and worsening of insulin resistance through the inflammatory response [44]. A successful inflammatory response leads to the resolution phase and restores homeostasis. However, the physiological mechanisms activated during inflammatory responses disrupt non-compatible homeostatic processes and might be permanently activated, thus promoting a phase of chronic inflammation.

1.4 Metaflammation: the inflammatory state in obesity

Despite using similar mechanisms and mediators, the inflammatory process in metabolic-related diseases differs from the set of changes that takes place during infectious inflammation. The response to infectious inflammation implicates a short and acute response, described as the principal response of the body to deal with injuries. The principal hallmarks of this short-term response include redness, pain, fever and swelling and the inflammatory response has a prominent importance in tissue repair [45].

Conversely, in metabolic alterations, the response differs in intensity and duration and just a few of the classic characteristics of inflammation are

present. The consequence of long-term caloric overfeeding involves a chronic (years to decades) and low-grade inflammatory response, which is manifested through heterogeneous and complex mechanisms [42], [46].

Hotamisligil G.S has proposed the use of a new term ("Metaflammation") to describe this state of inflammation. Metaflammation, defined as a metabolically triggered inflammation is reached due to an excess of nutrients, and promotes the activation of a similar network of signaling pathways and molecules to those involved in classical and acute inflammation [46], [47]. Metaflammation is the hallmark of metabolic diseases principally characterized by chronic low-grade metabolic inflammation caused by lipid-induced inflammation and cellular dysfunction and death. In metabolically active organs including liver, adipose tissue, muscle, pancreas, brain and gut, the inflammatory cell action and the interactions within the stromal components is determinant in the tight line between tissue homeostasis and metabolic disease [47]. Cells possess an integrated network of response to adapt to stress situations as the nutrient imbalance. Hence, although lipids are essential for homeostatic processes, in excess or improper composition can result in detrimental metabolic effects leading to disturbances in energy metabolism, organelle dysfunction, chronic inflammation and cell death [48] .

The immune responses are closely associated with lipid metabolism, so the accumulation of harmful lipid species and signaling intermediates can interfere with integrated immune response leading to lipotoxicity-mediated inflammation and immunometabolic dysregulation. These detrimental responses yield maladaptive effects promoting vicious pathological cycles that potentiate metabolic diseases [48].

Hallmarks of metaflammation

Obesity is associated with inflammation and is causally associated with the development of insulin resistant in a background of low-grade chronic inflammation. The inflammation caused in obese patients is different from the paradigm of classical inflammation, because the trigger is metabolic and caused by an excess of nutrient intake, and because metabolic cells like adipocytes are responsible for initiating the release of metabolic signals and inflammatory mediators [1].

The first evidence for a pathophysiological link between obesity and inflammation was provided at 1993 when *Hotamisligil et al.* demonstrated that TNF-α is overexpressed in the adipose tissue of obese mice compared to lean controls [49]. Moreover, the lack of TNF-α function in obese mouse models results in an improved glucose homeostasis, thus confirming that the inflammatory response initiated by this cytokine has a potent role as a negative regulator of insulin actions [46], [49]–[51].

A great number of studies published in the recent decade have reported the inflammatory differences displayed between obese and lean animal models and humans. Moreover, not only TNF-α is involved in the activation of inflammatory response, since various other inflammatory cytokines and chemokines are increased in obese tissues, mainly in adipose tissue. This array of cytokines includes IL-6, IL-1β and monocyte chemoattractant protein-1 (MCP-1, CCL2) [39], [46].

The main contributors that induce this inflammatory response in metabolic tissues have been identified as JNK, IKK and protein kinase R (PKR). These kinases and their downstream signaling pathways are highly increased in adipose tissue and liver in comparison with lean controls and converge on the induction of inflammatory target genes [1].

The phosphorylation and activation of JNK leads to the phosphorylation of the N terminus of c-Jun. Because of this, c-Jun dimers start a switch for c-Jun-c-Fos heterodimers (AP-1), which stimulate the transcription of pro-inflammatory gene sets. Similarly, the activation of IKKβ promotes the degradation of the inhibitor of NFκB, IκB, through its phosphorylation. This modification promotes the dissociation the NFκB complex, permits the translocation of NFκB to the nucleus and leads to the transactivation of inflammatory gene sets. NFκB and AP-1 induce the expression of inflammatory mediators that act in a paracrine and autocrine manner to exacerbate insulin resistance (Figure 3) [39], [52].

These inflammatory signaling is activated by different mechanisms. The activation through TNF-α and IL-1 and their surface receptors correspond to a classical activation. On the other hand, the inflammatory process can be activated through an alternatively mode via pattern recognition receptors (PRRs) which include Toll-like receptors (TLRs). Specifically, TLR4 displays an important role sensing saturated fatty acids to initiate an inflammatory response on macrophages [39], [53]. Furthermore, diverse studies have demonstrated that obesity is related to the activation of the inflammasome, in which caspase-1 controls the process of maturation from pro-IL-1β to IL-1β [54]–[56]. Finally, other cellular stresses such as lipotoxicity, ER stress, ROS production and hypoxia can stimulate the pathways to activate the inflammatory signaling.

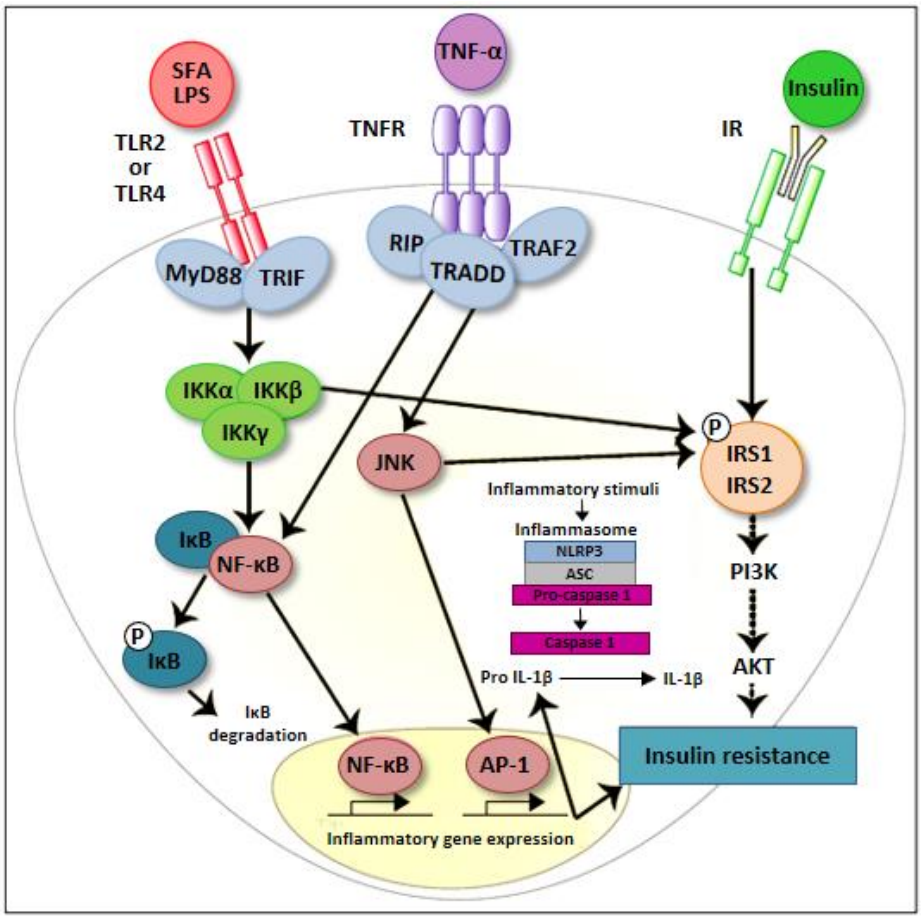

Figure 3. Inflammatory signaling pathways implicated in the development of insulin resistance. Activation of TLR2, TLR4 or TNFR leads to activation of IKK and JNK, causing serine kinase phosphorylation of IRS-1 or IRS-2 and inhibiting insulin downstream signaling. In addition, the phosphorylation of IKKβ permits the translocation of NFκB to the nucleus and the activation of JNK leads to the formation of AP-1 transcription factor. Both, NFκB and AP-1, increase the transcription of inflammatory genes and contribute to insulin resistance in a paracrine manner. Adapted from *McNelis JC et al.* [39].

Another feature of the inflammatory response triggered by obesity is an increase of immune cells infiltration in the target metabolic tissues. In 2003, two groups independently demonstrated that the macrophage infiltration is increased in the white adipose tissue of obese mice fed with a high-fat diet (HFD) in comparison with lean controls fed with a standard diet. This population of macrophages turned out to be the main source of inflammatory mediators, including TNF-α [57], [58]. Moreover, the existence of factors that attract and activate immune cells in obesity lead to a strong connection between immune cell infiltration and metabolic obese tissue [59]. Although the infiltration of macrophages triggers multiple alterations in obese tissues, natural killer T cells (NKT) and mast cells also contribute to the inflammatory response. Several studies reported that obesity promotes pathogenic adaptive responses of T cells [60], [61], namely $CD8^+$ T cells that interact with infiltrated macrophages and contribute to the inflammatory response [62]. The presence of regulatory T cells (Treg), which induce immunomodulatory suppressive effects, also decreases in the context of obesity [63]. Therefore, the immune system actively participates in the regulation and orchestration of the systemic inflammatory environment in adipose tissue during obesity.

An additional hallmark of the metabolic inflammatory response is chronicity. The infiltration of immune cells is gradual and appears to remain unresolved. A few years ago, *Xu et al.* demonstrated that the expression levels of inflammatory gene set and macrophage-related genes is directly correlated with the increase of fat mass, and that the inflammatory response is intensified by the development of insulin resistance [58]. In 2007, *Strissel et al.* suggested that adipocyte death and the removal of death cells by adipose tissue macrophages is part of a remodeling program to expand adipose tissue in response to an excess of energy [64].

In the issue of progression and duration of the inflammatory response evoked by an excess of nutrients, it seems that inflammatory signals occur at early and larger states, thus promoting a maintained chronic state of metabolic inflammation. As illustrated in Figure 4, the first hallmark of obese inflammation is that it initiates from metabolic cells, like adipocytes, in response to nutrient overload. Second, metabolic mediators activate the downstream response from the stress sensors as JNK, IKK or PKR, which induced a moderate and low-grade inflammation. Third, the maintenance of the inflammatory state induces the recruitment and infiltration of several immune cells that create a modified milieu that results in a higher inflammatory response. Finally, the inflammatory state is unresolved, no apparent resolution is observed and the inflammatory signaling pathways reinforce each other in a feedback loop, becoming a chronic inflammatory state [1].

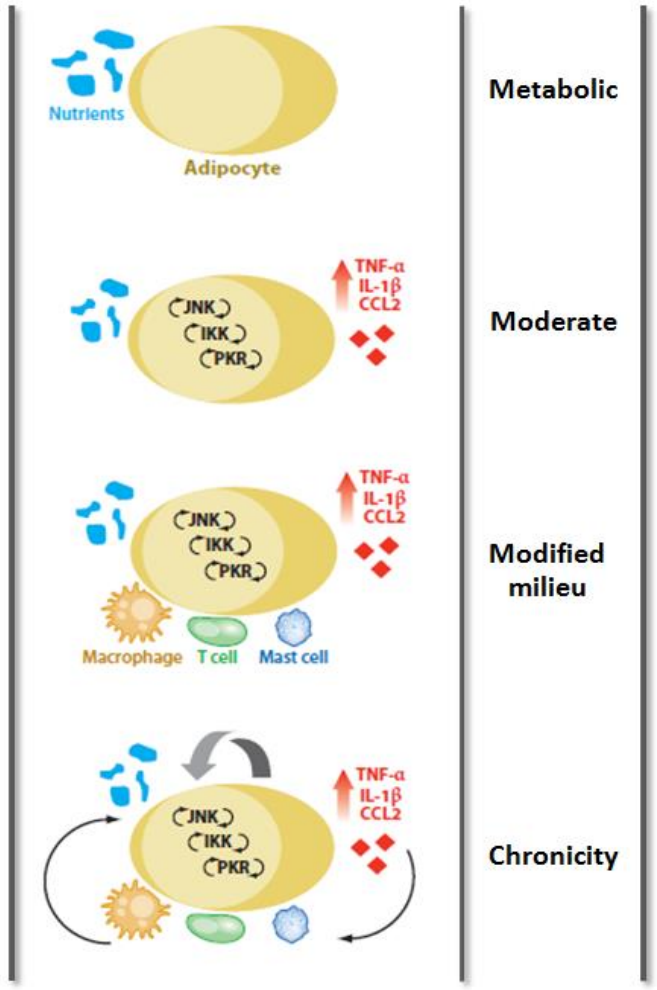

Figure 4. Hallmarks of metaflammation. The initiation of obese inflammation is metabolic and originated by metabolic cells such as adipocytes. Second, metabolic signals trigger inflammatory signaling pathways as JNK, IKK and PKR that mediate a modest, low-level induction of pro-inflammatory cytokines. Third, this low-grade inflammation induces the recruitment of immune cells, driving the metabolic tissue toward a modified milieu. At last, the nutrient excess is maintained and the inflammatory state is chronic and unresolved. Adapted from *Gregor MF et al.* [1].

1.5 Therapeutic perspectives

Chronic inflammation, the key factor in the pathogenesis of obesity, insulin-resistant states and associated complications, also underlies pathologies like rheumatoid arthritis, psoriasis, gout and Crohn's disease among others. Therefore, the development of therapeutic strategies to interfere with these inflammatory-mediated diseases has potential importance for the case of obesity. In fact, several anti-inflammatory drugs have been tried in clinical approaches and several are already in late stages of development or have been already approved [39], [65]. A major field of research involves the finding of optimal therapeutic strategies for chronic inflammatory diseases by interfering with inflammatory mediators, modulating inflammatory cascades and restoring anti-inflammatory molecules. In the case of obesity, these approaches also include the use of anti-inflammatory nutrients through diet as well as cell based-immunotherapies.

Because the blood levels of TNF-α and IL-1β are elevated in obesity [66], [67], blocking of TNF-α and IL-1β has been addressed in different therapies and clinical approaches. Anti-TNF-α antibodies have yielded positive results in rodent models of diabetes and insulin resistance [49]. However, in human therapies the results are unclear. Various human studies using etanercept, a TNF-α inhibitor, failed to demonstrate a positive effect on glucose metabolism in insulin-resistant patients without evident inflammatory disease [68], [69]. While these pilot studies were conducted for a short-term period, larger studies on the prolonged treatment with antagonists of TNF-α improved insulin sensitivity and other parameters in patients with inflammatory diseases, especially rheumatoid arthritis [70], [71]. Strategies directed against IL-1β have also been explored using IL-1β receptor antagonists and anti-IL-1β antibodies [72]–[74]. Specifically, high glucose concentrations induce IL-1β production in pancreatic β-cells of T2D patients,

leading to decreased cell proliferation and impaired insulin secretion. The blockade of IL-1 with anakinra, a recombinant human interleukin-1 receptor antagonist, seems to yield glucose-lowering effects, improves β-cell secretory functions and reduce markers of inflammation [75].

Therapies to reduce obesity-mediated inflammation also include approaches to block the action of certain kinases and inflammatory pathways. The drug family of salicylates, particularly salsalate, seems to exert an anti-inflammatory effect through the inhibition of IKK activity, preventing the action of NFκB and the gene set involved in the inflammatory response [76].

Another example of therapeutic strategies are thiazolidinediones (TZDs, e.g., rosiglitazone and pioglitazone), that contribute to overall anti-inflammatory effects by restoring insulin sensitization. These anti-diabetic drugs are agonists of peroxisome proliferator-activated receptor γ (PPARγ), a transcription factor essential for adipogenesis and adipocyte-specific functions [77]. The TZDs activate PPARγ and restore the lipogenic function in adipocytes, inhibit inflammatory pathways by decreasing the content of adipose tissue macrophages (ATMs), and increase the content of eosinophils in adipose tissue and the differentiation of anti-inflammatory Treg cells [78]. The main feature of TZDs is to produce insulin-sensitizing effects through many different mechanisms such as the redistribution of fat stores and the induction of adiponectin, an endogenous anti-inflammatory adipokine [39].

At present, the most studied anti-inflammatory nutrients might be the omega-3 polyunsaturated fatty acids (n-3 PUFAs) which have anti-inflammatory properties via docosahexaenoic acid (DHA) and eicosapentaenoic acid (EPA). An increased consumption of these fatty acids appears to decrease the risk of inflammatory diseases as obesity, diabetes, arthritis and cardiovascular disease [79], [80].

The interaction between macrophages and other immune cells, that promote a pro-inflammatory polarization of ATMs, also represents a target for immunotherapy. This field still has a great number of unanswered questions, but the option to shift pro-inflammatory macrophages toward an anti-inflammatory state, or targeting other immune cells to exert a similar final effect, may prove successful in having insulin sensitizing effects [39].

The option of immunotherapy has yielded positive metabolic effects in murine obesity models. Although the involvement of adaptive immune cells in metabolic diseases remains unclear, it is reported that the pathogenesis of obesity is associated by a huge abundance of T cells, B cells, macrophages, neutrophils and mast cells in adipose tissue [81], [82]. $CD4^+$ T lymphocytes have been identified to have a potential role in insulin resistance, adipocyte hypertrophy and regulation of body weight, implicating these immune cells in the progression of obesity or T2D [60]. Other studies have demonstrated the beneficial effects of deleting $CD11c^+$ [83], $CD8^+$T cells [62] or mast cells [84] in obese murine models. These results indicate that immune cells are potentially relevant targets for the development of new therapeutic approaches for treatment of T2D and obesity-induced insulin resistance in humans.

As indicated, several therapeutic approaches are under an exhaustive study. Metabolomics is taking special interest in the last decades as an invaluable tool in the research of the new biomarkers of disease and therapeutic strategies. In this way, targeted metabolomics to explore the energy management and mitochondrial function should be a non-invasive (specially in plasma), fast and easy alternative to an early diagnostic of these pathophysiological processes.

1.6 Animal models in scientific research

As stated before, inflammation-based diseases represent a growing socioeconomic trouble worldwide. For that reason, great efforts are focused on the finding of new treatments, especially pharmacological interventions. Regarding animal models of disease, it is however not possible to have the certainty that the effects observed will be translated to an improvement of the human health. The use of animals to model human diseases in the field of biomedical research is based on the fact that basic processes are sufficiently similar across species to permit the extrapolation. The ideal characteristics in an animal model is the similitude to the human condition in pathophysiology, etiology, symptomatology and response to therapeutic interventions [85], [86].

The capacity to create transgenic animal models, especially genetically engineered mouse models, has had a deep impact on the research of several diseases. Mice have several similarities to human in physiology, genetic and anatomy, and are cost effective, small and multiply quickly. The mouse genome is relatively easy to manipulate, so providing a useful tool for the study of diseases with mutated genes. Moreover, mice are really useful for the study of complex diseases such as hypertension or atherosclerosis due to the fact that many genes responsible for these diseases are shared between human and mice [87], [88]. Without doubt, and in biomedical research, mice have helped to accelerate the progress of research and have also permitted the development of effective pharmacological drugs and treatments.

2. Macrophages: linking immune system and metabolic disease

2.1 Ontogeny

Macrophages have long been considered as one of the main populations of immune effector cells. In 1908, Élie Metchinikoff was the first to identify these phagocytic cells as macrophages [89]. Metchnikoff credited that these phagocytes played a prominent role in organ development, homeostasis and protecting the host from infection. He also described a relationship between the mononuclear phagocytic cells in the lymph nodes, spleen and bone marrow and the macrophages outside these organs [89], [90].

In the late 1960s and early 1970s, van Furth and co-workers described the "mononuclear phagocyte system" which includes all highly phagocytic mononuclear cells and their bone marrow progenitors [90]. Further, they established the concept that these mononuclear cells are originated from precursor cells in the bone marrow, are transported as monocytes in the peripheral blood, and infiltrated into different tissues to mature into macrophages. However, this prevalent idea that monocytes are precursors of tissue macrophages has been recently redefined [90], [91], and the monocyte-to-macrophage differentiation process is now only known to exist during inflammatory responses and only in some tissues in homeostasis (gut, dermis and heart).

Macrophages differentiate from myeloid progenitor cells by several routes of differentiation [92]. Early in ontogeny macrophage derives from the yolk sac without a monocytic progenitor. Later, monocytic differentiation takes place in the fetal liver, which is initially seeded by hematopoietic progenitors from the yolk sac and subsequently by hematopoietic stem cells. Subsequently, the fetal liver becomes the source of definitive hematopoiesis that generates circulating monocytes during embryogenesis. After birth, and upon the

formation of bone, fetal liver hematopoiesis declines and is replaced by bone marrow hematopoiesis [93]–[95].

Brain-resident macrophages, known as microglia, are exclusively derived from yolk sac progenitors [96], [97], whereas Langerhans cells and epidermal macrophages have a mixed origin from fetal liver and yolk sac [98]. Kupffer cells in the liver and lung alveolar macrophages are derived from fetal liver monocytes during the embryonic state and, from then on, these populations are maintained autonomously under homeostatic conditions [94], [96]. This self-renewal process is regulated through cytokines and growth factors as macrophage colony-stimulating factor (M-CSF or CSF1) in most tissues and granulocyte-macrophage colony-stimulating factor (GM-CSF) in lung [93], [99], [100].

All these previous studies evidenced that monocyte do not contribute to the maintenance of tissue resident macrophages in homeostatic conditions, with the exception of dermis, gut and heart, where monocytes seed the tissue and differentiate in tissue macrophages [101]–[103]. By contrast, monocytes seed the tissues and differentiate in tissue macrophages in most inflammatory settings [99], [100].

2.2 Tissue-resident macrophages

All tissue macrophages exhibit common effector function that includes a role in immune response against pathogens, and the ability to initiate the process of resolution of inflammatory and wound healing. Besides, macrophages are also involved in tissue development by shaping the tissue architecture, and are key players in immune surveillance by acting as sentinel and effector immune cells. At last, they all participate in the clearance of senescent or apoptotic cells and tissue repair to maintain tissue homeostasis [93].

The different phenotypes adopted by monocyte-derived macrophages and resident macrophages are ultimately determined by tissue-specific cues. The different tissue-resident macrophage populations display distinct and specific transcriptional profiles that are perfectly suited for the tissue-specific requirements for maintaining, defending and regaining homeostasis [93], [94]. In fact, the alteration of homeostasis in tissue macrophages through an anomalous activation promotes the development of different pathologies according to the affected tissue (Table1).

Table 1. Macrophages functions and pathologies in the main tissues. Adapted from *Italiani et al.* [93].

Macrophages	Tissue	Functions	Pathology
Microglia	Brain	Brain development Immune surveillance Synaptic remodeling	Neurodegeneration
Osteoclasts	Bone	Bone resorption Bone modeling Support to hematopoiesis	Osteoporosis Osteopetrosis Arthritis
Heart macrophages	Heart and vasculature	Surveillance	Atherosclerosis
Kuppfer cells	Liver	Toxin removal Lipid metabolism Iron recycling Erythrocyte clearance	Fibrosis Impaired erythrocyte clearance
Alveolar macrophages	Lung	Surfactant clearance Surveillance for inhaled pathogens	Alveolar proteinosis
Adipose tissue macrophages	Adipose tissue	Metabolism Adipogenesis Adaptive thermogenesis	Obesity Diabetes Insulin resistance
Bone marrow macrophages	Bone marrow	Reservoir of monocytes Waste disposal	Disruption of hematopoiesis
Intestinal macrophages	Gut	Tolerance to microbiota Defense against pathogens Intestinal homeostasis	Inflammatory bowel disease
Langerhans cells	Skin	Immune surveillance	Insufficient healing Fibrosis

Marginal zone and red pulp macrophages	Spleen	Erythrocyte clearance Iron processing Capture of microbes from blood	Impaired iron recycling Erythrocyte clearance
Inflammatory macrophages	All tissues	Defense against pathogens Protection against dangerous stimuli	Chronic inflammation Tissue damage Autoimmunity
Healing macrophages	All tissues	Branched morphology Angiogenesis	Cancer Fibrosis

The heterogeneous population of tissue resident macrophages represents up to 10-15% of the total cell number in steady-state adult tissues. The homeostatic control of macrophages is principally influenced by M-CSF, which is produced by endothelial cells, macrophages, stromal cells, fibroblasts, osteoblasts and smooth muscle cells [104]. The main functions of M-CSF are promotion of proliferation, increased cell survival and differentiation, and its effects are restricted to the macrophage lineage. In a steady-state, M-CSF functions are mediated through its receptor (CSF-1R) [105].

The macrophage differentiation program induced by M-CSF is essential for in vivo generation of macrophages derived from bone marrow precursors. *Csf1*$^{op/op}$ mice display a dramatically reduced number of macrophages in kidney, liver, peritoneal cavity and dermis. Moreover, these mice are osteopetrotic due to an early and important deficiency of osteoclasts [105], [106]. However, *CSFR1*$^{-/-}$ mice exhibit a more severe phenotype in comparison with *Csf1*$^{op/op}$ mice because of the existence of a second ligand for CSF-1R, IL-34. This interleukin also has immunosuppressive properties, induces *in vitro* generation of macrophages from bone marrow precursors and specifically directs differentiation of Langerhans cells and microglia [104], [107], [108].

An important feature of macrophage differentiation is that the tissue microenvironment determines the final outcome of macrophage differentiation. In general, tissue macrophages are characterized by cell surface markers as tyrosine-protein kinase MER (MERTK) and FcγRI (CD64) together with the expression of the transcription factors PU.1, CCAAT/enhancer-binding protein (C/EBP), MAF and MAFB. However, the cytokines and metabolites produced in the macrophage microenvironment also promote the expression of specific transcription factors and the expression of tissue-specific markers. In the brain, cells derived from yolk sac are exposed to transforming growth factor-β (TGF-β), which induces SMAD phosphorylation and a transcriptional profile specific for microglia. In the lung, fetal liver monocytes are exposed to GM-CSF that leads to the induction of PPARγ expression and the differentiation into alveolar macrophages. In the spleen, SPI-C expression controls the differentiation to splenic red pulp macrophages and macrophages from marginal zone depends on the transcription factor liver X receptor-α (LXRα). Macrophages from peritoneal cavity are induced by the expression of GATA-binding protein 6 (GATA6). In the skin, the presence of TGF-β and IL-34 induces the expression of RUNX3 and ID2 and promotes the differentiation to Langerhans cells [109].

The maintenance, regulation and functional specialization of macrophages also depends on the surrounding metabolites and cytokines. M-CSF promotes proliferation and macrophage survival in most tissues, whereas GM-CSF or IL-34 are only produced in specific tissues to maintain local macrophages. For example, the expression of low doses of GM-CSF is required for the essential functions of macrophages in lung and intestine. However, at higher doses and together with inflammatory signals, GM-CSF contributes to the development of inflammatory processes [105], [109].

Finally, the involvement of M-CSF in several diseases has been reported. An increase in M-CSF circulating levels is found in arthritis, pulmonary fibrosis, inflammatory bowel disease, autoimmune diseases, kidney inflammation, atherosclerosis, obesity and cancer metastasis [106], [110], thus making CSF-1 signaling as an important option for therapeutic treatment [111].

2.3 Macrophages in inflammation

Macrophages are constantly sensing the local microenvironment, where metabolites together with tissue-specific cytokines contribute to shaping macrophage effector functions under homeostatic and inflammatory states. Macrophages can detect disruptions of tissue homeostasis, sensing pathogens or stress signals such as hypoxia or nutrient excess or deprivation [112]. The recognition of injurious signals induces tissue stress and defense response that lead to inflammation as a mean to restore homeostasis.

In the first phases of inflammatory response, the number of effector immune cells is increased to potentiate the immune defense. The main strategy is through recruitment of blood monocytes, a process that is essential for viral, bacterial or fungal infections. These bone marrow-derived monocytes infiltrate in the peripheral tissues and differentiate into inflammatory macrophages within tissues. However, newly recruited monocytes also contribute to the pathogenesis of inflammatory diseases [93], [113].

Another option to increase the number of effector cells is via enhancement of macrophage proliferation through self-renewal. Macrophage proliferation is observed in different human diseases including adipose tissue-associated macrophages in obesity. In this pathology, the increase in macrophage numbers is due to recruitment and accumulation of macrophages in the adipose tissue mediated by CCL2, also considered as a stimulus for macrophage proliferation in this inflammatory disease [114].

As described above, and upon tissue damage, monocytes migrate from circulation to target tissues and differentiate into macrophages showing a pro-inflammatory phenotype. Moreover, these newly recruited phagocytic cells are able to produce inflammatory mediators to protect tissue integrity. Although this response is initially beneficial, the secretion of pro-inflammatory mediators such as nitric oxide (NO), TNF-α and IL-1β trigger the activation of oxidative processes that contribute to kill the pathogens but also result in tissue damage [115]. Other secreted mediators are decisive to the polarization of T lymphocytes to a Th1 and Th17 response, which potentiate the inflammatory response. Therefore, this macrophage pro-inflammatory phenotype is associated with chronic inflammatory diseases like obesity, rheumatoid arthritis, Crohn's disease, multiple sclerosis and allergy and asthma [94], [116].

Importantly, and besides their innate phagocytic activity, tissue macrophages are also involved in wound repair. So, an anti-inflammatory macrophage response is involved in wound healing and fibrosis through the production of growth factors as TGFβ1 and platelet-derived growth factor (PDGF) [117]. These anti-inflammatory macrophages also produce matrix metalloproteinases (MMPs), eliminate death cells, secrete extracellular matrix (ECM) components and eliminate debris. Furthermore, these macrophages promote Th2 and Treg responses and produce IL-10, a critical immunoregulatory and anti-inflammatory cytokine [116].

The mechanisms that regulate the phenotypic switch of pro-inflammatory macrophages into anti-inflammatory cells, or the conversion of anti-inflammatory into a pro-inflammatory phenotype is decisive for the development and resolution of many chronic diseases [94]. Therefore, the factors controlling these functional shifts are excellent targets for the development of therapeutic alternatives for chronic inflammatory diseases.

The pathological relevance of the pro-inflammatory-to-anti-inflammatory shift is best exemplified in the case of tumors.

Macrophages in cancer display a heterogeneous phenotype which is either: pathogenic and protective. Pro-inflammatory macrophages activate mechanisms to promote an anti-tumor response and trigger the action of cytotoxic and tumor-killing mechanisms. However, the progression of tumor and the microenvironment drives a switch into a suppressive macrophage phenotype. These anti-inflammatory macrophages contribute to tumor progression and metastasis [115], [116], [118]. Similarly, macrophages participate in all phases of fibrotic diseases and their functional heterogeneity allows them to induce or inhibit the process [119], [120].

Macrophages have also an important role in metabolic disorders and obesity. In white adipose tissue, anti-inflammatory adipose tissue macrophages (ATMs) are induced by PPARγ and contribute to maintenance of adipocyte function and prevention of the development of insulin resistance [40]. However, as the obesity progresses, the anti-inflammatory ATMs switch into a pro-inflammatory phenotype that contributes to insulin resistance and adipose tissue inflammation [121] . In lean mice, macrophages are approximately 10-15% of cells of adipose tissue, while in obese animals the presence of these phagocytic cells increase up to 45-60% of total cells [57].

2.4. Macrophage activation

Macrophages represent the first line of defense against pathogens. The stimulation of macrophages by signals from microbes (pathogen-associated molecular patterns, PAMPs), damaged tissues (danger-associated molecular patterns, DAMPs) and resting or activated lymphocytes, undergo a reprogramming that leads to the acquisition of a wide spectrum of different

functional phenotypes [115], [122]. Macrophages are equipped with numerous cell surface (TLRs, lectins) and intracellular (NLRs) receptors that recognize either PAMPs or DAMPs. Activation of this sensors switches on intracellular signaling events that promote the acquisition of effector functions to eliminate the injury and, later, to repair the damage.

Plasticity and heterogeneity have long been known to be the principal hallmarks of the macrophage lineage. Consequently, the activation of macrophages, influenced by their systemic and local milieu, can generate a broad range of functional states, commonly referred to as "macrophage polarization states". Importantly, macrophage activation or polarization is associated with substantial modifications in the macrophage gene expression signature whose acquisition is critically dependent on the triggering stimulus [123], [124] (Figure 5).

A simplistic view of macrophage polarization states is based on a binary system: pro-inflammatory state and anti-inflammatory state [125]. In the first state, the macrophage phenotype is characterized by the expression of high levels of pro-inflammatory cytokines as TNF-α, IL-1β, IL-6 and type1-biasing cytokines such as IL-12 and IL-23, high production of reactive oxygen and nitrogen intermediates, promotion of polarized Th1 responses and resistance against intracellular pathogens and tumors (microbicidal and tumoricidal activity, respectively) [126], [127]. In contrast, anti-inflammatory macrophages produce high levels of IL-10, which limits the intensity and duration of inflammatory and immune responses. Thus, these phagocytic cells are involved in recruitment of eosinophils and basophils, amplification of Th2 response, angiogenesis, tumor progression and dampening inflammation through immunoregulatory functions [128], [129].

Macrophages: linking immune system and metabolic disease

The cytokines and stimuli that trigger macrophage activation are grouped according their ability to induce pro- or anti-inflammatory functions and associated markers. The main stimuli associated with pro-inflammatory activation are interferon (IFN)-γ, lipopolysaccharide (LPS) and GM-CSF, while those associated with anti-inflammatory polarization are IL-4, IL-13, IL-10, glucocorticoids and M-CSF [125].

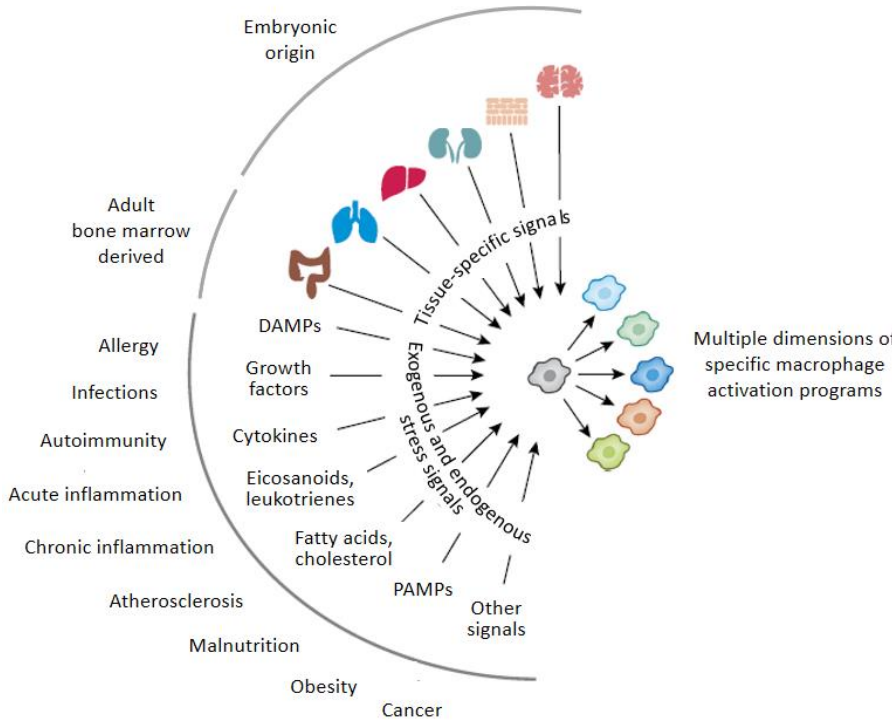

Figure 5. Integrative multidimensional model of macrophage activation. A multidimensional model is presented wherein the macrophage activation is determined by the macrophage ontogeny and the microenvironment (tissue-specific signals and stress signals). Microglia is derived from yolk sac, alveolar macrophages and Kupffer cells are derived from fetal liver monocytes and Langerhans cells are derived from both yolk sac macrophages and fetal liver monocytes. However, macrophages from gut and heart are replaced after birth with adult bone marrow monocytes. The same stress signals with the same kinetic will result in different activation programs in macrophages of different origins. Adapted from *Ginhoux F. et al.* [99].

2.5 Toll-like receptors

The first line of defense against pathogens in vertebrates is the innate immune response. Members of the TLR family of Pathogen Recognition Receptors (PRRs) play an essential role in the activation of innate immunity through the recognition of PAMPs and DAMPs. Each member of TLR family recognize a specific subset of pathogenic ligands and endogenous molecules (Table 2). TLRs are type I transmembrane proteins characterized by containing leucine-rich repeats for PAMPs recognition, a transmembrane helix domain and an intracellular Toll-interleukin 1 receptor (TIR) domain that dimerizes for signal transduction [130]–[132].

Table 2. Summary of pathogenic and endogenous stimuli of the human TLRs. Adapted from *Bryant C E. et al.*[130].

TLR	Pathogenic stimuli (PAMP)	Endogenous stimuli (DAMP)
TLR1/2/6	Lipoproteins (Gram + bacteria)	
TLR2	LTA (Gram + bacteria) Zymosan, β-glucan (fungus) GPI anchors (protozoa)	Hyaluronic acid Serum amyloid A Oxidized LDL HMGB1
TLR3	dsRNA (virus)	Mrna
TLR4	Lipopolysaccharides (Gram – bacteria) GPI anchors (protozoa)	Hyaluronic acid Serum amyloid A Oxidized LDL Saturated fatty acids HMGB1 Fetuin A
TLR5	Flagellin (bacteria)	
TLR7/8	ssRNA (virus)	SsRNA
TLR9	DNA (bacteria, virus, fungal, protozoa)	Mitocondrial DNA
TLR10	Not known	

The human genome encodes 10 TLRs, of which TLR1, TLR2, TLR4, TLR5, TLR6 and TLR10 are present on the cell surface, while TLR3, TLR7, TLR8 and TLR9, involved in the recognition of nucleic acid structures, are only found intracellularly. Importantly, TLR1, TLR2 and TLR4 are also recruited into phagosomes after ligand engagement [130], [131].

As other type I membrane receptors, the basic mechanism for signal transduction of TLRs is ligand-induced receptor dimerization. Dimerized TLR bind to adaptor proteins and activates specific signaling pathways that trigger pro-inflammatory responses and also promote the maturation of adaptive immune response. TLRs use five adaptor proteins that binds to TIR domains: MyD88 (Myeloid differentiation factor 88), TRIF (TIR domain-containing adaptor protein inducing interferon-β), TRAM (TRIF-related adaptor molecule), MAL and SARM. All TLRs can signal through MyD88 with the exception of TLR3, which only uses TRIF [132]–[134]. In general, TLR-initiated downstream signaling cascades can be classified as either MyD88-dependent pathways, responsible for the induction of pro-inflammatory cytokines, or TRIF-dependent pathways, which drives the induction of inflammatory cytokines and type I interferon, as shown in Figure 6.

Lipopolysaccharides from gram-negative bacteria are the main agonists for TLR4 but the activation of TLR4 signaling pathway also requires the co-receptor protein MD-2, to form TLR4/MD-2 complexes at cell surface. TLR4 activates both the MyD88- and TRIF-dependent pathways [134].

TLR4 recruits MyD88 through MAL and the activation of MyD88-dependent pathway involves the recruitment of IL-1 receptor-associated kinases: IRAK1, IRAK2, IRAK4 and IRAK-M. IRAK4 is activated and has an important role in NFκB and mitogen-activated protein kinase (MAPK) activation. IRAK1 and IRAK2 are sequentially phosphorylated and potentiate the activation of NFκB

and MAPK. IRAK activation promotes the interaction with TRAF6 which catalyzes the formation of polyubiquitin chains to activate TAK1. In one pathway, TAK1 activates the IKK complex through the phosphorylation of IKKβ, which targets the inhibitory protein IκB for degradation by proteasome, and leads to NFκB activation and translocation to the nucleus. Simultaneously, TAK1 activate a second branch of TLR pathways through the phosphorylation of MAPK kinases: Erk1, Erk2, Jnk and p38, which activate different transcription factors including AP-1 [131], [132], [134], [135].

Subsequently, TLR4 undergoes endocytosis and is transported to the endosome where the signaling through TRIF-dependent pathway requires TRAM as an adaptor molecule [132]. This TRAM-TRIF complex interacts with TRAF3 and promote the activation of TANK binding kinase 1 (TBK1) and IKKi (IKKε). The phosphorylation of TBK1 or IKKi activates interferon regulatory factor 3 (IRF3), which form homodimers or heterodimers with IRF7, and induce nuclear translocation. These dimers promote the transcription of interferon and interferon-inducible genes. Furthermore, TRAF6 is also involved in the activation of NFκB via TRIF-dependent pathway [133].

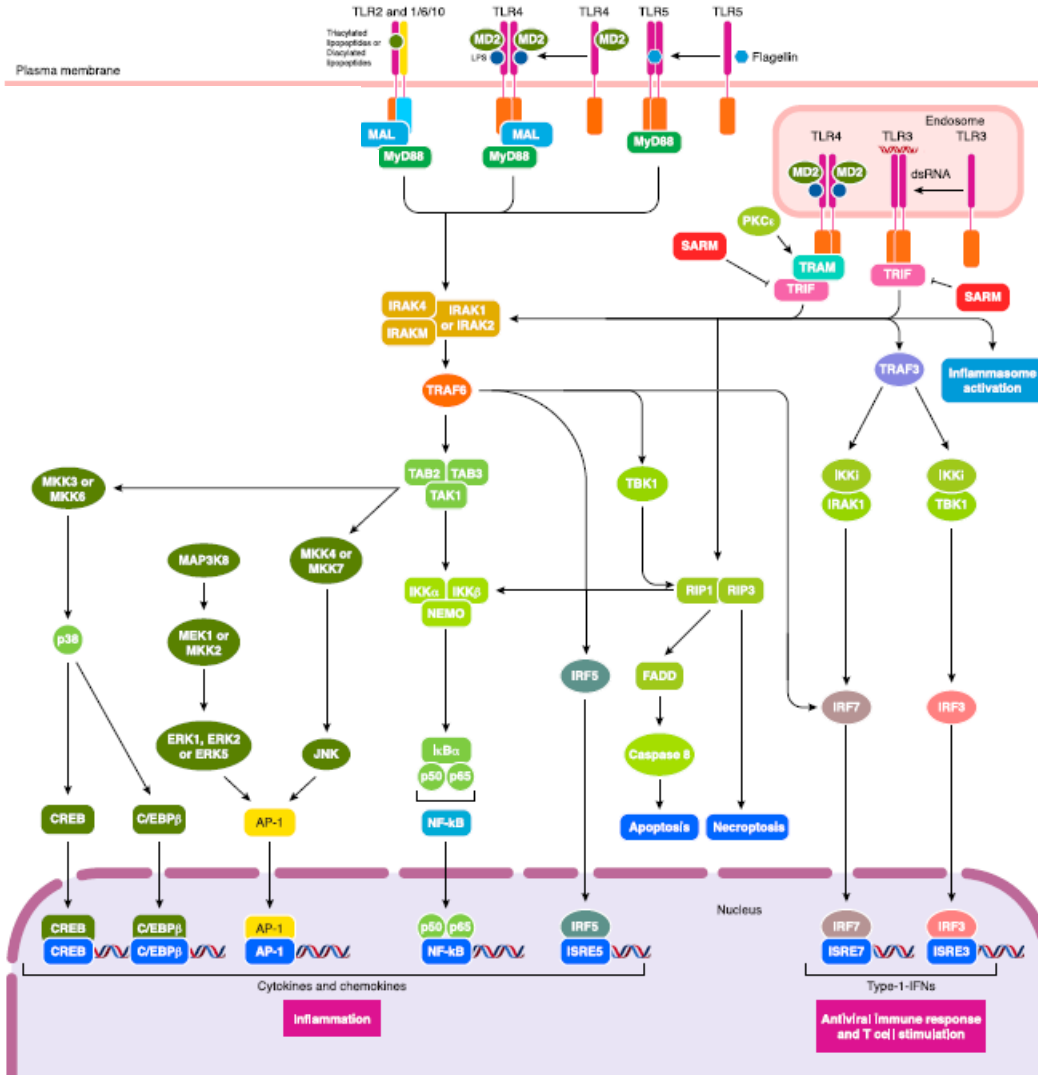

Figure 6. TRIF and MyD88-dependent TLR signaling pathways. TRIF-dependent signaling is responsible for the production of type-I IFNs and the MyD88-dependent signaling pathways are responsible for the production of inflammatory cytokines. Adapted from *Ullah M.O. et al.* [133].

The engagement of TLR4 on macrophages activates several transcription factors, including NFκB, AP-1, CREB, C/EBPβ and IRF3. TLR4-driven activation of monocyte-derived macrophages generated under the stimulus of GM-CSF are characterized by the expression of pro-inflammatory cytokines and type I interferon. Conversely, M-CSF-dependent macrophages respond to LPS primarily through the release of IL-10 [125], [133]. The production of this anti-inflammatory cytokines in monocyte-derived macrophages is mainly controlled by MAPKs as ERK [136] and p38 [137].

TLR4 as a mediator between innate immunity and saturated fatty acids

Several studies have reported the complex roles played by different immune cell populations in metabolic tissues [138]–[140]. These reports have demonstrated that saturated fatty acids (SFA) are capable of activating TLR4-signaling pathways through MyD88 and TRIF, and then activate transcription factors as NFκB, AP-1 and IRF3. The activation of these transcription factors promotes the expression of pro-inflammatory genes, cytokines, chemokines and other effectors related with the development of insulin resistance and chronic inflammation.

The inflammation of adipose tissue in obesity is a process driven by tissue macrophages [57]. As described above, ATMs are phenotypically heterogeneous and can display different phenotypes depending on the signals and microenvironment they are exposed to. In lean adipose tissue, macrophages display an anti-inflammatory phenotype mainly supported by eosinophil-derived IL-4. In turn, adipocytes produce adiponectin to maintain the homeostatic phenotype and macrophages release IL-10 that potentiates insulin signaling and sensitivity [141], [142] (Figure 7A).

The profile of ATMs in obesity is balanced toward a pro-inflammatory phenotype. The inflammatory mediators released from adipose tissue such

as cytokines, IFN-γ and saturated fatty acids induce the recruitment of monocytes and its differentiation to pro-inflammatory macrophages [39]. These immune cells are characterized by robust expression of inflammatory mediators such as TNF-α, IL-1β and IL-6 among others. This phenotypic switch generates an inflammatory circuit which blocks insulin action and promote insulin resistance, enhancing cellular stress and recruitment of additional immune cells [142] (Figure 7B).

Biochemical pathways are also associated with macrophage polarization. Anti-inflammatory macrophages display high rates of fatty acid oxidation whereas macrophages found in pro-inflammatory microenvironments are related with glycolytic metabolism [143], [144].

A better understanding of the molecular mechanisms underlying macrophage polarization and functional plasticity in vivo should provide useful knowledge for the development of new therapeutic approaches against chronic inflammatory diseases like obesity.

Macrophages: linking immune system and metabolic disease

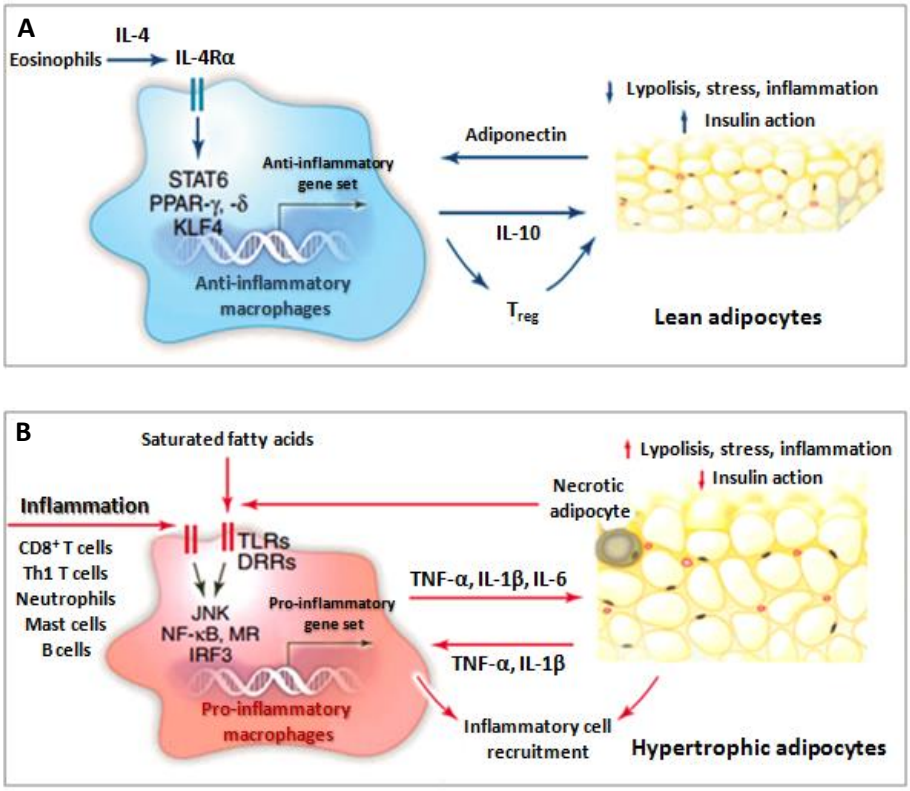

Figure 7. (A) Macrophages in lean adipose tissue are associated with an anti-inflammatory phenotype. These macrophages are characterized by production of IL-10, a tolerogenic cytokine. (B) In obese adipose tissue, the phenotype of macrophages is related with the production of pro-inflammatory cytokines that reinforce the inflammatory milieu. Adapted from *Odegaard J.I.* [9].

HYPOTHESIS & AIMS

Hypothesis

Chronic inflammation underlies the onset and maintenance of numerous human modern diseases. Metabolic diseases induced by high-fat diet represent a socially and clinically relevant example of pathologies where chronic low-grade inflammation plays a triggering role. A better understanding of the pathophysiological mechanisms operating in metabolic diseases should allow the identification of diagnostic and therapeutic biomarkers for these diseases. The development of tools to identify such biomarkers, including the presence of altered metabolites, is also of utmost importance. Therefore, we hypothesized that novel metabolomics approaches allow the identification of candidate biomarkers for metabolic diseases, and tested the validity of the hypothesis by analyzing tissues from mice exposed to either dietary restriction, metformin or both, as treatments to ameliorate metabolic damage. In addition, we have evaluated the hypothesis that macrophages, an immune cell critically involved in the initiation of inflammatory responses, respond to high levels of palmitate by expressing a specific set of genes, some of which might constitute novel diagnostic biomarkers for metabolic diseases.

Aims

- To assess the process of energy generation through the use of a targeted metabolomics method applicable to biological samples from experimental (cell-culture lysates) and clinical (patient plasma) origin, as well as to tissues from mouse models of metabolic disease.

- To determine the effect of metformin on *LDLr* knock-out mice fed with chow diet or high-fat diet, or metformin combined with "diet reversal", through biochemical, histological and metabolomics analysis.

- To define the palmitate-specific polarization state in human macrophages at transcriptomic and functional levels, and to evaluate the ability of palmitate to condition macrophage responses towards other inflammatory stimuli.

RESULTS

STUDY I

Exploring the process of energy generation in pathophysiology by targeted metabolomics: performance of a simple and quantitative method

J. Am. Soc. Mass Spectrom. (2016) 27(1): 168-77

Abstract

Abnormalities in mitochondrial metabolism and regulation of energy balance contribute to human diseases. The consequences of high fat and other nutrient intake, and the resulting acquired mitochondrial dysfunction, are essential to fully understand common disorders, including obesity, cancer, and atherosclerosis. To simultaneously and noninvasively measure and quantify indirect markers of mitochondrial function, we have developed a method based on gas chromatography coupled to quadrupole-time of flight mass spectrometry and an electron ionization interface, and validated the system using plasma from patients with peripheral artery disease, human cancer cells, and mouse tissues. This approach was used to increase sensibility in the measurement of a wide dynamic range and chemical diversity of multiple intermediate metabolites used in energy metabolism. We demonstrate that our targeted metabolomics method allows for quick and accurate identification and quantification of molecules, including the measurement of small yet significant biological changes in experimental samples. The apparently low process variability required for its performance in plasma, cell lysates, and tissues allowed a rapid identification of correlations between interconnected pathways. Our results suggest that delineating the process of energy generation by targeted metabolomics can be a valid surrogate for predicting mitochondrial dysfunction in biological samples. Importantly, when used in plasma, targeted metabolomics should be viewed as a robust and noninvasive source of biomarkers in specific pathophysiological scenarios.

Introduction

Energy metabolism is the process by which nutrients, such as carbohydrates and fats, are broken down to generate adenosine triphosphate (ATP), the main cellular energy store. A state of energy balance is achieved when energy intake matches expenditure. Deviations from this homeostatic regulation can result in obesity, where energy intake exceeds demands. Obesity is a pathologic condition that combines inflammatory and metabolic disturbances, which are the immediate cause and/or consequence of many chronic and lethal diseases, including diabetes, atherosclerosis, and cancer [1]. Some of the excess energy is stored as triglyceride in adipose tissue without deleterious effects, but the capacity to store energy is limited and regulated by poorly understood mechanisms. The subsequent excessive accumulation of lipids and other metabolites in tissues that are not designed to manage this condition (e.g., liver, muscle, and pancreas) commonly ensues in an unhealthy course of metabolic events [2, 3].

Detection and treatment of subclinical metabolic derangements are challenging. The clinical picture is difficult to assess because of the combination of multiple and variable stressors such as inflammation, macrophage recruitment, alterations in muscle function, or the chemical composition of the diet. However, the resulting metabolically-related disorders, each with distinct phenotypes, are united by acquired deficiencies in the mitochondrial function and handling of energy [4]. Whether this association is causal or consequential is a matter of debate. To provide cellular energy, mitochondria use the free energy derived from breakdown of fatty acids and glucose to produce ATP by oxidative phosphorylation. The immediate outcome of deranged energy processing is the reduced ability to switch from one fuel source (e.g., glucose) to another (e.g., fatty acids), resulting in altered flux between glycolytic pathways and oxidative capacity

within cells and tissues. The recognition that mitochondria may play a central role in disease has renewed interest in the Randle cycle and the Warburg effect in the pathogenesis of common diseases [5, 6], and may be relevant because the inefficient use of glucose, lipotoxicity, and decreased fat oxidation are key mechanisms to explain most noncommunicable diseases [7, 8]. Consequently, the pharmacologic modulation of mitochondrial function mimicking the effect of exercise and/or caloric restriction may be an attractive therapeutic strategy [9, 10]. In cell-based models, it is relatively simple to assess mitochondrial dynamics, mitophagy (mitochondrial elimination), and pathways aimed to restore and/or maintain mitochondrial function [11, 12]. Assessment in vivo is considerably more challenging and requires sophisticated analytical platforms and stable isotopes to measure metabolites [13, 14]. We recently demonstrated that mitochondrial dysfunction could be assessed in plasma (i.e., noninvasively) using indirect markers of altered cellular energy metabolism [15].

Contrary to the belief that a high-throughput platform for massive metabolite profiling without accurate quantification of each metabolite is the method of choice to provide useful data, we hypothesized that a targeted approach, avoiding the intensive use of bioinformatics and making available actual changes in the concentration of metabolites under different experimental conditions, would be a valuable addition to current analytical tools. To this end, we have designed a simple and rapid method using advances in the technology of gas chromatography coupled to quadrupole time-of-flight mass spectrometry with an electron impact source (GC-EI-QTOF-MS). The method is sensitive for the accurate and simultaneous measurement of organic acids participating in the citric acid cycle (CAC) and selected metabolites representative of the catabolic and anabolic status of several biological systems. We also reasoned that the quantitative

exploration of mitochondrial function might rapidly identify correlations between related pathways of metabolism, facilitating the understanding of metabolic conditions. Our results support the usefulness of this technique in in vitro and in vivo settings, and ongoing studies point to a potentially valuable role as a recently available methodology in the search for quantitative biomarkers of disease in epidemiologic cohorts and drug targets to restore cellular energy homeostasis [16–18].

Material and methods

Chemicals

Methanol (MS grade), methoxyamine hydrochloride (MA), pyridine, N-methyl-N-(trimethylsilyl)-trifluoroacetamide (TMS) and standards (2-hydroxyglutarate, 3-hydroxybutyrate, 3-phosphoglycerate, 6-phosphogluconate, α-ketoglutarate, acetyl-CoA, aconitate, alanine, aspartic acid, citrate, fructose- 1,6-bisphsophate, fructose-6-phosphate, fumarate, glucose, glucose-6-phosphate, glutamate, glutamine, glyceraldehyde- 3-phosphate, isoleucine, lactate, leucine, malate, malonylcoenzyme A, oxaloacetate, phosphoenolpyruvate, pyruvate, ribose-5-phosphate, serine, succinate, and succinyl-coenzyme A and valine) were purchased from Sigma-Aldrich (St. Louis, MO, USA).

Instrumentation

We used a 7890A gas chromatograph coupled with an electron impact source to a 7200 quadrupole time-of-flight mass spectrometer equipped with a 7693 autosampler module and a J&W Scientific HP-5MS column (30 m × 0.25 mm, 0.25 µm) (Agilent Technologies, Santa Clara, CA, USA). Helium was used as a carrier gas at a flow rate of 1.5 mL/min in constant flow mode. The initial oven temperature was set to 70°C, increased to 190°C at

12°C/min, then raised to 325°C at a rate of 20°C/min and held for 3.25 min. For the MS, ionization was performed using electron impact with a source temperature of 230°C using an electron energy of 70 eV, an emission intensity of 35 µA, and a mass-to-charge range from 70 to 400 *m/z*. The initially selected metabolites to be identified and quantified using this GC-EI-QTOF-MS method are shown in Figure 1, and the selection criteria were based on available knowledge [19].

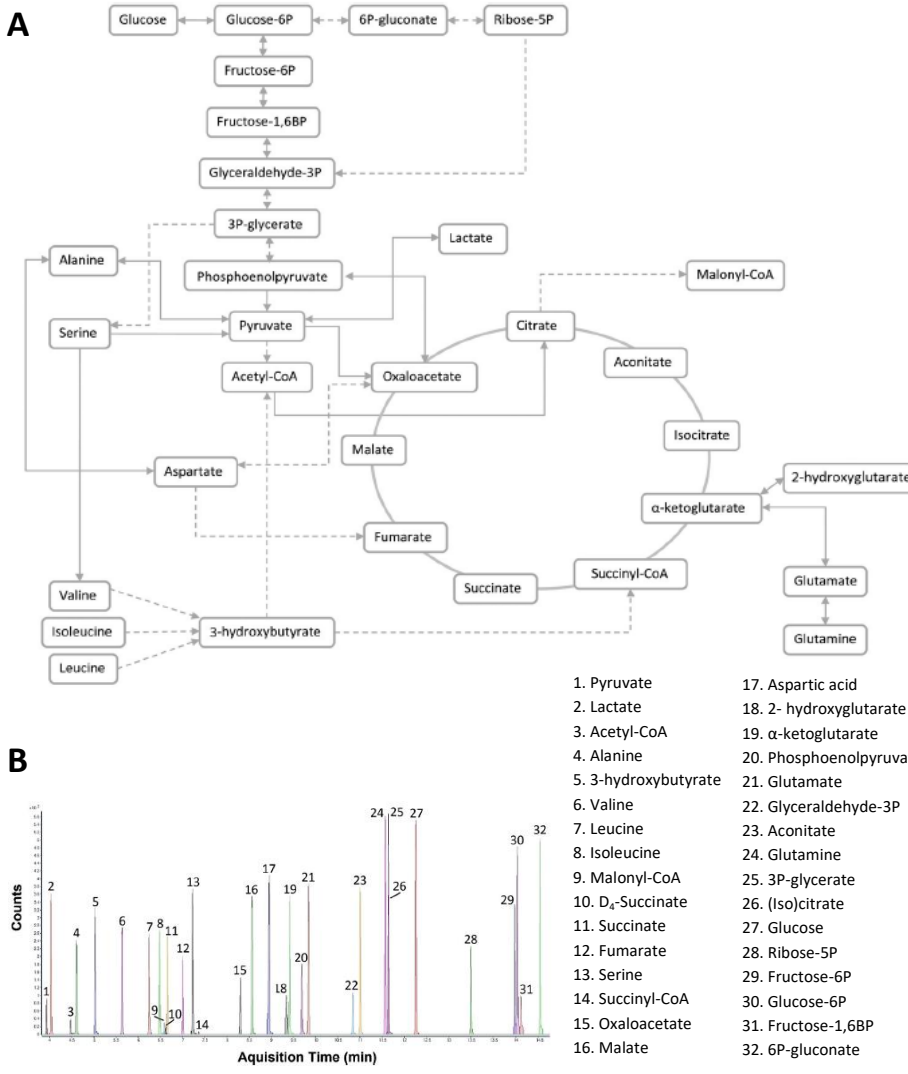

Figure 1. (A) Metabolic pathways of measured metabolites involved in energy metabolism. **(B)** Extracted compound chromatogram (ECC) of the quantifier ion of all metabolites, numbered according to their elution order.

Isolation and Preparation of Biological Samples

To test the analytical performance and robustness of the method in different biological systems, we used human plasma, cell culture lysates, and rodent tissues. The procedures used in humans were performed according to protocols approved by our Ethics Committee and Institutional Review Board, and all participants signed an informed consent (EPINOLS 12-03-29/3proj6). Briefly, these included the recruitment of 50 ostensibly healthy participants, aged between 55 and 65 y with an ankle-brachial index (ABI) >0.9, which were body weight- and age matched with patients presenting intermittent claudication (i.e., peripheral artery disease), ABI <0.9 and staged at grade II according to Fontaine. A sample of blood was drawn from each patient. Participants with diabetes mellitus were excluded to avoid metabolic bias and to limit variability. Further clinical details on the inclusion and exclusion criteria have been previously described [20].

To test the performance of the method in cultured cells, we used MCF10A cells infected with a retroviral $KRAS^{V12}$ expression construct, which were generously provided by the Ben-Ho Park's laboratory and maintained under the previously described culture conditions [21]. Cells were grown to confluence in 6-well plates, then trypsinized and counted (approximately 2×10^6 cells per experiment). We pooled the results obtained in four experiments in triplicate (n = 12). LDL receptor-deficient (*Ldlr*$^{-/-}$) mice develop spontaneous hyperlipidemia and are a useful model for studying atherosclerosis since they present features similar to those observed in the human metabolic syndrome. Mice (C57BL/6J background, The Jackson Laboratory) were housed under standard conditions and given a commercial low-fat mouse diet (14% protein rodent maintenance diet; Harlan, Barcelona, Spain). Male mice were sacrificed at 24 weeks of age following previously described procedures [22] and tissues (liver and epididymal white

adipose tissue; n = 10 samples, each tissue) were extracted. All procedures were carried out in accordance with institutional guidelines (CEIA, 2014-237). To ensure high quality data and reduced false discovery rates, a rigorous optimization of pre-analytical steps prior to chromatography was essential. This may vary between laboratories and experimental conditions but includes sample collection, storage, pretreatment and cleanup, as well as software parameters used in data alignment and peak picking. It is particularly important to minimize the time between sample collection and storage at –80°C to less than 1 h to reduce variability. Of note, this method may be used in the quantification of 13C isotopic substrates (data not shown), indicating its suitability for metabolic flux analysis to define the pattern of carbon flow through a metabolic network in cells and tissues [23].

Metabolite Extraction

We investigated different extraction protocols and found that methanol/water (4/1) extraction was efficient for these metabolites. To minimize complexity in the metabolite extraction, we used methanol/water (4/1) mixed with deuterated D_4-succinic acid as surrogate standard (MeOHW-D_4S) to obtain a final concentration of 1 µg/mL. The choice of a unique surrogate standard was considered sufficient as injection quality control and considerably simplifies the procedure. Further, although this method was designed for targeting metabolomics, during experimentations it is not uncommon to require measurement of additional metabolites in the same samples by nuclear magnetic resonance (NMR) or LC/MS. With these procedures, results did not differ significantly using isotopic compounds as internal standard, and there was no need for solvent exchange as previously described [24–26]. Thawed plasma (100 µL) was added to 900 µL of MeOHW-D_4S, vortexed, placed at –20°C for 2 h to precipitate proteins, and centrifuged at 14,000 rpm for 10 min at 4°C to collect the supernatant. As a

cautionary note, the use of lower amounts of plasma results in the lack of reliable detection of some metabolites present at low concentrations (e.g., acetyl-CoA or oxaloacetate). Cell pellets were resuspended in 500 µL of MeOHWD_4S, lysed with three cycles of freezing and thawing using liquid N2 and sonicated with three cycles of 30 s. Samples were maintained on ice for 1 min between each sonication step. Proteins were precipitated, samples centrifuged, and supernatant collected. Animal tissues (100 mg) were placed in plastic tubes containing 1 mL of MeOHW-D_4S and homogenized using a Precellys 24 system (Izasa, Barcelona, Spain). After centrifugation at 14,000 rpm 10 min at 4°C, supernatant was collected and the homogenization step was repeated. Then proteins were precipitated, samples centrifuged, and supernatant collected. The extraction of nonpolar compounds was performed adding chloroform to have a final proportion of chloroform/methanol (2/1), according to Folch protocol [27]. All supernatants were further vortexed, centrifuged, filtered using 0.22 µm filters, and freeze-dried overnight.

Derivatization

Samples were dried under N_2 and derivatized to rapidly form silyl derivatives. Briefly, in order to protect ketone groups [28], we added 30 µL of methoxylamine hydrochloride dissolved in pyridine [40 mg/mL (0.48 M)] to each sample, which was then incubated for 1.5 h at 37°C with agitation. Then, 45 µL of TMS was added and samples were agitated for 10 min and placed in the dark for 1 h and transferred into a vial before immediate analysis.

Data Analysis

Raw data were processed and compounds were detected and quantified using the Qualitative and Quantitative Analysis B.06.00 software (Agilent

Technologies), respectively. Results were compared by one-way ANOVA with Dunnett's multiple pair-wise comparison tests using a significance threshold of 0.05. Other calculations including comparisons with the U of Mann–Whitney test and/or correlations were made using GraphPad Prism software 6.01 (GraphPad Software, San Diego, CA, USA).

Results and discussion

Method Validation

Calibration curves were obtained for each metabolite by plotting the standard concentration as a function of the peak area. Because the differences in concentration of some metabolites may be highly variable, we required, in some cases, the simultaneous use of different calibration curves covering the expected concentration range for each metabolite. Recovery of each metabolite was calculated and the variation in the percentage of recovery was between 83% and 99%. Ten points of the selected range of all calibration curves were injected and showed linearity with regression coefficients higher than 0.99. The limit of detection (LOD) and quantification (LOQ) for each metabolite were calculated according to International Union of Pure and Applied Chemistry recommendations [29]. Within-day precision or repeatability was calculated injecting each standard on the same day, and between-day repeatability on 5 separate d (n = 5 replicates at three concentration levels) and expressed as relative standard deviation (RSD). Values for each metabolite were considered excellent (RSD from 0.65% to 3.68% and from 1.12 to 4.15%, respectively). Selected and relevant validation parameters are shown in Table 1, and results for other variables may be also examined in Supplemental Table 1.

Table 1. Validation method parameters: regression curve values (slope and intercept), linearity, limit of detection (LOD), limit of quantification (LOQ), intra- and interday % RSD, and recovery (see also Supplemental Table 1).

Metabolite	Slope / intercept	Linearity (R^2)	LOD (µM)	LOQ (µM)	Intraday RSD (%)	Interday RSD (%)	Recovery (%)
2-Hydroxyglutarate	330378 / –64056	0.9991	0.127	0.425	1.12	1.95	91.65
3-Hydroxybutirate	101090 / –15769	0.9976	0.010	0.032	0.65	1.15	96.74
3-Phosphoglycerate	237249 / –2135051	0.9993	0.065	0.215	2.24	3.05	85.65
6-Phospho-gluconate	526980 / –1258050	0.9987 0.9989	0.527	1.758	3.21	3.98	89.35
	87569 / –284587						
α-Ketoglutarate	128155 / 14577	0.9997	0.029	0.098	1.14	2.08	94.99
Acetyl-coenzyme A	10158 / 1785	0.9972	0.610	2.030	1.98	3.01	84.12
Aconitate	749201 / –788502	0.9990	0.010	0.032	2.98	3.65	88.68
Alanine	1987694 / –229517	0.9994	0.288	0.959	1.25	2.34	97.48
Aspartic acid	1715209/ –28378	0.9996	0.835	2.783	0.84	1.25	98.02
(Iso)citrate	1469611 / –271860	0.9996	0.039	0.130	2.54	2.96	93.58
Fructose-1,6-bisphosphate	140842 / –428131	0.9981	0.117	0.389	1.65	2.15	83.26
Fructose-6-phosphate	824733 / –956090	0.9987	0.146	0.487	1.29	1.99	88.69
Fumarate	1119413 / –117375	0.9997	0.040	0.132	0.99	1.34	91.68
Glucose	113676 / –74297	0.9997	0.009	0.029	1.54	2.03	97.35
Glucose-6-phosphate	1040659 / –2961082	0.9990	0.039	0.129	2.14	2.97	96.67
Glutamate	1371976 / –306806	0.9989	0.334	1.114	3.05	4.01	94.31
	284354 / –76489	0.9990					
Glutamine	477954 / –224408	0.9988	0.114	0.380	2.87	3.56	93.11
	957845 / –79154	0.9987					
Glyceraldehyde-3-phosphate	85106 / –44424	0.9979	0.029	0.096	1.32	1.68	87.64
Isoleucine	1652773 / 219943	0.9996	0.108	0.360	0.96	1.42	98.39
Lactate	23667 / 77898	0.9998	0.021	0.070	0.86	1.74	98.96
Leucine	1735828 / 422255	0.9993	0.102	0.340	1.33	1.89	96.84
Malate	336640 / –57888	0.9992	0.113	0.377	0.92	1.12	91.64
Malonyl-coenzyme A	16769 / –359	0.9989	0.039	0.130	2.73	3.06	85.23
Oxaloacetate	70439 / –43811	0.9991	0.590	1.966	3.68	4.15	89.34
Phosphoenolpyruvate	285046 / –222284	0.9981	0.313	1.044	2.38	3.18	92.48
Pyruvate	379309 / 156902	0.9991	0.060	0.200	1.01	1.69	94.67
Ribose-5-phosphate	553740 / –344047	0.9976	0.202	0.675	1.79	2.06	94.58
Serine	1461082 / 11922	0.9999	0.304	1.012	1.14	1.79	97.46
Succinate	176185 / 7109	0.9997	0.077	0.258	0.91	1.35	98.74
Succinyl-coenzyme A	34216 / 5480	0.9998	0.020	0.086	2.06	2.67	87.56
Valine	1836799 / 46946	0.9994	0.098	0.326	1.05	1.68	98.12

Identification and Quantification

The relevant analytical data are summarized in Supplemental Table 2. For some organic acids (3- hydroxybutyrate, fumarate, lactate, oxaloacetate, phosphoenolpyruvate, pyruvate, and succinate) and the internal standard (D_4-succinate), the ion $[M]^+$ was used as qualifier ion and the most abundant ion $[M\text{-}CH3]^+$ resulting from the characteristic loss of a methyl group in TMS after the electron impact, was used as quantifier ion. As shown in Figure 2A, the proposed quantifier ion of acetyl-CoA was observed at *m/z* 219, which is the result of acetate moiety linked to S–C_2H_4–N–TMS from the 4' phosphopantetheine moiety included in the CoA moiety. The subsequent loss of 15 u suggests the loss of a methyl group from the TMS resulting in an ion at *m/z* 204 that was used as qualifier. For malonyl-CoA, the loss of the

TMS from the acid group in malonate moiety linked to $S–C_2H_4–N–TMS$ from the CoA moiety gives a qualifier ion with *m/z* at 262. The presence of other minor ions with a consecutive loss of 16 u (*m/z* 246 and 230) suggest the loss of the TMS group linked to the acid group of the malonate moiety, which can lose two oxygen atoms consecutively. This is followed by the loss of the methoxyl group from the methoxyamine, giving an ion at *m/z* 187. To stabilize this ion, a rearrangement is made through a cyclation between the radicals CH_2• in malonate moiety and the N• linked to the TMS (Figure 2B). A similar reasoning was used to explain the presence in succinyl-CoA of an ion at *m/z* 276 (qualifier) and minor ions at *m/z* 260 and 244. The N– TMS group and the methyl group from the methoxyamine are finally lost, giving a quantifier ion at *m/z* 174. In this case, to stabilize this structure, the CH_2• radical should be linked to the oxygen from the oxyamine group (Figure 2C). Special attention is required in the identification of phosphate compounds (Figure 2D) because they yield three characteristic fragments [30] and retention time is crucial. Quantifier and qualifier ions used to identify phosphate compounds are summarized in Supplemental Table 2. Of note, with this method isocitrate and citrate have the same retention time. In addition, both give a qualifier ion corresponding to the loss of a carboxyl group and the most abundant ion was $[M\text{-}COOTMS\text{-}OTMS]^+$ due to the consecutive loss of an OTMS group from the ion ($[M\text{-}COOTMS]^+$ (Figure 2E). Although the signal for isocitrate using pure standards is significantly less intense, results were expressed as (iso)citrate to denote the lack of chromatographic separation. The quantifier ion for glucose, which is derivatized with five TMS and one MA group (Figure 2F) is $[M\text{-}CH_2\text{-}CH\text{-}NOCH_3\text{-}2OTMS]^+$ (attributable to the loss of the methoxyamine group and the CH where it is linked, an OTMS group and a CH_2-OTMS group), and the subsequent loss of an additional CH-OTMS group results in the qualifier ion $[M\text{-}CH_2\text{-}2CH\text{-}NOCH_3\text{-}3OTMS]^+$ [31]. In contrast, the interpretation for alanine,

valine, leucine, isoleucine, serine, aspartic acid, glutamic acid, malate, and glutamine is simpler because $[M\text{-}CH_3]^+$ is constant (qualifier ion) and $[M\text{-}COOTMS]^+$ is identified as the quantifier ion. $[M\text{-}CH_3]^+$, however, was the qualifier ion and $[M\text{-}COOTMS]^+$ the quantifier ion for 2-hydroxyglutarate. Aconitate also shows $[M\text{-}CH_3]^+$ as qualifier ion after derivatization with three TMS groups. The loss of two TMS groups and a methyl from the third TMS group yields the quantifier ion $[M\text{-}2TMS\text{-}CH_3]^+$. Finally, $[M\text{-}OCH_3]^+$ (loss of the OCH3 from the methoxiamine group) is the qualifier ion for α- ketoglutarate, and the additional loss of an OTMS results in the quantifier ion [M-OCH3-OTMS]+.

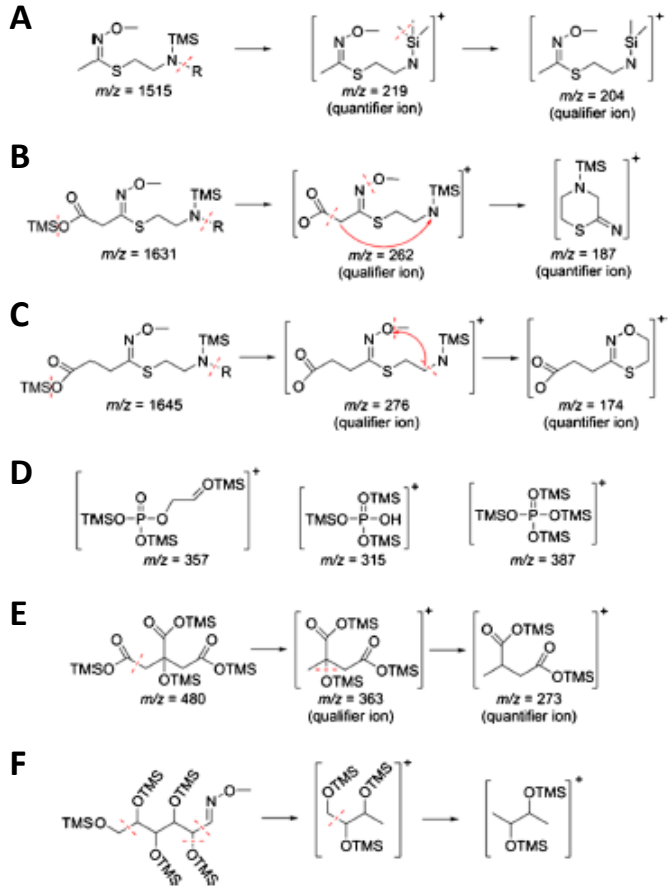

Figure 2. Fragmentation pattern of **(A)** acetyl-CoA, **(B)** malonyl-CoA, **(C)** succinyl-CoA, **(D)** phosphate group, **(E)** (iso)citrate, and **(F)** glucose.

Applications in Biological Samples

In our previous efforts with untargeted metabolomics using LC/MS and GC/MS platforms, we found that comparisons between groups were limited by the lack of accurate quantification [32–34]. Conversely, the use of a nuclear magnetic resonance platform [25, 26] provided excellent reproducibility to quantify certain metabolites but low sensitivity to quantitatively measure the selected metabolites as indirect markers of energy metabolism and mitochondrial function, which included intermediates of glycolysis, the pentose phosphate pathway, branched chain amino acids, and the organic acids of the CAC. We therefore developed the present GC-EI-QTOF-MS analytical platform to measure, after derivatization, these selected compounds, and we found it reliable for use in different biological systems (Tables 2, 3 and 4).

In the first analysis, we compared plasma from healthy controls and patients with stage II peripheral artery disease. Samples injected in triplicate produce RSD values that were similar to those obtained in the precision study. The concentrations of these metabolites have not been previously examined in this condition but metabolites involved in the CAC have been previously suggested as biomarkers of myocardial infarction [35]. Blood was drawn from our patients when they were free of clinical signs of ischemia (i.e., after 1 h of inactivity). Controls with uncompromised circulation in the limb arteries (i.e., ABI > 0.9) had similar cardiovascular risk factors including age, hyperlipidemia, body weight, and current (not past) smoking habit (data not shown). This comparison was designed exclusively for testing analytical performance in plasma and no clinical implications were intended. Nevertheless, the high concentrations of aconitate, isocitrate, malate, α-ketoglutarate, and succinyl-coenzyme A in patients indicate that mitochondrial function is stimulated rather than inhibited (i.e., contrary to

that expected in ischemic conditions) (Table 2). In addition, we found elevated levels of branched chain amino acids, which may also indicate an increased mitochondrial function via their conversion to β-hydroxybutyrate and succinyl-coenzyme A. This may seem paradoxical because elevated levels of branched chain amino acids are usually associated with poor health and cardiovascular disease. One explanation might be the increased endothelial proliferation and accumulation of immune cells resulting in a higher diffusion of these metabolites into the circulation, but may also indirectly point to increased breakdown in the leg muscles [36, 37]. The lack of circulating phosphate compounds was expected considering the hydrophobic nature of the cellular membrane, and it may similarly indicate an absence of significant cellular destruction. Under these conditions, only lactate, which is significantly decreased, may indirectly indicate normal to low glycolytic flux. Also, significant increases of glutamate and glutamine were observed in patients with active atherosclerosis in the limbs, indicating a distinct use of these metabolites in this setting. Our results confirm the validity of our hypothesis with respect to the usefulness of the method to explore the energy metabolism in vivo. These findings may have implications in the search for possible biomarkers and to assess the effectiveness of therapeutic strategies.

Table 2. Metabolite concentrations in plasma (in µM) from selected participants and expressed as mean ± SD. Fold change and significance (P value) are also reported and decimals were set according to the first significant digit of the measured SD.

Metabolite	Plasma control (n = 50)	Plasma PAD (n = 50)	Fold change	*P* value
2-Hydroxyglutarate	9.2 ± 0.4	9.0 ± 0.3	–1.02	N.S.
3-Hydroxybutirate	0.13 ± 0.01	0.31 ± 0.07	2.38	<0.0001
3-Phosphoglycerate	-	-	-	-
6-Phosphogluconate	-	-	-	-
α-Ketoglutarate	3.3 ± 0.2	4.6 ± 0.4	1.39	0.0091
Aconitate	0.52 ± 0.01	4.4 ± 0.9	8.46	<0.0001
Alanine	211 ± 11	203 ± 27	–1.04	N.S.
Aspartic acid	133 ± 3	199 ± 11	1.50	<0.0001
(Iso)citrate	279 ± 13	706 ± 22	2.53	<0.0001
Fructose-1,6-bisphosphate	-	-	-	-
Fructose-6-phosphate	-	-	-	-
Fumarate	0.33 ± 0.02	0.26 ± 0.03	–1.27	<0.0001
Glucose	4856 ± 305	5044 ± 346	1.04	N.S.
Glucose-6-phosphate	N.Q.	N.Q.	-	-
Glutamate	462 ± 366	5197 ± 317	11.25	<0.0001
Glutamine	1115 ± 206	3691 ± 237	3.31	<0.0001
Glyceraldehyde-3-phosphate	-	-	-	-
Isoleucine	49 ± 1	63 ± 2	1.29	<0.0001
Lactate	395 ± 8	359 ± 13	–1.10	0.0323
Leucine	73 ± 2	90 ± 3	1.23	0.0032
Malate	1.57 ± 0.08	3.0 ± 0.3	1.91	<0.0001
Malonyl-coenzyme A	N.Q.	N.Q.	-	-
Oxaloacetate	54 ± 5	N.Q.	-	-
Phosphoenolpyruvate	-	-	-	-
Pyruvate	11 ± 1	10 ± 1	–1.1	0.0270
Ribose-5-phosphate	-	-	-	-
Serine	104 ± 2	145 ± 4	1.39	<0.0001
Succinate	10.7 ± 0.1	12.2 ± 0.4	1.14	N.S.
Succinyl-coenzyme A	6.6 ± 0.9	11.9 ± 0.9	1.80	0.0014
Valine	88 ± 2	105 ± 3	1.19	N.S.

PAD: Peripheral Artery Disease
N.Q.: detected metabolite, but under limit of quantification
N.S.: not significant p-value

We found that the metabolic activity of MCF10A cells engineered to overexpress oncogenic KRAS was significantly higher than MCF10A parental cells under the same culture conditions, strongly suggesting that metabolic reprogramming occurs in breast epithelial cells carrying the constitutively active $KRAS^{V12}$ gene (Table 3). Of note, we were able to detect 2-hydroxyglutarate in MCF10A-$KRAS^{V12}$ cells, which is a product of the mutated isocitrate dehydrogenase and is considered to be an oncometabolite [38]. Further, the increased concentration in some amino acids and indirect markers (ribose-5-phosphate) of metabolic activity in the pentose phosphate pathway were considered as an indication of a higher generation of biomass and endogenous antioxidants in MCF10A-$KRAS^{V12}$ cells to eradicate the reactive oxygen species generated by the accelerated metabolism [39] (Table 3).

Table 3. Metabolite concentration in MCF10A and MCF10A-KRAS^{V12} cells (in µM/mg of protein) expressed as mean ± SD, fold change, and significance (P value). Decimals are reported according to the first significant digit of the measured SD.

Metabolite	MCF10A (n = 12)	MCF10A-KRAS^{V12} (n = 12)	Fold change	*P* value
2-Hydroxyglutarate	-	0.22 ± 0.04	-	-
3-Hydroxybutirate	5.0 ± 0.4	1.78 ± 0.09	–2.81	0.0079
3-Phosphoglycerate	0.28 ± 0.09	36.73 ± 5.13	131.18	<0.0001
6-Phosphogluconate	8.8 ± 1	19.34 ± 2.32	2.20	0.0167
α-Ketoglutarate	0.23 ± 0.08	2.18 ± 0.23	9.48	<0.0001
Aconitate	0.21 ± 0.07	0.14 ± 0.01	–1.50	0.0387
Alanine	65 ± 6	156 ± 21	2.40	0.0067
Aspartic acid	48 ± 6	408 ± 32	8.50	<0.0001
(Iso)citrate	6.3 ± 0.9	5.3 ± 0.6	–1.19	N.S.
Fructose-1,6-bisphosphate	N.Q.	6.4 ± 0.9	-	-
Fructose-6-phosphate	-	N.Q.	-	-
Fumarate	2.4 ± 0.4	10.6 ± 0.6	4.42	<0.0001
Glucose	2.7 ± 0.2	0.22 ± 0.01	–12.27	<0.0001
Glucose-6-phosphate	0.16 ± 0.03	0.64 ± 0.07	4.00	0.0268
Glutamate	10.9 ± 0.6	289 ± 52	26.51	<0.0001
Glutamine	5.8 ± 0.7	5.9 ± 0.7	1.02	N.S.
Glyceraldehyde-3-phosphate	1.6 ± 0.4	1.3 ± 0.4	–1.23	N.S.
Isoleucine	14 ± 2	35 ± 6	2.50	0.0341
Lactate	288 ± 34	812 ± 12	2.82	<0.0001
Leucine	41 ± 8	34 ± 4	–1.21	N.S.
Malate	0.7 ± 0.2	5.0 ± 0.3	7.14	<0.0001
Malonyl-coenzyme A	88 ± 1	40.7 ± 0.6	–2.16	0.0048
Oxaloacetate	-	14 ± 2	-	-
Phosphoenolpyruvate	N.Q.	13 ± 4	-	-
Pyruvate	7 ± 1	94 ± 14	13.43	<0.0001
Ribose-5-phosphate	-	4.9 ± 0.8	-	-
Serine	47 ± 9	48 ± 3	1.02	N.S.
Succinate	12 ± 2	11 ± 2	–1.09	N.S.
Succinyl-coenzyme A	17.3 ± 0.5	31 ± 6	1.79	0.031
Valine	25 ± 2	24 ± 1	–1.04	N.S.

N.Q.: detected metabolite, but under limit of quantification
N.S.: not significant p-value

The increased concentration of glucose-6-phosphate suggests both increased glucose transport and glycolysis, and indeed lactate production was significantly increased in mutated cells with respect to their isogenic controls. The overall results suggest the dependence on glycolysis for growth, indicative of the Warburg effect. Consequently, our analytical method may be used to perform experiments under different glucose environments and to explore the effect of drugs acting on either glucose uptake or mitochondrial functioning. We next wished to determine whether this method could be used to explore energy metabolism in a relevant disease model. The simplest approach to test the functionality of the technique was to isolate tissues from mice with different mitochondrial load and importance in energy production. Thus, we compared the concentration of metabolites in adipose tissue and hepatic tissue and found significant differences in the concentration of measured metabolites (Table 4). Some were immediately expected (e.g., amino acids and CAC intermediates). We

also found that oxaloacetate and phosphoenolpyruvate were barely detectable in adipose tissue, and the concentration of malonyl-CoA was similar in both tissues. No attempt was made to explore the putative metabolic pathways involved (e.g., lipogenesis), but results show that this method can be used to interrogate metabolic alterations related to excessive energy intake, obesity, and the development of associated metabolic dysfunction in the liver (e.g., fatty liver disease).

Table 4. Metabolite concentration in mouse tissue samples (in µM/100 mg of tissue) expressed as mean ± SD. Decimals are reported according to the first significant digit of the measured SD. The number of decimals varies according to the concentration

Metabolite	Liver tissue (n = 10)	Adipose tissue (n = 10)
2-Hydroxyglutarate	19 ± 1	0.87 ± 0.09
3-Hydroxybutirate	0.11 ± 0.01	0.064 ± 0.003
3-Phosphoglycerate	18 ± 3	0.24 ± 0.05
6-Phosphogluconate	38206 ± 1648	297 ± 45
α-Ketoglutarate	5.2 ± 0.6	0.15 ± 0.01
Aconitate	47 ± 3	0.061 ± 0.004
Alanine	1663± 188	63 ± 7
Aspartic acid	4259 ± 128	305 ± 59
(Iso)citrate	425 ± 46	31 ± 8
Fructose-1,6-bisphosphate	12 ± 1	1.7 ± 0.4
Fructose-6-phosphate	1323 ± 110	28 ± 3
Fumarate	26 ± 5	0.25 ± 0.04
Glucose	1802 ± 103	249 ± 21
Glucose-6-phosphate	1302 ± 147	191 ± 17
Glutamate	49043 ± 6746	1889 ± 394
Glutamine	2104 ± 273	532 ± 97
Glyceraldehyde-3-phosphate	16 ± 3	0.11 ± 0.05
Isoleucine	730 ± 74	15 ± 3
Lactate	667 ± 47	59 ± 2
Leucine	1009 ± 104	30 ± 6
Malate	319 ± 49	3.8 ± 0.8
Malonyl-coenzyme A	23 ± 2	22 ± 1
Oxaloacetate	2.3 ± 0.3	N.Q.
Phosphoenolpyruvate	12 ± 2	N.Q.
Pyruvate	5.6 ± 0.5	0.32 ± 0.03
Ribose-5-phosphate	470 ± 82	1.7 ± 0.3
Serine	5531 ± 710	182 ± 18
Succinate	138 ± 19	13.1 ± 0.8
Succinyl-coenzyme A	291 ± 7	7.0 ± 0.9
Valine	460 ± 60	22 ± 3

N.Q.: detected metabolite, but under limit of quantification

Method Limitations

This method requires a derivatization procedure, which increases the time used for sample preparation. It should also be considered that the stability of derivatized compounds is limited to a relatively short period of time (not

more than 24 h). Although most authors consider citric acid as the only compound found at its time of retention, our efforts to distinguish between isomers were unsuccessful. Finally, because of the low ionization of acetyl CoA, the concentration in biological samples is not readily detected using GC-MS. To detect this and other possibly useful important metabolites, other analytical platforms are required. Methods using liquid chromatography-mass spectrometry [40–42] are available and provide an accurate approach.

Conclusion

We have developed a simple analytical method using GC-EI-QTOF-MS to separate, detect, and quantify numerous metabolites involved in energy metabolism, including glycolysis, the CAC, and pathways involved in metabolism of lipids, amino acids, and pentose phosphate. This method delivers an overall assessment of metabolism in biological samples used in preclinical and clinical investigation: namely, cell-culture lysates, mouse models of disease, and patient plasma. We have found that GC-EI-QTOF-MS provides better resolution and reproducibility than other available analytical platforms [43] to accurately quantify multiple metabolites. In particular, the measurement of intermediates involved in mitochondrial metabolism, in all likelihood, represents a major advance in the assessment, in vitro, of mitochondrial dysfunction in cells and tissues. The indirect measurement of these intermediates in plasma should be considered as an alternative to assess the mitochondrial dysfunction in vivo for the clinical management of common metabolic diseases.

References

1. Kotas, M.E., Medzhitov, R.: Homeostasis, inflammation, and disease susceptibility. Cell 160, 816–827 (2015)

2. Chowdhury, R., Warnakula, S., Kunutsor, S., Crowe, F., Ward,H.A., Johnson, L., Franco, O.H., Butterworth, A.S., Forouhi, N.G., Thompson, S.G., Khaw, K.T.,Mozaffarian, D., Danesh, J., Di Angelantonio, E.: Association of dietary, circulating, and supplement fatty acids with coronary risk: a systematic review and meta-analysis. Ann. Intern. Med. 160, 398–406 (2014)

3. Masoodi, M., Kuda, O., Rossmeisl, M., Flachs, P., Kopecky, J.: Lipid signaling in adipose tissue: connecting inflammation and metabolism. Biochim. Biophys. Acta. 1851, 503–518 (2015)

4. Rull, A., Camps, J., Alonso-Villaverde, C., Joven, J.: Insulin resistance, inflammation, and obesity: role of monocyte chemoattractant protein-1 (or CCL2) in the regulation of metabolism. Mediat. Inflamm. 2010, Article ID 326580 (2010)

5. Menendez, J.A., Alarcon, T., Joven, J.: Gerometabolites: the pseudohypoxic aging side of cancer oncometabolites. Cell Cycle 13, 699–709 (2014)

6. Menendez, J.A., Joven, J., Cufi, S., Corominas-Faja, B., Oliveras-Ferraros, C., Cuyas, E., Martin-Castillo, B., López-Bonet, E., Alarcón, T., Vazquez-Martin, A.: The Warburg effect version 2.0: metabolic reprogramming of cancer stem cells. Cell Cycle 12, 1166–1179 (2013)

7. Patergnani, S., Pinton, P.: Mitophagy and mitochondrial balance. Methods Mol. Biol. 1241, 181–194 (2015)

8. Peti-Peterdi, J.: Mitochondrial TCA cycle intermediates regulate body fluid and acid-base balance. J. Clin. Invest. 123, 2788–2790 (2013)

9. Phielix, E., Meex, R., Moonen-Kornips, E., Hesselink, M.K., Schrauwen, P.: Exercise training increases mitochondrial content and ex vivo mitochondrial function similarly in patients with type 2 diabetes and in control individuals. Diabetologia 53, 1714–1721 (2010)

10. Szeto, H.H., James, L.P., Atkinson, A.J.: Mitochondrial pharmacology: its future is now. Clin. Pharmacol. Ther. 96, 629–633 (2014)

11. Divakaruni, A.S., Rogers, G.W., Murphy, A.N.: Measuring mitochondrial function in permeabilized cells using the Seahorse XF analyzer or a Clarktype oxygen electrode. Curr. Protoc. Toxicol. 60, 25.22.21–25.22.16 (2014)

12. Phelan, J.J., MacCarthy, F., Feighery, R., O'Farrell, N.J., Lynam-Lennon, N., Doyle, B., O'Toole, D., Ravi, N., Reynolds, J.V., O'Sullivan, J.: Differential expression of mitochondrial energy metabolism profiles across the metaplasia-dysplasia-adenocarcinoma disease sequence in Barrett's oesophagus. Cancer Lett. 354, 122–131 (2014)

13. Abdurrachim, D., Ciapaite, J., Wessels, B., Nabben, M., Luiken, J.J., Nicolay, K., Prompers, J.J.: Cardiac diastolic dysfunction in high-fat diet fed mice is associated with lipotoxicity without impairment of cardiac energetics in vivo. Biochim. Biophys. Acta. 1842, 1525–1537 (2014)

14. Prompers, J.J., Wessels, B., Kemp, G.J., Nicolay, K.: Mitochondria: investigation of in vivo muscle mitochondrial function by 31P magnetic resonance spectroscopy. Int. J. Biochem. Cell. Biol. 50, 67–72 (2014)

15. Rodriguez-Gallego, E., Guirro, M., Riera-Borrull, M., Hernandez-Aguilera, A., Marine-Casado, R., Fernandez-Arroyo, S., Beltrán-Debón, R., Sabench, F., Hernández, M., del Castillo, D., Menendez, J.A., Camps, J., Ras, R., Arola, L., Joven, J.: Mapping of the circulating metabolome reveals alpha-ketoglutarate as a predictor of morbid obesity-associated nonalcoholic fatty liver disease. Int. J. Obes. 39, 279–287 (2015)

16. Floegel, A., Stefan, N., Yu, Z., Muhlenbruch, K., Drogan, D., Joost, H.G., Fritsche, A., Häring, H.U., Hrabě de Angelis, M., Peters, A., Roden, M., Prehn, C., Wang-Sattler, R., Illig, T., Schulze, M.B., Adamski, J., Boeing, H., Pischon, T.: Identification of serum metabolites associated with risk of type 2 diabetes using a targeted metabolomic approach. Diabetes 62, 639– 648 (2013)

17. Inouye, M., Kettunen, J., Soininen, P., Silander, K., Ripatti, S., Kumpula, L.S., Hämäläinen, E., Jousilahti, P.,Kangas, A.J., Männistö, S., Savolainen, M.J., Jula, A., Leiviskä, J., Palotie, A., Salomaa, V., Perola, M., Ala-Korpela, M., Peltonen, L.: Metabonomic, transcriptomic, and genomic variation of a population cohort. Mol. Syst. Biol. 6, 441 (2010)

18. Shah, S.H., Kraus, W.E., Newgard, C.B.: Metabolomic profiling for the identification of novel biomarkers and mechanisms related to common cardiovascular diseases: form and function. Circulation 126, 1110–1120 (2012)

19. Shin, S.Y., Fauman, E.B., Petersen, A.K., Krumsiek, J., Santos, R., Huang, J., Arnold, M., Erte, I., Forgetta, V., Yang, T.P., Walter, K., Menni, C., Chen, L., Vasquez, L., Valdes, A.M., Hyde, C.L., Wang, V., Ziemek, D., Roberts, P., Xi, L., Grundberg, E.: Multiple TissueHuman Expression Resource (MuTHER) Consortium, Waldenberger, M., Richards, J.B., Mohney, R.P., Milburn, M.V., John, S.L.,Trimmer, J., Theis, F.J., Overington, J.P., Suhre, K., Brosnan, M.J., Gieger, C., Kastenmüller, G., Spector, T.D., Soranzo, N.: An atlas of genetic influences on human blood metabolites. Nat. Genet. 46, 543–550 (2014)

20. Rull, A., Hernandez-Aguilera, A., Fibla, M., Sepulveda, J., Rodriguez-Gallego, E., Riera-Borrull, M., Sirvent, J.J., Martín-Paredero, V., Menendez, J.A., Camps, J., Joven, J.: Understanding the role of circulating chemokine (C C motif) ligand 2 in patients with chronic ischemia threatening the lower extremities. Vasc. Med. 19, 442–451 (2014)

21. Konishi, H., Karakas, B., Abukhdeir, A.M., Lauring, J., Gustin, J.P., Garay, J.P., Konishi, Y., Gallmeier, E., Bachman, K.E., Park, B.H.: Knock-in of mutant K-ras in nontumorigenic human epithelial cells as a new model for studying K-ras mediated transformation. Cancer Res. 67, 8460–8467 (2007)

22. Joven, J., Rull, A., Ferre, N., Escola-Gil, J.C., Marsillach, J., Coll, B., Alonso-Villaverde, C., Aragones, G., Claria, J., Camps, J.: The results in rodent models of atherosclerosis are not interchangeable: the influence of diet and strain. Atherosclerosis 195, e85–e92 (2007)

23. Sauer, U.: Metabolic networks in motion: 13C-based flux analysis. Mol. Syst. Biol. 2, 62 (2006)

24. Beltran, A., Suarez, M., Rodriguez, M.A., Vinaixa, M., Samino, S., Arola, L., Correig, X., Yanes, O.: Assessment of compatibility between extraction methods for NMR- and LC/MS-based metabolomics. Anal. Chem. 84, 5838–5844 (2012)

25. Rull, A., Vinaixa, M., Angel Rodriguez, M., Beltran, R., Brezmes, J., Canellas, N., Correig, X., Joven, J.: Metabolic phenotyping of genetically modified mice: an NMR metabonomic approach. Biochimie. 91, 1053–1057 (2009)

26. Vinaixa, M., Rodriguez,M.A., Rull, A., Beltran, R., Blade, C., Brezmes, J., Correig, X., Joven, J.: Metabolomic assessment of the effect of dietary cholesterol in the progressive development of fatty liver disease. J. Proteome. Res. 9, 2527–2538 (2010)

27. Folch, J., Lees,M., Sloane Stanley, G.H.: A simple method for the isolation and purification of total lipides from animal tissues. J. Biol. Chem. 226, 497 -509 (1957)

28. Yang, L.,Kombu, R.S.,Kasumov, T., Zhu, S.H., Cendrowski,A.V.,David, F.: Metabolomic and mass isotopomer analysis of liver gluconeogenesis and citric acid cycle. I. Interrelation between gluconeogenesis and cataplerosis; formation of methoxamates from aminooxyacetate and ketoacids. J. Biol. Chem. 283, 21978–21987 (2008)

29. Currie, L.A.: Nomenclature in evaluation of analytical methods including detection and quantification capabilities (IUPAC Recommendations 1995). Anal. Chim. Acta. 391, 105–126 (1999)

30. Wegner, A., Weindl, D., Jager, C., Sapcariu, S.C., Dong, X., Stephanopoulos, G., Hiller, K.: Fragment formula calculator (FFC): determination of chemical formulas for fragment ions in mass spectrometric data. Anal. Chem. 86, 2221–2228 (2014)

31. Sakamoto, Y., Nakagawa, K., Miyagawa, H., Kawana, S., Fukumoto, S.: Quantitative analysis of stable isotopes of glucose in blood plasma using quadrupole GC-MS. Shimadzu Corporation, GC-MS technical repport No. 2 (2010)

32. Garcia-Heredia, A., Kensicki, E., Mohney, R.P., Rull, A., Triguero, I., Marsillach, J., Tormos, C., Mackness, B., Mackness, M., Shih, D.M., Pedro-Botet, J., Joven, J., Sáez, G., Camps, J.: Paraoxonase-1 deficiency is associated with severe liver steatosis in mice fed a high-fat high-cholesterol diet: a metabolomic approach. J. Proteome. Res. 12, 1946–1955 (2013)

33. Holvoet, P., Rull, A., Garcia-Heredia, A., Lopez-Sanroma, S., Geeraert, B., Joven, J., Camps, J.: Stevia-derived compounds attenuate the toxic effects of ectopic lipid accumulation in the liver of obese mice: a transcriptomic and metabolomic study. Food Chem. Toxicol. 77, 22–33 (2015)

34. Rull, A., Geeraert, B., Aragones, G., Beltran-Debon, R., Rodriguez-Gallego, E., Garcia-Heredia, A., Pedro-Botet, J., Joven, J., Holvoet, P., Camps, J.: Rosiglitazone and fenofibrate exacerbate liver steatosis in a mouse model of obesity and hyperlipidemia. A transcriptomic and metabolomic study. J. Proteome. Res. 13, 1731–1743 (2014)

35. Yao, H., Shi, P., Zhang, L., Fan, X., Shao, Q., Cheng, Y.: Untargeted metabolic profiling reveals potential biomarkers in myocardial infarction and its application. Mol. Biosyst. 6, 1061–1070 (2010)

36. Greenhaff, P.L., Karagounis, L.G., Peirce, N., Simpson, E.J., Hazell, M., Layfield, R., Wackerhage, H., Smith, K., Atherton, P., Selby, A., Rennie, M.J.: Disassociation between the effects of amino acids and insulin on signaling, ubiquitin ligases, and protein turnover in human muscle. Am. J. Physiol. Endocrinol. Metab. 295, E595–E604 (2008)

37. Suhre, K., Meisinger, C., Doring, A., Altmaier, E., Belcredi, P., Gieger, C., Chang, D., Milburn, M.V., Gall, W.E., Weinberger, K.M., Mewes, H.W., Hrabé de Angelis,M., Wichmann, H.E., Kronenberg, F., Adamski, J., Illig, T.: Metabolic footprint of diabetes: a multiplatform metabolomics study in an epidemiological setting. PLoS ONE 5, e13953 (2010)

38. Krell, D., Mulholland, P., Frampton, A.E., Krell, J., Stebbing, J., Bardella, C.: IDH mutations in tumorigenesis and their potential role as novel therapeutic targets. Future Oncol. 9, 1923–1935 (2013)

39. Chen, X., Qian, Y., Wu, S.: The Warburg effect: evolving interpretations of an established concept. Free Radic. Biol. Med. 79, 253–263 (2015)

40. Armando, J.W., Boghigian, B.A., Pfeifer, B.A.: LC-MS/MS quantification of short-chain acyl-CoA's in Escherichia coli demonstrates versatile propionyl CoA synthetase substrate specificity. Lett. Appl. Microbiol. 54, 140–148 (2012)

41. Gilibili, R.R., Kandaswamy, M., Sharma, K., Giri, S., Rajagopal, S., Mullangi, R.: Development and validation of a highly sensitive LC-MS/MS method for simultaneous quantitation of acetyl-CoA and malonyl-CoA in animal tissues. Biomed. Chromatogr. 25, 1352–1359 (2011)

42. Hayashi, O., Satoh, K.: Determination of acetyl-CoA and malonyl-CoA in germinating rice seeds using the LC-MS/MS technique. Biosci. Biotechnol. Biochem. 70, 2676–2681 (2006)

43. Lei, Z., Huhman, D.V., Sumner, L.W.: Mass spectrometry strategies in metabolomics. J. Biol. Chem. 286, 25435–25442 (2011)

STUDY II

Metformin potentiates the benefits of dietary restraint: a metabolomic study

Nutrients, 2017

Abstract

Identification of therapeutic approaches to protect against the metabolic consequences of chronic energy-dense/high-fat diet (HFD) remains a public health priority because associated diseases are the leading causes of death worldwide. Here, we evaluated whether metformin could protect against HFD-induced metabolic disturbances in low-density lipoprotein receptor-knockout mice. Once rendered obese, glucose-intolerant and hyperlipidemic, mice were switched to diet reversal with or without metformin to explore how proinflammatory and metabolic changes respond. Metabolic phenotypes were evaluated by integrating biochemical, histological, and metabolomic components closely related to the multi-faceted metabolic disturbances provoked by HFD. Metformin combined with diet reversal promoted a more effective weight loss along with better glucose control, notably lowered levels of circulating cholesterol and triglycerides, and moderately reduced adipose tissue content. Moreover, mice treated with metformin showed a dramatically improved protection against HFD-induced hepatic steatosis, a beneficial effect that was accompanied by a lowering of liver-infiltrating proinflammatory macrophages and lower release of proinflammatory cytokines. The ability of metformin to target the contribution of branched chain amino acids to adipose tissue metabolism while suppressing mitochondrial-dependent biosynthesis in hepatic tissue might contribute to the additional beneficial effects elicited beyond those of dietary restriction alone. Our findings underscore how the adipose tissue and liver crosstalk provides clinical potential for combining metformin and dietary modifications as a therapeutic maneuver to protect against the metabolic damage occurring upon excessive dietary fat intake.

Introduction

Contemporary high-energy and high-fat poor quality diets coupled with the effect of sedentary lifestyles are closely related to the convergent epidemics of obesity, insulin resistance; type 2 diabetes (T2D) and non-alcoholic fatty liver disease (NAFLD). These metabolic comorbidities foster patterns of functional decline and major chronic diseases that compromise health span and quality of life [1]. Therefore, to identify therapeutic options aimed to protect against dietary-induced, multifaceted metabolic damage is a clinical priority. Lifestyle modification approaches are commonly indicated to manage the vicious cycle of metabolic damage triggered by energy-dense/high-fat diets (HFD) but the efficacy is seriously hampered by relatively unknown cellular metabolic strategies and compensatory pathways induced by reducing fat intake or taking regular exercise [2, 3]. The typical diets in industrialized countries and calorie (energy) restriction (CR) would be expected to exert the opposite effect by operating as extreme ends of the same disease-health metabolic spectrum. However, the adoption of a CR-like lifestyle seems impractical outside of research settings [4, 5]. An alternative strategy might combine lifestyle modification with pharmacotherapy, and in this context efficacy is likely for adenosine monophosphate-activated protein kinase (AMPK) activators [6].

The biguanide metformin, a first-line diabetes drug, has been repeatedly suggested to promote long-term programming of metabolic health with little or no toxicological significance [7-10] and may take new routes (i.e., to treat patients without diabetes) to clinical usefulness [11, 12] with the potential to differentially affect medical outcomes [13-17]. Despite the growing evidence demonstrating the multiple protective effects of metformin against metabolic diseases, the combined effects of diet planning along with metformin have been scarcely investigated. For example, the combination of

metformin and a 70% restriction in calories yielded superior results than either treatment alone in diabetic rats [18] and metformin alone improved liver damage without modifying adipose tissue in HFD-fed C57BL6/J mice [19]. Using a metabolomic approach, we tested the hypothesis that concomitant metformin and simple diet reversal treatment could ameliorate HFD-induced disturbances in energy metabolism. We performed an integrated analysis of the metabolic phenotypes occurring upon feeding experimental diets with or without metformin treatment in low-density lipoprotein receptor-deficient mice (*Ldlr* $^{-/-}$). We have previously shown that this is a robust model to assess the effect of nutrition in a context of subclinical chronic inflammation, which reproducibly measure objective and quantifiable metabolic characteristics, and includes hyperlipidemia without the confounding effects of diabetes [20, 21]. We provide evidence that switching to normal diet in combination with metformin can significantly alleviate the metabolic disturbances provoked by previous HFD.

Material and methods

Animals and animal care

Male *Ldlr*$^{-/-}$ mice in a C57BL/6 genetic background were obtained by breeding animals purchased from Jackson Laboratory (Bar Harbor, ME, USA) and maintained under controlled temperature (22ºC), humidity (50%) and lighting (12h-12h light-dark cycle). To prevent sex-dependent variability, female animals were not included [18]. Mice had ad libitum access to water and control breeder chow diet (CD; crude fat 3.1% and 71.8% available carbohydrate) prepared by Scientific Animal Food & Engineering, Augy, France, until the experiments began at 10 weeks of age. All procedures were performed by dedicated staff in accordance with current regulations and

supervision by the Ethics Committee on Animal Experimentation of the Universitat Rovira i Virgili following European guidelines (Directive 2010/63/EU). Diets were chosen to examine relevant differences. In CD, calories (3.3 Kcal/g) were from protein (19%), fat (roughly 9%) and carbohydrates (72%). In the high-fat diet (HFD), Ssnif Spezialdiäten (Soest, Germany), calories (5.7 Kcal/g) were from protein (19%), fat (roughly 60%) and carbohydrates (21%).

Experimental design

We explored the metformin response in mice fed with either the original CD or HFD for 14 weeks. The animals were allocated to experimental groups using computer-generated randomization schedules and the investigators responsible for the assessment of outcomes had no knowledge of the experimental group to which the animals belonged. No animals were excluded from the analysis. First, mice were allocated into two dietary groups (n=16, each) and further divided in mice receiving metformin (Sigma, Madrid, Spain) or placebo (Monteloeder, Elche, Spain) daily (n=8, each) (Fig 1A). Mice were sacrificed at 24 weeks using isoflurane inhalation. The route of administration and dose of metformin was designed after confirming that metformin does not accumulate in plasma after repeated administration and that the mean plasma concentration in mice was similar to that obtained in humans with a dose of 1.25 g/day as described [22]. Hence, we used metformin dissolved in drinking water (5 mg/mL) to provide 250 mg/Kg/day in concordance with previously published data [23, 24]. We then examined in parallel experiments the metformin response in mice with adverse inflammatory and metabolic status established through feeding animals with HFD for 6 weeks. Some animals (n=6) were sacrificed at this time for comparative analysis. Other littermates were then fed with HFD or CD for other 8 weeks. Those mice fed with CD were divided to receive metformin or

placebo (n=8, each) as stated above (Fig 1B). Mice were sacrificed at 24 weeks after a similar fasting time (4 hours with a maximum difference of 15 min).

Sample collection and analytical methods

Glucose tolerance tests (GTT) were performed in all animals one week before their sacrifice by injecting intraperitoneally glucose in saline solution (2 mg/g of body weight) after 4 hours of fasting. Blood was drawn from the tail to measure glucose levels (Roche Diagnostics, Basel, Switzerland), 0, 15, 30, 60 and 120 min after the injection. Blood samples were also collected from anesthetized animals into EDTA treated blood collection tubes during sacrifice and immediately centrifuged and stored at -80ºC until analysis. There were no detectable iatrogenic experimental variables. Plasma concentrations of glucose, cholesterol, triglycerides and liver enzymes were measured by standard assays in an automated analyzer Synchron LXi 725 (Beckman Coulter, IZASA, Barcelona, Spain). Plasma lipoproteins were separated by fast-performance liquid chromatography (FPLC) using a Bio-Rad Bio Logic Duo Flow 10 system (Bio-Rad, Alcobendas, Spain). Serum pooled samples from each group (200 µl) were injected into a Superose 6 /300 GL column (GE Healthcare Europe GmbH, Munich, Germany), and 500 µl fractions were collected. Cholesterol and triglycerides concentrations were analyzed in each fraction as reported [17]. Organs were perfused in phosphate buffered saline and tissue samples removed and fixed for 24h in 10% neutral-buffered formalin for histology.

Histological analysis

Paraffin-embedded tissues were stained with hematoxylin and eosin (H&E). The extent of steatosis in the liver and adipocyte size of epididymal white adipose tissue (eWAT) were estimated by image analysis software (AnalySIS,

Soft Imaging System, Munster, Germany) and the hepatic proportion of macrophages (anti F4/80, Serotec, Oxford, UK) was determined by immunohistochemistry essentially as described [25, 26].

Cytokines measurements

Liver samples were homogenized using a Precellys 24 homogenizer (Bertin Technologies, Toulouse, France) in lysis buffer containing protease inhibitors at a concentration of 250 µg/mL. The levels of interleukin (IL)-1β, IL-2, IL-6, IL-10, interferon-γ, chemokine (C-C motif) ligand 2 (CCL2), and tumor necrosis factor-α (TNF- α) were measured in the homogenates following the manufacturer's instructions using Bio-plexProTM magnetic bead-based assays (Bio-Rad, Madrid, Spain) on the Luminex platform (Bio-Rad).

Targeted metabolomics

The list of metabolites of major pathways related to energy metabolism was designed with the rationale that cells must allocate nutrients toward boosting glycolysis, and to generate ATP and intermediates for macromolecule biosynthesis. Metabolites were quantitatively measured as described [21]. Briefly, metabolites in liver (50 mg) and epididymal white adipose tissue (eWAT; 100 mg) were extracted in 1 mL of methanol/water (8:2) using a Precellys 24 system (Izasa, Barcelona, Spain). After centrifugation at 14,000 rpm 10 min at 4°C, supernatants were collected and the homogenization step repeated. Nonpolar compounds were further extracted in chloroform/methanol (2:1). All supernatants were centrifuged, filtered using 0.22 µm filters, and freeze-dried overnight. Samples were dried under N2, derivatized using methoxyamine dissolved in pyridine (40 mg/mL) and N-methyl-N-(trimethylsilyl)-trifluoroacetamide and injected into a 7890A gas chromatograph coupled with an electron impact source to a 7200 quadrupole time-of-flight mass spectrometer (MS) equipped with a 7693

auto-sampler module and a J&W Scientific HP-5MS column (30 m × 0.25 mm, 0.25 µm) (Agilent Technologies, Santa Clara, CA, USA). We measured 31 metabolites in related pathways, including the pentose-phosphate, glycolysis and gluconeogenesis, citric acid cycle (CAC) and metabolism of amino acids (see Figures). Values in eWAT homogenates were lower than in liver and malonyl-CoA and succinyl-CoA were not considered because, although detected, they were under the limit of quantification using these conditions.

Statistical analyses

All results are shown as the mean ± SD unless otherwise stated. Differences between groups were assessed with the Mann-Withney *U* test (nonparametric) and considered statistically significant when $P < 0.05$. Some comparisons required one-way ANOVA. All statistical analyses were carried out using the GraphPad Prism 6.0 Software, Inc (USA). For the metabolomic analysis, the obtained raw data were processed and compounds were detected and quantified using the Qualitative and Quantitative Analysis B.06.00 software (Agilent Technologies). Results were compared by one-way ANOVA with Dunnett's multiple pair-wise comparison tests using a significance threshold of 0.05. MetaboAnalyst 3.0, available on the web (http://www.metaboanalyst.ca/) was used to generate meaningful scores/loading plots [27].

Results

Effects on the regulation of body weight and food intake

Predictably, mice in the HFD group gained weight quicker than CD littermates. Whereas metformin treatment had no effect on body weight regulation in mice challenged with HFD, it led to a significant reduction in body weight gain in mice on CD from the fourth week until the end of the

follow-up (24 weeks) (Figure 1A). Body weight gain of HFD-fed mice decreased immediately after switching to CD. Remarkably, administration of metformin was significantly more effective than CD alone in reducing body weight gain, particularly after 6–7 weeks of diet reversal when mice fed CD alone began to regain lost body weight (Figure 1B). Mice on HFD exhibited decreased food intake relative to CD-fed mice; however, the total caloric intake by body weight was similar in both groups when considering the food energy density in the diets. Metformin treatment had no effect on food consumption between groups (Figure 2A, B).

Effects on glucose homeostasis

Fasting serum glucose levels were significantly higher in the HFD group than in the CD group. To assess in more detail the impact of chronic HFD exposure on glucose homeostasis, both groups were subjected to a glucose tolerance test (GTT). Intraperitoneally injected glucose resulted in a more rapid increase of blood glucose in the HFD group than in the CD group, indicating the development of HFD-induced systemic glucose intolerance. The effect of metformin administration on plasma glucose levels and glucose tolerance was negligible in CD and HFD groups. We then re-evaluated glucose homeostasis in HFD-fed mice subjected to diet reversal with or without metformin treatment. Diet reversal and metformin were similarly effective in reducing the HFD-provoked increase in plasma glucose. Of note, although peak values of blood glucose levels were similar for diet reversal alone and with metformin in the GTT, animals treated with metformin exhibited faster glucose clearance (Figure 2C-F).

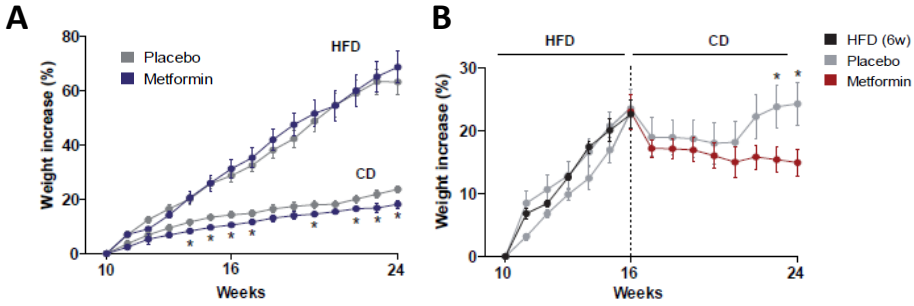

Figure 1. Dietary-induced changes and the effect of metformin on weight control. Overall design in experimental animals. **(A)** Values obtained in mice upon feeding with experimental diets for 14 weeks. CD, chow diet; HFD, high-fat diet. **(B)** Values obtained after a 6 weeks period of HFD feeding and shift to CD. Asterisks denote significant (P < 0.05) changes compared to the respective group.

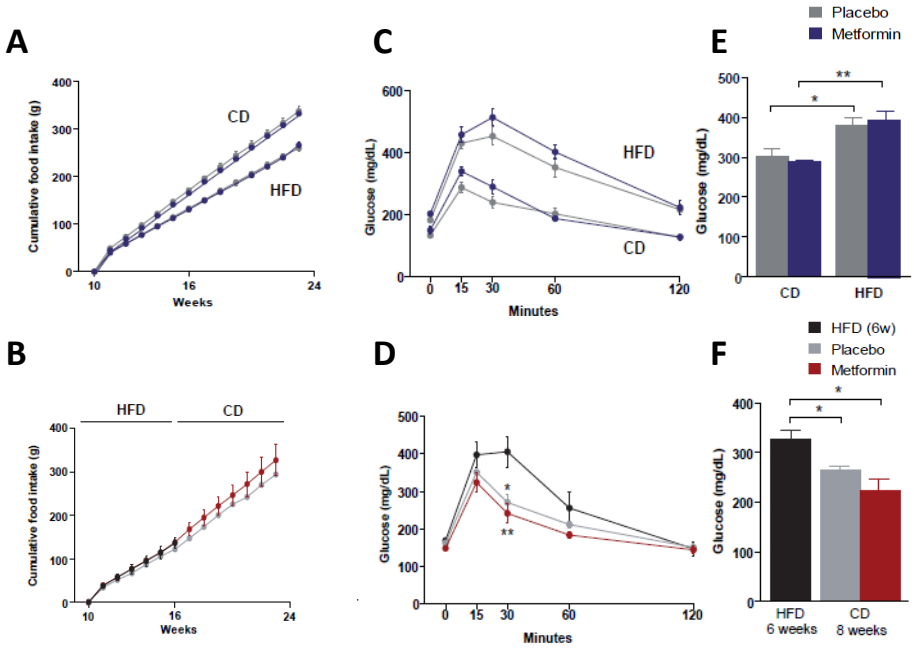

Figure 2. Dietary-induced changes and the effect of metformin on food intake and glucose homeostasis. (A, B) Cumulative food intake, **(C, D)** glucose tolerance tests, and **(E, F)** plasma glucose levels segregated by the type of dietary experiment and use of metformin as indicated. Asterisks denote significant ($^{*}P$ < 0.05; $^{**}P$ < 0.01) changes.

Effects on hyperlipidemia

Plasma levels of cholesterol and triglycerides were significantly higher in the HFD group than in the CD group (Figure 3A). Metformin treatment resulted in a significant reduction in the concentration of total serum cholesterol and of dense LDL-cholesterol in CD-fed animals (Figure 3A, B). Metformin-induced changes to LDL levels in CD-fed mice were accompanied by a significant decrease in serum triglyceride concentrations and of triglycerides in the LDL fraction (Figure 3 A, B). Diet reversal to CD abolished the increase in circulating cholesterol promoted by HFD feeding (Figure 3C). Indeed, lipoprotein distribution in mice subjected to diet reversal with or without metformin largely resembled that commonly observed in wild-type animals (i.e., almost all cholesterol in the HDL fraction) (Figure 3D). Remarkably, administration of metformin promoted a further reduction in the circulating levels of cholesterol in diet-switched mice and also a statistically significant reduction in serum triglyceride concentration (Figure 3C).

Effects on white adipose tissue

Given the changes to triglyceride levels between CD and HFD groups, we next questioned how metformin might impact eWAT content. Morphometric analysis of visceral/eWAT depots revealed that average adipocyte size in HFD-fed mice was significantly greater than that found in CD-fed mice (Figure 4A, B). Metformin administration significantly decreased adipocyte size and also the relative weight of the eWAT depot in CD-fed mice (Figure 4A, B). By contrast, metformin treatment further increased adipocyte size and also the relative weight of WAT in HFD-fed animals (Figure 4A, B). Whereas metformin treatment augmented the loss of the WAT depot in animals subjected to diet reversal and led to a significant decrease in adipocyte size, the average size of adipocytes remained larger than in those from animals treated with diet reversal alone (Figure 4C, D).

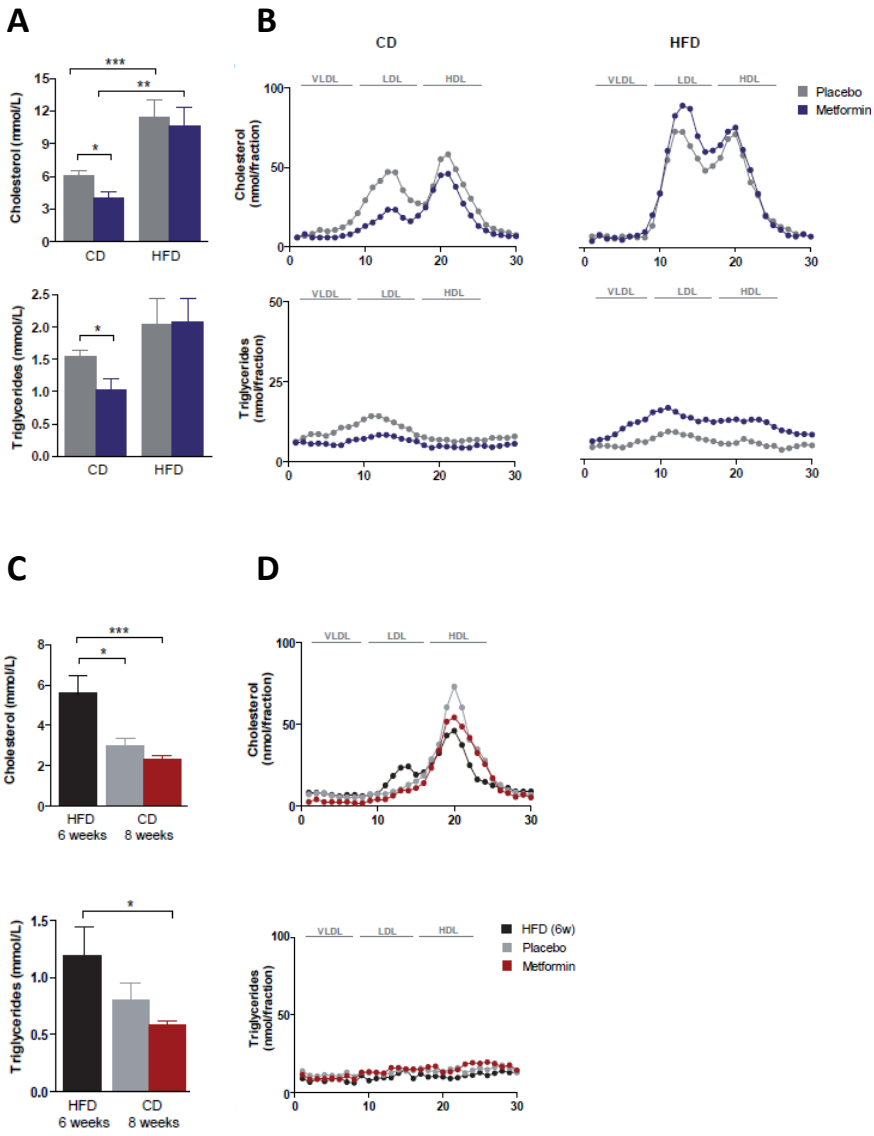

Figure 3. Dietary-induced changes and the effect of metformin on plasma lipids and lipoprotein distribution. (A) Plasma lipids and **(B)** lipoprotein distribution as measured with fast-performance liquid chromatography in mice upon feeding with experimental diets for 14 weeks. CD, chow diet; HFD, high-fat diet. **(C, D)** Same measurements in mice after diet reversal with or without metformin. Asterisks denote significant ($^{*}P < 0.05$; $^{**}P < 0.01$; $^{***}P < 0.001$) changes as indicated.

Study II

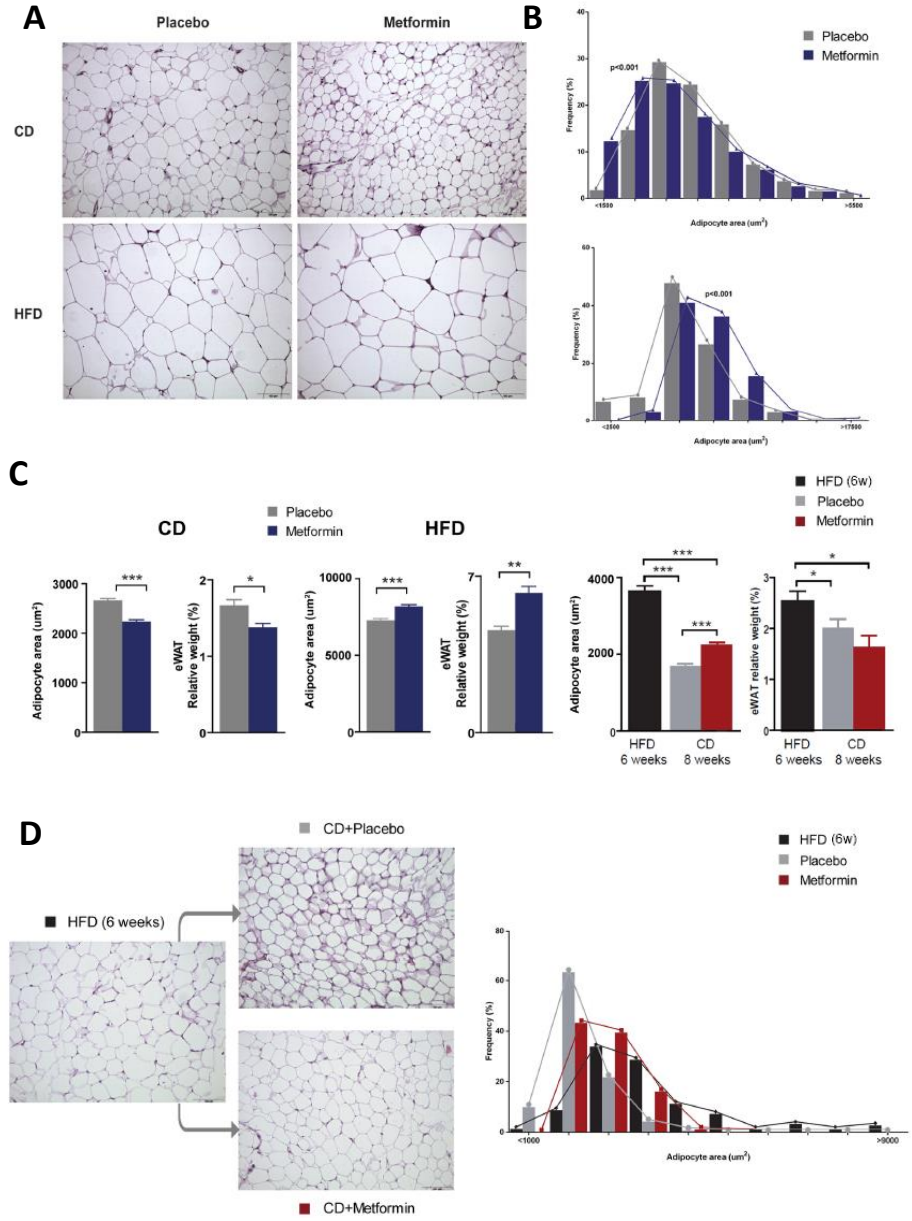

Figure 4. Dietary-induced changes and the effect of metformin on the epididymal WAT phenotype. (A) Representative microphotographs (200x) showing the differential effects of diet and metformin in epididymal white adipose tissue (eWAT) and **(B)** frequency distribution of adipocyte size. **(C)** Mean values for adipocyte area and relative weight with respect to body weight in experiments. **(C, D)** Phenotypic changes and frequency distribution of adipocyte size combining shift in diets and metformin. Legends as in Figure 1 and asterisks denote significant ($^{*}P < 0.05$; $^{**}P < 0.01$; $^{***}P < 0.001$) changes as indicated.

Effects on hepatic steatosis

Chronic HFD exposure is known to cause lipid accumulation in the liver, a process that ultimately leads to NAFLD and eventually to nonalcoholic steatohepatitis. As expected, HFD-fed animals presented with severe fatty liver disease. No significant differences in hepatic steatosis were found in the CD and HFD groups following metformin administration (Figure 5A). Remarkably, whereas diet reversal alone failed to ameliorate HFD-induced hepatic steatosis, the combination of diet reversal and metformin treatment significantly reduced the occurrence of steatosis (Figure 5B).

Effects on hepatic inflammation

There were no signs of ballooning or fibrosis and liver enzymes were not differentially affected by diet but we detected a significantly increased number of macrophages in liver of HFD-fed animals when compared with CD-fed animals, as revealed by immunohistochemistry for F4/80, a pan-marker for murine tissue macrophages (Figure 5C). Diet reversal ameliorated liver inflammation in the HFD group, as demonstrated by the significant decrease in the number of $F4/80^+$ inflammatory cells (Figure 5D). Of note, metformin treatment of diet-reversed animals almost completely eliminated the presence of $F4/80^+$ macrophages (Figure 5D), which also appeared to be enlarged; a morphology that might be suggestive of an activated state following HFD. The ability of metformin to reduce HFD-induced chronic inflammation might involve the reduced production of prototypical pro-inflammatory cytokines including interleukin (IL)-1β and tumor necrosis factor-α (TNF-α), as levels of these cytokines were significantly reduced in metformin-treated mice. Quantitative and qualitative changes were similar in both CD and HFD regimens and values obtained in CD fed mice with or without metformin are shown in Figure 5E.

Study II

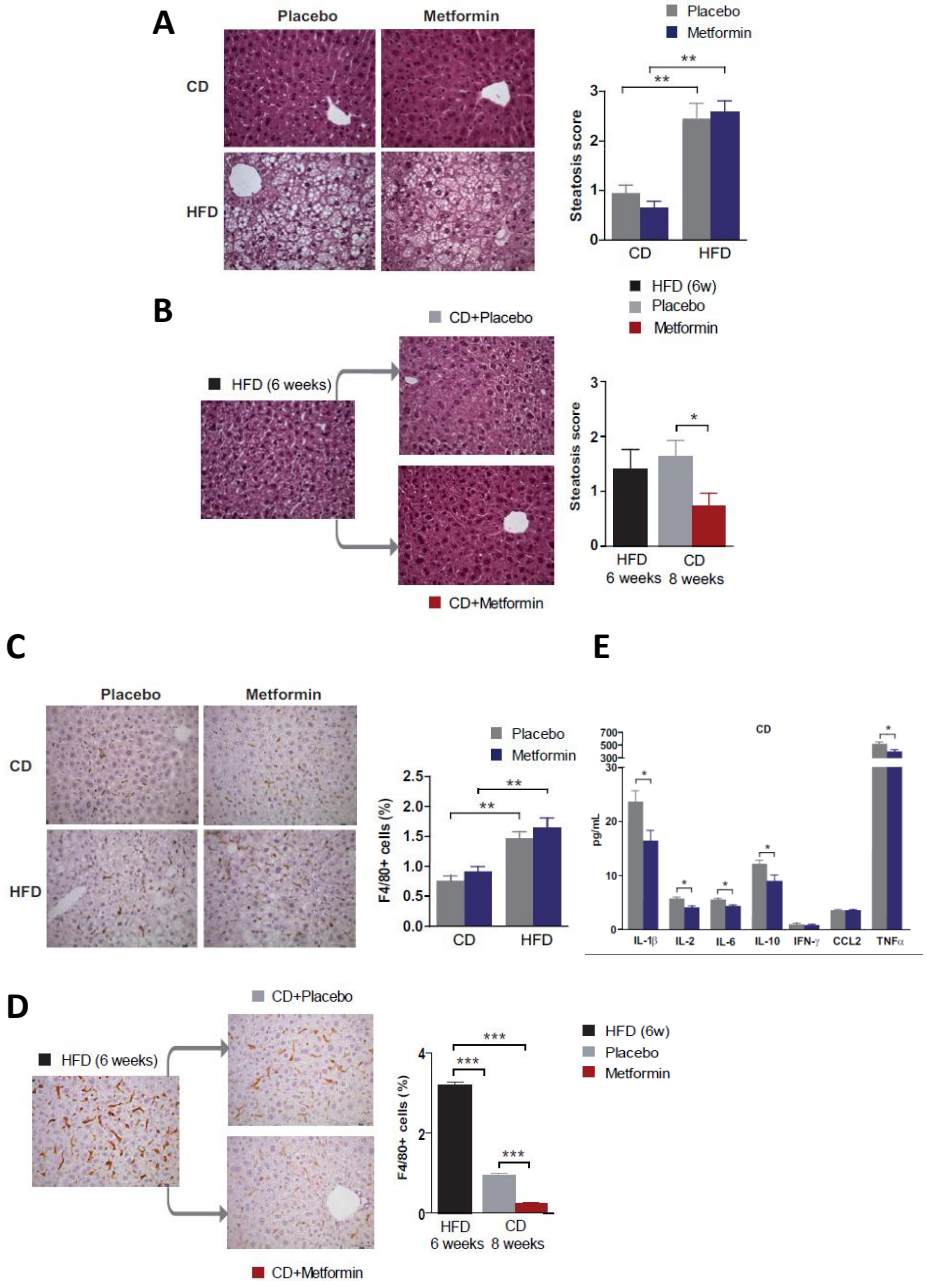

Figure 5. Dietary-induced changes and the effect of metformin on the liver phenotype. Effects of diet and metformin at indicated times during nutritional variations. Representative microphotographs (100x) of liver sections stained with H&E **(A, B)** and F4/80 immunochemistry **(C, D)** showing the effects of diet and metformin in steatosis score and proportion of macrophages. **(E)** The effect of metformin in the hepatic concentration of selected cytokines. Legends as in Figure 1 and asterisks denote significant ($^{*}P < 0.05$; $^{**}P < 0.01$; $^{***}P < 0.001$) changes as indicated.

Effects on the levels of energy metabolites in hepatic and adipose tissue

The exposure of mice to HFD has an impact on levels of energy metabolites, which is different in WAT and liver. In WAT, HFD led to a decrease in the levels of glycolytic intermediates proximal to glucose-6-phosphate, while increasing the TCA cycle intermediates citrate/isocitrate and α-ketoglutarate. Conversely, HFD promoted in liver the accumulation of glycolytic intermediates proximal to glucose-6-phosphate, that is, those intermediates involved in glucose transport and phosphorylation, while significantly decreasing branched-chain amino acids (BCAAs) (Figure 6). We then evaluated the tissue-specific (WAT versus liver) nature of the impact of metformin for energy metabolites. Metformin treatment led to a significant decrease in the levels of the BCAAs valine, leucine, and isoleucine in WAT of mice fed CD, and additionally increased glycolytic intermediates distal to glucose-6-phosphate (phosphoenolpyruvate, pyruvate, and lactate) and most of the TCA cycle intermediates (Figure 7A). Whereas the decrease in the glycolytic intermediates proximal to glucose-6-phosphate remained unaltered by metformin treatment, neither glycolytic intermediates distal to glucose-6-phosphate nor TCA intermediates were significantly altered by metformin in WAT of mice on HFD. Metabolite-based clustering in WAT obtained by the partial least squares-discriminant analysis (PLS-DA) model revealed a clear and significant separation between CD and HFD regimens in the absence or presence of metformin treatment in two-dimensional score plots (Figure 7B). When the criteria of variable importance in the projection (VIP scores ≥1) in the PLS-DA model were used to maximize the difference of metabolic profiles between the different diet groups, the subset of metabolites majorly impacted were early glycolytic intermediates and BCAAs (Figure 7C). Heatmap visualization, commonly used for unsupervised

clustering, revealed a similar segregation of metformin-impacted glycolytic and amino acids metabolites in WAT from CD and HFD groups (Figure 7D).

A completely different picture emerged when assessing metformin-driven metabolomic shifts in liver from CD and HFD groups. The significant reduction of phosphoenolpyruvate and acetyl-CoA, accompanied by an increase in the levels of glycolytic intermediates proximal to glucose-6-phosphate, including glucose-6-phosphate itself, 6-phosphogluconate, and fructose 1,6-bisphosphate, suggested a reduced entry of glucose carbon into mitochondrial biosynthetic metabolism in mice fed CD together with metformin treatment (Figure 8A). Mitochondria from liver of mice fed HFD apparently exhibited an increased dependency in reductive glutamine metabolism capable of replenishing the high levels of lipogenic acetyl-CoA/malonyl-CoA as an adaptive response to metformin (Figure 8A). Metabolite-based clustering in liver obtained by the PLS-DA model confirmed a clear and significant separation of animals fed a CD alone and with metformin (Figure 8B). Conversely, a small overlap occurred in animals fed HFD alone and with metformin (Figure 8B). When the distinct metabolites between hepatic groups were selected with the criteria of VIP ≥1 in the PLS-DA model, the subset of metabolites majorly impacted were glycolytic intermediates and those metabolites related to the biosynthetic fates of glutamine metabolism (Figure 8C). Unlike the scenario observed with the similar impact of metformin for WAT metabolites in CD- and HFD-fed mice, the segregation of the selected metabolites obtained by using heatmap visualization confirmed a completely distinct segregation of metformin-impacted metabolites in liver of CD- and HFD-fed mice (Figure 8D).

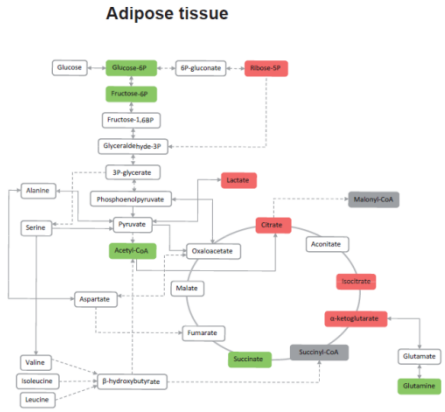

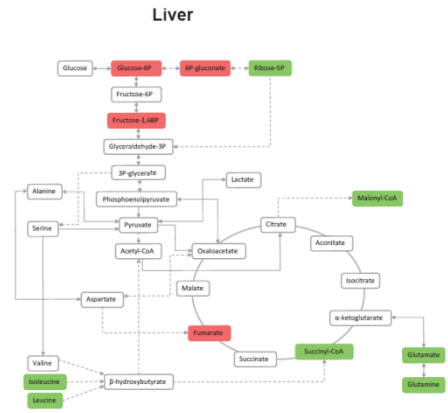

Metabolite	HFD (µM)	CD (µM)	HFD/CD
3P-glycerate	0.14 ± 0.05	0.24 ± 0.05	0.58
6P-gluconate	194.70 ± 35.73	296.90 ± 44.49	0.66
α-ketoglutarate	0.27 ± 0.02	0.15 ± 0.02	1.83 ***
β-hydroxybutyrate	0.04 ± 0.00	0.04 ± 0.00	0.89
Acetyl-CoA	0.002 ± 0.00	0.004 ± 0.00	0.43 ***
Aconitate	0.08 ± 0.01	0.05 ± 0.00	1.73
Alanine	80.94 ± 6.60	63.13 ± 7.35	1.28
Aspartate	252 ± 38.84	304.50 ± 58.62	0.83
Citrate-Isocitrate	102.50 ± 22.56	30.65 ± 8.53	3.34 *
Fructose-1,6BP	0.20 ± 0.08	1.74 ± 0.43	0.11
Fructose-6P	7.03 ± 0.85	28.21 ± 3.27	0.25 *
Fumarate	0.34 ± 0.06	0.25 ± 0.04	1.35
Glyceraldehyde-3P	0.06 ± 0.03	0.11 ± 0.05	0.56
Glucose	324.50 ± 35.59	248.60 ± 20.99	1.31
Glucose-6P	33.22 ± 5.72	191.10 ± 17.21	0.17 *
Glutamate	28293 ± 8985	18839 ± 3194	1.50
Glutamine	274.80 ± 65.95	532.30 ± 96.81	0.52 *
Isoleucine	7.72 ± 1.28	14.93 ± 2.52	0.52
Lactate	90.31 ± 7.49	59.45 ± 2.46	1.52 **
Leucine	15.24 ± 2.00	29.67 ± 5.56	0.51
Malate	5.84 ± 1.27	3.83 ± 0.79	1.53
Malonyl-CoA	n.q.	n.q.	-
Oxaloacetate	0.04 ± 0.01	0.01 ± 0.00	2.76
Phosphoenolpyruvate	0.03 ± 0.01	0.08 ± 0.03	0.38
Pyruvate	0.33 ± 0.02	0.32 ± 0.03	1.05
Ribose-5P	7.28 ± 1.14	2.19 ± 0.51	3.33 **
Serine	56.50 ± 14.64	89.36 ± 26.89	0.63
Succinate	9.08 ± 0.62	13.06 ± 0.84	0.69 **
Succinyl-CoA	n.q.	n.q.	-
Valine	22.95 ± 4.71	21.80 ± 3.06	1.05

Metabolite	HFD (µM)	CD (µM)	HFD / CD
3P-glycerate	12.49 ± 1.75	18.05 ± 3.28	0.69
6P-gluconate	57168 ± 7366	38206 ± 1648	1.50 *
α-ketoglutarate	4.57 ± 0.41	5.16 ± 0.57	0.88
β-hydroxybutyrate	0.14 ± 0.02	0.10 ± 0.02	1.39
Acetyl-CoA	0.03 ± 0.01	0.06 ± 0.01	0.56
Aconitate	64.22 ± 18.12	46.98 ± 2.67	1.37
Alanine	1644 ± 125.60	1663 ± 185.70	0.99
Aspartate	3261 ± 240	4259 ± 127.70	0.77
Citrate-Isocitrate	208.40 ± 12.65	425.20 ± 46.36	0.49
Fructose-1,6BP	36.58 ± 8.76	12.03 ± 1.28	3.04 *
Fructose-6P	1800 ± 337.80	1323 ± 110.20	1.36
Fumarate	61.76 ± 7.05	25.67 ± 4.79	2.41 **
Glyceraldehyde-3P	16.02 ± 3.74	16.14 ± 2.71	0.99
Glucose	1346 ± 244.40	1802 ± 103	0.75
Glucose-6P	6383 ± 1454	1302 ± 147	4.90 **
Glutamate	81941 ± 14649	490043 ± 67246	0.17 **
Glutamine	977.80 ± 113	2104 ± 272.90	0.46 ***
Isoleucine	262.20 ± 59.81	730.30 ± 73.83	0.36 *
Lactate	818.80 ± 92.73	667.10 ± 46.51	1.23
Leucine	536.60 ± 66.27	1009 ± 103.90	0.53 *
Malate	445.20 ± 80.17	318 ± 48.51	1.40
Malonyl-CoA	0.11 ± 0.04	0.36 ± 0.09	0.31 *
Oxaloacetate	1.98 ± 0.31	2.33 ± 0.28	0.85
Phosphoenolpyruvate	7.46 ± 0.98	11.86 ± 1.99	1.59
Pyruvate	7.54 ± 0.61	5.61 ± 0.54	1.34
Ribose-5P	156.10 ± 45.16	470 ± 81.70	0.33 *
Serine	3898 ± 269.20	5531 ± 709.80	0.70
Succinate	156.30 ± 10.29	137.80 ± 19.17	1.13
Succinyl-CoA	0.47 ± 0.06	0.99 ± 0.12	0.47 **
Valine	345.10 ± 43.53	460.30 ± 60.05	0.75

Figure 6. The relative impact of dietary fat on the levels of metabolites associated with energy metabolism in adipose tissue and liver. Metabolites are marked in green or red if they were significantly decreased or increased respectively according to the impact of HFD alone.

Study II

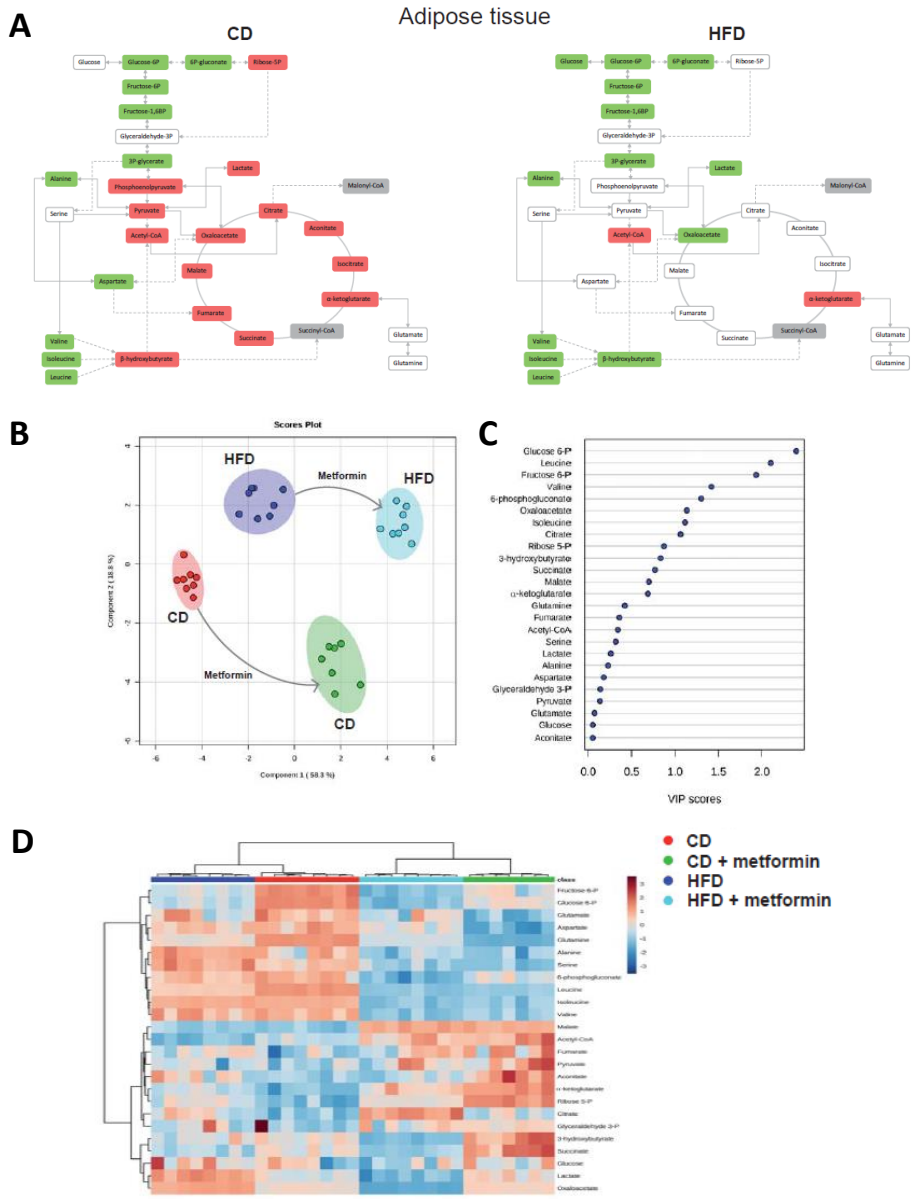

Figure 7. Dietary-induced changes and the effect of metformin on WAT energy metabolites. **(A)** The effect of both diets is segregated to highlight specific changes in metformin response; metabolites are marked in green or red if they were significantly decreased or increased respectively. **(B)** Partial least square discriminant analysis indicates visually the role of the measured metabolites in discriminating among the different experimental groups. **(C)** Random forests were used to rank without supervision the importance of metabolites to explain the differential effect of metformin. **(D)** Standardized metabolite concentrations represented as a heatmap. Mice populations with different diets and metformin treatment are reported as a color code in the upper part of the graph, while metabolite names have been assigned to rows.

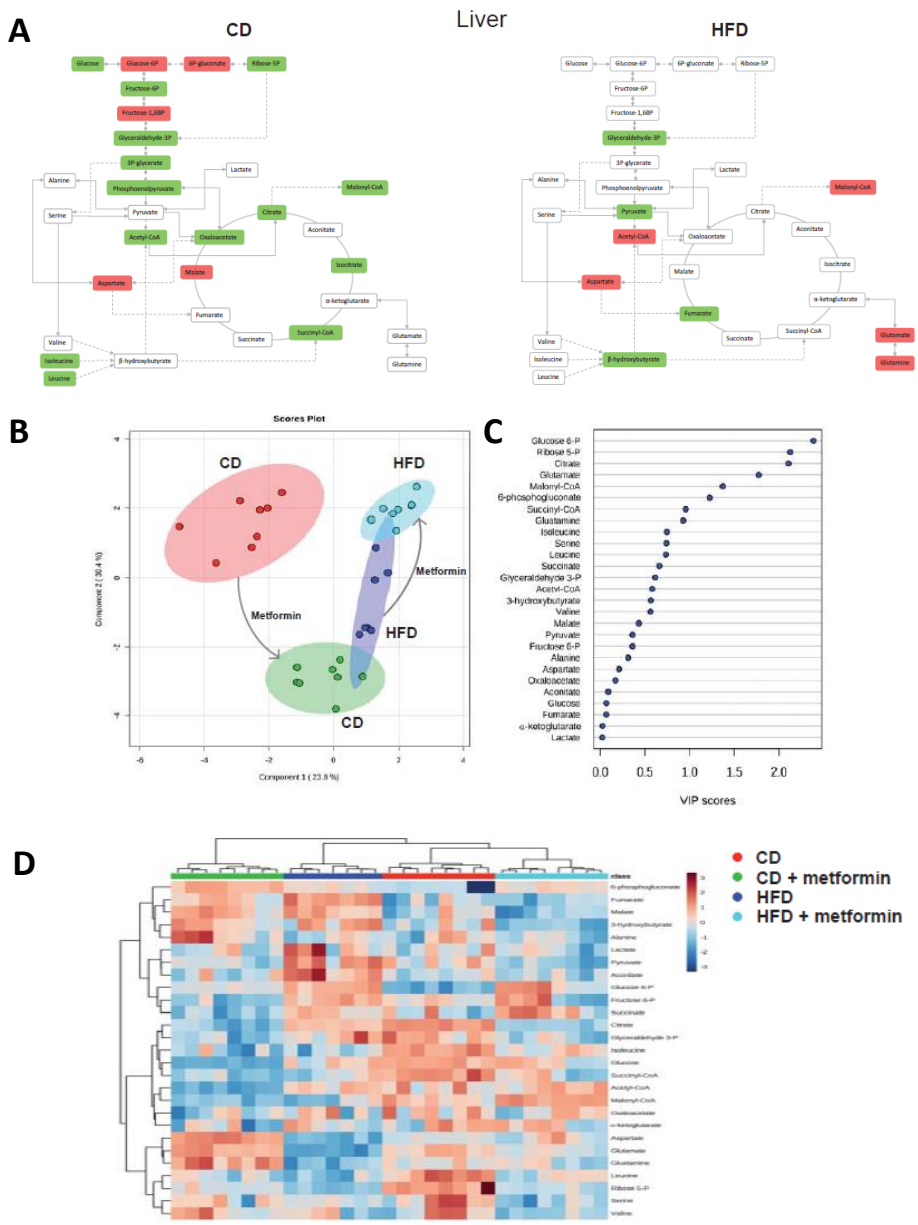

Figure 8. Dietary-induced changes and the effect of metformin on hepatic energy. (A) The effect of both diets is segregated to highlight specific changes in metformin response; metabolites are marked in green or red if they were significantly decreased or increased respectively. **(B)** Partial least square discriminant analysis indicates visually the role of the measured metabolites in discriminating among the different experimental groups. **(C)** Random forests were used to rank without supervision the importance of metabolites to explain the differential effect of metformin. **(D)** Standardized metabolite concentrations represented as a heatmap. Mice populations with different diets and metformin treatment are reported as a color code in the upper part of the graph, while metabolite names have been assigned to rows.

Discussion

Our major finding is that metformin treatment might play a major role in preventing the metabolic disturbances caused by earlier exposure to HFD in both adipose and liver tissues. Metformin also enlarges the benefits of simple dietary restrain as a stand-alone intervention. Feeding *Ldlr*$^{-/-}$ mice with HFD promoted the appearance of classical metabolic derangements occurring after excessive intake of dietary lipids (i.e., weight gain, glucose intolerance, hyperlipidemia, hepatic steatosis and liver inflammation). When HFD-fed animals were subjected to diet reversal alone and also to metformin for a short duration, it became apparent that switching to regular feeding alone (which mimics patients guided towards a healthier overall pattern of eating) could not fully reverse the full spectrum of metabolic abnormalities provoked by the initial exposure to HFD. However, the addition of metformin treatment to diet reversal remarkably ameliorated the metabolic status associated with the previous HFD pattern.

Animals started to regain body weight 6 weeks after switching to normal diet but the trend towards lower weight gain remained unaltered in the presence of metformin, likely indicating that the effect of metformin in weight loss maintenance could prevent the long-term consequences of HFD-associated overweight. Similarly, feeding mice HFD induced an insulin resistance phenotype. Although the reduction of energy intake by switching the diet from HFD to CD significantly improved the hyperglycemia induced by HFD, it was noteworthy that metformin treatment elicited additional glycemic control. The significantly better-preserved glucose tolerance of mice on metformin was accompanied by an improved attenuation of the circulating levels of cholesterol and triglycerides, thus revealing its capacity to protect from the long-term effects of HFD-imposed periods of metabolic hyperlipidemia. These effects are attributable to metformin [28] and our

data suggest that can reverse an HFD-established obese and insulin-resistant phenotype.

Exposure to HFD causes chronic inflammation in the liver, a critical factor for the development of obesity-related glucose intolerance and insulin resistance [29]. Glucose intolerance and hepatic insulin resistance, in turn, can promote the development and progression of NAFLD [30, 31], thereby driving a harmful cycle of metabolic disturbances. This key mechanistic component of the lifelong risk for developing metabolic complications in response to energy overload appears to be the one most profoundly affected by metformin. Metformin treated mice exhibited a dramatically improved protection against HFD-induced hepatic steatosis, which was accompanied by a significant lowering of liver-infiltrating pro-inflammatory macrophages as well as lower levels of major proinflammatory cytokines. The ability of metformin to modulate the polarization or migration of these cells has been recently demonstrated in tumor-associated macrophages [32, 33]. Future studies should examine whether the ability of metformin to restore impaired glucose and hepatic lipid metabolism may have aided in the reduction of hepatic tissue inflammation by preventing either the recruitment or pro-inflammatory activation of macrophages (or both).

Liver and WAT from HFD-fed *Ldlr*$^{-/-}$ mice appear to have a significantly different metformin-induced response to the inability of HFD-damaged tissues to benefit from the expected response to diet reversal [34-37]. On the one hand, diet reversal failed to restore HFD-induced hepatic damage unless combined with metformin. Metformin decreased the flow of glucose- and glutamine-derived metabolic intermediates into the TCA cycle and appears to overcome the hepatic ability to store and metabolize carbohydrates, thereby better preventing HFD-induced hepatic damage when switching to normal diet occurs. This metformin effect has already

been appreciated in proliferating cells, suppressing the mitochondrial-dependent biosynthetic activity and *de novo* lipogenesis [38,39]. Hence, our findings support the notion that elevated mitochondrial TCA function and increased flow through anabolic pathways plays a crucial role in the pathology of fatty liver and insulin resistance induced by an obesogenic diet [40]. This is in accordance with recent data indicating that metformin might alleviate oxidative stress and inflammation [41]. Mitochondrial adaptations might therefore be explored as mechanisms of HFD-induced hepatic complications. On the other hand, it appears that adipocyte hypertrophy in WAT of *Ldlr*$^{-/-}$ mice, a hallmark of WAT enlargement in obesity, is clearly corrected upon diet reversal. The frequency distribution of adipocyte sizes across the WAT depot suggests an apparently limited capacity of metformin to remodel WAT tissue architecture, likely indicating a specific protection from hepatic insulin resistance rather than a protection from systemic insulin resistance. We now know that, in contrast to the usage of glucose and glutamine for mitochondrial generation of lipogenic pools of acetyl-CoA in proliferating cells, differentiated adipocytes exhibit an increased catabolic flux of BCCAs such as leucine and isoleucine that account for a significant amount of lipogenic acetyl-CoA pools [42, 43]. In this regard, it is noteworthy that the capacity of metformin to target the contribution of BCAAs to WAT metabolism, likely by up-regulating the BCAA degradation pathway [44], might contribute to the additional beneficial effects elicited by metformin beyond those of diet reversal alone by altering the functional integrity of this tissue. Future research should include the effect of metformin and other drugs apparently converging in mechanisms involving BCAAs.

The health-promoting effects of metformin are largely viewed as the consequence of its ability to simultaneously target the core nutrient-sensing networks insulin/IGF-1, at the non-cell autonomous level, and AMPK/mTOR,

at the cell-autonomous level [7, 24, 45, 46]. Alternatively, they might reflect downstream consequences of a primary action on a single master mechanism that has not yet been identified. Along this line, very recent reports are providing evidence for epigenetic targets potentially contributing to the protective effects of metformin against several diseases [47-49]. Because the pathogenesis of HFD-induced metabolic disturbances causally involves the long-term persistence of epigenetic alterations [34-36, 50-52], there is an urgent need to elucidate the mechanism of metformin to mediate global epigenetic programming in multiple host tissues [48, 53]. We have found robust patterns indicating the potential of metformin to serve as a model compound for preventing HFD-driven progression of metabolic complications despite attainment of changes in dietary habits. The clinical combination of metformin-based pharmacotherapy with dietary modification might herald the development of much-needed therapeutic and preventive strategies against metabolic consequences of excessive dietary fat intake.

References

1. Hernández-Aguilera A, Fernández-Arroyo S, Cuyàs E, Luciano-Mateo F, Cabre N, Camps J, et al. Epigenetics and nutrition-related epidemics of metabolic diseases: Current perspectives and challenges. Food Chem Toxicol. 2016; 96:191-204. doi: 10.1016/j.fct.2016.08.006. PMID: 27503834.

2. Hardie DG, Schaffer BE, Brunet A. AMPK: An Energy-Sensing Pathway with Multiple Inputs and Outputs. Trends Cell Biol. 2016; 26(3): 190-201. doi: 10.1016/j.tcb.2015.10.013. PMID: 26616193.

3. Massucci FA, Wheeler J, Beltrán-Debón R, Joven J, Sales-Pardo M, Guimerà R. Inferring propagation paths for sparsely observed perturbations on complex networks. Sci Adv. 2016; 2(10): e1501638. PMID: 27819038.

4. Mattison JA, Roth GS, Beasley TM, Tilmont EM, Handy AM, Herbert RL, et al. Impact of caloric restriction on health and survival in rhesus monkeys from the NIA study. Nature. 2012; 489(7415): 318-321. doi: 10.1038/nature11432. PMID: 22932268.

5. Roth GS, Ingram DK. Manipulation of health span and function by dietary caloric restriction mimetics. Ann N Y Acad Sci. 2016; 1363: 5-10. doi: 10.1111/nyas.12834. PMID: 26214681.

6. Smith BK, Marcinko K, Desjardins EM, Lally JS, Ford RJ, Steinberg GR. Treatment of nonalcoholic fatty liver disease: role of AMPK. Am J Physiol Endocrinol Metab. 2016; 311(4): E730-E740. doi: 10.1152/ ajpendo. 00225.2016. PMID: 27577854.

7. Barzilai N, Crandall JP, Kritchevsky SB, Espeland MA. Metformin as a Tool to Target Aging. Cell Metab. 2016; 23(6): 1060-1065. doi: 10.1016/j.cmet.2016.05.011. PMID: 27304507.

8. Menendez JA, Joven J. One-carbon metabolism: an aging-cancer crossroad for the gerosuppressant metformin. Aging (Albany NY). 2012; 4(12): 894-898. PMID: 23525940.

9. Corominas-Faja B, Quirantes-Piné R, Oliveras-Ferraros C, Vazquez-Martin A, Cufí S, Martin-Castillo B, et al. Metabolomic fingerprint reveals that metformin impairs one-carbon metabolism in a manner similar to the antifolate class of chemotherapy drugs. Aging (Albany NY). 2012; 4(7): 480-498. PMID: 22837425

10. Viollet B, Guigas B, Sanz Garcia N, Leclerc J, Foretz M, Andreelli F. Cellular and molecular mechanisms of metformin: an overview. Clin Sci (Lond). 2012; 122(6): 253-270. doi: 10.1042/CS20110386.

11. Foretz M, Viollet B. Metformin takes a new route to clinical efficacy Nat Rev Endocrinol. 2015; 11(7): 390-392. doi: 10.1038/nrendo.2015.85. PMID: 26032104.

12. Pernicova I, Korbonits M. Metformin--mode of action and clinical implications for diabetes and cancer. Nat Rev Endocrinol. 2014;10(3):143-156. doi: 10.1038/nrendo.2013.256.

13. Saisho Y. Metformin and Inflammation: Its Potential Beyond Glucose-lowering Effect. Endocr Metab Immune Disord Drug Targets. 2015; 15(3):196-205. PMID: 25772174.

14. Song YM, Lee YH, Kim JW, Ham DS, Kang ES, Cha BS, Lee HC, Lee BW. Metformin alleviates hepatosteatosis by restoring SIRT1-mediated autophagy induction via an AMP-activated protein kinase-independent pathway. Autophagy. 2015; 11(1): 46-59. doi: 10.4161/15548627. 2014.984271. PMID: 25484077.

15. Jadhav KS, Dungan CM, Williamson DL. Metformin limits ceramide-induced senescence in C2C12 myoblasts. Mech Ageing Dev. 2013; 134(11-12): 548-559. doi: 10.1016/j.mad.2013.11.002. PMID: 24269881.

16. Domecq JP, Prutsky G, Leppin A, Sonbol MB, Altayar O, Undavalli C, et al. Clinical review: Drugs commonly associated with weight change: a systematic review and meta-analysis. J Clin Endocrinol Metab. 2015; 100(2): 363-70. doi: 10.1210/jc.2014-3421.

17. Foretz M, Hébrard S, Leclerc J, Zarrinpashneh E, Soty M, Mithieux G, et al. Metformin inhibits hepatic gluconeogenesis in mice independently of the LKB1/AMPK pathway via a decrease in hepatic energy state. J Clin Invest. 2010; 120(7): 2355-2369. doi: 10.1172/JCI40671. PMID: 20577053.

18. Linden MA, Lopez KT, Fletcher JA, Morris EM, Meers GM, Siddique S, et al. Combining metformin therapy with caloric restriction for the management of type 2 diabetes and nonalcoholic fatty liver disease in obese rats. Appl Physiol Nutr Metab. 2015; 40(10):1038-47. doi: 10.1139/apnm-2015-0236. PMID: 26394261.

19. Woo SL, Xu H, Li H, Zhao Y, Hu X, Zhao J, et al. Metformin ameliorates hepatic steatosis and inflammation without altering adipose phenotype

in diet-induced obesity. PLoS One. 2014; 9(3):e91111. doi:10.1371/ journal. pone. 0091111. PMID: 24638078.

20. Joven J, Rull A, Ferré N, Escolà-Gil JC, Marsillach J, Coll B, et al. The results in rodent models of atherosclerosis are not interchangeable: the influence of diet and strain. Atherosclerosis. 2007; 195(2): e85-92. PMID: 17651742.

21. Riera-Borrull M, Rodríguez-Gallego E, Hernández-Aguilera A, Luciano F, Ras R, Cuyàs E, et al. Exploring the Process of Energy Generation in Pathophysiology by Targeted Metabolomics: Performance of a Simple and Quantitative Method. J Am Soc Mass Spectrom. 2016; 27(1): 168-77. doi: 10.1007/s13361-015-1262-3. PMID: 26383735.

22. Cufí S, Corominas-Faja B, Lopez-Bonet E, Bonavia R, Pernas S, López IÁ, et al. Dietary restriction-resistant human tumors harboring the PIK3CA-activating mutation H1047R are sensitive to metformin. Oncotarget. 2013; 4(9): 1484-1495. PMID: 23986086.

23. García-Heredia A, Riera-Borrull M, Fort-Gallifa I, Luciano-Mateo F, Cabré N, Hernández-Aguilera A, Joven J, Camps J. Metformin administration induces hepatotoxic effects in paraoxonase-1-deficient mice. Chem Biol Interact. 2016; 249:56-63. doi: 10.1016/j.cbi.2016.03.004. PMID: 26945512.

24. Anisimov VN. Metformin for Prevention and Treatment of Colon Cancer: A Reappraisal of Experimental and Clinical Data. Curr Drug Targets. 2016; 17(4): 439-46. PMID: 25738299.

25. García-Heredia A, Kensicki E, Mohney RP, Rull A, Triguero I, Marsillach J, et al. Paraoxonase-1 deficiency is associated with severe liver steatosis in mice fed a high-fat high-cholesterol diet: a metabolomic approach. J Proteome Res. 2013; 12(4): 1946-1955. doi: 10.1021/pr400050u. PMID: 23448543.

26. Joven J, Espinel E, Rull A, Aragonès G, Rodríguez-Gallego E, Camps J, et al. Plant-derived polyphenols regulate expression of miRNA paralogs miR-103/107 and miR-122 and prevent diet-induced fatty liver disease in hyperlipidemic mice. Biochim Biophys Acta. 2012; 1820(7): 894-899. Doi: 10.1016/j.bbagen.2012.03.020. PMID: 22503922.

27. Xia J, Sinelnikov IV, Han B, Wishart DS. MetaboAnalyst 3.0--making metabolomics more meaningful. Nucleic Acids Res. 2015; 43(W1): W251-257. doi: 10.1093/nar/gkv380.

28. Menendez JA, Martin-Castillo B, Joven J. Metformin and cancer: Quo vadis et cui bono? Oncotarget. 2016. doi: 10.18632/oncotarget.10262. PMID: 27356748.

29. Shoelson SE, Herrero L, Naaz A. Obesity, inflammation, and insulin resistance. Gastroenterology. 2007; 132: 2169-2180. Doi: 10.1053/j.gastro.2007.03.059 PMID: 17498510.

30. Ota T, Takamura T, Kurita S, Matsuzawa N, Kita Y, Uno M, et al. Insulin resistance accelerates a dietary rat model of nonalcoholic steatohepatitis. Gastroenterology. 2007; 132: 282-293. PMID: 17241878.

31. Pfluger PT, Herranz D, Velasco-Miguel S, Serrano M, Tschöp MH. Sirt1 protects against high-fat diet-induced metabolic damage. Proc Natl Acad Sci U S A. 2008; 105: 9793-9798. Doi: 10.1073/pnas.0802917105. PMID: 18599449.

32. Ding L, Liang G, Yao Z, Zhang J, Liu R, Chen H, et al. Metformin prevents cancer metastasis by inhibiting M2-like polarization of tumor associated macrophages. Oncotarget. 2015; 6: 36441-36455. doi: 10.18632/oncotarget.5541. PMID: 26497364.

33. Incio J, Suboj P, Chin SM, Vardam-Kaur T, Liu H, Hato T, Babykutty S, et al. Metformin Reduces Desmoplasia in Pancreatic Cancer by Reprogramming Stellate Cells and Tumor-Associated Macrophages. PLoS One. 2015; 10:e0141392. doi: 10.1371/journal.pone.0141392. PMID: 26641266.

34. Tonna S, El-Osta A, Cooper ME, Tikellis C. Metabolic memory and diabetic nephropathy: potential role for epigenetic mechanisms. Nat Rev Nephrol. 2010; 6: 332-341. Doi: 10.1038/nrneph.2010.55. PMID: 20421885.

35. Villeneuve LM, Natarajan R. The role of epigenetics in the pathology of diabetic complications. Am J Physiol Renal Physiol. 2010; 299: F14-25. doi: 10.1152/ajprenal.00200.2010. PMID: 20462972.

36. Kumar S, Pamulapati H, Tikoo K. Fatty acid induced metabolic memory involves alterations in renal histone H3K36me2 and H3K27me3. Mol Cell Endocrinol. 2016; 422: 233-242. Doi: 10.1016/j.mce.2015.12.019. PMID: 26747726.

37. Tikoo K, Sharma E, Amara VR, Pamulapati H, Dhawale VS. Metformin improves metabolic memory in high fat diet (HFD)-induced renal dysfunction. J Biol Chem. 2016. pii: jbc.C116.732990. Doi: 10.1074/jbc.C116.732990. PMID: 27551045.

38. Griss T, Vincent EE, Egnatchik R, Chen J, Ma EH, Faubert B, et al. Metformin Antagonizes Cancer Cell Proliferation by Suppressing Mitochondrial-Dependent Biosynthesis. PLoS Biol. 2015; 13:e1002309. Doi: 10.1371/journal.pbio.1002309. PMID: 26625127.

39. Cuyàs E, Fernández-Arroyo S, Alarcón T, Lupu R, Joven J, Menendez JA. Germline BRCA1 mutation reprograms breast epithelial cell metabolism towards mitochondrial-dependent biosynthesis: evidence for metformin-based "starvation" strategies in BRCA1 carriers. Oncotarget. 2016; 7: 52974-52992. doi: 10.18632/oncotarget.9732. PMID: 27259235.

40. Satapati S, Sunny NE, Kucejova B, Fu X, He TT, Méndez-Lucas A, Shelton JM, Perales JC, Browning JD, Burgess SC. Elevated TCA cycle function in the pathology of diet-induced hepatic insulin resistance and fatty liver. J Lipid Res. 2012; 53:1080-1092. doi: 10.1194/jlr.M023382. PMID: 22493093.

41. Satapati S, Kucejova B, Duarte JA, Fletcher JA, Reynolds L, Sunny NE, et al. Mitochondrial metabolism mediates oxidative stress and inflammation in fatty liver. J Clin Invest. 2015; 125: 4447-4462. doi: 10.1172/JCI82204. PMID: 26571396.

42. Herman MA, She P, Peroni OD, Lynch CJ, Kahn BB. Adipose tissue branched chain amino acid (BCAA) metabolism modulates circulating BCAA levels. J Biol Chem. 2010; 285: 11348-11356. DOI: 10.1074/jbc.M109.075184. PMID: 20093359.

43. Green CR, Wallace M, Divakaruni AS, Phillips SA, Murphy AN, Ciaraldi TP, Metallo CM. Branched-chain amino acid catabolism fuels adipocyte differentiation and lipogenesis. Nat Chem Biol. 2016; 12: 15-21. Doi: 10.1038/nchembio.1961. PMID: 26571352.

44. De Haes W, Frooninckx L, Van Assche R, Smolders A, Depuydt G, Billen J, et al. Metformin promotes lifespan through mitohormesis via the peroxiredoxin PRDX-2. Proc Natl Acad Sci U S A. 2014; 111: E2501-2509. Doi: 10.1073/pnas.1321776111. PMID: 24889636.

45. López-Otín C, Galluzzi L, Freije JM, Madeo F, Kroemer G. Metabolic Control of Longevity. Cell. 2016; 166: 802-821. Doi: 10.1016/j.cell.2016.07.031. PMID: 27518560.

46. Anisimov VN. Metformin: do we finally have an anti-aging drug? Cell Cycle. 2013; 12: 3483-3489. PMID: 24189526.

47. de Kreutzenberg SV, Ceolotto G, Cattelan A, Pagnin E, Mazzucato M, Garagnani P, et al. Metformin improves putative longevity effectors in peripheral mononuclear cells from subjects with prediabetes. A randomized controlled trial. Nutr Metab Cardiovasc Dis. 2015; 25: 686-693. doi: 10.1016/j.numecd.2015.03.007. PMID: 25921843.

48. Cuyàs E, Fernández-Arroyo S, Joven J, Menendez JA. Metformin targets histone acetylation in cancer-prone epithelial cells. Cell Cycle. 2016; 15: 3355-3361. doi: 10.1080/15384101.2016.1249547. PMID: 27792453.

49. Niu N, Liu T, Cairns J, Ly RC, Tan X, Deng M, et al. Metformin pharmacogenomics: a genome-wide association study to identify genetic and epigenetic biomarkers involved in metformin anticancer response using human lymphoblastoid cell lines. Hum Mol Genet. 2016. pii: ddw301. Doi: 10.1093/hmg/ddw301. PMID: 27616566.

50. Zhong T, Men Y, Lu L, Geng T, Zhou J, Mitsuhashi A, et al. Metformin alters DNA methylation genome-wide via the H19/SAHH axis. Oncogene. 2016. doi: 10.1038/onc.2016.391. PMID: 27775072.

51. Reddy MA, Tak Park J, Natarajan R. Epigenetic modifications in the pathogenesis of diabetic nephropathy. Semin Nephrol. 2013; 33: 341-353. Doi: 10.1016/j.semnephrol.2013.05.006. PMID: 24011576.

52. Reddy MA, Zhang E, Natarajan R. Epigenetic mechanisms in diabetic complications and metabolic memory. Diabetologia. 2015; 58: 443-455. doi: 10.1007/s00125-014-3462-y. PMID: 25481708.

53. Krautkramer KA, Kreznar JH, Romano KA, Vivas EI, Barrett-Wilt GA, Rabaglia ME, et al. Diet-Microbiota Interactions Mediate Global Epigenetic Programming in Multiple Host Tissues. Mol Cell. 2016; 64(5): 982-992. doi: 10.1016/j.molcel.2016.10.025. PMID: 27889451.

STUDY III

Palmitate conditions macrophages for enhanced responses towards pro-inflammatory stimuli via JNK activation.

Molecular Metabolism, 2017

Abstract

Obesity is associated with low-grade inflammation and elevated levels of circulating saturated fatty acids (SFA), which trigger inflammatory responses by engaging pattern recognition receptors in macrophages. Since tissue homeostasis is maintained through an adequate balance of pro- and anti-inflammatory macrophages, we assessed the transcriptional and functional profile of M-CSF-dependent monocyte-derived human macrophages (M-MØ) exposed to concentrations of SFA found in obese individuals. We report that palmitate (C16:0, 200 μM) lowers the expression of transcription factors that positively regulate IL-10 expression (MAFB, AhR), modulates significantly the macrophage gene signature, and promotes a pro-inflammatory state whose acquisition requires JNK activation. Unlike LPS, palmitate exposure does not activate STAT1, and its transcriptional effects can be distinguished from those triggered by LPS as both agents oppositely regulate the expression of CCL19 and *TRIB3*. Besides, palmitate conditions macrophages for exacerbated pro-inflammatory responses (lower IL-10 and CCL2, higher TNFα, IL-6 and IL1-β) towards pathogenic stimuli, a process also mediated by JNK activation. All these effects of palmitate are fatty acid-specific since oleate (C18:1, 200 μM) does not modify the macrophage transcriptional and functional profiles. Therefore, pathologic palmitate concentrations promote the acquisition of a specific polarization state in human macrophages and condition macrophages for enhanced responses towards inflammatory stimuli, what provides a further insight on the macrophage contribution to obesity-associated inflammation.

Introduction

Obesity has become a major worldwide health problem due to its association with the development of metabolic diseases (type 2 diabetes, metabolic syndrome, non-alcoholic fatty liver disease), and its correlation with several types of cancer [1, 2]. Numerous studies have demonstrated that inflammation underlies the link between obesity and metabolic diseases. So, an excessive nutrient intake results in the accumulation of saturated fatty acids (SFA, like palmitate), which correlates with an increase in pro-inflammatory cytokines [3]. Moreover, adipose and liver tissues from obese individuals exhibit infiltration by immune cells, primarily macrophages, an event proposed as a primary trigger for obesity-induced inflammation [4]. Chronic obesity produces a low-grade activation of the innate immune system that affects homeostasis over time [5]. A key role for macrophages in the pathogenesis of metabolic disorders has been demonstrated in mouse models of obesity, where defective CCR2-dependent monocyte/macrophage recruitment towards adipose tissue protects from obesity-induced inflammation and insulin resistance [6]. Likewise, depletion of CD11c-positive cells in mice reduces adipose tissue inflammation [7], and myeloid cell-specific deletion of IKKβ or JNK1 also protects mice from high-fat diet induced insulin resistance [8, 9]. *In vitro* and in vivo studies have suggested that SFA activate macrophage inflammatory signaling pathways leading to adipose tissue inflammation and systemic insulin resistance in a TLR4-dependent manner [10]. However, recent reports suggest that the link between SFA and insulin resistance might not be a direct consequence of a canonical TLR4 activation [11-13] because MyD88 KO mice display a more severe metabolic disease in response to a high fat diet [12] and TLR4 deficiency exacerbates diet-induced obesity, steatosis, and insulin resistance on the C57BL/10 genetic background [13]. Palmitate may also induce TLR-independent actions through epigenetic modifications [14, 15]. Chronic

palmitate exposure reprograms gene expression of human pancreatic islets by altering DNA methylation level [14]. Likewise, palmitate treatment increases DNA methylation levels at PPARγ1 promoter in mouse macrophages [15]. Therefore, whereas the role of macrophages in obesity-induced diseases in mice is well established, the triggers for the inflammatory activation of macrophages by SFA and the underlying molecular mechanisms have not been completely elucidated.

Inflamed tissues contain heterogeneous populations of resident and newly recruited macrophages that display a continuum of functional (activation/polarization) states whose appropriate balance allows elimination of tissue injuries and recovery and maintenance of tissue homeostasis. The huge macrophage functional and phenotypic heterogeneity derives from their ability to integrate information from the surrounding environment [16]. Our group and others have functionally and transcriptionally characterized human monocyte-derived macrophages generated in the presence of either GM-CSF (GM-MØ) or M-CSF (M-MØ), and shown that they resemble macrophages found in vivo under inflammatory conditions (GM-MØ) or in homeostatic/anti-inflammatory settings (M-MØ) [17-20]. Accordingly, TLR-mediated activation of GM-MØ results in the production of large levels of pro-inflammatory cytokines, whereas M-MØ activation primarily leads to release of the anti-inflammatory cytokine IL-10 [20]. Moreover, LPS activation of GM-MØ and M-MØ has allowed the identification of novel gene sets whose expression is regulated by LPS in a macrophage subtype-specific manner (*Cuevas et al., unpublished*). Since palmitate exerts its activation, at least partly, via TLR4, the analysis of the transcriptional and functional responses of GM-MØ and M-MØ to palmitate should help clarify the mechanisms behind macrophage activation by SFA. Besides, since identified mouse macrophage polarization-specific genes cannot be extrapolated to the

case of human macrophages [21, 22], it is mandatory to identify genes whose expression correlates with SFA activation in human macrophages as a primary step to determine the polarization state of adipose tissue macrophages under homeostatic and pathological conditions. We have now analyzed the effects of palmitate on human macrophages at the transcriptomic and functional levels, and found that palmitate triggers a JNK-dependent pro-inflammatory shift in human macrophages and primes macrophages for exacerbated pro-inflammatory response towards other pathogenic stimuli. Our results illustrate the existence of a palmitate-specific polarization state in human macrophages and demonstrate that palmitate, but not oleate, primes macrophages for exacerbated responses towards inflammatory stimuli.

Material and methods

Generation of human monocyte-derived macrophages

Human Peripheral Blood Mononuclear Cells (PBMC) were isolated from buffy coats from normal donors over Lymphoprep (Nycomed Pharma, Oslo, Norway) gradient according to standard procedures. Monocytes were purified from PBMC by magnetic cell sorting using anti-CD14 microbeads (Miltenyi Biotec, Bergisch Gladbach, Germany) (>95% CD14+ cells). Monocytes (0.5 x 10^6 cells/ml, >95% CD14+ cells) were cultured in RPMI 1640 supplemented with 10% fetal bovine serum (FBS) for 7 days in the presence of 1000 U/ml GM-CSF or 10 ng/ml M-CSF (ImmunoTools, Friesoythe, Germany) to generate GM-CSF-polarized macrophages (hereafter termed GM-MØ) or M-CSF-polarized macrophages (hereafter termed M-MØ), respectively [23]. Cytokines were added every two days. Where indicated, macrophages were treated with 10 ng/ml E. coli 055:B5 LPS (Sigma-Aldrich, MO, USA), palmitate (C16:0, 200 µM) or BSA for the indicated periods of

time. Cells were cultured in 21% O_2 and 5% CO_2. For intracellular signaling inhibition, macrophages were exposed to JNK inhibitor SP600125 (30 μM), GSK3 inhibitor (LiCl 30 mM) during 1 hour before treatment with BSA or palmitate (C16:0).

Fatty acid preparation

Sodium palmitate (P9767, Sigma-Aldrich, Steinheim, Germany) and sodium oleate (O7501, Sigma-Aldrich) were prepared by diluting a 200 mM stock solution in 70% ethanol into 10% fatty acid-free, low endotoxin BSA (A-8806, Sigma-Aldrich; adjusted to pH 7.4) to obtain a 5 mM palmitate-BSA stock solution that was filtered using a 0.22μm low protein binding filter (Millipore, Billerica, MA, USA).

Quantitative real-time RT-PCR

Total RNA was extracted using the NucleoSpin RNA/Protein kit (Macherey-Nagel, Düren, Germany), retrotranscribed, and amplified using the Universal Human Probe library (Roche Diagnostics, Mannheim, Germany). Oligonucleotides for selected genes were designed according to the Roche software for quantitative real-time PCR (Roche Diagnostics, Mannheim, Germany). Assays were made in triplicate and results normalized according to the expression levels of TBP (TATA box-binding protein) mRNA. Results were expressed using the ΔΔCT method for quantification. Analyzed genes included the “Pro-inflammatory gene set” and the “Anti-inflammatory gene set” that have been previously defined [18, 25]. Where indicated, microfluidic gene cards were custom-made (Roche Diagnostics) and designed to analyze the expression of a set of genes whose expression is variably modulated by LPS (10 ng/ml E. coli 055:B5, 4h) in either GM-MØ and/or M-MØ [26] (*Delgado-Cuevas et al., unpublished*). Specifically, the gene cards included 10 genes upregulated by LPS in both GM-MØ and M-MØ, 9 genes

upregulated by LPS exclusively in GM-MØ, 3 genes downregulated by LPS exclusively in GM-MØ, 28 genes upregulated by LPS exclusively in M-MØ, 20 genes downregulated by LPS exclusively in M-MØ, 7 genes upregulated by LPS in GM-MØ but downregulated in M-MØ, and 9 genes downregulated by LPS in GM-MØ but upregulated in M-MØ. Assays were made in triplicate on two independent samples of each type, and the results normalized according to the mean of the expression level of endogenous reference genes *HPRT1*, *TBP* and *RPLP0*. In all cases (quantitative real-time PCR or gene cards), the results were expressed using the ΔΔCT method for quantitation. Non-supervised hierarchical clustering was done on the mean expression level of each gene in BSA- or palmitate-treated LPS-activated M-MØ, and using Genesis software (http://genome.tugraz.at/genesisclient/genesisclient_description.shtml) [27].

ELISA

Macrophage supernatants were assayed for the presence of cytokines using commercial ELISA kits for TNF-α, CCL2 (BD Biosciences, CA, USA), IL-10, IL-6, IL-1β (Biolegend, CA, USA) and CCL19 (Sigma-Aldrich) according to the protocols supplied by the manufacturers.

Western blot

Cell lysates were obtained in 10 mM Tris-HCl (pH 8), 150 mM NaCl, 1% Nonidet P-40 lysis buffer containing 2 mM Pefabloc, 2 mg/ml aprotinin/ antipain/leupeptin/pepstatin, 10 mM NaF, and 1 mM Na3VO4. 10-15 µg of cell lysate was subjected to SDS-PAGE and transferred onto an Immobilon polyvinylidene difluoride membrane (Millipore). Protein detection was carried out using antibodies against MAFB (sc-10022, Santa Cruz, CA, USA), AHR (sc-8087, Santa Cruz) and CEBP/β (sc-150, Santa Cruz), phospho-ERK1/2, phospho-JNK, phospho-p38, phospho-p65, phospho-IKK, total IKK, ERK 1/2

and IKBα (all from Cell Signaling), total and phosphorylated STAT1 and STAT 3 (BD Bioscences), phospho-IRF3 (Cell Signaling) and total IRF3 (Santa Cruz). Protein loading was normalized using a monoclonal antibody against GAPDH (Santa Cruz) or an antibody against human Vinculin (Sigma-Aldrich).

Phosphoarrays

Intracellular signaling in response to palmitate was assessed with lysates from macrophages exposed to palmitate for 4 hours and using the Human Phospho-Kinase Antibody Array (R&D Systems), which detects the relative phosphorylation levels of 46 intracellular serine/threonine/tyrosine kinases, and following the manufacturer recommendations.

Statistical analysis

Statistical analysis was performed using Student's t-test, and $p<0.05$ was considered significant (*$p<0.05$; **$p<0.01$; ***$p<0.001$).

Results

Palmitate modifies the functional, transcriptomic and protein profile of human anti-inflammatory M-MØ.

Numerous evidences indicate that macrophage dysfunction in states of lipid excess contribute to the development of obesity-related diseases [6-9]. To determine to what extent fatty acid exposure modifies the functional properties of human macrophages, GM-MØ and M-MØ were exposed to palmitate (200 µM, 24 h) and the production of pro- and anti-inflammatory cytokines was assessed. Palmitate was efficiently captured by both macrophage subtypes (Figure 1A) and significantly increased the production of TNF-α and IL-1β, while diminished the basal production of CCL2, in M-MØ (Figure 1B). Palmitate stimulation also modified macrophage polarization at

the transcriptomic level, as it drastically down-regulated all the M-MØ-specific genes assayed ("Anti-inflammatory gene set", *HTR2B, HTR7, FOLR2, IL10, IGF1, CCL2, FABP4, MAFB*) [18, 25] (Figure 1C), while increased the mRNA expression of GM-MØ-associated *INHBA, EGLN3, PPARG1*, *TNF*, *IL6* and *IDO1* genes ("Pro-inflammatory gene set") (Figure 1C). In the case of GM-MØ, palmitate significantly enhanced the basal production of TNF-α, IL-6 and IL-1β (Figure 1B), enhanced the mRNA levels of *TNF*, *IL1B*, *IL6* and *IDO1*, and reduced the expression of various GM-MØ- and M-MØ-specific genes (Figure 1C). Kinetics analysis revealed that the expression of prototypical genes within "Anti-inflammatory gene set" (*CCL2, IL10, HTR2B, HTR7*) was already decreased 4h after palmitate treatment (Figure 1D) whereas upregulation of genes of the "Pro-inflammatory gene set" (*INHBA, EGLN3, TNF, IL6*) was only seen at later time points after palmitate exposure (Figure 1D). The ability of palmitate to down-regulate M-MØ-specific gene expression prompted us to determine its effects on the expression of transcription factors that control macrophage polarization (AhR, MAFB, C/EBPβ) [18, 25, 26, 28, 29]. M-MØ exhibited considerably higher levels of MAFB and AhR than GM-MØ, whereas the latter exhibit a higher content of C/EBPβ (Figure 1E). Palmitate treatment significantly reduced MAFB and AhR protein levels, and increased C/EBPβ, in M-MØ (Figure 1E), and these changes in transcription factor levels were evident 4-10 hours after palmitate treatment (Figure 1F). Therefore, palmitate promotes M-MØ to acquire a GM-MØ-like pro-inflammatory signature at the transcriptional and cytokine levels, and also induces M-MØ to gain a transcription factor profile that resembles that of GM-MØ. The palmitate-induced downregulation of MAFB protein expression is especially significant given the involvement of MAFB in the acquisition of an anti-inflammatory profile by human macrophages [26].

Results

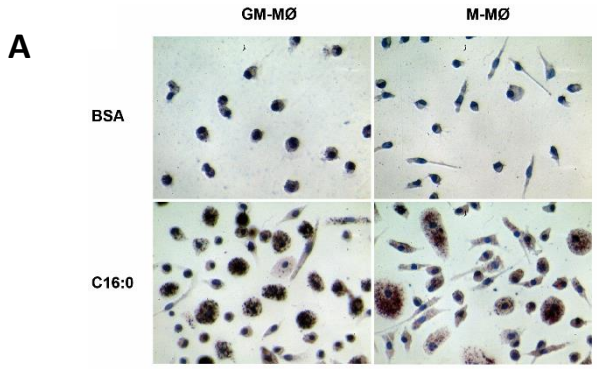
A
GM-MØ
M-MØ
BSA
C16:0

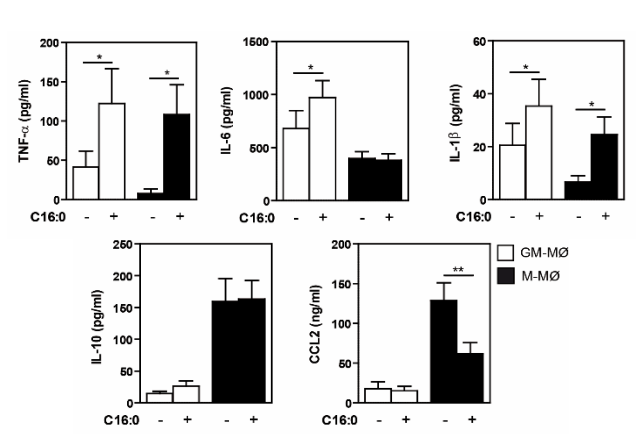
B
TNF-α (pg/ml)
IL-6 (pg/ml)
IL-1β (pg/ml)
IL-10 (pg/ml)
CCL2 (ng/ml)
C16:0
GM-MØ
M-MØ

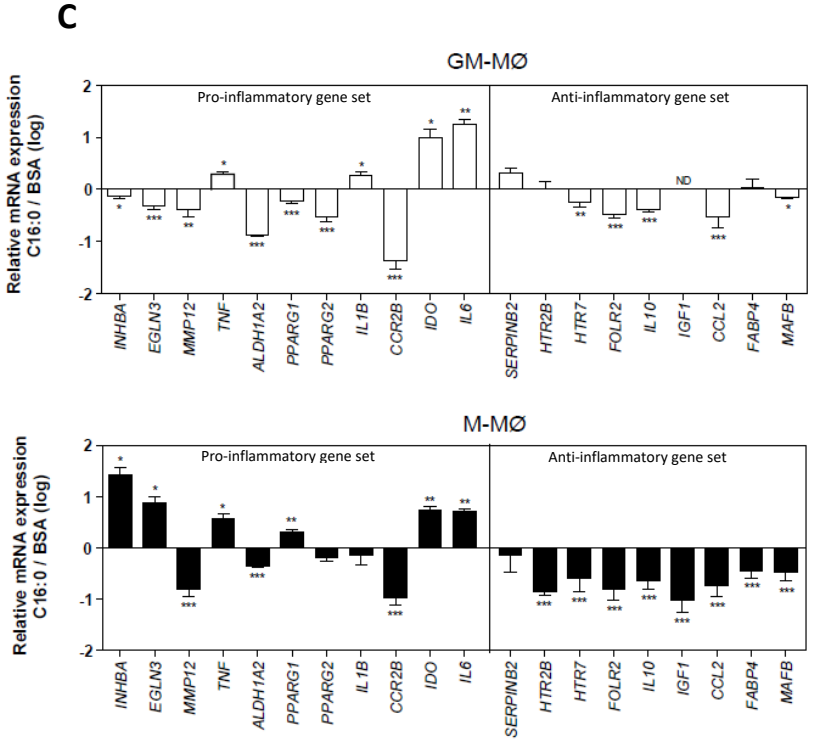
C
GM-MØ
M-MØ
Relative mRNA expression C16:0 / BSA (log)
Pro-inflammatory gene set
Anti-inflammatory gene set
ND
INHBA
EGLN3
MMP12
TNF
ALDH1A2
PPARG1
PPARG2
IL1B
CCR2B
IDO
IL6
SERPINB2
HTR2B
HTR7
FOLR2
IL10
IGF1
CCL2
FABP4
MAFB

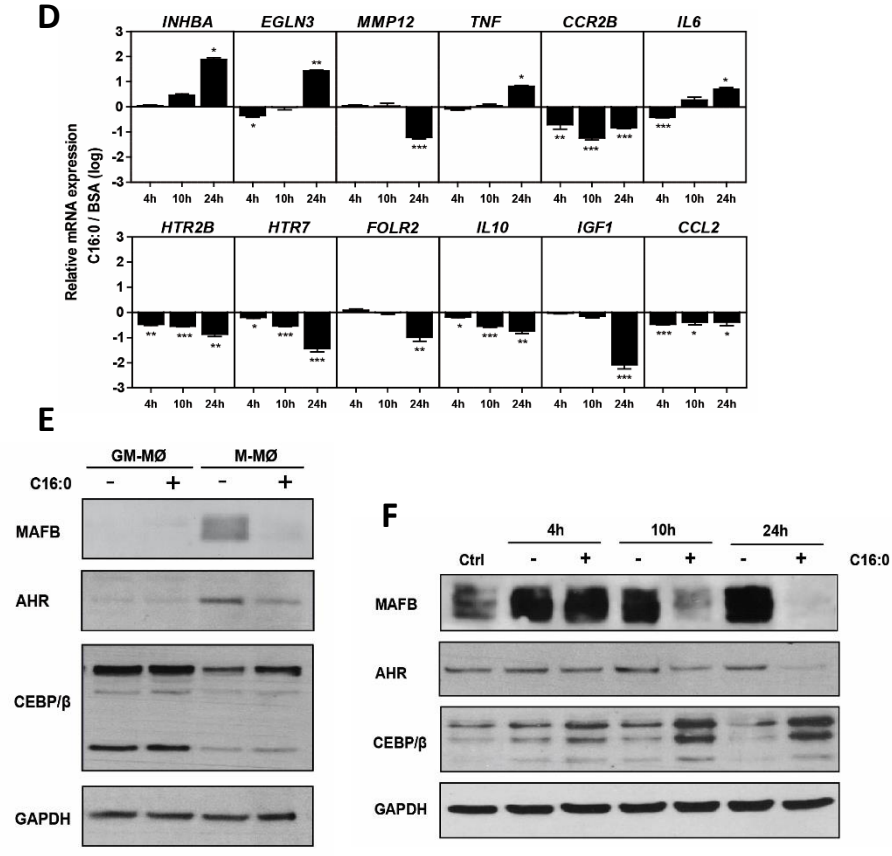

Figure 1. Functional, transcriptomic and transcription factor profile of palmitate-treated human macrophages. (A) Palmitate (C16:0) uptake by human macrophages (GM-MØ and M-MØ), as determined by Oil Red staining after 24 hours. For comparative purposes, macrophages were exposed in parallel to BSA (upper panels). **(B)** Levels of the indicated cytokines in the culture media of macrophages (GM-MØ and M-MØ) exposed to 200 µM palmitate (C16:0) or BSA for 24h, as determined ELISA. Shown is the mean ± SEM of ten independent experiments. **(C)** Relative mRNA expression of the indicated genes in GM-MØ and M-MØ exposed to 200 µM palmitate or BSA for 24h, as determined by qRT-PCR using *TBP* as a reference. Shown is the expression of each gene after palmitate treatment and relative to its expression after BSA treatment. Shown is the mean ± SEM of ten independent experiments. **(D)** Relative mRNA expression of the indicated genes in M-MØ exposed to 200 µM palmitate or BSA for 4h, 10h or 24h, as determined by qRT-PCR using *TBP* as a reference. Shown is the expression of each gene after palmitate treatment and relative to its expression after BSA treatment. Shown is the mean ± SEM of three independent experiments (*, $p<0.05$; **, $p<0.01$; ***, $p<0.001$). **(E)** Expression of MAFB, AhR and CEBP/β in macrophages (GM-MØ and M-MØ) treated with 200 µM palmitate or BSA (-) for 24h, as determined by Western blot. **(F)** Expression of MAFB, AhR and CEBP/β in M-MØ non-treated (Ctrl) or treated with 200 µM palmitate or BSA (-) for 4h, 10h or 24h, as determined by Western blot. In **(E-F)**, three independent experiments were done and one of them is shown, and GAPDH protein levels were determined in parallel as a protein loading control.

Palmitate and LPS induce distinct transcriptional profiles in human macrophages.

Innate immune cells sense palmitate as a danger signal via TLR4 [30, 31] and additional receptors [30, 32-34]. Numerous studies have already defined the LPS-induced transcriptional changes in mouse and human macrophages [35], and we have previously determined the global transcriptional profile of LPS-treated GM-MØ and M-MØ, and identified gene sets whose LPS responsiveness is distinct in GM-MØ and M-MØ (*Cuevas et al., unpublished*). Given the ability of TLR4 to recognize LPS or palmitate, we next compared the transcriptomic changes elicited by palmitate (200 µM) or LPS (10 ng/ml) for 4 h and 24 h on M-MØ. LPS and palmitate exhibited distinct transcriptional effects on genes of the "Pro-inflammatory gene set" and "Anti-inflammatory gene set" (Figure 2A), including opposite actions on the expression of *MMP12*, *PPARG1*, *CCR2B*, *IL10* and *CCL2* after 24 hours in M-MØ (Figure 2B). The differences in the transcriptional responses of M-MØ to LPS and palmitate were also observed upon analysis of a large set of LPS-regulated genes (Figure 3B) as *IDO1*, *MAOA*, *TNFRSF1B*, *EMR2*, *CCL19*, *LAMB3* and *TRIB3* expression was oppositely modified upon exposure to LPS or palmitate for 4h (Figure 3C) and 24h (Figure 3D). The differential regulation of IFN-regulated genes (*IDO1*, *CXCL10*) by LPS and palmitate was in agreement with the effect of either stimulus on STAT1, whose activation was exclusively promoted by LPS (Figure 3E). Altogether, this set of experiments indicate that palmitate induces a unique and specific transcriptional response in human macrophages, and that the palmitate-induced macrophage pro-inflammatory shift is only partly reminiscent of that triggered by LPS.

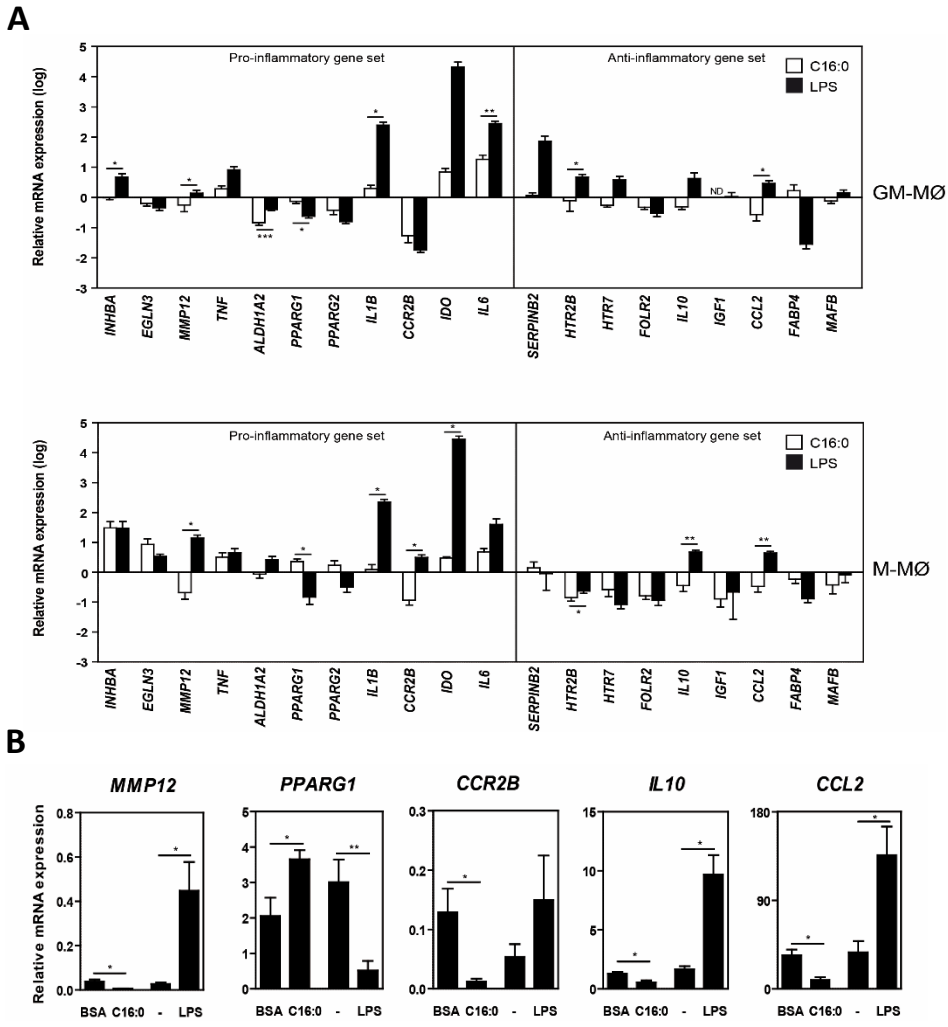

Figure 2. Comparison of the transcriptomic changes elicited by palmitate or LPS on human macrophages. (A) Relative mRNA expression of the "Pro-inflammatory gene set" and "Anti-inflammatory gene set" in GM-MØ and M-MØ exposed to either 200 µM palmitate (C16:0) or 10 ng/ml LPS for 24 hours. Results are presented as the mRNA expression of each gene after palmitate or LPS treatment and relative to the mRNA expression of the same gene after treatment with either BSA (control for palmitate treatment) or no treatment (control for LPS stimulation). **(B)** Relative mRNA expression of the indicated polarization-specific genes in M-MØ untreated (-) or exposed to 10 ng/ml LPS, 200 µM palmitate (C16:0) or BSA for 24h, as determined by qRT-PCR using *TBP* as a reference. Results are shown as mean ± SEM of five independent experiments (*, p<0.05; **, p<0.01; ***, p<0.001).

Results

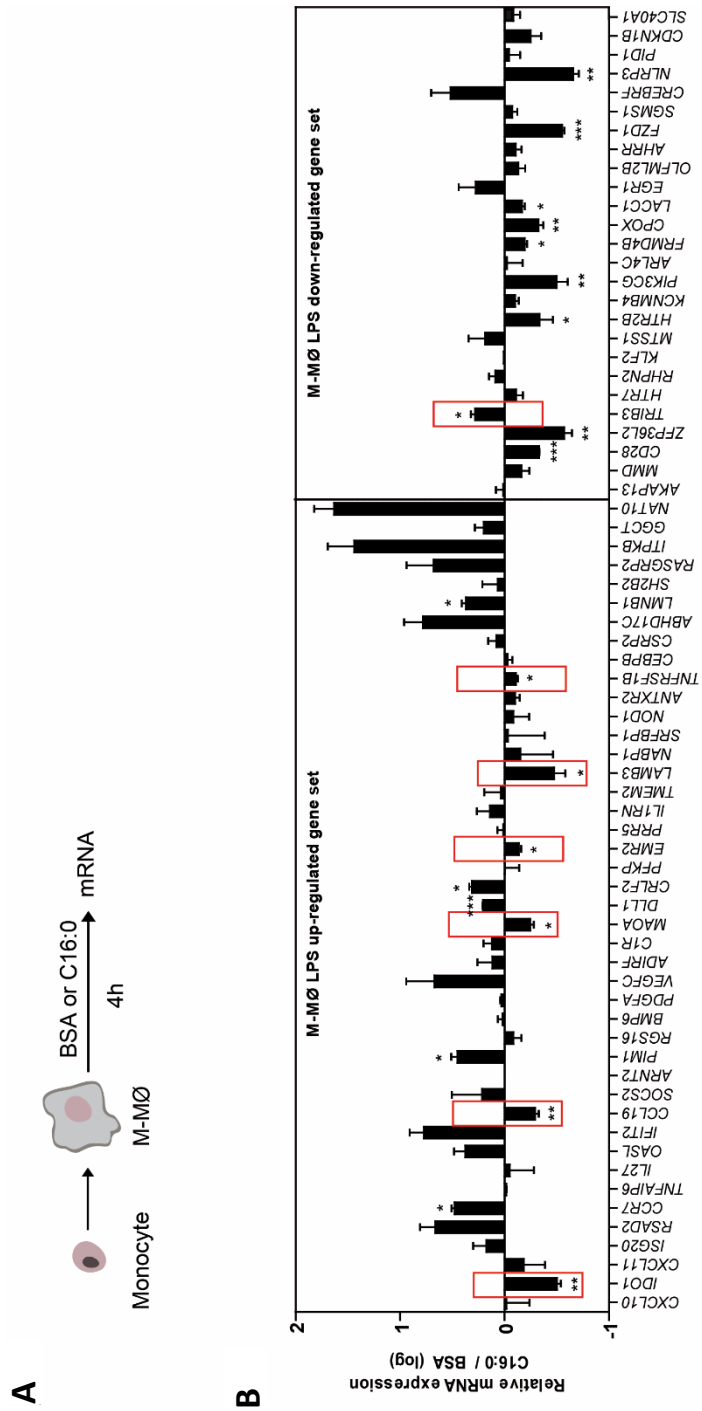
A
Monocyte
M-MØ
BSA or C16:0
4h
mRNA
B
M-MØ LPS up-regulated gene set
M-MØ LPS down-regulated gene set
Relative mRNA expression
C16:0 / BSA (log)
2
1
0
-1
CXCL10
IDO1
CXCL11
ISG20
RSAD2
CCR7
TNFAIP6
IL27
OASL
IFIT2
CCL19
SOCS2
ARNT2
PIM1
RGS16
BMP6
PDGFA
VEGFC
ADIRF
C1R
MAOA
DLL1
CRLF2
PFKP
EMR2
PRR5
IL1RN
TMEM2
LAMB3
NABP1
SRFBP1
NOD1
ANTXR2
TNFRSF1B
CEBPB
CSRP2
ABHD17C
LMNB1
SH2B2
RASGRP2
ITPKB
GGCT
NAT10
AKAP13
MMD
CD28
ZFP36L2
TRIB3
HTR7
RHPN2
KLF2
MTSS1
HTR2B
KCNMB4
PIK3CG
ARL4C
FRMD4B
CPOX
LACC1
EGR1
OLFML2B
AHRR
FZD1
SGMS1
CREBRF
NLRP3
PID1
CDKN1B
SLC40A1

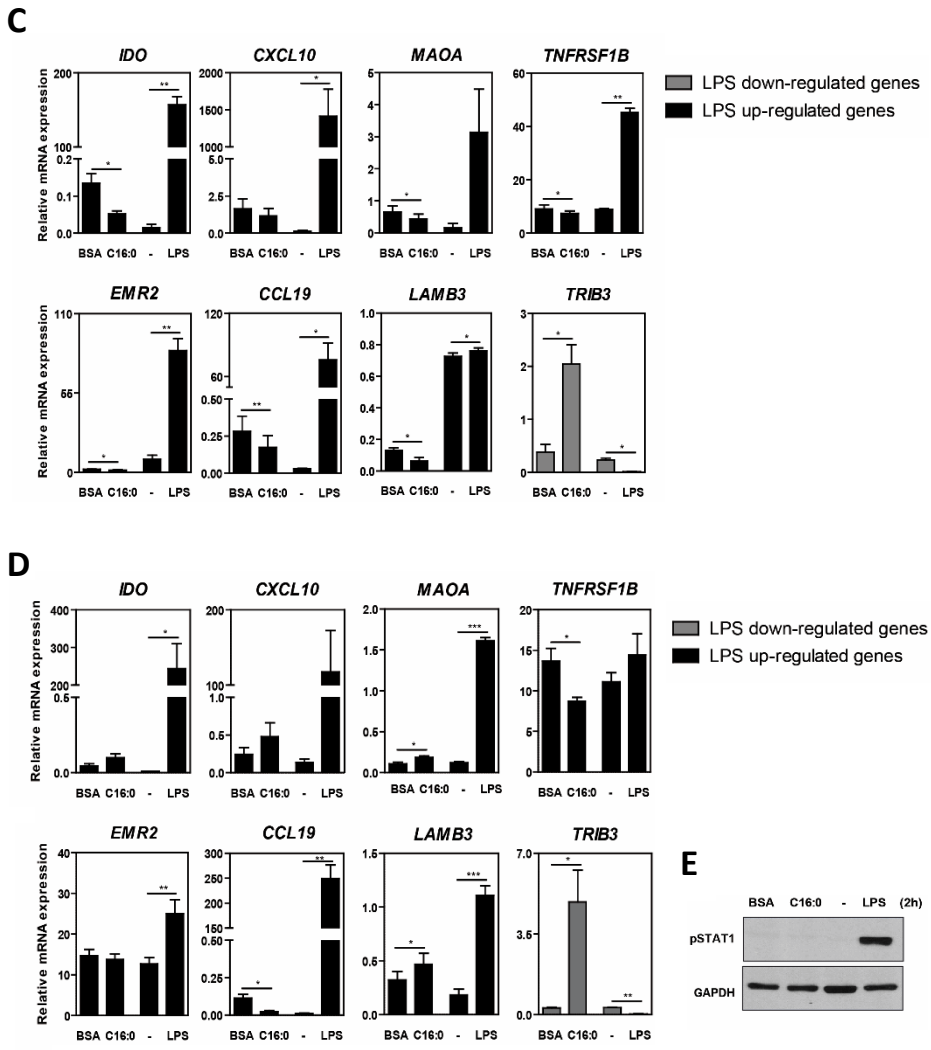

Figure 3. Comparison of the transcriptomic changes elicited by palmitate or LPS-regulated genes on human macrophages. (A) Experimental design of the experiment. **(B)** Relative mRNA expression of the indicated LPS-responsive genes in M-MØ exposed to either 200 µM palmitate (C16:0) or BSA for 4 hours. Results are presented as the mRNA expression of each gene after palmitate treatment and relative to the mRNA expression of the same gene after treatment with BSA. Shown is the mean ± SEM of three independent experiments. **(C, D)** Relative mRNA expression of the indicated LPS-regulated genes in M-MØ untreated (-) or exposed to 10 ng/ml LPS, 200 µM palmitate or BSA for **(C)** 4h or **(D)** 24h, as determined by qRT-PCR using *TBP* as a reference. In **(C-D)** results are shown as mean ± SEM of five independent experiments. **(E)** Expression of activated STAT1 in M-MØ non-treated (-) or treated with 10 ng/ml LPS, 200 µM palmitate or BSA for 2h, as determined by Western blot. GAPDH protein levels were determined in parallel as a protein loading control. (#, $p<0.06$; *, $p<0.05$; **, $p<0.01$; ***, $p<0.001$).

JNK activation mediates the transcriptional changes triggered by palmitate on human macrophages.

Screening of the phosphorylation state of intracellular signaling molecules after palmitate treatment identified JNK as the kinase with the higher level of palmitate-induced activation (Figure 4A,B). Correspondingly, c-Jun was also found to be phosphorylated in M-MØ exposed to palmitate for 4h (Figure 4A). The contribution of the palmitate-induced JNK activation to the transcriptional changes promoted by the fatty acid was next assessed using the selective JNK inhibitor SP600125 (Figure 4C). JNK inhibition significantly impaired the palmitate effect on the expression of *INHBA*, *TNF*, *IL10*, *IGF1*, *MAFB* and *TRIB3* (Figure 4D). In addition, the JNK inhibitor also diminished the palmitate-induced downregulation of MAFB protein expression (Figure 4E). Therefore, JNK activation mediates the palmitate-dependent modification of the transcriptional profile of human macrophages and also contributes to the palmitate-induced loss of MAFB, whose expression is required for the acquisition of the macrophage anti-inflammatory profile [26].

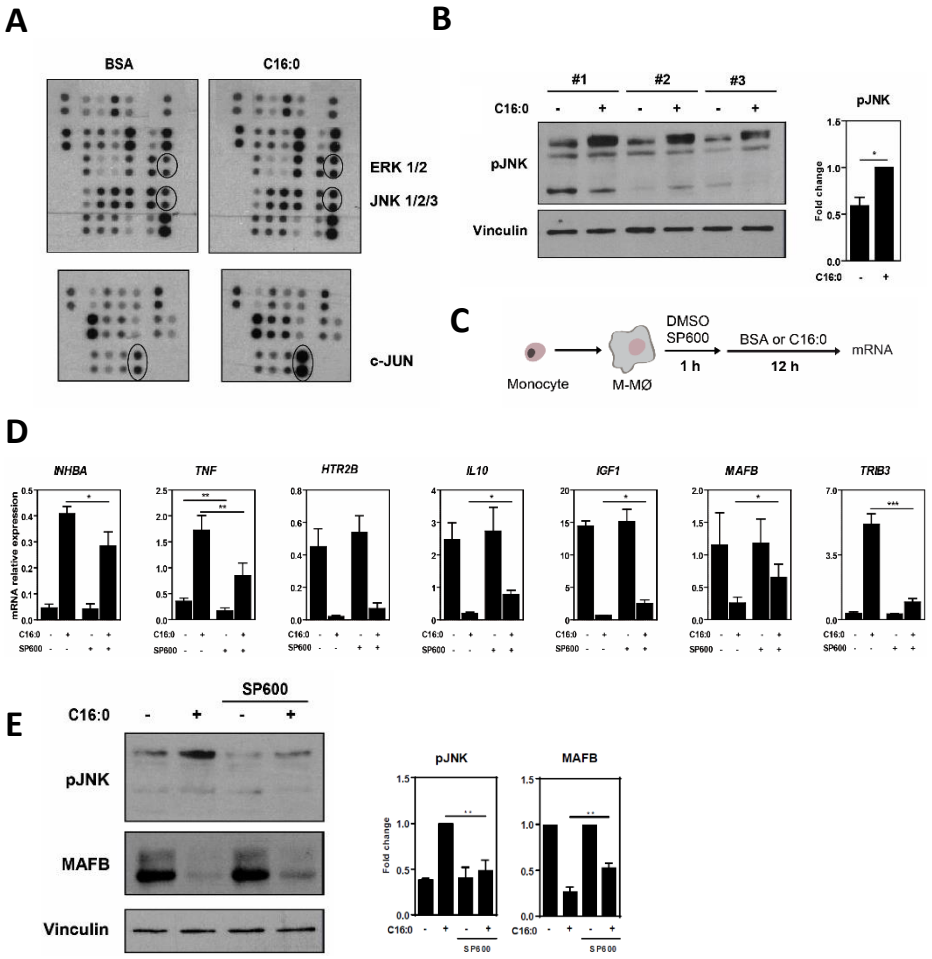

Figure 4. Effect of JNK activation on the palmitate-induced transcriptional changes in human macrophages. (A) M-MØ were left untreated (BSA) or exposed to 200 µM palmitate (C16:0) for 4h, and the phosphorylation state of representative signaling molecules was determined using the Proteome Profiler® protein array (R&D Systems, USA). The kinases specifically mentioned in the text are indicated. **(B)** M-MØ from three independent donors (#1-3) were left treated with BSA (-) or exposed to 200 µM palmitate (C16:0) for 4h, and the phosphorylation state of JNK was determined by Western blot using specific antibodies. The level of vinculin was determined in parallel as a protein loading control. Right panels show the mean ± SEM of the densitometric analysis of the three experiments (*, $p<0.05$). **(C)** Schematic representation of the experimental procedure. **(D)** Relative mRNA expression of the indicated genes in M-MØ exposed to SP600125 (SP600) or DMSO (-) for 1 hour and exposed to BSA (-) or 200 µM palmitate (C16:0) for 12h, as determined by qRT-PCR using *TBP* as a reference. Results are shown as mean ± SEM of five independent experiments (*, $p<0.05$; **, $p<0.01$; ***, $p<0.001$). **(E)** JNK activation and MAFB protein levels in M-MØ untreated or exposed to SP600125 (SP600) for 1 hour and then exposed to BSA (-) or 200 µM palmitate (C16:0) for 12h, as determined by determined by Western blot using specific antibodies. The level of vinculin was determined in parallel as a protein loading control. The experiment was performed on four independent M-MØ preparations, and one of them is shown. Right panels show the mean ± SEM of the densitometric analysis of the four experiments (**, $p<0.01$).

Palmitate conditions the LPS-induced cytokine profile of M-MØ.

Macrophages are extremely sensitive to the surrounding extracellular milieu and their exposure to an initial stimulus determines their subsequent functional responses to additional stimuli [36-39]. Since palmitate levels are enhanced in obesity-related pathologies, whose comorbidities include altered inflammatory responses, we hypothesized that palmitate exposure might also condition human macrophages for altered responses to additional stimuli. Thus, we initially assessed whether palmitate influences LPS-initiated intracellular signaling in M-MØ. Palmitate alone caused only a very low NFκB activation (as illustrated by a weak phosphorylation of p65) (Figure 5A) and a weak reduction in basal STAT3 phosphorylation levels (Figure 5B). However, palmitate had a remarkable effect on the intracellular signaling pathways activated by LPS. Specifically, palmitate pre-treatment (24h) led to more potent LPS-induced activation of NFκB (as evidenced by increased phosphorylation of IKKαβ and p65 and a more profound loss of IκBα, Figure 5A), lower LPS-induced STAT1 and STAT3 phosphorylation, and higher LPS-induced activation of IRF3, p38MAPK and JNK (Figure 5A,B). Therefore, the presence of palmitate conditions the intracellular signaling triggered by a pathogenic stimulus in macrophages.

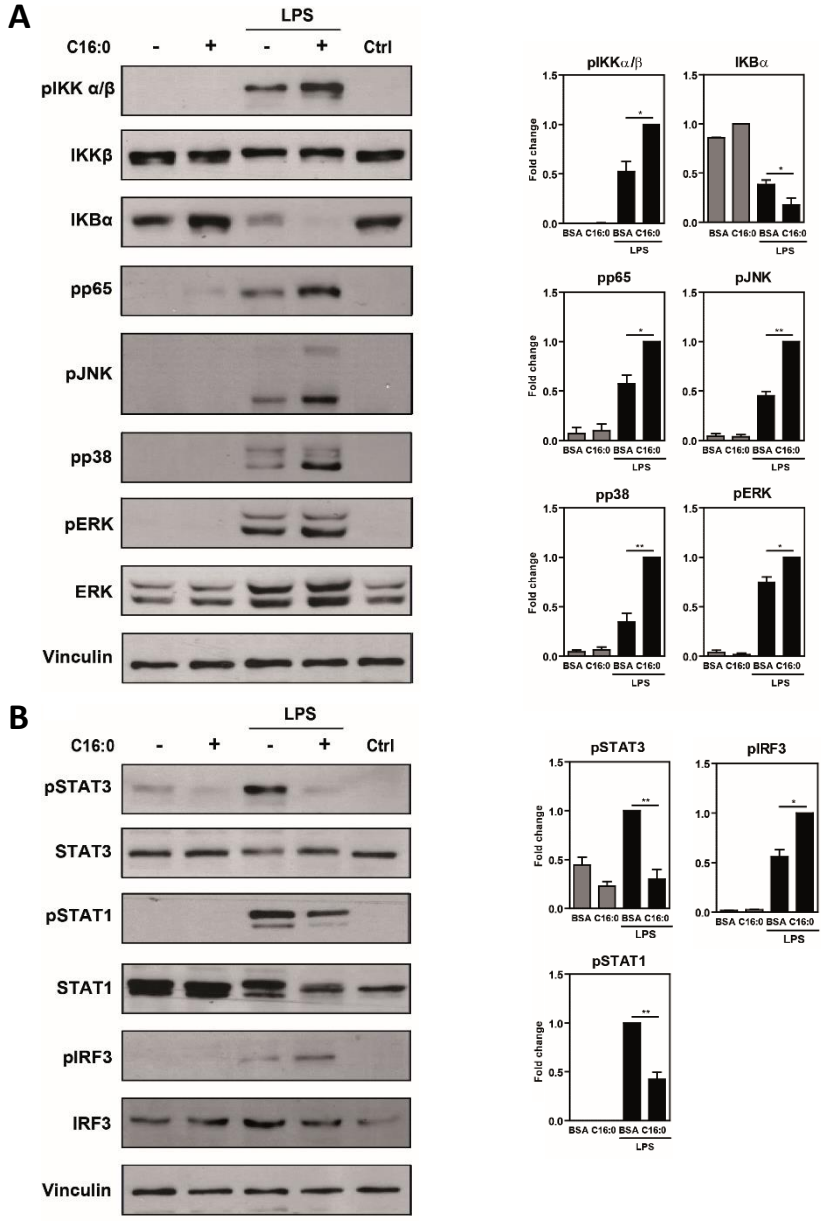

Figure 5. Palmitate exposure modulates LPS-initiated intracellular signalling in human macrophages. (A,B) Determination of the phosphorylation state of **(A)** IKKα/β, IκBα, NFκB p65, ERK1/2, JNK, p38 MAPK, STAT3, STAT1 and IRF3 in M-MØ exposed to BSA (-) or palmitate (C16:0) for 24 h and then stimulated with LPS (10 ng/ml) for 15-30 min **(A)** or 120 min **(B)**. The total levels of IKKα/β, ERK1/2, STAT3, STAT1 and IRF3 were determined in parallel. The levels of vinculin were determined as a protein loading control. The levels of each protein were also determined in untreated cells (Ctrl). In all cases, four independent experiments were performed, and one of them is shown. In **(A,B)**, right panels show the mean ± SEM of the densitometric analysis of the four experiments (*, $p<0.05$; **, $p<0.01$).

Next, we evaluated whether palmitate also modulates the transcriptional responses initiated by LPS in M-MØ. To that end, macrophages were exposed to palmitate (24 h) before stimulation with LPS (4 h), and the expression of the gene sets whose LPS responsiveness is distinct in GM-MØ and M-MØ (*Cuevas et al., unpublished*) was determined. Palmitate pre-treatment greatly altered the LPS-induced transcriptional response, with a profound effect on the expression of genes upregulated by LPS exclusively in M-MØ (Figure 6B,C). Specifically, palmitate significantly impaired the LPS-induced upregulation of 25% of the genes whose expression in enhanced by LPS only in M-MØ (Figure 6B,D), an effect that was most pronounced on genes with the highest M-MØ-specific upregulation by LPS (*CCL19, ARNT2, RGS16, ADIRF, MAOA*) (*Cuevas et al., unpublished*) (Figure 6B). Regarding the gene set whose expression in diminished by LPS only in M-MØ (Figure 6B), palmitate impaired the LPS-induced downregulation of 25% of them (5 out of 26), and concomitantly potentiated the LPS-induced downregulation of six genes (Figure 6B,D). Therefore, exposure to palmitate significantly affects the LPS-regulated gene expression in human macrophages.

Study III

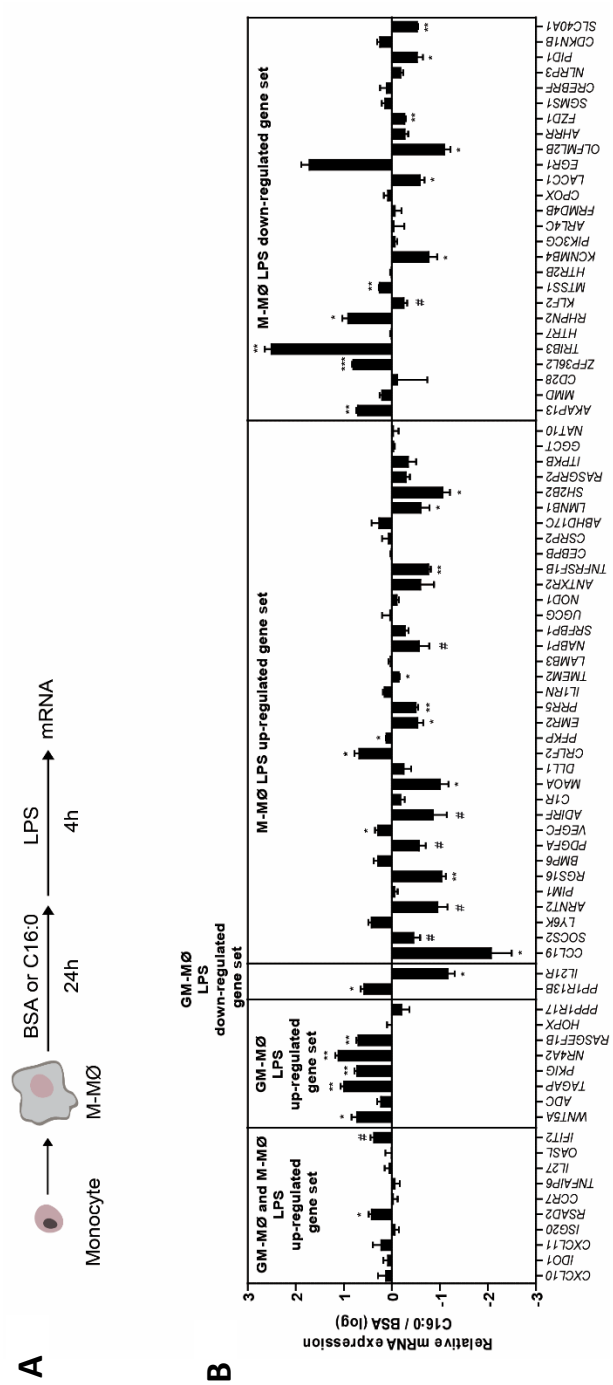
A
Monocyte
M-MØ
BSA or C16:0
24h
LPS
4h
mRNA
B
GM-MØ and M-MØ LPS up-regulated gene set
GM-MØ LPS up-regulated gene set
GM-MØ LPS down-regulated gene set
M-MØ LPS up-regulated gene set
M-MØ LPS down-regulated gene set
Relative mRNA expression C16:0 / BSA (log)
3
2
1
0
-1
-2
-3
CXCL10
IDO1
CXCL11
ISG20
RSAD2
CCR7
TNFAIP6
IL27
OASL
IFIT2
WNT5A
ADC
TAGAP
PKIG
NR4A2
RASGEF1B
HOPX
PPP1R17
PPP1R13B
IL21R
CCL19
SOCS2
LY6K
ARNT2
PIM1
RGS16
BMP6
PDGFA
VEGFC
ADIRF
C1R
MAOA
DLL1
CRLF2
PFKP
EMR2
PRR5
IL1RN
TMEM2
LAMB3
NAIP1
SRFBP1
UGCG
NOD1
ANTXR2
TNFRSF1B
CEBPB
CSRP2
ABHD17C
LMNB1
SH2B2
RASGRP2
ITPKB
GGCT
NAT10
AKAP13
MMD
CD28
ZFP36L2
TRIB3
HTR7
RHPN2
KLF2
MTSS1
HTR2B
KCNMB4
PIK3CG
ARL4C
FRMD4B
CPOX
LAC1
EGR1
OLFML2B
AHRR
FZD1
SGMS1
CREBRF
NLRP3
PID1
CDKN1B
SLC40A1

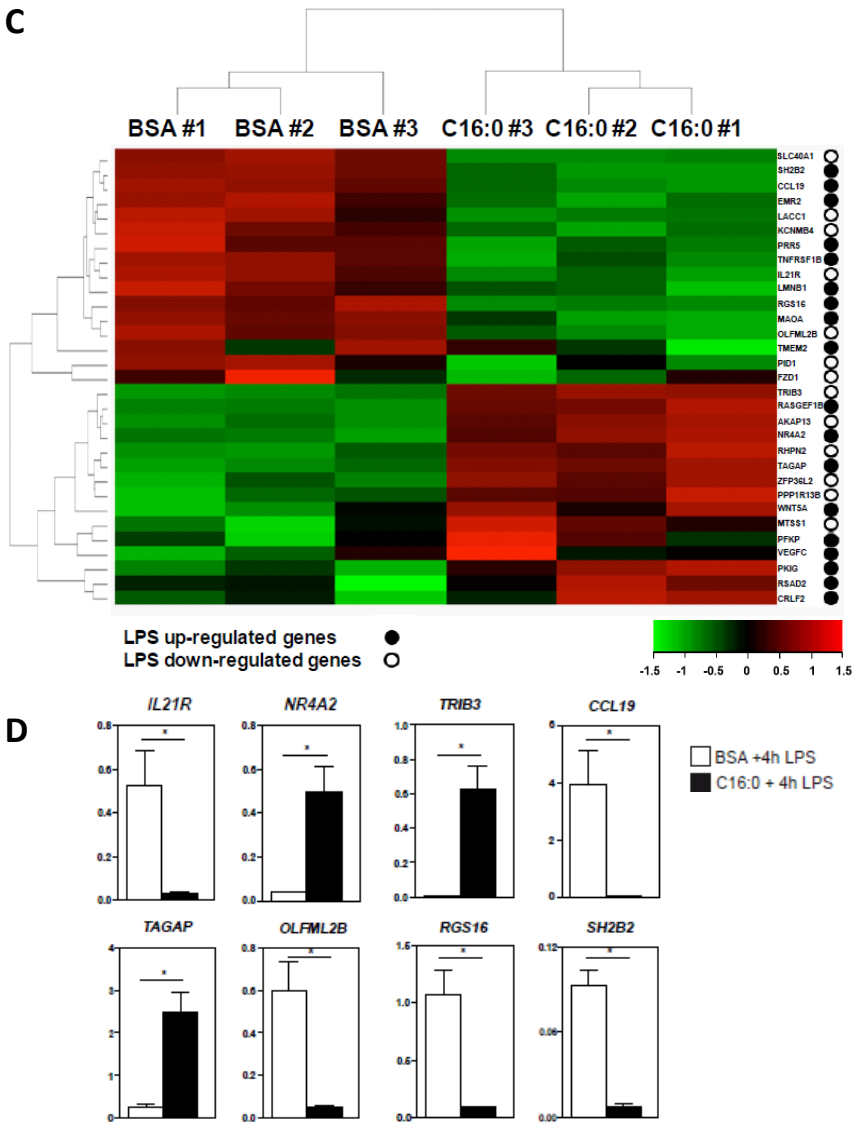

Figure 6. Palmitate pre-treatment alters the LPS-induced transcriptomic response in human macrophages. (A) Experimental design of the experiment. **(B)** Relative mRNA expression of the indicated LPS-responsive genes in M-MØ exposed to either 200 µM palmitate (C16:0) or BSA for 24 h and later stimulated with 10 ng/ml LPS for 4 hours. Results represent the LPS-induced changes in the mRNA expression of each gene in cells pre-treated with palmitate and relative to the expression of the same gene in cells pre-treated with BSA. Shown is the mean ± SEM of three independent experiments. **(C)** Heat map representation of the mRNA expression of the LPS-regulated genes whose expression is significantly different ($p < 0.05$) in M-MØ exposed to either BSA or 200µM palmitate (C16:0) (24 h) before stimulation with LPS (10ng/ml) for 4 hours. The effect of LPS on the expression of the analysed genes is shown. **(D)** Relative mRNA expression of the indicated genes in M-MØ exposed to either BSA or 200µM palmitate (C16:0) (24 h) before stimulation with LPS (10ng/ml) for 4 hours, as determined by qRT-PCR using *TBP* as a reference. Shown is the mean ± SEM of three independent experiments (#, $p<0.06$; *, $p<0.05$; **, $p<0.01$; ***, $p<0.001$).

Finally, we evaluated whether pre-exposure to palmitate affected the production of LPS-induced cytokines of human macrophages. To that end, M-MØ were exposed to palmitate for 24 h and then stimulated with LPS (Figure 7A). Palmitate pre-treatment significantly enhanced the LPS-induction of the pro-inflammatory cytokines TNFα, IL-6 and IL-1β, while inhibited LPS-induced IL-10 and CCL2 production, by M-MØ (Figure 7B). Therefore, palmitate not only limits the differentiation of anti-inflammatory (M-CSF-dependent) M-MØ but primes M-MØ for increased production of pro-inflammatory cytokines, and reduced production of anti-inflammatory cytokines, in response to a pathogenic stimulus like LPS. Importantly, these effects of palmitate are fatty-acid-specific since the unsaturated free fatty acid oleate (C18:1) was efficiently taken up by human macrophages (Figure 8A) but neither modified the basal level of expression of MAFB, AhR and C/EBPβ in M-MØ (Figure 8B) nor altered the LPS-induced production of TNFα, IL-6 and CCL2 (Figure 8C). Besides, and lending further relevance to its transcriptional effects, palmitate pre-treatment completely blocked the LPS-induced production of the CCL19 chemokine by M-MØ (Figure 7B).

JNK activation mediates the ability of palmitate to condition macrophage responses to LPS.

The ability of palmitate to modify the LPS-induced cytokine profile of M-MØ correlates with its capacity to modulate LPS-initiated intracellular signaling (shown in Figure 5). Such a correlation is especially relevant in the case of JNK, which play a central role in the development of inflammation in adipose tissue and insulin resistance in animal models [40]. Given the ability of palmitate to activate JNK, we analyzed whether the palmitate-induced JNK activation contributes to its macrophage-conditioning effect. Inhibition of JNK activation by SP600125 reduced the palmitate-dependent inhibition in

the production of LPS-induced IL-10 (Figure 7D). Therefore, the palmitate-induced JNK activation modifies the macrophage transcriptome and also mediates the ability of palmitate to alter macrophage responses towards pathogenic stimuli like LPS.

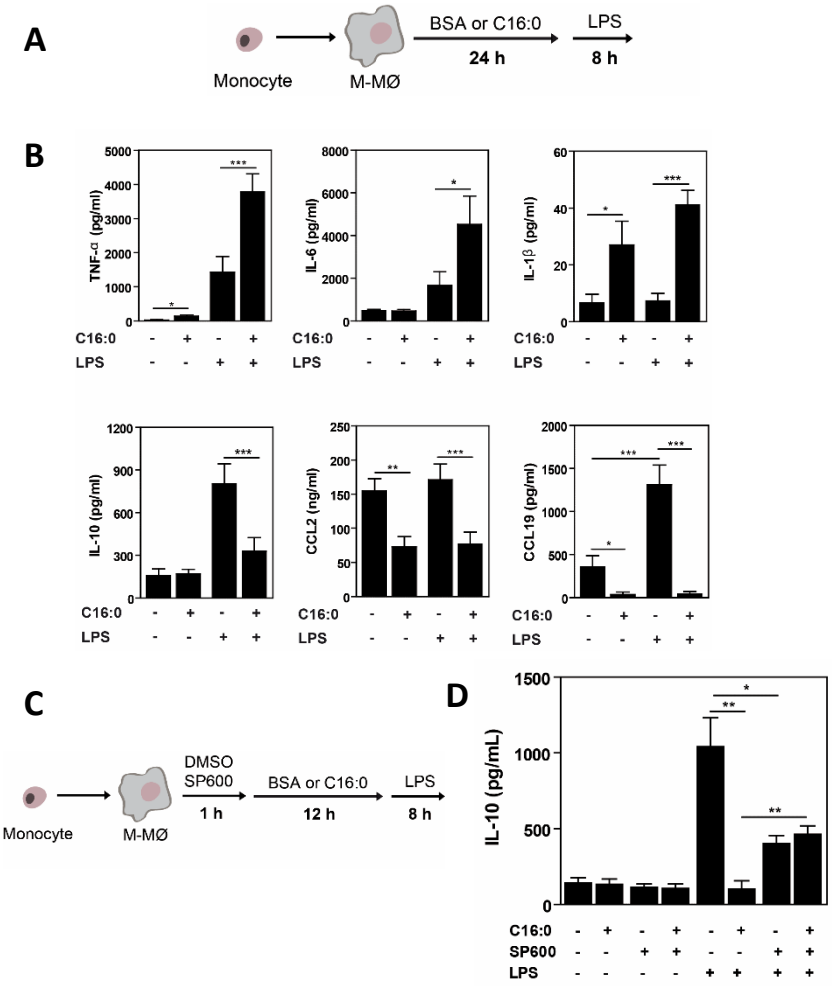

Figure 7. Effect of palmitate treatment on the LPS-induced cytokine profile in human macrophages. (A) Schematic representation of the experimental procedure. **(B)** Levels of the indicated cytokines in the culture supernatants of macrophages (M-MØ) exposed to 200 µM palmitate (C16:0) or BSA (-) for 24h before stimulation with 10 ng/ml LPS for 8 hours. Shown is the mean ± SEM of eight independent experiments (*, p<0.05; **, p<0.01; ***, p<0.001). **(C)** Schematic representation of the experimental procedure. **(D)** Levels of IL-10 in the culture media of macrophages (M-MØ) not treated o treated with SP600125 (SP600), and then exposed to 200 µM palmitate (C16:0) or BSA (-) (24h) before stimulation with 10 ng/ml LPS (8h). Shown is the mean ± SEM of four independent experiments (*, p<0.05; **, p<0.01).

Study III

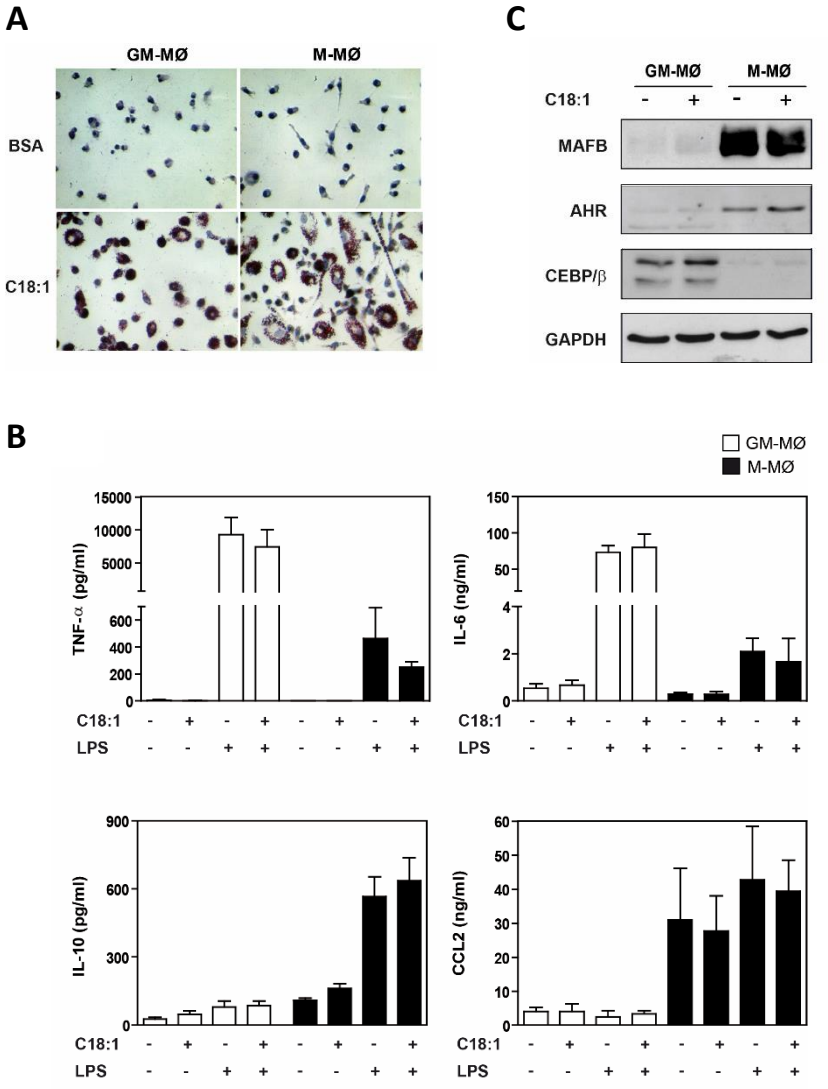

Figure 8. Functional and transcription factor profile of oleate-treated human macrophages. **(A)** Oleate uptake by human macrophages (GM-MØ and M-MØ), as determined by Oil Red staining. For comparative purposes, macrophages were exposed in parallel to BSA (upper panels). **(B)** Expression of MAFB, AhR and CEBP/β in macrophages (GM-MØ and M-MØ) treated with 200 µM oleate (C18:1) or BSA (-) for 24h, as determined by Western blot. GAPDH protein levels were determined in parallel as a protein loading control. **(C)** Levels of the indicated cytokines in the culture media of macrophages (GM-MØ and M-MØ) exposed to 200 µM oleate (C18:1) or BSA (-) for 24h before stimulation with 10 ng/ml LPS for 8 hours. Shown is the mean ± SEM of three independent experiments (*, $p<0.05$).

Lithium chloride impairs the palmitate-induced loss of MAFB and abrogates the ability of palmitate to inhibit LPS-induced IL-10 production

We have previously shown that MAFB regulates the expression of the "Anti-inflammatory gene set", and that MAFB protein levels correlate with IL-10 production in human macrophages [26]. Interestingly, MAFB regulates human adipose tissue inflammation [41] and its deficiency in hematopoietic cells accelerates obesity [42]. MAFB protein stability is regulated by the JNK and ubiquitin–proteasome pathway [43], what agrees with the JNK-dependent ability of palmitate to downregulate MAFB protein levels (Figure 4). However, MAFB degradation is also controlled by a GSK3β-mediated phosphorylation of the transcriptional activation domain [44]. Since palmitate activates GSK3β [45, 46] and GSK3β inhibition suppresses palmitate-induced JNK phosphorylation in human liver cells [45], we hypothesized that GSK3β inhibition might alter palmitate effects on the macrophage cytokine profile. To determine whether the GSK3β/MAFB axis contributes to the inhibitory action of palmitate on the LPS-induced IL-10 production, we exposed macrophages to palmitate in the presence of Lithium Chloride (LiCl, 30 mM), a well-known GSK3β inhibitor [47, 48]. As shown in Figure 9A, LiCl inhibited the palmitate-induced MAFB downregulation, an effect not observed in the presence of NaCl. LiCl also significantly reduced the inhibitory effect of palmitate on the expression of MAFB-regulated genes like *SLC40A1*, *IL10* and *CCL2* (Figure 9B). More importantly, the presence of LiCl, but not a similar concentration of NaCl, completely abrogated the inhibitory effect of palmitate on the LPS-induced IL-10 production in human macrophages (Figure 9C). Therefore, Lithium chloride impairs two relevant palmitate-dependent effects (MAFB downregulation and loss of LPS-induced expression), thus suggesting that

modulation of the GSK3β/MAFB axis also contributes to the pro-inflammatory activity of palmitate.

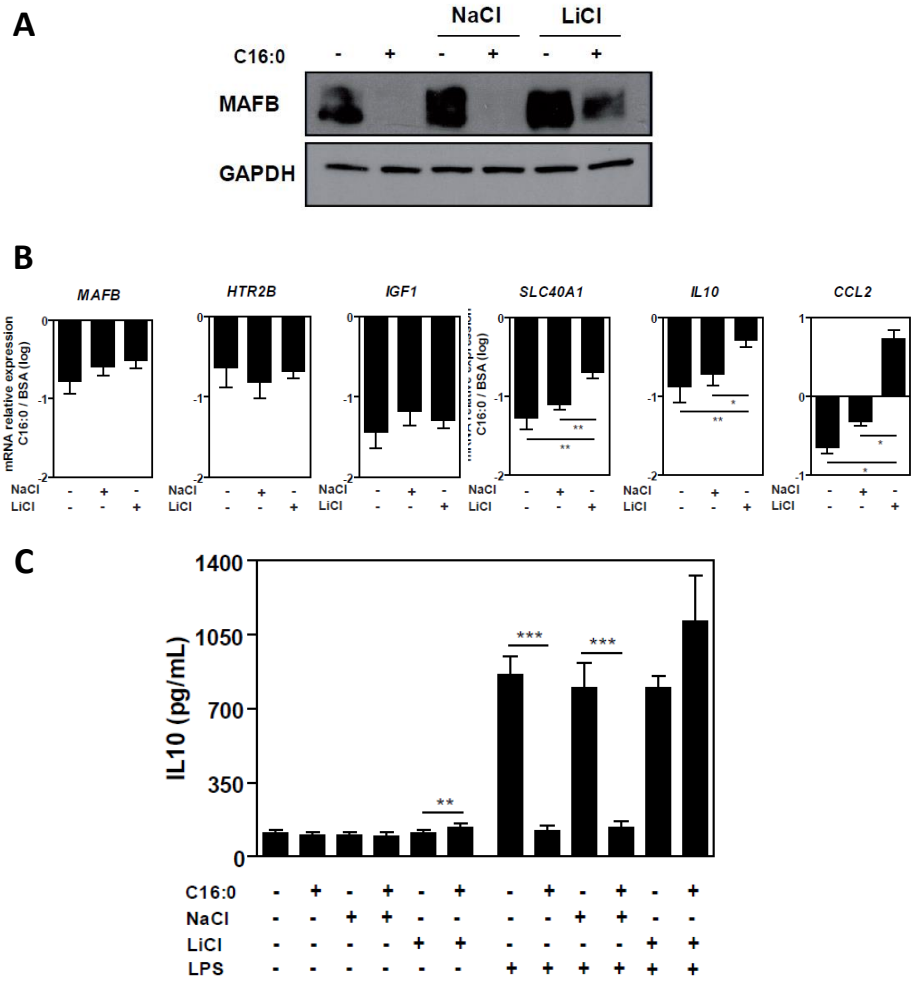

Figure 9. Lithium chloride inhibits palmitate-dependent effects in human macrophages. (A) Expression of MAFB in macrophages (M-MØ) treated with LiCl or NaCl before exposure to 200 µM palmitate (C16:0) or BSA (-) for 24h, as determined by Western blot. **(B)** Relative mRNA expression of the indicated genes in M-MØ treated with LiCl or NaCl before exposure to 200 µM palmitate (C16:0) or BSA for 24h, as determined by qRT-PCR using *TBP* as a reference. The expression of each gene after palmitate treatment and relative to its expression after BSA treatment is indicated. Shown is the mean ± SEM of six independent experiments (*, p<0.05; **, p<0.01). **(C)** Levels of IL-10 in the culture media of macrophages (M-MØ) not treated o treated with LiCl or NaCl, and then exposed to 200 µM palmitate (C16:0) or BSA (-) (24h) before stimulation with 10 ng/ml LPS (8h). Shown is the mean ± SEM of six independent experiments (**, p<0.01; ***, p<0.001).

Discussion

Macrophages are critically involved in the initiation and resolution of inflammatory processes, and their deregulated activation contributes to chronic inflammatory diseases [4]. In the case of chronic inflammation associated to metabolic syndromes, the production of pro-inflammatory cytokines by macrophages correlates with the serum concentration of SFA [49], whose increased levels modify macrophage effector functions either by itself (e.g., palmitate) [10] or in combination with high levels of glucose and insulin [50]. Taking advantage of the previous identification of gene sets that specifically define the pro-inflammatory and anti-inflammatory state of human macrophage [18, 25], we now report that palmitate promotes the acquisition of a pro-inflammatory state that depends on JNK and differs from the LPS-induced pro-inflammatory activation at the transcriptional and functional levels. Further supporting the specificity of the palmitate-induced macrophage activation, we also provide evidences that, unlike LPS, palmitate conditions ("trains") human macrophages for stronger pro-inflammatory responses towards pathogenic stimuli.

Since metabolic diseases are driven by a low-grade inflammation and elevated levels of pro-inflammatory cytokines [51], the ability of palmitate to condition macrophage responses to other inflammatory stimuli (e.g., LPS) has very relevant pathological implications. It is now well established that metabolic endotoxemia initiates obesity and insulin resistance and, in fact, lowering plasma LPS concentration has been proposed as a strategy to tackle metabolic diseases [52]. Consequently, the palmitate pro-inflammatory conditioning that we now report might exacerbate the pro-inflammatory responses of monocyte/macrophage towards pathogen-associated molecular patterns (PAMP) (e.g., LPS) derived from bacteria translocating from the gut, thus enhancing the production of PAMP-induced inflammatory

cytokines. In agreement with the palmitate-induced increased LPS-responsiveness, palmitate conditions macrophages for stronger LPS-induced NFκB, IRF3, p38, ERK and JNK signaling. Since NFκB and JNK are chronically activated in adipose tissue from obese and insulin resistance subjects [53] and JNK activation in mouse macrophages is required for obesity-induced insulin resistance and inflammation [40], the macrophage-conditioning ability of palmitate that we now report might contribute to the known association between bacterial DNA translocation and increased insulin resistance [54].

The macrophage-conditioning ability of palmitate also resembles the effect of PAMPs like β-glucan, which render macrophages more responsive to a subsequent stimulation by LPS [38, 39]. This "boosting" effect has led to the concept of "trained immunity" and allowed the demonstration that innate immunity cells like macrophages produce much higher levels of pro-inflammatory cytokines if previously exposed to certain "training" stimuli [38, 39]. From this point of view, the changes that we have detected in palmitate-treated macrophages (loss of AhR and MAFB expression, reduced expression of the anti-inflammatory gene set) are compatible with the acquisition of a "palmitate-trained state" that would confer palmitate-conditioned macrophages with the ability to produce higher levels of pro-inflammatory cytokines upon exposure to a second stimulus.

The capacity of palmitate to downregulate MAFB protein expression in macrophages is especially relevant for the whole set of transcriptional and functional changes triggered by this SFA. Palmitate exerts rapid transcriptional effects and upregulates the expression of the macrophage "pro-inflammatory gene set" (*INHBA, EGLN3*) [18, 25] in less than 24 hours, a time at which palmitate has also provoked the loss of the transcription factors that drive "anti-inflammatory gene set" expression (AhR, MAFB) [18,

25]. The loss of MAFB expression appears to critically underlie the pro-inflammatory ability of palmitate because MAFB is a major positive regulator for the expression of a significant number of genes that characterize anti-inflammatory IL-10-producing macrophages (e.g., *IL10, IGF1, CCL2*) [26]. Importantly, the palmitate-induced loss of MAFB expression is partly mediated by JNK, an effect that is in line with the ability of JNK to promote MAFB ubiquitination [43] and agrees with the known pro-inflammatory nature of JNK in vivo [40]. Besides, MAFB protein levels are also controlled by other kinases like GSK3β [44], whose activation state might be also affected by palmitate [46]. In this regard, it is worth noting that the diminished LPS-induced production of IL-10 seen in palmitate-treated macrophages can be prevented by lithium chloride, a well-known GSK3β inhibitor [55] (*Riera-Borrull and Corbí, data not shown*). Whereas this effect of lithium chloride (enhanced levels of IL-10 after macrophage re-stimulation) would fit with the potential ability of GSK3 inhibitors to overcome insulin resistance, the involvement of the GSK3β kinase in the human macrophage "palmitate training" is also counterintuitive since GSK3β mediates TNFα-induced cross-tolerance [56].

Previous studies have assumed that palmitate activation of macrophages mostly resembles LPS-induced mechanisms because palmitate is recognized by TLR4 and activates pro-inflammatory signaling pathways *in vitro* and in vivo [10]. However, and in line with previous reports [11-13], our results indicate that palmitate and LPS differ in their respective transcriptional and functional effects on human macrophages. Thus, palmitate and LPS oppositely modulate the expression of genes like *IDO1*, *MAOA*, *EMR2* and *LAMB3*. Palmitate and LPS also differ in terms of the intracellular signaling triggered in human macrophages. Palmitate leads to JNK activation at late time points, but causes a very weak NFκB activation and has not effect on

STAT1/STAT3 or IRF3 phosphorylation (Figure 5). In fact, palmitate pre-treatment even reduces the LPS-induced activation of STAT1 and STAT3. This differential signaling ability of palmitate and LPS correlates with their distinct effect on the expression of IFN-regulated genes like *IDO1*, and strongly suggests that the palmitate-initiated intracellular signaling originates from TLR4 and additional PAMP/DAMP receptors.

Especially relevant is the fact that palmitate and LPS differentially regulate the expression of *CCL19* and *TRIB3*. Contrarily to the effect of LPS, which greatly enhances *CCL19* mRNA (*Cuevas and Corbí, data not shown*), palmitate significantly downregulates CCL19 at the mRNA and protein level (Figure 3) and even abrogates the LPS-induced upregulation of CCL19 production (Figure 7). Together with CCL21, the chemokine CCL19 is a ligand of CCR7, whose expression critically determines lymph node homing of T cells and dendritic cells [57]. Interestingly, CCL19, but not CCL21, promotes CCR7 phosphorylation, internalization and desensitization towards CCL21 [57]. Therefore, the ability of 200 μM palmitate to ablate the basal and LPS-mediated CCL19 expression implies that stronger CCR7-dependent responses (dendritic cell homing and maturation, and antigen-presentation) [58] must take place in the presence of the palmitate concentrations found in obese individuals. This prediction would be in line with the ability of palmitate to foster the acquisition of the cytokine and transcriptional profile of pro-inflammatory (and immunogenic) macrophages that we now report.

Regarding the palmitate-mediated upregulation of *TRIB3* gene expression, our results agree with the ability of palmitate to induce TRIB3 expression in human liver cells [59] and podocytes [60]. TRIB3 is a pseudokinase that modulates many signaling cascades associated with ER stress, nutrient deficiency and insulin resistance [61], and that acts as a negative regulator of NFκB-dependent transcription [62]. Since TRIB3 negatively regulates CCL2

expression in podocytes [60], it is tempting to speculate that palmitate-induce TRIB3 upregulation might underlie the negative effect that palmitate has on the basal and LPS-induced expression of CCL2 in human macrophages.

References

1. Gallagher, E.J. and D. LeRoith, Epidemiology and molecular mechanisms tying obesity, diabetes, and the metabolic syndrome with cancer. Diabetes Care, 2013. 36 Suppl 2: p. S233-9.

2. Hopkins, B.D., M.D. Goncalves, and L.C. Cantley, Obesity and Cancer Mechanisms: Cancer Metabolism. J Clin Oncol, 2016. 34(35): p. 4277-4283.

3. Das, U.N., Is obesity an inflammatory condition? Nutrition, 2001. 17(11-12): p. 953-66.

4. Chawla, A., K.D. Nguyen, and Y.P. Goh, Macrophage-mediated inflammation in metabolic disease. Nat Rev Immunol, 2011. 11(11): p. 738-49.

5. Lumeng, C.N. and A.R. Saltiel, Inflammatory links between obesity and metabolic disease. J Clin Invest, 2011. 121(6): p. 2111-7.

6. Weisberg, S.P., et al., CCR2 modulates inflammatory and metabolic effects of high-fat feeding. J Clin Invest, 2006. 116(1): p. 115-24.

7. Patsouris, D., et al., Ablation of CD11c-positive cells normalizes insulin sensitivity in obese insulin resistant animals. Cell Metab, 2008. 8(4): p. 301-9.

8. Arkan, M.C., et al., IKK-beta links inflammation to obesity-induced insulin resistance. Nat Med, 2005. 11(2): p. 191-8.

9. Solinas, G., et al., JNK1 in hematopoietically derived cells contributes to diet-induced inflammation and insulin resistance without affecting obesity. Cell Metab, 2007. 6(5): p. 386-97.

10. Shi, H., et al., TLR4 links innate immunity and fatty acid-induced insulin resistance. J Clin Invest, 2006. 116(11): p. 3015-25.

11. Erridge, C. and N.J. Samani, Saturated fatty acids do not directly stimulate Toll-like receptor signaling. Arterioscler Thromb Vasc Biol, 2009. 29(11): p. 1944-9.
12. Hosoi, T., et al., Myeloid differentiation factor 88 (MyD88)-deficiency increases risk of diabetes in mice. PLoS One, 2010. 5(9).

13. Vijay-Kumar, M., et al., Loss of function mutation in toll-like receptor-4 does not offer protection against obesity and insulin resistance induced by a diet high in trans fat in mice. J Inflamm (Lond), 2011. 8(1): p. 2.

14. Hall, E., et al., Effects of palmitate on genome-wide mRNA expression and DNA methylation patterns in human pancreatic islets. BMC Med, 2014. 12: p. 103.

15. Wang, X., et al., Epigenetic regulation of macrophage polarization and inflammation by DNA methylation in obesity. JCI Insight, 2016. 1(19): p. e87748.

16. Gordon, S. and P.R. Taylor, Monocyte and macrophage heterogeneity. Nat Rev Immunol, 2005. 5(12): p. 953-64.

17. Escribese, M.M., et al., The prolyl hydroxylase PHD3 identifies proinflammatory macrophages and its expression is regulated by activin A. J Immunol, 2012. 189(4): p. 1946-54.

18. Sierra-Filardi, E., et al., Activin A skews macrophage polarization by promoting a proinflammatory phenotype and inhibiting the acquisition of anti-inflammatory macrophage markers. Blood, 2011. 117(19): p. 5092-101.

19. Soler Palacios, B., et al., Macrophages from the synovium of active rheumatoid arthritis exhibit an activin A-dependent pro-inflammatory profile. J Pathol, 2015. 235(3): p. 515-26.

20. Verreck, F.A., et al., Human IL-23-producing type 1 macrophages promote but IL-10-producing type 2 macrophages subvert immunity to (myco)bacteria. Proc Natl Acad Sci U S A, 2004. 101(13): p. 4560-5.

21. Lacey, D.C., et al., Defining GM-CSF- and Macrophage-CSF-Dependent Macrophage Responses by In Vitro Models. J Immunol, 2012. 188(11): p. 5752-65.

22. Raes, G., et al., Arginase-1 and Ym1 are markers for murine, but not human, alternatively activated myeloid cells. J Immunol, 2005. 174(11): p. 6561; author reply 6561-2.

23. Izquierdo, E., et al., Reshaping of Human Macrophage Polarization through Modulation of Glucose Catabolic Pathways. J Immunol, 2015. 195(5): p. 2442-51.

24. Xu, S., et al., Evaluation of foam cell formation in cultured macrophages: an improved method with Oil Red O staining and DiI-oxLDL uptake. Cytotechnology, 2010. 62(5): p. 473-81.

25. Gonzalez-Dominguez, E., et al., Atypical Activin A and IL-10 Production Impairs Human CD16+ Monocyte Differentiation into Anti-Inflammatory Macrophages. J Immunol, 2016. 196(3): p. 1327-37.

26. Cuevas, V.D., et al., MAFB Determines Human Macrophage Anti-Inflammatory Polarization: Relevance for the Pathogenic Mechanisms Operating in Multicentric Carpotarsal Osteolysis. J Immunol, 2017.

27. Sturn, A., J. Quackenbush, and Z. Trajanoski, Genesis: cluster analysis of microarray data. Bioinformatics, 2002. 18(1): p. 207-8.

28. Kimura, A., et al., Aryl hydrocarbon receptor in combination with Stat1 regulates LPS-induced inflammatory responses. J Exp Med, 2009. 206(9): p. 2027-35.

29. Ruffell, D., et al., A CREB-C/EBPbeta cascade induces M2 macrophage-specific gene expression and promotes muscle injury repair. Proc Natl Acad Sci U S A, 2009. 106(41): p. 17475-80.

30. Huang, S., et al., Saturated fatty acids activate TLR-mediated proinflammatory signaling pathways. J Lipid Res, 2012. 53(9): p. 2002-13.

31. Pal, D., et al., Fetuin-A acts as an endogenous ligand of TLR4 to promote lipid-induced insulin resistance. Nat Med, 2012. 18(8): p. 1279-85.

32. Ibrahimi, A., et al., Expression of the CD36 homolog (FAT) in fibroblast cells: effects on fatty acid transport. Proc Natl Acad Sci U S A, 1996. 93(7): p. 2646-51.

33. Senn, J.J., Toll-like receptor-2 is essential for the development of palmitate-induced insulin resistance in myotubes. J Biol Chem, 2006. 281(37): p. 26865-75.

34. Nguyen, M.T., et al., A subpopulation of macrophages infiltrates hypertrophic adipose tissue and is activated by free fatty acids via Toll-like receptors 2 and 4 and JNK-dependent pathways. J Biol Chem, 2007. 282(48): p. 35279-92.

35. Xue, J., et al., Transcriptome-based network analysis reveals a spectrum model of human macrophage activation. Immunity, 2014. 40(2): p. 274-88.

36. Erwig, L.P., et al., Initial cytokine exposure determines function of macrophages and renders them unresponsive to other cytokines. J Immunol, 1998. 161(4): p. 1983-8.

37. Cheng, S.C., et al., mTOR- and HIF-1alpha-mediated aerobic glycolysis as metabolic basis for trained immunity. Science, 2014. 345(6204): p. 1250684.

38. Netea, M.G., et al., Trained immunity: A program of innate immune memory in health and disease. Science, 2016. 352(6284): p. aaf1098.

39. Saeed, S., et al., Epigenetic programming of monocyte-to-macrophage differentiation and trained innate immunity. Science, 2014. 345(6204): p. 1251086.

40. Han, M.S., et al., JNK expression by macrophages promotes obesity-induced insulin resistance and inflammation. Science, 2013. 339(6116): p. 218-22.

41. Pettersson, A.M., et al., MAFB as a novel regulator of human adipose tissue inflammation. Diabetologia, 2015. 58(9): p. 2115-23.

42. Tran, M.T., et al., MafB deficiency accelerates the development of obesity in mice. FEBS Open Bio, 2016. 6(6): p. 540-7.

43. Tanahashi, H., et al., MafB protein stability is regulated by the JNK and ubiquitin-proteasome pathways. Arch Biochem Biophys, 2010. 494(1): p. 94-100.

44. Herath, N.I., et al., GSK3-mediated MAF phosphorylation in multiple myeloma as a potential therapeutic target. Blood Cancer J, 2014. 4: p. e175.

45. Cao, J., et al., Saturated free fatty acid sodium palmitate-induced lipoapoptosis by targeting glycogen synthase kinase-3beta activation in human liver cells. Dig Dis Sci, 2014. 59(2): p. 346-57.

46. Choi, S.E., et al., Involvement of glycogen synthase kinase-3beta in palmitate-induced human umbilical vein endothelial cell apoptosis. J Vasc Res, 2007. 44(5): p. 365-74.

47. Eldar-Finkelman, H. and A. Martinez, GSK-3 Inhibitors: Preclinical and Clinical Focus on CNS. Front Mol Neurosci, 2011. 4: p. 32.

48. Freland, L. and J.M. Beaulieu, Inhibition of GSK3 by lithium, from single molecules to signaling networks. Front Mol Neurosci, 2012. 5: p. 14.

49. Ray, I., S.K. Mahata, and R.K. De, Obesity: An Immunometabolic Perspective. Front Endocrinol (Lausanne), 2016. 7: p. 157.

50. Kratz, M., et al., Metabolic dysfunction drives a mechanistically distinct proinflammatory phenotype in adipose tissue macrophages. Cell Metab, 2014. 20(4): p. 614-25.

51. Johnson, A.R., J.J. Milner, and L. Makowski, The inflammation highway: metabolism accelerates inflammatory traffic in obesity. Immunol Rev, 2012. 249(1): p. 218-38.

52. Cani, P.D., et al., Metabolic endotoxemia initiates obesity and insulin resistance. Diabetes, 2007. 56(7): p. 1761-72.

53. Odegaard, J.I. and A. Chawla, Alternative macrophage activation and metabolism. Annu Rev Pathol, 2011. 6: p. 275-97.

54. Ortiz, S., et al., Bacterial DNA translocation holds increased insulin resistance and systemic inflammatory levels in morbid obese patients. J Clin Endocrinol Metab, 2014. 99(7): p. 2575-83.

55. Phiel, C.J. and P.S. Klein, Molecular targets of lithium action. Annu Rev Pharmacol Toxicol, 2001. 41: p. 789-813.

56. Park, S.H., et al., Tumor necrosis factor induces GSK3 kinase-mediated cross-tolerance to endotoxin in macrophages. Nat Immunol, 2011. 12(7): p. 607-15.

57. Forster, R., A.C. Davalos-Misslitz, and A. Rot, CCR7 and its ligands: balancing immunity and tolerance. Nat Rev Immunol, 2008. 8(5): p. 362-71.

58. Sanchez-Sanchez, N., L. Riol-Blanco, and J.L. Rodriguez-Fernandez, The multiple personalities of the chemokine receptor CCR7 in dendritic cells. J Immunol, 2006. 176(9): p. 5153-9.

59. Yan, W., et al., Palmitate induces TRB3 expression and promotes apoptosis in human liver cells. Cell Physiol Biochem, 2014. 33(3): p. 823-34.

60. Morse, E., et al., TRB3 is stimulated in diabetic kidneys, regulated by the ER stress marker CHOP, and is a suppressor of podocyte MCP-1. Am J Physiol Renal Physiol, 2010. 299(5): p. F965-72.

61. Mondal, D., A. Mathur, and P.K. Chandra, Tripping on TRIB3 at the junction of health, metabolic dysfunction and cancer. Biochimie, 2016. 124: p. 34-52.

62. Wu, M., et al., SINK is a p65-interacting negative regulator of NF-kappaB-dependent transcription. J Biol Chem, 2003. 278(29): p. 27072-9.

DISCUSSION

Nutrients and energy intake require highly regulated and coordinated functions of homeostatic systems. In our societies, these systems are under the pressure of continuous exposure to excess amounts of nutrients, lack of physical activity, new dietary components, changes in dietary patterns and an increased lifespan. Consequently, the biological responses are unable to deal with these challenges and the homeostatic systems deteriorate, promoting the development of different pathologies [145].

All these changes derived from modern lifestyle are closely associated with chronic metabolic diseases such as obesity, fatty liver disease, type 2 diabetes (T2D), atherosclerosis and cardiovascular diseases. These modern human diseases are mainly characterized by chronic low-grade inflammation and homeostasis disruption [44], [146]. In fact, it is now recognized that obesity-associated tissue inflammation is an important contributor for the development of comorbidities, and that, the combined action of metabolism and the immune system causes the pathogenesis of metabolic diseases [82], [147].

The mechanistic link between inflammatory processes and insulin resistance was established after the finding that signaling pathways involving IKKβ and NFκB are activated in obesity and insulin resistance [82]. Several studies have demonstrated that the inhibition, deletion or blocking of IKKβ can attenuate the development of insulin resistance induced by a high-fat diet (HFD) [148]–[153]. Moreover, chronic low-grade inflammation induced by an excess of nutrient intake also leads to JNK activation and the ablation of JNK in mice can also protect them from diet-induced inflammation and obesity [154], [155]. Subsequently, obesity and insulin resistance lead to further activation of inflammatory signaling pathways in target organs such as liver, fat and muscle, thus contributing to pathogenesis at a systemic level. Furthermore, this state of chronic low-grade inflammation also induces alterations in

immune cell functions and increase the production of cytokines and other inflammatory mediators [82], [156].

In 2003, two different reports [57], [58] demonstrated that obese adipose tissue is infiltrated by macrophages and that these immune cells produce several inflammatory factors that contribute to aggravate obesity-related complications. The initial trigger of inflammation in adipose tissue is not unique. Dead cells, excess of free fatty acids and hypoxia can initiate the inflammatory process to attract macrophages [57], [58], [156]. All these factors contribute to recruitment and activation of macrophages towards a pro-inflammatory phenotype that leads to the activation of JNK, IKKβ and other serine kinases and, consequently, the expression and activity of the transcription factor AP-1 and NFκB. This type of macrophage activation (commonly referred to as M1 or pro-inflammatory polarization) induces the release of different cytokines (TNF-α, IL-6, IL-1β) and chemokines that exert autocrine and paracrine effects contributing to decreased insulin sensitivity [59]. Further, these macrophages also promote a feed-forward process that increase the recruitment of additional immune cells and propagate the chronic inflammatory state.

Metabolomics allow us to measure the entire set of metabolites of a wide range of biological specimens under specific conditions. Consequently, large-scale studies of metabolite fingerprint have emerged as a valuable and versatile tool to investigate the pathophysiology and etiology of complex diseases. Metabolomics approaches have identified novel biomarkers that allow a clear characterization of the onset and progression of chronic diseases. While the identified biomarkers should be validated and confirmed in different samples, and should be reproducible, sensitive and specific [157], [158], these novel biomarkers hold the promise to be relevant tools in clinical and provide an improvement on treatment effectiveness.

Metabolomics technologies can, thus, identify a specific "metabolic profile" of disease through the detection of variations on metabolite levels in pathways that play a role in metabolic dysfunctions. Since many diseases are characterized by changes in metabolic signature, various metabolites have been identified as reliable biomarkers [159], [160]. However, in the last few years, the new high-throughput technologies as metabolomics have been focused, more frequently, in the field of new biomarkers discovery [157], [161], [162]. As representative examples, abnormalities in the kynurenine pathway appear to be associated with progressive forms of multiple sclerosis [163], [164]. Catecholamine metabolism, caffeine, xanthine and ornithine pathways and redox homeostasis have been found altered in patients with Parkinson disease [165].

Regarding obesity-related pathologies like T2D, high levels of branched-chain amino acids (BCAAs) affect the fatty acids oxidation (FAO) producing incomplete FAO by-products related to mitochondrial stress and impaired insulin signaling [166], [167]. Another hypothesized mechanism linking high levels of BCAA and T2D is the activation of mTOR pathway which induces hepatic insulin resistance [157], [168]. The search for NAFLD biomarkers have identified metabolites like cytokeratin 18 fragment (CK18-F) (the major intermediate filament protein in the liver) [169] and α-ketoglutarate (a citric acid cycle intermediate) [170] that distinguish, NAFLD patients from healthy controls [171].

Since, metabolomics offers the possibility to identify the alterations in specific pathways that underlie chronic low-grade inflammatory diseases, we made use of targeted metabolomics as a mean to explore, determinate and quantify key intermediates involved in the pathogenesis of obesity-related diseases. Therefore, and as outlined in the first study, we designed a method based on gas chromatography coupled to a quadrupole-time-of-flight mass

spectrometer and using an electron ionization interface (GC-EI-QTOF-MS) that allows measurement and quantification of intermediate metabolites as indirect markers of energy metabolism and mitochondrial function. To evaluate whether this analytical platform could be effective for predicting impairments on energy generation and mitochondrial disruption in different biological samples, we validated the developed analytical method in plasma, tissues and cell lysates. In plasma samples of patients with peripheral artery disease (PAD), we found elevated levels of BCAAs, what indicates an impaired short-term metabolic control [172], [173], and significant increases of glutamate and glutamine, indicating a possible function of these metabolites in patients affected by PAD. Several studies have deepened in metabolic changes in patients with atherosclerosis, and a recent study with patients affected with PAD have also demonstrated that serum levels of aspartate, glutamate, leucine and serine among others, were significantly higher in patients with atherosclerosis [174].

We next explored metabolite concentration in breast epithelial cells carrying the constitutively active oncogenic-KRAS^{V12} gene (MCF10A-KRAS^{V12}) and we found that the basal metabolic activity was higher than in control cells (MCF10A). Moreover, we also detected the presence of an oncometabolite (2-hydroxglutarate) in mutated cells [175], [176], and an increased concentration of ribose-5-phosphate, an intermediate in the pentose phosphate pathway, indicating an active generation of nucleic acids for biomass production and endogenous antioxidants to prevent the oxidative stress produced due to the high metabolic rate [177], [178]. Finally, the lactate production was also increased in mutant cells, a finding indicative of an active Warburg effect [179].

The experimental approach was also evaluated in tissues, specifically in adipose and hepatic tissue from LDL receptor-deficient (*Ldlr*$^{-/-}$) mice. As

expected, levels of metabolites in liver, the most important metabolic organ, were higher than those found in adipose tissue, where some metabolites such oxaloacetate or phosphoenolpyruvate could not be detected. In conclusion, the analytical platform used, as well as the targeted metabolomics approach followed, provides the reproducibility, sensitivity and accuracy to detect and unequivocally quantify several metabolites involved in energy generation. Therefore, the use of targeted metabolomics in plasma can be applied to define metabolic perturbations in disease states and consequently, in the search of new non-invasive biomarkers of disease [180], [181].

The second study focused on the effects of metformin and caloric restraint in *Ldlr*$^{-/-}$ mice. The main finding was that metformin potentiates the beneficial effects of caloric restriction, and that this intervention yielded better results than metformin monotherapy. HFD-fed mice subjected to diet switch could not fully reverse the metabolic derangements caused by the initial excessive nutrient intake. However, mice fed with a HFD subjected to a diet reversal together with metformin administration displayed an ameliorated metabolic profile. Thus, the addition of metformin to caloric restriction improved the metabolic pattern developed by early HFD intake. These effects were observed in weight loss maintenance and in the improvement on insulin resistance. Although “diet reversal” improved the levels of cholesterol, the addition of metformin to caloric restriction further improved the lipid profile. Metabolic disturbances generated by the initial HFD exposure promoted the development of NAFLD [182], adipocyte hypertrophy and an increase of WAT weight in mice [183]. While liver injury was only reduced with the addition of metformin to caloric restriction, the effects in WAT were ameliorated with caloric restriction with or without metformin. Finally, the early HFD intake increased the macrophage infiltration in liver. Nevertheless, this immune

response was reduced with caloric restriction and further improved with metformin treatment and non-excess caloric intake.

It is widely known that caloric restriction represents the most robust method for health maintenance and increased lifespan [184]–[186]. However, recent studies have also demonstrated that the combination of metformin and caloric restriction may provide a better approach than either therapy alone in the management of metabolic diseases as NAFLD or insulin resistance [187], [188]. Specifically, a recent study demonstrated that the metformin administration together with overnutrition reduction further improved mitophagy and liver injury markers, hepatic *de novo* lipogenesis and glucose response in diabetic rats [187].

The main differences in the study of energy metabolism, focused in the main metabolic tissues in diet groups treated with metformin or placebo, were found in the concentration of BCAAs in WAT. It has been reported that differentiated adipocytes showed increased catabolic flux of BCAAs and the inhibition of this catabolism compromises adipogenesis [189], [190]. Metformin treatment in HFD-fed mice targeted the contribution of valine, leucine and isoleucine to energy metabolism, probably up-regulating the degradation pathway and decreasing the capacity of BCAAs to generate TCA intermediates such as acetyl-CoA that can be used for the lipid synthesis [191].

The effects of metformin as a metabolic modulator [192] are evidenced in several diseases. This biguanide is the most common anti-diabetic prescribed drug [193], but the therapeutic potential of metformin is also observed in cancer treatment [194] and, additionally there are evidences to suggest that metformin delays the aging process [195]. These health-promoting effects are mainly related with a key regulator of cellular energy homeostasis, 5' adenosine monophosphate-activated protein kinase (AMPK). Caloric

restriction and metformin promotes energetic changes and increase AMPK activity [192], [196]. In line with our findings, it has been described that the metformin and caloric restriction have the ability to restore the mitochondrial function through AMPK in fibroblasts from patients affected by fibromyalgia [197]. Other studies reported that the senescence due to the epithelial-mesenchymal transition (EMT) in aging kidney is alleviated by caloric restriction and metformin through the AMPK/mTOR signaling [198]. All these data suggest the potential for improved efficacy with the combination of pharmacological therapies and lifestyle.

Importantly, the pathogenesis of metabolic alterations induced by HFD involved long-term epigenetic modifications [199], [200] and further studies are needed to elucidate the ability of metformin-mediated epigenetic changes [201], [202]. These novel approaches suggest new epigenetics mechanism for the physiological function of metformin and might guide the development of new therapeutic strategies [203].

The ability of saturated fatty acids (e.g., palmitate) to modify the polarization state of human macrophages and their response against inflammatory stimuli is detailed in the third study. The rationale for this study stems from the close link between metabolism and immunity, and from the fact that macrophages are critical initiators and regulators of the inflammatory processes that promote metabolic diseases like obesity and insulin resistance [39], [59]. In fact, a dysregulation of fatty acid homeostasis contributes to metabolic disturbances, and fatty acids have been postulated as triggers for macrophage pro-inflammatory polarization [40]. In line with previous findings establishing chronic low-grade inflammation and pro-inflammatory cytokines as hallmarks of metabolic diseases, our results indicate that palmitate promotes the acquisition of a pro-inflammatory phenotype in human macrophages via JNK activation, and that palmitate-initiated

intracellular signaling differs from the signals triggered by a paradigmatic pathogenic stimulus like LPS. More importantly, we have obtained evidences that palmitate conditions macrophage responses to other pathogenic (pro-inflammatory) stimuli like LPS, a finding with huge implications because metabolic endotoxemia initiates insulin resistance and obesity [204], [205]. At the molecular level, we have observed that, palmitate primes macrophages for an exacerbated pro-inflammatory response towards LPS, by enhancing LPS-initiated activation of, NFκB, ERK, p38, IRF3 and JNK signaling. Especially relevant is the palmitate effect on LPS-induced activation of JNK [155], [206] and NFκB [207], since both signaling pathways are directly involved in the development of obesity and insulin resistance [148], [154]. In fact, inhibition of palmitate-induced JNK activation partially restores markers of "anti-inflammatory gene set", and reduces the ability of palmitate to inhibit LPS-induced IL-10 production.

Altogether, the effects of palmitate on macrophages are compatible with palmitate promoting a state of "trained immunity" by which palmitate-conditioned macrophages produce increased levels of pro-inflammatory cytokines in response to a second stimuli such as LPS. The term "Trained immunity" has been recently coined to describe the ability of macrophages to modify their responses towards exogenous stimuli depending on the previous stimulus they have encountered [208]–[210]. Trained immunity has been found to depend on epigenetic mechanisms initiated at the level of HIF1 and mTOR [211]. We have not tested the ability of palmitate to trigger epigenetic changes in macrophages. However, it is worth noting that the effects of palmitate on M-MØ resemble the actions of hypoxia, which is also capable of increasing LPS-induced production of pro-inflammatory cytokines [212]. Therefore, it is tempting to speculate that palmitate might increase HIF1 expression as a primary signal for the establishment of the "palmitate-induced trained state" [213], [214]. On the other hand, since M-MØ

preferentially secrete IL-10 upon stimulation and since palmitate exposure reduces the production of IL-10 and CCL2 in response to LPS, the effect of palmitate can be also classified as a "tolerance" process (by analog to the well-known LPS tolerance effect) [215], [216]. As a whole, this combined effect of palmitate on LPS-induced cytokines production (higher levels of pro-inflammatory cytokines, lower levels of IL-10 and CCL2) clearly illustrates the ability of palmitate to modify macrophage responses, and justifies further analysis of the underlying molecular mechanisms.

One of the factors that deserves additional attention for its involvement in the macrophage-conditioning ability of palmitate is activin A. Activin A is a member of the TGF-β family of factors [217], [218], and its expression is elevated in most inflammatory pathologies (e.g., inflammatory bowel disease, rheumatoid arthritis, bacterial septicemia) and induced with faster kinetic than classical pro-inflammatory cytokines after LPS injection [219]. Moreover, activin A is a critical promoter of the pro-inflammatory polarization of macrophages [220]–[222]. Since palmitate causes an increase in the expression of INHBA (the gene encoding the activin A polypeptide), it is tempting to speculate that activin A levels might be elevated in the peripheral blood of patients with high-levels of palmitate [223], an analysis that is currently being designed. Furthermore, it is also formally possible that activin A might contribute to the palmitate-induced training of macrophages, a hypothesis that correlates well with the unpublished effects of other immunomodulatory agents on macrophage-derived activin A (*Dominguez-Soto et al., unpublished).*

Another relevant aspect of the palmitate action on macrophages is its ability to reduce the expression of the MAFB transcription factor. MAFB is a member of the large MAF transcription factor family (c-MAF, MAFA, MAFB and NRL), all of which share a transcriptional activation domain at their N

termini [224], [225]. The large MAF proteins regulate terminal differentiation in a variety of tissues, such as the bone, brain, kidney, lens, pancreas and retina [226], [227], and they appear to have specific and non-redundant functions. In hematopoietic cells, MAFB is expressed in the monocyte lineage [228], where the lack of MAFB and c-MAF cause differentiated macrophages to self-renew without malignant transformation [229]. MAFB is a critical determinant for the anti-inflammatory macrophage polarization state [230]. In line with this effect, palmitate downregulates the expression of a previously defined MAFB-dependent gene set that marks anti-inflammatory macrophages and, in parallel, upregulates the "pro-inflammatory gene set". The correlation between the palmitate-induced MAFB downregulation and the palmitate ability to limit the expression of "anti-inflammatory gene set" is especially interesting because a recent study demonstrated that MafB deficiency in the hematopoietic system increases the body fat storage and the adipocyte size and accelerates weight gain developing an obesity phenotype in mice [231]. Moreover, another report has described the relation between MAFB and ischemic stroke pathologies and suggested that MAFB has an essential role for the efficient clearance of DAMPs to resolver inflammation and to prevent the exacerbation of the pathology [232]. These data indicate a role for MAFB in the resolution of inflammation that correlates with our results, and indicate that the loss of MAFB due to palmitate exposure associates with a macrophage pro-inflammatory phenotype and has relevant pathological consequences.

MAFB protein expression is commonly regulated by GSK3β-mediated phosphorylation and subsequent ubiquitination for degradation [233], [234]. Although we have not been able to demonstrate any effect of palmitate on GSK3β activity, it is worth noting that lithium chloride, a well-known GSK3β inhibitor [235], [236], was able to impair the palmitate-induced MAFB downregulation, and that this effect of lithium chloride correlated with its

ability to abolish the inhibitory effect of palmitate on the production of IL-10 in response to LPS. Therefore, although we have no demonstrated the existence of a palmitate-GSK3β-MAFB axis, the effects of lithium chloride are of interest, because GSK3β participates in insulin resistance improvement [237], [238] and because GSK3β also mediates the cross-tolerance towards LPS induced by TNF-α [239].

Besides GSK3β, MAFB protein expression can be also abrogated via JNK dependent ubiquitination [240]. Since palmitate exposure leads to JNK phosphorylation, the palmitate-induced MAFB downregulation could be viewed as a secondary phenomenon after the palmitate-induced JNK activation, what suggests that the palmitate-JNK-MAFB axis might be of importance for the pathological response of macrophages towards high levels of saturated fatty acids. The link between palmitate and MAFB expression deserves further analysis because MAFB (and other related MAF family factors) is involved in numerous physiological processes, including lymphangiogenesis [241], osteoclast differentiation [242], [243] and the control of expression of insulin and glucagon by pancreatic cells [227]. Therefore, it would be of interest to determine whether the ability of palmitate to limit MAFB expression also operates in other cell types.

A second transcription factor whose expression in macrophages is diminished upon palmitate exposure is Aryl Hydrocarbon receptor (AhR). AhR is activated by xenobiotics and endogenous ligands like kynurenine, regulates the proliferation and differentiation of numerous cell lineages [244], and is an important factor for Th differentiation during the polarization step of the adaptive immune response. Importantly, AhR has been identified as a critical factor for the establishment of the LPS tolerance mechanism [245], and is preferentially expressed by anti-inflammatory macrophages. Therefore, the effect of palmitate on macrophages might also

disrupt their ability to eliminate xenobiotics and other environmental contaminants, an hypothesis that deserves further analysis [246].

The results derived from the third study indicate that palmitate and LPS exert different transcriptional effects, although both are recognized by TLR4 in human macrophages [139]. We have found that several genes associated with the polarization state (*CCL2*, *IL10*) and modulated during LPS response (*CCL19*, *TRIB3*, *IDO1*, *MAOA*, *LAMB3* and *EMR2*) are oppositely modulated by palmitate and LPS. CCL19 is greatly increased by LPS stimulation whereas palmitate treatment abrogates CCL19 expression and even limits the LPS-induced CCL19 production. Conversely, *TRIB3* expression is significantly upregulated by palmitate but downregulated by LPS. Moreover, these differential effects are also seen at the signaling level, since STAT3 and STAT1 are not activated by palmitate. Consequently, the capacity of palmitate to regulate the expression of CCL19 and *TRIB3* in an opposite manner to LPS suggests their possible use as biomarkers for palmitate-induced macrophage polarization.

Like CCL21, CCL19 is a ligand of CCR7, that contributes to dendritic cell migration towards lymph nodes during the initiation of adaptive immunity [247]. The ability of palmitate to abrogate CCL19 production would also imply that CCR7-dependent responses like antigen presentation, chemotaxis or dendritic cell maturation would be altered in obese patients with high levels of peripheral blood palmitate [248].

Regarding TRIB3, previous reports have demonstrated that palmitate induces TRIB3 expression in podocytes [249] and human liver cells [250]. TRIB3 is a pseudokinase that modulates many signals transduction cascades associated with insulin resistance, ER stress and nutrient availability [251]. Interestingly, hepatic TRIB3 mRNA levels strongly correlate with plasma insulin and triglycerides and hepatic steatosis score in obese individuals, and *TRIB3*

transcript levels are also increased in visceral tissue samples [252]. Since TRIB3 inhibits CCL2 expression at the transcriptional level [249], the increased TRIB3 expression after palmitate exposure might contribute to the palmitate-induced downregulation of CCL2 in macrophages.

CONCLUSIONS

- The analytical method developed using GC-EI-QTOF-MS provides a valid tool to detect and quantify multiple metabolites involved in energy metabolism, and specifically in intermediates from mitochondrial metabolism, and can be used in a wide range of biological samples, including cell-culture lysates, tissues from mouse models of disease and patient plasma.

- Metformin and "reduction of nutrient intake" ameliorate biochemical metabolism, improve hepatic steatosis and reduce the immune response in liver from HFD-fed hyperlipemic mice. In fact, metformin combined with caloric restriction constitutes a better approach to protect against metabolic diseases, and represents a potential therapeutic strategy.

- Metformin targets Branched Chain Amino Acids (BCAAs) metabolism in adipose tissue, what might contribute to its protective effects against the metabolic damage induced by a high-fat diet.

- Palmitate limits the expression of anti-inflammatory markers and induces the expression of a pro-inflammatory phenotype in human macrophages, with both effects being dependent on JNK activation.

- Palmitate and LPS trigger distinct transcriptional and functional profile in human macrophages: CCL19 expression is exclusively upregulated by LPS, whereas palmitate promotes an enhanced expression of TRIB3 that is not observed upon LPS stimulation.

- Palmitate conditions human macrophages for exacerbated pro-inflammatory responses towards pathogenic stimuli like LPS, and this conditioning effect is also dependent on activation of JNK.

- GSK3 inhibition might contribute to restore the inhibitory action of palmitate on the LPS-induced IL-10 production.

REFERENCES

References

[1] M. F. Gregor and G. S. Hotamisligil, “Inflammatory mechanisms in obesity.,” *Annu. Rev. Immunol.*, vol. 29, pp. 415–45, 2011.

[2] OMS, “Obesity : Preventing and Managing the Global Epidemic,” 2000.

[3] “World Health Organization. Obesity and overweight. Fact sheet N°311 Updated June 2016 http://www.who.int/mediacentre/ factsheets/fs311/en/.”

[4] K. M. Flegal, D. Kruszon-Moran, M. D. Carroll, C. D. Fryar, and C. L. Ogden, “Trends in obesity among adults in the united states, 2005 to 2014,” *JAMA*, vol. 315, no. 21, pp. 2284–2291, 2016.

[5] K. E. Corey and L. M. Kaplan, “Obesity and liver disease. The epidemic of the twenty-first century,” *Clin. Liver Dis.*, vol. 18, no. 1, pp. 1–18, 2014.

[6] B. Swinburn, G. Egger, and F. Raza, “Dissecting obesogenic environments: the development and application of a framework for identifying and prioritizing environmental interventions for obesity.,” *Prev. Med. (Baltim).*, vol. 29, no. 6 Pt 1, pp. 563–570, 1999.

[7] A. A. Martin and T. L. Davidson, “Human cognitive function and the obesogenic environment,” *Physiol. Behav.*, vol. 136, pp. 185–193, 2014.

[8] G. S. Hotamisligil, “Inflammation and metabolic disorders,” *Nature*, vol. 444, no. 7121, pp. 860–867, 2006.

[9] J. I. Odegaard and A. Chawla, “Pleiotropic actions of insulin resistance and inflammation in metabolic homeostasis.,” *Science*, vol. 339, no. 6116, pp. 172–7, 2013.

[10] D. G. Tiniakos, M. B. Vos, and E. M. Brunt, “Nonalcoholic Fatty Liver Disease: Pathology and Pathogenesis,” *Annu. Rev. Pathol. Mech. Dis.*, vol. 5, no. 1, pp. 145–171, 2010.

[11] V. L. Misra, M. Khashab, and N. Chalasani, “Non-Alcoholic Fatty Liver Disease and Cardiovascular Risk,” *Curr. Gastroenterol. Rep.*, vol. 11, no. 1, pp. 50–55, 2009.

[12] K. M. Korenblat, E. Fabbrini, B. S. Mohammed, and S. Klein, “Liver, Muscle, and Adipose Tissue Insulin Action Is Directly Related to Intrahepatic Triglyceride Content in Obese Subjects,” *Gastroenterology*, vol. 134, no. 5, pp. 1369–1375, 2008.

References

[13] Y. Fazel, A. B. Koenig, M. Sayiner, Z. D. Goodman, and Z. M. Younossi, "Epidemiology and natural history of non-alcoholic fatty liver disease," *Metabolism.*, vol. 65, no. 8, pp. 1017–1025, 2016.

[14] Z. M. Younossi, A. B. Koenig, D. Abdelatif, Y. Fazel, L. Henry, and M. Wymer, "Global epidemiology of nonalcoholic fatty liver disease—Meta-analytic assessment of prevalence, incidence, and outcomes," *Hepatology*, vol. 64, no. 1, pp. 73–84, 2016.

[15] K. Ray, "NAFLD—the next global epidemic," *Nat. Rev. Gastroenterol. Hepatol..*, vol. 10, no. 11, p. 621, 2013.

[16] A. Wree, L. Broderick, A. Canbay, H. M. Hoffman, and A. E. Feldstein, "From NAFLD to NASH to cirrhosis-new insights into disease mechanisms.," *Nat. Rev. Gastroenterol. Hepatol.*, vol. 10, no. 11, pp. 627–36, 2013.

[17] J. C. Cohen, J. D. Horton, and H. H. Hobbs, "Human Fatty Liver Disease: Old Questions and New Insights," *Science*, vol. 332, no. 6037, pp. 1519–1523, 2011.

[18] E. Fabbrini, S. Sullivan, and S. Klein, "Obesity and nonalcoholic fatty liver disease: Biochemical, metabolic, and clinical implications," *Hepatology*, vol. 51, no. 2, pp. 679–689, 2010.

[19] H. Esterbauer, R. J. Schaur, and H. Zollner, "Chemistry and biochemistry of 4-hydroxynonenal, malonaldehyde and related aldehydes," *Free Radic. Biol. Med.*, vol. 11, no. 1, pp. 81–128, 1991.

[20] C. MATTEONI, Z. YOUNOSSI, T. GRAMLICH, N. BOPARAI, Y. LIU, and A. MCCULLOUGH, "Nonalcoholic fatty liver disease: A spectrum of clinical and pathological severity," *Gastroenterology*, vol. 116, no. 6, pp. 1413–1419, 1999.

[21] M. V Machado and H. Cortez-Pinto, "Cell death and nonalcoholic steatohepatitis: where is ballooning relevant?," *Expert Rev. Gastroenterol. Hepatol.*, vol. 5, no. 2, pp. 213–222, 2011.

[22] H. Malhi, G. J. Gores, and J. J. Lemasters, "Apoptosis and necrosis in the liver: A tale of two deaths?," *Hepatology*, vol. 43, no. 2 SUPPL. 1, pp. 31–44, 2006.

[23] W. Peverill, L. W. Powell, and R. Skoien, "Evolving concepts in the pathogenesis of NASH: Beyond steatosis and inflammation," *Int. J. Mol. Sci.*, vol. 15, no. 5, pp. 8591–8638, 2014.

References

[24] S. De Minicis *et al.*, "Gene Expression Profiles During Hepatic Stellate Cell Activation in Culture and In Vivo," *Gastroenterology*, vol. 132, no. 5, pp. 1937–1946, 2007.

[25] S. L. Friedman, "Mechanisms of Hepatic Fibrogenesis," *Gastroenterology*, vol. 134, no. 6, pp. 1655–1669, 2010.

[26] J. Crespo *et al.*, "Gene Expression of Tumor Necrosis Factor α and TNF-Receptors , p55 and p75 , in Nonalcoholic Steatohepatitis Patients," *Hepatology*, vol. 34, no. 6, pp. 1158–1163, 2001.

[27] Y. Hori, Y. Takeyama, T. Ueda, M. Shinkai, K. Takase, and Y. Kuroda, "Macrophage-derived transforming growth factor-beta1 induces hepatocellular injury via apoptosis in rat severe acute pancreatitis," *Surgery*, vol. 127, no. 6, pp. 641–649, 2000.

[28] K.-S. Jeong, "Therapeutic target for chronic liver fibrosis by regulation of transforming growth factor-beta," *Basic Appl. Pathol.*, vol. 1, no. 2, pp. 56–60, 2008.

[29] Y. Zhan and W. An, "Roles of liver innate immune cells in nonalcoholic fatty liver disease," *World J. Gastroenterol.*, vol. 16, no. 37, pp. 4652–4660, 2010.

[30] G. Baffy, "Kupffer cells in non-alcoholic fatty liver disease: The emerging view," *J. Hepatol.*, vol. 51, no. 1, pp. 212–223, 2010.

[31] S. Romeo *et al.*, "Genetic variation in PNPLA3 confers susceptibility to nonalcoholic fatty liver disease," *Nat. Genet.*, vol. 40, no. 12, pp. 1461–1465, 2009.

[32] L. Valenti *et al.*, "Homozygosity for the patatin-like phospholipase-3/adiponutrin i148m polymorphism influences liver fibrosis in patients with nonalcoholic fatty liver disease," *Hepatology*, vol. 51, no. 4, pp. 1209–1217, 2010.

[33] World Health Organization, "Global Report on Diabetes," vol. 978, p. 88, 2016.

[34] M. F. White, "IRS proteins and the common path to diabetes.," *Am. J. Physiol. Endocrinol. Metab.*, vol. 283, no. 3, pp. E413-22, 2002.

[35] S. Schinner, W. a Scherbaum, S. R. Bornstein, and a Barthel, "Molecular mechanisms of insulin resistance.," *Diabet. Med.*, vol. 22, no. 6, pp. 674–682, 2005.

References

[36] V. T. Samuel and G. I. Shulman, "Mechanisms for insulin resistance: Common threads and missing links," *Cell*, vol. 148, no. 5, pp. 852–871, 2012.

[37] K. E. Wellen and G. S. Hotamisligil, "Obesity-induced inflammatory changes in adipose tissue," *J. Clin. Invest.*, vol. 112, no. 12, pp. 1785–1788, 2003.

[38] M. Quatanani and M. A. Lazar, "Mechansims of obesity-associated insulin resistance : many choice on the menu," *Genes Dev.*, vol. 21, no. 12, pp. 1443–1455, 2016.

[39] J. C. Mcnelis and J. M. Olefsky, "Macrophages, Immunity, and Metabolic Disease," *Immunity*, vol. 41, no. 1, pp. 36–48, 2014.

[40] A. Chawla, K. D. Nguyen, and Y. P. S. Goh, "Macrophage-mediated inflammation in metabolic disease," *Nat. Rev. Immunol.*, vol. 11, no. 11, pp. 738–749, 2011.

[41] S. E. Kahn, R. L. Hull, and K. M. Utzschneider, "Mechanisms linking obesity to insulin resistance and type 2 diabetes," *Nature*, vol. 444, no. 7121, pp. 840–846, 2006.

[42] S. Schenk, M. Saberi, and J. M. Olefsky, "Insulin sensitivity: Modulation by nutrients and inflammation," *J. Clin. Invest.*, vol. 118, no. 9, pp. 2992–3002, 2008.

[43] R. Medzhitov, "Origin and physiological roles of inflammation," *Nature*, vol. 454, no. 7203, pp. 428–453, 2008.

[44] M. E. Kotas and R. Medzhitov, "Homeostasis, Inflammation, and Disease Susceptibility," *Cell*, vol. 160, no. 5, pp. 816–827, 2015.

[45] G. L. Larsen and P. M. Henson, "Mediators of Inflammation," *Annu. Rev. Immunol.*, vol. 1, pp. 335–359, 1983.

[46] M. Zeyda and T. M. Stulnig, "Obesity, inflammation, and insulin resistance," *Gerontology*, vol. 55, no. 4, pp. 379–386, 2009.

[47] G. S. Hotamisligil, "Inflammation, metaflammation and immunometabolic disorders," *Nature*, vol. 542, no. 7640, pp. 177–185, 2017.

[48] M. Erikci Ertunc and G. S. Hotamisligil, "Lipid signaling and lipotoxicity in metaflammation: indications for metabolic disease pathogenesis and treatment.," *J. Lipid Res.*, vol. 57, no. 12, pp. 2099–2114, 2016.

[49] G. S. Hotamisligil, S. Shargill, and B. M. Spiegelman, "Adipose Expression of Tumor Necrosis Factor-α : Direct Role in Obesity-Linked Insulin Resistance," *Science*, vol. 259, no. 5091, pp. 87–91, 1993.

[50] K. T. Uysal, S. M. Wiesbrock, M. W. Marino, and G. S. Hotamisligil, "Protection from obesity-induced insulin resistance in mice lacking TNF function.," *Nature*, vol. 389, no. 6651, pp. 610–614, 1997.

[51] J. Ventre *et al.*, "Targeted Disruption of the Tumor Necrosis Factor- Gene: Metabolic Consequences in Obese and Nonobese Mice," *Diabetes*, vol. 46, no. 9, pp. 1526–1531, 1997.

[52] G. Solinas and M. Karin, "JNK1 and IKKβ: molecular links between obesity and metabolic dysfunction," *FASEB J.*, vol. 24, no. 8, pp. 2596–2611, 2010.

[53] J. S. Orr, M. J. Puglisi, K. L. J. Ellacott, C. N. Lumeng, D. H. Wasserman, and A. H. Hasty, "Toll-like receptor 4 deficiency promotes the alternative activation of adipose tissue macrophages," *Diabetes*, vol. 61, no. 11, pp. 2718–2727, 2012.

[54] R. Stienstra *et al.*, "Inflammasome is a central player in the induction of obesity and insulin resistance," *Proc. Natl. Acad. Sci.*, vol. 108, no. 37, pp. 15324–15329, 2011.

[55] B. Vandanmagsar *et al.*, "The NALP3/NLRP3 Inflammasome Instigates Obesity-Induced Autoinflammation and Insulin Resistance," *Nat. Med.*, vol. 17, no. 2, pp. 179–188, 2011.

[56] H. Wen *et al.*, "Fatty acid-induced NLRP3-ASC inflammasome activation interferes with insulin signaling.," *Nat. Immunol.*, vol. 12, no. 5, pp. 408–15, 2011.

[57] S. P. Weisberg, D. McCann, M. Desai, M. Rosenbaum, R. L. Leibel, and A. W. Ferrante, "Obesity is associated with macrophage accumulation in adipose tissue," *J. Clin. Invest.*, vol. 112, no. 12, pp. 1796–1808, 2003.

[58] H. Xu *et al.*, "Chronic inflammation in fat plays a crucial role in the development of obesity-related insulin resistance," *J. Clin. Invest.*, vol. 112, no. 12, pp. 1821–1830, 2003.

[59] J. M. Olefsky and C. K. Glass, "Macrophages, Inflammation, and Insulin Resistance," *Annu. Rev. Physiol.*, vol. 72, pp. 219–246, 2010.

[60] S. Winer *et al.*, "Normalization of obesity-associated insulin resistance

through immunotherapy.," *Nat. Med.*, vol. 15, no. 8, pp. 921–9, 2009.

[61] U. Kintscher *et al.*, "T-lymphocyte infiltration in visceral adipose tissue: A primary event in adipose tissue inflammation and the development of obesity-mediated insulin resistance," *Arterioscler. Thromb. Vasc. Biol.*, vol. 28, no. 7, pp. 1304–1310, 2008.

[62] S. Nishimura *et al.*, "CD8+ effector T cells contribute to macrophage recruitment and adipose tissue inflammation in obesity," *Nat. Med.*, vol. 15, no. 8, pp. 914–920, 2009.

[63] M. Feuerer *et al.*, "Fat Treg cells: a liaison between the immune and metabolic systems," *Nat. Med.*, vol. 15, no. 8, pp. 930–939, 2009.

[64] K. J. Strissel *et al.*, "Adipocyte death, adipose tissue remodeling, and obesity complications," *Diabetes*, vol. 56, no. 12, pp. 2910–2918, 2007.

[65] M. Y. Donath, "Targeting inflammation in the treatment of type 2 diabetes," *Diabetes, Obes. Metab.*, vol. 15, no. S3, pp. 193–196, 2013.

[66] G. Winkler *et al.*, "Elevated serum TNF-alpha level as a link between endothelial dysfunction and insulin resistance in normotensive obese patients," *Diabet. Med.*, vol. 16, no. 3, pp. 207–211, 1999.

[67] C. A. Meier, E. Bobbioni, C. Gabay, F. Assimacopoulos-Jeannet, A. Golay, and J. M. Dayer, "IL-1 receptor antagonist serum levels are increased in human obesity: A possible link to the resistance to leptin?," *J. Clin. Endocrinol. Metab.*, vol. 87, no. 3, pp. 1184–1188, 2002.

[68] H. Dominguez *et al.*, "Metabolic and vascular effects of tumor necrosis factor-α blockade with etanercept in obese patients with type 2 diabetes," *J. Vasc. Res.*, vol. 42, no. 6, pp. 517–525, 2005.

[69] F. Ofei, S. Hurel, J. Newkirk, M. Sopwith, and R. Taylor, "Effects of an engineered human anti-TNF-a antibody (CDP571) on insulin sensitivity and glycemic control in patients with NIDDM," *Diabetes*, vol. 45, no. 7, pp. 881–885, 1996.

[70] D. H. Solomon, E. Massarotti, and C. Canning, "Association Between Disease-Modifying Antirheumatic Drugs and Diabetes Risk in Patients With Rheumatoid Arthritis and Psoriasis," *JAMA*, vol. 305, no. 24, pp. 2525–2531, 2011.

[71] M. A. Gonzalez-Gay, C. Gonzalez-Juanatey, T. R. Vazquez-Rodriguez, J.

A. Miranda-Filloy, and J. Llorca, "Insulin resistance in rheumatoid arthritis: the impact of the anti-TNF-alpha therapy," *Ann. N. Y. Acad. Sci.*, vol. 1193, no. 1, pp. 153–159, 2010.

[72] K. H. Shen, C. K. Chang, M. T. Lin, and C. P. Chang, "Interleukin-1 receptor antagonist restores homeostatic function and limits multiorgan damage in heatstroke," *Eur. J. Appl. Physiol.*, vol. 103, no. 5, pp. 561–568, 2008.

[73] S. Perrier, F. Darakhshan, and E. Hajduch, "IL-1 receptor antagonist in metabolic diseases: Dr Jekyll or Mr Hyde?," *FEBS Lett.*, vol. 580, no. 27, pp. 6289–6294, 2006.

[74] D. Ballak, R. Stienstra, C. Tack, C. Dinarello, and J. van Diepen, "IL-1 family members in the pathogenesis and treatment of metabolic disease: Focus on adipose tissue inflammation and insulin resistance," *Cytokine*, vol. 75, no. 2, pp. 280–290, 2015.

[75] C. M. Larsen *et al.*, "Interleukin-1-Receptor Antagonist in Type 2 Diabetes Mellitus," *N. Engl. J. Med.*, vol. 357, no. 15, pp. 1517–1526, 2007.

[76] N. Esser, N. Paquot, and A. J. Scheen, "Anti-inflammatory agents to treat or prevent type 2 diabetes, metabolic syndrome and cardiovascular disease," *Expert Opin Investig Drugs*, vol. 24, no. 3, pp. 283–307, 2014.

[77] B. Gross, M. Pawlak, P. Lefebvre, and B. Staels, "PPARs in obesity-induced T2DM, dyslipidaemia and NAFLD," *Nat. Rev. Endocrinol.*, vol. 13, no. 1, pp. 36–49, 2017.

[78] M. Hamaguchi and S. Sakaguchi, "Regulatory T cells expressing PPAR-γ control inflammation in obesity," *Cell Metab.*, vol. 16, no. 1, pp. 4–6, 2012.

[79] R. Wall, R. P. Ross, G. F. Fitzgerald, and C. Stanton, "Fatty acids from fish: The anti-inflammatory potential of long-chain omega-3 fatty acids," *Nutr. Rev.*, vol. 68, no. 5, pp. 280–289, 2010.

[80] T. M. Stulnig, "Immunomodulation by polyunsaturated fatty acids: Mechanisms and effects," *Int. Arch. Allergy Immunol.*, vol. 132, no. 4, pp. 310–321, 2003.

[81] T.-D. Kanneganti and V. D. Dixit, "Immunological complications of obesity," *Nat. Immunol.*, vol. 13, no. 8, pp. 707–712, 2012.

[82] O. Osborn and J. M. Olefsky, "The cellular and signaling networks linking the immune system and metabolism in disease.," *Nat. Med.*, vol. 18, no. 3, pp. 363–74, 2012.

[83] D. Patsouris, P. P. Li, D. Thapar, J. Chapman, J. M. Olefsky, and J. G. Neels, "Ablation of CD11c-Positive Cells Normalizes Insulin Sensitivity in Obese Insulin Resistant Animals," *Cell Metab.*, vol. 8, no. 4, pp. 301–309, 2008.

[84] J. Liu *et al.*, "Genetic deficiency and pharmacological stabilization of mast cells reduce diet-induced obesity and diabetes in mice.," *Nat. Med.*, vol. 15, no. 8, pp. 940–5, 2009.

[85] M. J. Arends, E. S. White, and C. B. a Whitelaw, "Animal and cellular models of human disease.," *J. Pathol.*, vol. 238, no. 2, pp. 137–40, 2016.

[86] C. Nilsson, K. Raun, F. Yan, M. O. Larsen, and M. Tang-Christensen, "Laboratory animals as surrogate models of human obesity.," *Acta Pharmacol. Sin.*, vol. 33, no. 2, pp. 173–81, 2012.

[87] P. McGonigle and B. Ruggeri, "Animal models of human disease: Challenges in enabling translation," *Biochem. Pharmacol.*, vol. 87, no. 1, pp. 162–171, 2014.

[88] O. E. Varga, A. K. Hansen, P. Sandoe, and A. S. Olsson, "Validating Animal Models for Preclinical Research: A Scientific and Ethical Discussion," *Altern. Lab. Anim.*, vol. 38, no. 3, pp. 245–248, 2010.

[89] C. Nathan, "Metchnikoff's Legacy in 2008," *Nat. Immunol.*, vol. 9, no. 7, pp. 695–698, 2008.

[90] R. van Furth, Z. Cohn, J. Hirsh, J. Humphrey, W. Spector, and H. Langevoort, "The mononuclear phagocyte system: a new classification of macrophages, monocytes, and their precursor cells," *Bull. World Heal. Organ.*, vol. 46, no. 6, pp. 845–852, 1972.

[91] K. Takahashi, "Development and Differentiation of Macrophages and Related Cells: Historical Review and Current Concepts," *J. Clin. Exp. Hematop.*, vol. 41, no. 1, pp. 1–33, 2001.

[92] D. A. Hume, "Differentiation and heterogeneity in the mononuclear phagocyte system," *Mucosal Immunol.*, vol. 1, no. 6, pp. 432–441, 2008.

[93] P. Italiani and D. Boraschi, "From monocytes to M1/M2 macrophages:

Phenotypical vs. functional differentiation," *Front. Immunol.*, vol. 5, pp. 514–522, 2014.

[94] T. A. Wynn, A. Chawla, and J. W. Pollard, "Macrophage biology in development, homeostasis and disease.," *Nature*, vol. 496, no. 7446, pp. 445–55, 2013.

[95] G. Hoeffel and F. Ginhoux, "Ontogeny of tissue-resident macrophages," *Front. Immunol.*, vol. 6, no. 486, pp. 1–14, 2015.

[96] J. Sheng, C. Ruedl, and K. Karjalainen, "Most Tissue-Resident Macrophages Except Microglia Are Derived from Fetal Hematopoietic Stem Cells," *Immunity*, vol. 43, no. 2, pp. 382–393, 2015.

[97] F. Ginhoux *et al.*, "Fate Mapping Analysis Reveals That Adult Microglia Derive from Primitive Macrophages," *Science (80-.).*, vol. 330, no. 6005, pp. 841–845, 2010.

[98] G. Hoeffel *et al.*, "Adult Langerhans cells derive predominantly from embryonic fetal liver monocytes with a minor contribution of yolk sac-derived macrophages.," *J. Exp. Med.*, vol. 209, no. 6, pp. 1167–81, 2012.

[99] F. Ginhoux, J. L. Schultze, P. J. Murray, J. Ochando, and S. K. Biswas, "New insights into the multidimensional concept of macrophage ontogeny, activation and function.," *Nat. Immunol.*, vol. 17, no. 1, pp. 34–40, 2015.

[100] F. Ginhoux and S. Jung, "Monocytes and macrophages: developmental pathways and tissue homeostasis," *Nat. Rev. Immunol.*, vol. 14, no. 6, pp. 392–404, 2014.

[101] C. C. Bain *et al.*, "Constant replenishment from circulating monocytes maintains the macrophage pool in the intestine of adult mice.," *Nat. Immunol.*, vol. 15, no. 10, pp. 929–37, 2014.

[102] S. Epelman *et al.*, "Embryonic and adult-derived resident cardiac macrophages are maintained through distinct mechanisms at steady state and during inflammation," *Immunity*, vol. 40, no. 1, pp. 91–104, 2014.

[103] S. Tamoutounour *et al.*, "Origins and functional specialization of macrophages and of conventional and monocyte-derived dendritic cells in mouse skin," *Immunity*, vol. 39, no. 5, pp. 925–938, 2013.

[104] J. A. Hamilton, "Colony-stimulating factors in inflammation and

autoimmunity John," *Trends Immunol.*, vol. 23, no. 8, pp. 403–408, 2002.

[105] I. Ushach and A. Zlotnik, "Biological role of granulocyte macrophage colony-stimulating factor (GM-CSF) and macrophage colony-stimulating factor (M-CSF) on cells of the myeloid lineage.," *J. Leukoc. Biol.*, vol. 100, no. September, pp. 1–9, 2016.

[106] X. Dai *et al.*, "Targeted disruption of the mouse CSF-1 receptor gene results in osteopetrosis, mononuclear phagocyte deficiency, increased primititive progenitor cell frequencies and reproductive defects.," *Blood*, vol. 99, no. 1, pp. 111–120, 2002.

[107] S. Wei *et al.*, "Functional overlap but differential expression of CSF-1 and IL-34 in their CSF-1 receptor-mediated regulation of myeloid cells," *J. Leukoc. Biol.*, vol. 88, no. 3, pp. 495–505, 2010.

[108] Y. Wang *et al.*, "IL-34 is a tissue-restricted ligand of CSF1R required for the development of Langerhans cells and microglia," *Nat. Immunol.*, vol. 13, no. 8, pp. 753–760, 2014.

[109] Y. Lavin, A. Mortha, A. Rahman, and M. Merad, "Regulation of macrophage development and function in peripheral tissues.," *Nat. Rev. Immunol.*, vol. 15, no. 12, pp. 731–44, 2015.

[110] V. Chitu and E. R. Stanley, "Colony-stimulating factor-1 in immunity and inflammation," *Curr. Opin. Immunol.*, vol. 18, no. 1, pp. 39–48, 2006.

[111] D. A. Hume and K. P. A. MacDonald, "Therapeutic applications of macrophage colony-stimulating factor-1 (CSF-1) and antagonists of CSF-1 receptor (CSF-1R) signaling," *Blood*, vol. 119, no. 8, pp. 1810–1820, 2012.

[112] R. Chovatiya and R. Medzhitov, "Stress, inflammation, and defense of homeostasis," *Mol. Cell*, vol. 54, no. 2, pp. 281–288, 2014.

[113] C. Shi and E. G. Pamer, "Monocyte Recruitment During Infection and Inflammation," *Nat Rev Immunol*, vol. 11, no. 11, pp. 762–774, 2014.

[114] S. U. Amano *et al.*, "Local proliferation of macrophages contributes to obesity-associated adipose tissue inflammation," *Cell Metab.*, vol. 19, no. 1, pp. 162–171, 2014.

[115] D. M. Mosser and J. P. Edwards, "Exploring the full spectrum of macrophage activation.," *Nat. Rev. Immunol.*, vol. 8, no. 12, pp. 958–

69, 2008.

[116] P. J. Murray and T. A. Wynn, "Protective and pathogenic functions of macrophage subsets," *Nat. Rev. Immunol.*, vol. 11, no. 11, pp. 723–737, 2011.

[117] a B. Roberts *et al.*, "Transforming growth factor type β: rapid induction of fibrosis and angiogenesis in vivo and stimulation of collagen formation in vitro.," *Proc. Natl. Acad. Sci. U. S. A.*, vol. 83, no. 12, pp. 4167–71, 1986.

[118] B. Ruffell and L. M. Coussens, "Macrophages and therapeutic resistance in cancer," *Cancer Cell*, vol. 27, no. 4, pp. 462–472, 2015.

[119] L. Barron and T. a Wynn, "Fibrosis is regulated by Th2 and Th17 responses and by dynamic interactions between fibroblasts and macrophages.," *Am. J. Physiol. Gastrointest. Liver Physiol.*, vol. 300, no. 5, pp. G723-8, 2011.

[120] T. A. Wynn and K. M. Vannella, "Macrophages in Tissue Repair, Regeneration, and Fibrosis," *Immunity*, vol. 44, no. 3, pp. 450–462, 2016.

[121] C. N. Lumeng, J. L. Bodzin, and A. R. Saltiel, "Obesity induces a phenotipic switch in adipose tissue macrophage polarization," *J Clin Invest*, vol. 117, no. 1, pp. 175–184, 2007.

[122] A. B. Sanz *et al.*, "Macrophages and recently identified forms of cell death.," *Int. Rev. Immunol.*, vol. 33, no. 1, pp. 9–22, 2014.

[123] P. J. Murray *et al.*, "Macrophage Activation and Polarization: Nomenclature and Experimental Guidelines," *Immunity*, vol. 41, no. 1, pp. 14–20, 2014.

[124] J. L. Schultze, T. Freeman, D. A. Hume, and E. Latz, "A transcriptional perspective on human macrophage biology," *Semin. Immunol.*, vol. 27, no. 1, pp. 44–50, 2015.

[125] F. O. Martinez and S. Gordon, "The M1 and M2 paradigm of macrophage activation: time for reassessment.," *F1000Prime Rep.*, vol. 6, p. 13, 2014.

[126] A. Sica and A. Mantovani, "Macrophage plasticity and polarization: in vivo veritas," *J. Clin. Invest.*, vol. 122, no. 3, pp. 787–795, 2012.

[127] F. O. Martinez, S. Gordon, M. Locati, and A. Mantovani,

"Transcriptional profiling of the human monocyte-to-macrophage differentiation and polarization: new molecules and patterns of gene expression," *J. Immunol.*, vol. 177, no. 10, pp. 7303–7311, 2006.

[128] S. K. Biswas and A. Mantovani, "Macrophage plasticity and interaction with lymphocyte subsets : cancer as a paradigm," *Nat. Immunol.*, vol. 11, no. 10, pp. 889–896, 2010.

[129] F. O. Martinez, A. Sica, A. Mantovani, and M. Locati, "Macrophage activation and polarization," *Front. Biosci.*, vol. 13, no. 4, pp. 453–461, 2008.

[130] C. E. Bryant, N. J. Gay, S. Heymans, S. Sacre, L. Schaefer, and K. S. Midwood, "Advances in Toll-like receptor biology: Modes of activation by diverse stimuli.," *Crit. Rev. Biochem. Mol. Biol.*, vol. 50, no. 5, pp. 359–379, 2015.

[131] S. Akira and K. Takeda, "Toll-like receptor signalling," *Nat. Rev. Immunol.*, vol. 4, no. 7, pp. 499–511, 2004.

[132] T. Kawai and S. Akira, "The role of pattern-recognition receptors in innate immunity: update on Toll-like receptors.," *Nat. Immunol.*, vol. 11, no. 5, pp. 373–384, 2010.

[133] M. O. Ullah, M. J. Sweet, A. Mansell, S. Kellie, and B. Kobe, "TRIF-dependent TLR signaling, its functions in host defense and inflammation, and its potential as a therapeutic target.," *J. Leukoc. Biol.*, vol. 100, no. 1, pp. 27–45, 2016.

[134] N. J. Gay and M. Gangloff, "Structure and Function of Toll Receptors and Their Ligands," *Annu. Rev. Biochem.*, vol. 76, no. 1, pp. 141–165, 2007.

[135] K. Takeda and S. Akira, "TLR signaling pathways," *Semin. Immunol.*, vol. 16, no. 1, pp. 3–9, 2004.

[136] A. Agrawal, S. Dillon, T. L. Denning, and B. Pulendran, "ERK1-/- mice exhibit Th1 cell polarization and increased susceptibility to experimental autoimmune encephalomyelitis.," *J. Immunol.*, vol. 176, pp. 5788–5796, 2006.

[137] W. Ma *et al.*, "The p38 Mitogen Activated Kinase Pathway Regulates the Human IL-10 Promoter via the Activation of Sp1 Transcription Factor in Lipopolysaccharide-Stimulated Human Macrophages," *J. Biol. Chem.*, vol. 276, no. 17, pp. 13664–13674, 2001.

[138] K. Eguchi and I. Manabe, "Toll-Like Receptor, Lipotoxicity and Chronic inflammation: The Pathological Link Between Obesity and Cardiometabolic Disease.," *J. Atheroscler. Thromb.*, vol. 21, no. 7, pp. 629–639, 2014.

[139] H. Shi, M. V Kokoeva, K. Inouye, I. Tzameli, H. Yin, and J. S. Flier, "TLR4 links innate immunity and fatty acid – induced insulin resistance," *J. Clin. Invest.*, vol. 116, no. 11, pp. 3015–3025, 2006.

[140] B. Ruiz-Núñez, D. A. J. Dijck-Brouwer, and F. A. J. Muskiet, "The relation of saturated fatty acids with low-grade inflammation and cardiovascular disease," *J. Nutr. Biochem.*, vol. 36, pp. 1–20, 2016.

[141] J. Clària, A. González-Périz, C. López-Vicario, B. Rius, and E. Titos, "New insights into the role of macrophages in adipose tissue inflammation and fatty liver disease: Modulation by endogenous omega-3 fatty acid-derived lipid mediators," *Front. Immunol.*, vol. 2, no. 49, pp. 1–8, 2011.

[142] S. K. Biswas and A. Mantovani, "Orchestration of metabolism by macrophages," *Cell Metab.*, vol. 15, no. 4, pp. 432–437, 2012.

[143] K. Ganeshan and A. Chawla, "Metabolic Regulation of Immune Responses," *J. Clin. Invest.*, vol. 32, no. 1, pp. 609–634, 2014.

[144] E. Izquierdo *et al.*, "Reshaping of Human Macrophage Polarization through Modulation of Glucose Catabolic Pathways.," *J. Immunol.*, vol. 195, no. 5, pp. 2442–51, 2015.

[145] G. S. Hotamisligil, "Endoplasmic Reticulum Stress and the Inflammatory Basis of Metabolic Disease," *Cell*, vol. 140, no. 6, pp. 900–917, 2010.

[146] G. S. Hotamisligil and E. Erbay, "Nutrient sensing and inflammation in metabolic diseases.," *Nat. Rev. Immunol.*, vol. 8, no. 12, pp. 923–934, 2008.

[147] A. Rull, J. Camps, C. Alonso-Villaverde, and J. Joven, "Insulin resistance, inflammation, and obesity: Role of monocyte chemoattractant protein-1 (or CCL2) in the regulation of metabolism," *Mediators Inflamm.*, vol. 2010, no. Figure 1, 2010.

[148] S. E. Shoelson, J. Lee, and M. Yuan, "Inflammation and the IKK beta/I kappa B/NF-kappa B axis in obesity- and diet-induced insulin resistance," *Int J Obes Relat Metab Disord*, vol. 27 Suppl 3, pp. S49-52, 2003.

References

[149] M. C. Arkan *et al.*, "IKK-beta links inflammation to obesity-induced insulin resistance.," *Nat. Med.*, vol. 11, no. 2, pp. 191–198, 2005.

[150] L. Weissmann *et al.*, "IKKε is key to induction of insulin resistance in the hypothalamus, and its inhibition reverses obesity," *Diabetes*, vol. 63, no. 10, pp. 3334–3345, 2014.

[151] C. Cao *et al.*, "Deficiency of IKKε inhibits inflammation and induces cardiac protection in high-fat diet-induced obesity in mice," *Int. J. Mol. Med.*, vol. 34, no. 1, pp. 244–252, 2014.

[152] S. M. Reilly *et al.*, "An inhibitor of the protein kinases TBK1 and IKK-ε improves obesity-related metabolic dysfunctions in mice.," *Nat. Med.*, vol. 19, no. 3, pp. 313–21, 2013.

[153] M. Yuan, "Reversal of Obesity- and Diet-Induced Insulin Resistance with Salicylates or Targeted Disruption of Ikkbeta," *Science*, vol. 293, no. 5535, pp. 1673–1677, 2001.

[154] J. Hirosumi *et al.*, "A central role for JNK in obesity and insulin resistance.," *Nature*, vol. 420, no. 6913, pp. 333–336, 2002.

[155] M. S. Han *et al.*, "JNK Expression by Macrophages Promotes Obesity-induced Insulin Resistance and Inflammation," *Science*, vol. 339, no. 6116, pp. 218–222, 2013.

[156] V. Subramanian and A. W. Ferrante, "Obesity , Inflammation , and Macrophages," *Nesté Nutr Inst Work. Ser Pediatr Progr.*, vol. 63, pp. 151–162, 2009.

[157] A. Sussulini, *Metabolomics: From Fundamentals to Clinical Applications*, vol. 965. 2017.

[158] R. Bujak, W. Struck-Lewicka, M. J. Markuszewski, and R. Kaliszan, "Metabolomics for laboratory diagnostics," *J. Pharm. Biomed. Anal.*, vol. 113, pp. 108–120, 2014.

[159] C. R. Roe, D. S. Millington, and D. A. Maltby, "Identification of 3-Methylglutarylcarnitine," *J. Clin. Invest.*, vol. 77, no. 4, pp. 1391–1394, 1986.

[160] E. Jellum, E. A. Kvittingen, and O. Stokke, "Mass spectrometry in diagnosis of metabolic disorders," *Biol. Mass Spectrom.*, vol. 16, no. 1–12, pp. 57–62, 1988.

[161] L. D. Roberts and R. E. Gerszten, "Toward new biomarkers of

cardiometabolic diseases," *Cell Metab.*, vol. 18, no. 1, pp. 43–50, 2013.

[162] A. Zhang, H. Sun, and X. Wang, "Power of metabolomics in biomarker discovery and mining mechanisms of obesity," *Obes. Rev.*, vol. 14, no. 4, pp. 344–349, 2013.

[163] C. K. Lim *et al.*, "Kynurenine pathway metabolomics predicts and provides mechanistic insight into multiple sclerosis progression," *Sci. Rep.*, vol. 7, p. 41473, 2017.

[164] M. D. Lovelace *et al.*, "Current evidence for a role of the kynurenine pathway of tryptophan metabolism in multiple sclerosis," *Front. Immunol.*, vol. 7, pp. 1–22, 2016.

[165] T. Hatano, S. Saiki, A. Okuzumi, R. P. Mohney, and N. Hattori, "Identification of novel biomarkers for Parkinson's disease by metabolomic technologies," *J. Neurol. Neurosurg. Psychiatry*, vol. 87, no. 3, pp. 295–301, 2016.

[166] S. J. Mihalik *et al.*, "Metabolomic profiling of fatty acid and amino acid metabolism in youth with obesity and type 2 diabetes: Evidence for enhanced mitochondrial oxidation," *Diabetes Care*, vol. 35, no. 3, pp. 605–611, 2012.

[167] C. B. Newgard, "Interplay between lipids and branched-chain amino acids in development of insulin resistance," *Cell Metab.*, vol. 15, no. 5, pp. 606–614, 2012.

[168] C. J. Lynch and S. H. Adams, "Branched-chain amino acids in metabolic signaling and insulin resistance," *Nat Rev Endrocrinol*, vol. 10, no. 12, pp. 723–736, 2014.

[169] Y. Aida *et al.*, "Serum cytokeratin 18 fragment level as a noninvasive biomarker for non-alcoholic fatty liver disease," *Int. J. Clin. Exp. Med.*, vol. 7, no. 11, pp. 4191–4198, 2014.

[170] E. Rodríguez-Gallego *et al.*, "Mapping of the circulating metabolome reveals α-ketoglutarate as a predictor of morbid obesity-associated non-alcoholic fatty liver disease.," *Int. J. Obes. (Lond).*, vol. 39, no. 2, pp. 279–87, 2015.

[171] A. Sahebkar, E. Sancho, D. Abello, J. Camps, and J. Joven, "Novel Circulating Biomarkers for Non-Alcoholic Fatty Liver Disease: A Systematic Review.," *J. Cell. Physiol.*, January, 2017.

[172] K. Suhre *et al.*, "Metabolic footprint of diabetes: A multiplatform metabolomics study in an epidemiological setting," *PLoS One*, vol. 5, no. 11, p. e13953, 2010.

[173] P. Vannini *et al.*, "Branched-Chain Amino Acids and Alanine as Indices of the Metabolic Control in Type 1 (Insulin-Dependent) and Type 2 (Non-Insulin-Dependent) Diabetic Patients P.," *Diabetologia*, vol. 22, pp. 217–219, 1982.

[174] M. Zagura *et al.*, "Metabolomic signature of arterial stiffness in male patients with peripheral arterial disease.," *Hypertens. Res.*, vol. 38, no. 12, pp. 840–846, 2015.

[175] L. Dang *et al.*, "Cancer-associated IDH1 mutations produce 2-hydroxyglutarate.," *Nature*, vol. 462, no. 7274, pp. 739–44, 2009.

[176] P. S. Ward *et al.*, "Identification of additional IDH mutations associated with oncometabolite R(−)-2-hydroxyglutarate production," *Oncogene*, vol. 31, no. 19, pp. 2491–2498, 2012.

[177] P. Jiang, W. Du, and M. Wu, "Regulation of the pentose phosphate pathway in cancer," *Protein Cell*, vol. 5, no. 8, pp. 592–602, 2014.

[178] A. Ramos-Montoya *et al.*, "Pentose phosphate cycle oxidative and nonoxidative balance: A new vulnerable target for overcoming drug resistance in cancer," *Int. J. Cancer*, vol. 119, no. 12, pp. 2733–2741, 2006.

[179] M. Vander Heiden, L. Cantley, and C. Thompson, "Understanding the Warburg effect: The metabolic Requiremetns of cell proliferation," *Science*, vol. 324, no. 5930, pp. 1029–1033, 2009.

[180] P. E. Minkler, J. Kerner, T. Kasumov, W. Parland, and C. L. Hoppel, "Quantification of malonyl-coenzyme A in tissue specimens by high-performance liquid chromatography/mass spectrometry," *Anal. Biochem.*, vol. 352, no. 1, pp. 24–32, 2006.

[181] R. R. Gilibili, M. Kandaswamy, K. Sharma, S. Giri, S. Rajagopal, and R. Mullangi, "Development and validation of a highly sensitive LC-MS/MS method for simultaneous quantitation of acetyl-CoA and malonyl-CoA in animal tissues," *Biomed. Chromatogr.*, vol. 25, no. 12, pp. 1352–1359, 2011.

[182] T. Ota *et al.*, "Insulin Resistance Accelerates a Dietary Rat Model of Nonalcoholic Steatohepatitis," *Gastroenterology*, vol. 132, no. 1, pp. 282–293, 2007.

References

[183] Y. Li, V. Periwal, S. W. Cushman, and K. G. Stenkula, "Adipose cell hypertrophy precedes the appearance of small adipocytes by 3 days in C57BL/6 mouse upon changing to a high fat diet," *Adipocyte*, vol. 5, no. 1, pp. 81–87, 2016.

[184] G. S. Roth and D. K. Ingram, "Manipulation of health span and function by dietary caloric restriction mimetics," *Ann. N. Y. Acad. Sci.*, vol. 1363, no. 1, pp. 5–10, 2016.

[185] C. Selman, "Dietary restriction and the pursuit of effective mimetics," *Proc. Nutr. Soc.*, vol. 73, p. 260–270., 2014.

[186] J. R. Speakman and S. E. Mitchell, "Caloric restriction," *Mol. Aspects Med.*, vol. 32, no. 3, pp. 159–221, 2011.

[187] M. A. Linden *et al.*, "Combining metformin therapy with caloric restriction for the management of type 2 diabetes and nonalcoholic fatty liver disease in obese rats," *Appl. Physiol. Nutr. Metab.*, vol. 40, no. 10, pp. 1038–1047, 2016.

[188] Y. M. Song *et al.*, "Metformin alleviates hepatosteatosis by restoring SIRT1-mediated autophagy induction via an AMP-activated protein kinase-independent pathway," *Autophagy*, vol. 11, no. 1, pp. 46–59, 2015.

[189] M. A. Herman, P. She, O. D. Peroni, C. J. Lynch, and B. B. Kahn, "Adipose tissue Branched Chain Amino Acid (BCAA) metabolism modulates circulating BCAA levels," *J. Biol. Chem.*, vol. 285, no. 15, pp. 11348–11356, 2010.

[190] C. R. Green *et al.*, "Branched-chain amino acid catabolism fuels adipocyte differentiation and lipogenesis," *Nat Chem Biol*, vol. 12, no. 1, pp. 15–21, 2016.

[191] I. Estrada-Alcalde *et al.*, "Metabolic Fate of Branched-Chain Amino Acids During Adipogenesis, in Adipocytes from Obese Mice and C2C12 Myotubes," *J. Cell. Biochem.*, vol. 118, no. 4, pp. 808–818, 2016.

[192] R. Pryor and F. Cabreiro, "Repurposing metformin: an old drug with new tricks in its binding pockets," *Biochem. J.*, vol. 471, no. 3, pp. 307–322, 2015.

[193] M. R. Owen, E. Doran, and A. P. Halestrap, "Evidence that metformin exerts its anti-diabetic effects through inhibition of complex 1 of the mitochondrial respiratory chain," *Biochem. J.*, vol. 348, no. 3, pp. 607–614, 2000.

[194] A. Vazquez-Martin *et al.*, "Metformin limits the tumourigenicity of iPS cells without affecting their pluripotency," *Sci Rep*, vol. 2, p. 964, 2012.

[195] N. Barzilai, J. P. Crandall, S. B. Kritchevsky, and M. A. Espeland, "Metformin as a Tool to Target Aging," *Cell Metab.*, vol. 23, no. 6, pp. 1060–1065, 2016.

[196] G. Zhou *et al.*, "Role of AMP-Activated Protein Kinase in Mechanism of Metformin Action Role of AMP-activated protein kinase in mechanism of metformin action," *J. Clin. Invest.*, vol. 108, no. 8, pp. 1167–1174, 2001.

[197] E. Alcocer-Gómez *et al.*, "Metformin and caloric restriction induce an AMPK-dependent restoration of mitochondrial dysfunction in fibroblasts from Fibromyalgia patients," *Biochim. Biophys. Acta*, vol. 1852, no. 7, pp. 1257–1267, 2015.

[198] D. Dong *et al.*, "Alleviation of senescence and epithelial-mesenchymal transition in aging kidney by short-term caloric restriction and caloric restriction mimetics via modulation of AMPK/mTOR signaling," *Oncotarget*, vol. 8, no. 10, pp. 16109–16121, 2016.

[199] A. Leung, C. Trac, J. Du, R. Natarajan, and D. E. Schones, "Persistent Chromatin Modifications Induced by High Fat Diet.," *J. Biol. Chem.*, vol. 291, no. 20, pp. 10446–55, 2016.

[200] A. Leung *et al.*, "Open chromatin profiling in mice livers reveals unique chromatin variations induced by high fat diet," *J. Biol. Chem.*, vol. 289, no. 34, pp. 23557–23567, 2014.

[201] Q. Yang *et al.*, "AMPK/a-Ketoglutarate Axis Dynamically Mediates DNA Demethylation in the Prdm16 Promoter and Brown Adipogenesis," *Cell Metab.*, vol. 24, no. 4, pp. 542–554, 2016.

[202] E. Cuyàs, S. Fernández-Arroyo, J. Joven, and J. Menéndez, "Metformin targets histone acetylation in cancer-prone epithelial cells," *Cell Cycle*, vol. 15, no. 24, pp. 3355–3361, 2016.

[203] L. Nie *et al.*, "The Landscape of Histone Modifications in a High-Fat-Diet-Induced Obese (DIO) Mouse Model," *Mol. Cell. Proteomics*, pp. 1–32, 2017.

[204] P. D. Cani *et al.*, "Metabolic Endotoxemia Initiates Obesity and Insulin Resistance," *Diabetes*, vol. 56, no. 7, pp. 1761–1772, 2007.

References

[205] P. D. Cani, R. Bibiloni, C. Knauf, A. M. Neyrinck, and N. M. Delzenne, "Changes in gut microbiota control metabolic diet–induced obesity and diabetes in mice," *Diabetes*, vol. 57, no. 6, pp. 1470–81, 2008.

[206] G. Solinas and B. Becattini, "JNK at the crossroad of obesity, insulin resistance, and cell stress response," *Mol. Metab.*, vol. 6, no. 2, pp. 174–184, 2016.

[207] R. G. Baker, M. S. Hayden, and S. Ghosh, "NFκB, inflammation, and metabolic disease," *Cell Metab.*, vol. 13, no. 1, pp. 11–22, 2011.

[208] J. W. M. van der Meer, L. A. B. Joosten, N. Riksen, and M. G. Netea, "Trained immunity: A smart way to enhance innate immune defence," *Mol. Immunol.*, vol. 68, no. 1, pp. 40–44, 2015.

[209] M. G. Netea *et al.*, "Trained immunity: A program of innate immune memory in health and disease," *Science*, vol. 352, no. 6284, p. aaf1098, 2016.

[210] S. Saeed *et al.*, "Epigenetic programming during monocyte to macrophage differentiation and trained innate immunity," *Science*, vol. 345, no. 6204, pp. 1–26, 2014.

[211] S.-C. Cheng *et al.*, "mTOR/HIF1 alpha-mediated aerobic glycolysis as metabolic basis for trained immunity," *Science*, vol. 345, no. 6204, pp. 1–18, 2014.

[212] M. M. Escribese *et al.*, "The prolyl hydroxylase PHD3 identifies proinflammatory macrophages and its expression is regulated by activin A.," *J. Immunol.*, vol. 189, no. 4, pp. 1946–54, 2012.

[213] S. Fujisaka *et al.*, "Adipose tissue hypoxia induces inflammatory M1 polarity of macrophages in an HIF-1α-dependent and HIF-1α-independent manner in obese mice," *Diabetologia*, vol. 56, no. 6, pp. 1403–1412, 2013.

[214] R. G. Snodgrass *et al.*, "Hypoxia potentiates palmitate-induced pro-inflammatory activation of primary human macrophages," *J. Biol. Chem.*, vol. 291, no. 1, pp. 413–424, 2016.

[215] S. K. Biswas and E. Lopez-Collazo, "Endotoxin tolerance: new mechanisms, molecules and clinical significance," *Trends Immunol.*, vol. 30, no. 10, pp. 475–487, 2009.

[216] a E. Medvedev, K. M. Kopydlowski, and S. N. Vogel, "Inhibition of lipopolysaccharide-induced signal transduction in endotoxin-tolerized

mouse macrophages: dysregulation of cytokine, chemokine, and toll-like receptor 2 and 4 gene expression.," *J. Immunol.*, vol. 164, pp. 5564–5574, 2000.

[217] Y. Shav-Tal and D. Zipori, "The role of activin A in regulation of hemopoiesis.," *Stem Cells*, vol. 20, no. 6, pp. 493–500, 2002.

[218] Y.-G. Chen, Q. Wang, S.-L. Lin, C. D. Chang, J. Chuang, and S.-Y. Ying, "Activin signaling and its role in regulation of cell proliferation, apoptosis, and carcinogenesis.," *Exp. Biol. Med. (Maywood).*, vol. 231, no. 5, pp. 534–544, 2006.

[219] D. J. Phillips, D. M. de Kretser, and M. P. Hedger, "Activin and related proteins in inflammation: Not just interested bystanders," *Cytokine Growth Factor Rev.*, vol. 20, no. 2, pp. 153–164, 2009.

[220] E. Gonzalez-Dominguez *et al.*, "Atypical Activin A and IL-10 Production Impairs Human CD16+ Monocyte Differentiation into Anti-Inflammatory Macrophages," *J. Immunol.*, vol. 196, no. 3, pp. 1327–1337, 2016.

[221] E. Sierra-Filardi *et al.*, "Activin A skews macrophage polarization by promoting a proinflammatory phenotype and inhibiting the acquisition of anti-inflammatory macrophage markers," *Blood*, vol. 117, no. 19, pp. 5092–5101, 2011.

[222] B. S. Palacios *et al.*, "Macrophages from the synovium of active rheumatoid arthritis exhibit an activin a-dependent pro-inflammatory profile," *J. Pathol.*, vol. 235, no. 3, pp. 515–526, 2015.

[223] C. Dani, "Activins in adipogenesis and obesity," *Int. J. Obes.*, vol. 37, no. 2, pp. 163–166, 2012.

[224] M. Tsuchiya, R. Misaka, K. Nitta, and K. Tsuchiya, "Transcriptional factors, Mafs and their biological roles.," *World J. Diabetes*, vol. 6, no. 1, pp. 175–83, 2015.

[225] K. Kataoka, K. T. Fujiwara, M. Noda, and M. Nishizawa, "MafB, a new Maf family transcription activator that can associate with Maf and Fos but not with Jun.," *Mol. Cell. Biol.*, vol. 14, no. 11, pp. 7581–7591, 1994.

[226] H. M. Reza, A. Urano, N. Shimada, and K. Yasuda, "Sequential and combinatorial roles of maf family genes define proper lens development.," *Mol. Vis.*, vol. 13, no. January, pp. 18–30, 2007.

[227] I. Artner *et al.*, "MafB is required for islet beta cell maturation," *Proc. Natl. Acad. Sci. U. S. A.*, vol. 104, no. 16, pp. 3853–3858, 2007.

[228] L. M. Kelly, U. Englmeier, I. Lafon, M. H. Sieweke, and T. Graf, "MafB is an inducer of monocytic differentiation.," *EMBO J.*, vol. 19, no. 9, pp. 1987–97, 2000.

[229] A. Aziz, E. Soucie, S. Sarrazin, and M. H. Sieweke, "MafB/c-Maf Deficiency Enables Self-Renewal of Differentiated Functional Macrophages," *Science*, vol. 326, no. 5954, pp. 867–872, 2009.

[230] V. D. Cuevas *et al.*, "MAFB Determines Human Macrophage Anti-Inflammatory Polarization: Relevance for the Pathogenic Mechanisms Operating in Multicentric Carpotarsal Osteolysis," *J. Immunol.*, vol. 198, no. 5, pp. 2070–2081, 2017.

[231] A. M. L. Pettersson *et al.*, "MAFB as a novel regulator of human adipose tissue inflammation," *Diabetologia*, vol. 58, no. 9, pp. 2115–2123, 2015.

[232] T. Shichita *et al.*, "MAFB prevents excess inflammation after ischemic stroke by accelerating clearance of damage signals through MSR1," *Nat. Med.*, no. April, pp. 1–12, 2017.

[233] N. I. Herath, N. Rocques, A. Garancher, A. Eychène, and C. Pouponnot, "GSK3-mediated MAF phosphorylation in multiple myeloma as a potential therapeutic target.," *Blood Cancer J.*, vol. 4, p. e175, 2014.

[234] M. Niceta *et al.*, "Mutations impairing GSK3-mediated MAF phosphorylation cause cataract, deafness, intellectual disability, seizures, and a down syndrome-like facies," *Am. J. Hum. Genet.*, vol. 96, no. 5, pp. 816–825, 2015.

[235] V. Stambolic, L. Ruel, and J. R. Woodgett, "Lithium inhibits glycogen synthase kinase-3 activity and mimics wingless signalling in intact cells.," *Curr. Biol.*, vol. 6, no. 12, pp. 1664–1668, 1996.

[236] P. S. Klein and D. A. Melton, "A molecular mechanism for the effect of lithium on development.," *Proc. Natl. Acad. Sci. U. S. A.*, vol. 93, no. 16, pp. 8455–8459, 1996.

[237] O. Kaidanovich and H. Eldar-Finkelman, "The role of glycogen synthase kinase-3 in insulin resistance and type 2 diabetes.," *Expert Opin. Ther. Targets*, vol. 6, no. 5, pp. 555–61, 2002.

[238] H. Eldar-Finjelman, S. Schreyer, M. Shinohara, R. LeBoueuf, and E.

Krebs, "Increased Glycogen Synthase Kinase-3 Activity in Diabetes- and Obesity-Prone C57BL/6J Mice," *Diabetes*, vol. 48, no. 8, pp. 1662–1666, 1999.

[239] S. Park, K. Park-Min, J. Chen, X. Hu, and L. Ivashkiv, "TNF Induces Endotoxin Tolerance Mediated by GSK3 in Macrophages," *Nat. Immunol.*, vol. 12, no. 7, pp. 607–615, 2012.

[240] H. Tanahashi, K. Kito, T. Ito, and K. Yoshioka, "MafB protein stability is regulated by the JNK and ubiquitin-proteasome pathways," *Arch. Biochem. Biophys.*, vol. 494, no. 1, pp. 94–100, 2010.

[241] L. C. Dieterich *et al.*, "DeepCAGE Transcriptomics Reveal an Important Role of the Transcription Factor MAFB in the Lymphatic Endothelium," *Cell Rep.*, vol. 13, no. 7, pp. 1493–1504, 2015.

[242] P. Henning, H. H. Conaway, and U. H. Lerner, "Retinoid receptors in bone and their role in bone remodeling," *Front. Endocrinol. (Lausanne).*, vol. 6, no. 31, pp. 1–13, 2015.

[243] M. P. Menéndez-Gutiérrez and M. Ricote, "The multi-faceted role of retinoid X receptor in bone remodeling," *Cell. Mol. Life Sci.*, vol. 74, no. 12, pp. 2135-2149, 2017.

[244] F. J. Quintana, "The aryl hydrocarbon receptor: A molecular pathway for the environmental control of the immune response," *Immunology*, vol. 138, no. 3, pp. 183–189, 2013.

[245] A. Bessede *et al.*, "Aryl hydrocarbon receptor control of a disease tolerance defense pathway," *Nature*, vol. 511, no. 7508, pp. 184–190, 2015.

[246] Y. Kawano *et al.*, "Activation of the aryl hydrocarbon receptor induces hepatic steatosis via the upregulation of fatty acid transport," *Arch. Biochem. Biophys.*, vol. 504, no. 2, pp. 221–227, 2010.

[247] M. A. Hauser and D. F. Legler, "Common and biased signaling pathways of the chemokine receptor CCR7 elicited by its ligands CCL19 and CCL21 in leukocytes," *J. Leukoc. Biol.*, vol. 99, no. 6, pp. 869–882, 2016.

[248] N. Sánchez-Sánchez, L. Riol-Blanco, J. L. Rodríguez-Fernández, "The Multiple Personalities of the Chemokine Receptor," *J. Immunol.*, vol. 176, no. 9, pp. 5153–5159, 2006.

[249] E. Morse *et al.*, "TRB3 is stimulated in diabetic kidneys , regulated by

the ER stress marker CHOP , and is a suppressor of podocyte MCP-1," *AM J Physiol Ren. Physiol*, vol. 299, no. 5, pp. 965–972, 2010.

[250] W. Yan *et al.*, "Palmitate Induces TRB3 Expression and Promotes Apoptosis in Human Liver Cells," *Cell Physiol Biochem*, vol. 33, no. 3, pp. 823–834, 2014.

[251] S. Prudente *et al.*, "The Mammalian Tribbles Homolog TRIB3, Glucose Homeostasis, and Cardiovascular Diseases," *Endocr Rev*, vol. 33, no. 4, pp. 526–546, 2012.

[252] H. Oberkofler, A. Pfeifenberger, S. Soyal, and T. Felder, "Aberrant hepatic TRIB3 gene expression in insulin-resistant obese humans," *Diabetologia*, vol. 53, no. 9, pp. 1971–1975, 2010.

SUPPLEMENTARY MATERIAL

J. Am. Soc. Mass Spectrom. (2016) 27:168–177
DOI: 10.1007/s13361-015-1262-3

RESEARCH ARTICLE

Exploring the Process of Energy Generation in Pathophysiology by Targeted Metabolomics: Performance of a Simple and Quantitative Method

Marta Riera-Borrull,[1,2] Esther Rodríguez-Gallego,[1,2] Anna Hernández-Aguilera,[1,2] Fedra Luciano,[1,2] Rosa Ras,[3] Elisabet Cuyàs,[4,5] Jordi Camps,[1,2] Antonio Segura-Carretero,[6,7] Javier A. Menendez,[4,5] Jorge Joven,[1,2] Salvador Fernández-Arroyo[1,2]

[1]Unitat de Recerca Biomèdica, Hospital Universitari de Sant Joan, IISPV, Universitat Rovira i Virgili, Reus, Spain
[2]Campus of International Excellence Southern Catalonia, Tarragona, Spain
[3]Center for Omics Sciences, Reus, Spain
[4]Metabolism and Cancer Group, Translational Research Laboratory, Catalan Institute of Oncology (ICO), Girona, Spain
[5]Girona Biomedical Research Institute (IDIBGI), Girona, Spain
[6]Department of Analytical Chemistry, University of Granada, Granada, Spain
[7]Research and Development of Functional Food Centre (CIDAF), Granada, Spain

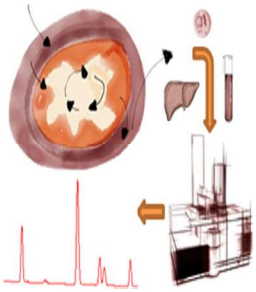

Abstract. Abnormalities in mitochondrial metabolism and regulation of energy balance contribute to human diseases. The consequences of high fat and other nutrient intake, and the resulting acquired mitochondrial dysfunction, are essential to fully understand common disorders, including obesity, cancer, and atherosclerosis. To simultaneously and noninvasively measure and quantify indirect markers of mitochondrial function, we have developed a method based on gas chromatography coupled to quadrupole-time of flight mass spectrometry and an electron ionization interface, and validated the system using plasma from patients with peripheral artery disease, human cancer cells, and mouse tissues. This approach was used to increase sensibility in the measurement of a wide dynamic range and chemical diversity of multiple intermediate metabolites used in energy metabolism. We demonstrate that our targeted metabolomics method allows for quick and accurate identification and quantification of molecules, including the measurement of small yet significant biological changes in experimental samples. The apparently low process variability required for its performance in plasma, cell lysates, and tissues allowed a rapid identification of correlations between interconnected pathways. Our results suggest that delineating the process of energy generation by targeted metabolomics can be a valid surrogate for predicting mitochondrial dysfunction in biological samples. Importantly, when used in plasma, targeted metabolomics should be viewed as a robust and noninvasive source of biomarkers in specific pathophysiological scenarios.

Keywords: Arteriosclerosis, Biomarkers, Cancer, Energy metabolism, Gas chromatography, Mitochondrial dysfunction, Targeted metabolomics

Received: 17 June 2015/Revised: 23 August 2015/Accepted: 27 August 2015/Published Online: 17 September 2015

Introduction

Energy metabolism is the process by which nutrients, such as carbohydrates and fats, are broken down to generate adenosine triphosphate (ATP), the main cellular energy store. A state of energy balance is achieved when energy intake matches expenditure. Deviations from this homeostatic

Jorge Joven and Salvador Fernández-Arroyo contributed equally to this work.

Electronic supplementary material The online version of this article (doi:10.1007/s13361-015-1262-3) contains supplementary material, which is available to authorized users.

Correspondence to: Jorge Joven; *e-mail:* jorge.joven@urv.cat, Salvador Fernández–Arroyo; *e-mail:* sfernandez@fiispv.cat

regulation can result in obesity, where energy intake exceeds demands. Obesity is a pathologic condition that combines inflammatory and metabolic disturbances, which are the immediate cause and/or consequence of many chronic and lethal diseases, including diabetes, atherosclerosis, and cancer [1]. Some of the excess energy is stored as triglyceride in adipose tissue without deleterious effects, but the capacity to store energy is limited and regulated by poorly understood mechanisms. The subsequent excessive accumulation of lipids and other metabolites in tissues that are not designed to manage this condition (e.g., liver, muscle, and pancreas) commonly ensues in an unhealthy course of metabolic events [2, 3]. Detection and treatment of subclinical metabolic derangements are challenging. The clinical picture is difficult to assess because of the combination of multiple and variable stressors such as inflammation, macrophage recruitment, alterations in muscle function, or the chemical composition of the diet. However, the resulting metabolically-related disorders, each with distinct phenotypes, are united by acquired deficiencies in the mitochondrial function and handling of energy [4]. Whether this association is causal or consequential is a matter of debate.

To provide cellular energy, mitochondria use the free energy derived from breakdown of fatty acids and glucose to produce ATP by oxidative phosphorylation. The immediate outcome of deranged energy processing is the reduced ability to switch from one fuel source (e.g., glucose) to another (e.g., fatty acids), resulting in altered flux between glycolytic pathways and oxidative capacity within cells and tissues. The recognition that mitochondria may play a central role in disease has renewed interest in the Randle cycle and the Warburg effect in the pathogenesis of common diseases [5, 6], and may be relevant because the inefficient use of glucose, lipotoxicity, and decreased fat oxidation are key mechanisms to explain most noncommunicable diseases [7, 8]. Consequently, the pharmacologic modulation of mitochondrial function mimicking the effect of exercise and/or caloric restriction may be an attractive therapeutic strategy [9, 10].

In cell-based models, it is relatively simple to assess mitochondrial dynamics, mitophagy (mitochondrial elimination), and pathways aimed to restore and/or maintain mitochondrial function [11, 12]. Assessment in vivo is considerably more challenging and requires sophisticated analytical platforms and stable isotopes to measure metabolites [13, 14]. We recently demonstrated that mitochondrial dysfunction could be assessed in plasma (i.e., noninvasively) using indirect markers of altered cellular energy metabolism [15]. Contrary to the belief that a high-throughput platform for massive metabolite profiling without accurate quantification of each metabolite is the method of choice to provide useful data, we hypothesized that a targeted approach, avoiding the intensive use of bioinformatics and making available actual changes in the concentration of metabolites under different experimental conditions, would be a valuable addition to current analytical tools. To this end, we have designed a simple and rapid method using advances in the technology of gas chromatography coupled to quadrupole time-of-flight mass spectrometry with an electron impact source (GC-EI-QTOF-MS). The method is sensitive for the accurate and simultaneous measurement of organic acids participating in the citric acid cycle (CAC) and selected metabolites representative of the catabolic and anabolic status of several biological systems. We also reasoned that the quantitative exploration of mitochondrial function might rapidly identify correlations between related pathways of metabolism, facilitating the understanding of metabolic conditions. Our results support the usefulness of this technique in in vitro and in vivo settings, and ongoing studies point to a potentially valuable role as a recently available methodology in the search for quantitative biomarkers of disease in epidemiologic cohorts and drug targets to restore cellular energy homeostasis [16–18].

Material and Methods

Chemicals

Methanol (MS grade), methoxyamine hydrochloride (MA), pyridine, *N*-methyl-*N*-(trimethylsilyl)-trifluoroacetamide (TMS) and standards (2-hydroxyglutarate, 3-hydroxybutyrate, 3-phosphoglycerate, 6-phosphogluconate, α-ketoglutarate, acetyl-CoA, aconitate, alanine, aspartic acid, citrate, fructose-1,6-bisphsophate, fructose-6-phosphate, fumarate, glucose, glucose-6-phosphate, glutamate, glutamine, glyceraldehyde-3-phosphate, isoleucine, lactate, leucine, malate, malonyl-coenzyme A, oxaloacetate, phosphoenolpyruvate, pyruvate, ribose-5-phosphate, serine, succinate, and succinyl-coenzyme A and valine) were purchased from Sigma-Aldrich (St. Louis, MO, USA).

Instrumentation

We used a 7890A gas chromatograph coupled with an electron impact source to a 7200 quadrupole time-of-flight mass spectrometer equipped with a 7693 autosampler module and a J&W Scientific HP-5MS column (30 m × 0.25 mm, 0.25 µm) (Agilent Technologies, Santa Clara, CA, USA). Helium was used as a carrier gas at a flow rate of 1.5 mL/min in constant-flow mode. The initial oven temperature was set to 70°C, increased to 190°C at 12°C/min, then raised to 325°C at a rate of 20°C/min and held for 3.25 min. For the MS, ionization was performed using electron impact with a source temperature of 230°C using an electron energy of 70 eV, an emission intensity of 35 µA, and a mass-to-charge range from 70 to 400 *m/z*. The initially selected metabolites to be identified and quantified using this GC-EI-QTOF-MS method are shown in Figure 1, and the selection criteria were based on available knowledge [19].

Isolation and Preparation of Biological Samples

To test the analytical performance and robustness of the method in different biological systems, we used human plasma, cell-culture lysates, and rodent tissues. The procedures used in humans were performed according to protocols approved by our Ethics Committee and Institutional Review Board, and all

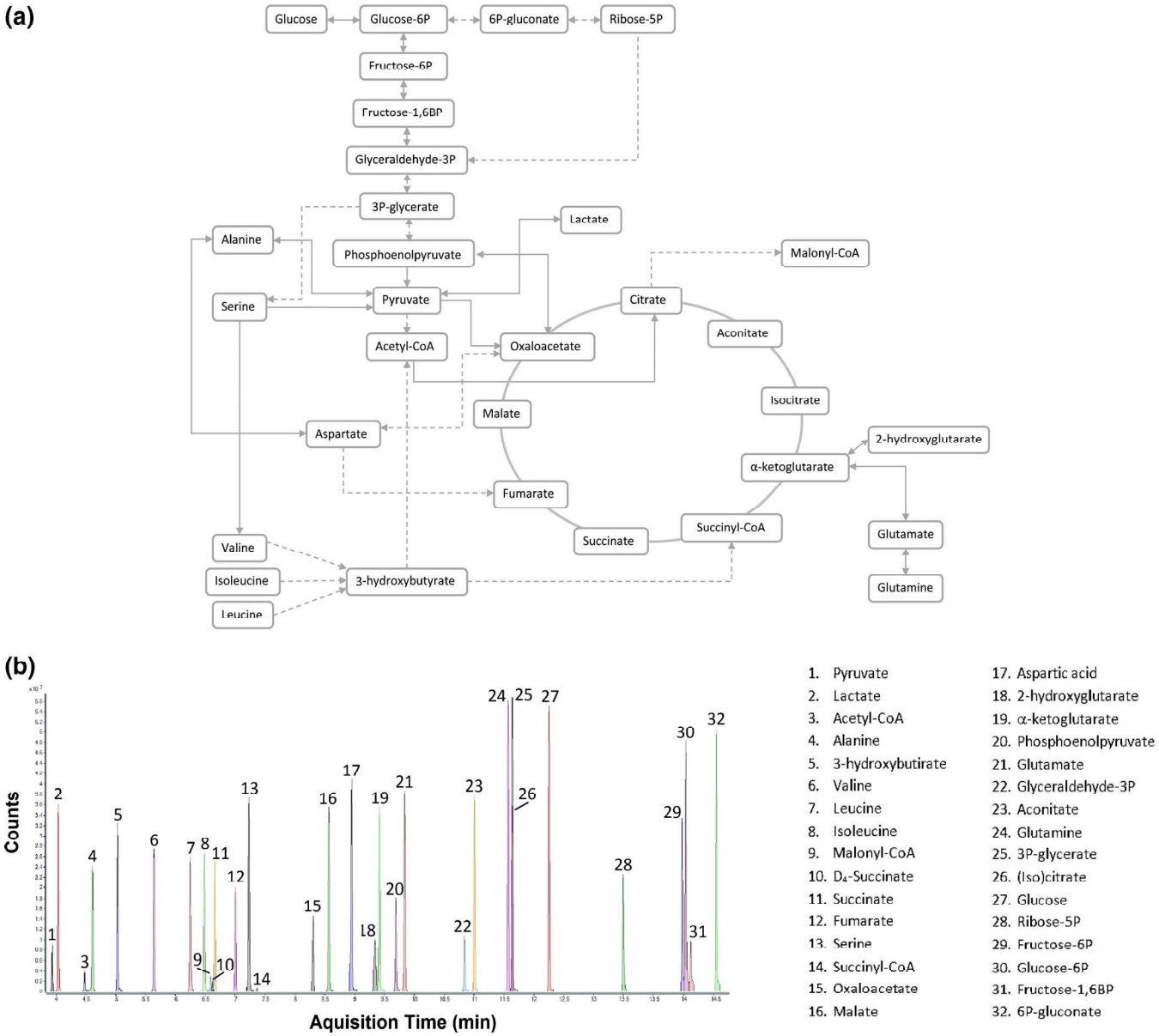

Figure 1. **(a)** Metabolic pathways of measured metabolites involved in energy metabolism. **(b)** Extracted compound chromatogram (ECC) of the quantifier ion of all metabolites, numbered according to their elution order. ECC was obtained after deconvolution of raw data with a retention time window size factor of 100.00, a signal-to-noise threshold of 2.00 and an absolute area filter of 5000 counts

participants signed an informed consent (EPINOLS 12-03-29/3proj6). Briefly, these included the recruitment of 50 ostensibly healthy participants, aged between 55 and 65 y with an ankle-brachial index (ABI) >0.9, which were body weight- and age-matched with patients presenting intermittent claudication (i.e., peripheral artery disease), ABI <0.9 and staged at grade II according to Fontaine. A sample of blood was drawn from each patient. Participants with diabetes mellitus were excluded to avoid metabolic bias and to limit variability. Further clinical details on the inclusion and exclusion criteria have been previously described [20].

To test the performance of the method in cultured cells, we used MCF10A cells infected with a retroviral $KRAS^{V12}$ expression construct, which were generously provided by the Ben-Ho Park's laboratory and maintained under the previously described culture conditions [21]. Cells were grown to confluence in 6-well plates, then trypsinized and counted (approximately 2×10^6 cells per experiment). We pooled the results obtained in four experiments in triplicate (n = 12).

LDL receptor-deficient ($Ldlr^{-/-}$) mice develop spontaneous hyperlipidemia and are a useful model for studying atherosclerosis since they present features similar to those observed in the human metabolic syndrome. Mice (C57BL/6J background, The Jackson Laboratory) were housed under standard conditions and given a commercial low fat mouse diet (14% protein rodent maintenance diet; Harlan, Barcelona, Spain). Male mice were sacrificed at 24 wk of age following previously described procedures [22] and tissues (liver and epididymal white

adipose tissue; n = 10 samples, each tissue) were extracted. All procedures were carried out in accordance with institutional guidelines (CEIA, 2014-237).

To ensure high quality data and reduced false discovery rates, a rigorous optimization of pre-analytical steps prior to chromatography was essential. This may vary between laboratories and experimental conditions but includes sample collection, storage, pretreatment and clean-up, as well as software parameters used in data alignment and peak picking. It is particularly important to minimize the time between sample collection and storage at –80°C to less than 1 h to reduce variability. Of note, this method may be used in the quantification of ^{13}C isotopic substrates (data not shown), indicating its suitability for metabolic flux analysis to define the pattern of carbon flow through a metabolic network in cells and tissues [23].

Metabolite Extraction

We investigated different extraction protocols and found that methanol/water (4/1) extraction was efficient for these metabolites. To minimize complexity in the metabolite extraction, we used methanol/water (4/1) mixed with deuterated D_4-succinic acid as surrogate standard (MeOHW-D_4S) to obtain a final concentration of 1 µg/mL. The choice of a unique surrogate standard was considered sufficient as injection quality control and considerably simplifies the procedure. Further, although this method was designed for targeting metabolomics, during experimentations it is not uncommon to require measurement of additional metabolites in the same samples by nuclear magnetic resonance (NMR) or LC/MS. With these procedures, results did not differ significantly using isotopic compounds as internal standard, and there was no need for solvent exchange as previously described [24–26].

Thawed plasma (100 µL) was added to 900 µL of MeOHW-D_4S, vortexed, placed at –20°C for 2 h to precipitate proteins, and centrifuged at 14,000 rpm for 10 min at 4°C to collect the supernatant. As a cautionary note, the use of lower amounts of plasma results in the lack of reliable detection of some metabolites present at low concentrations (e.g., acetyl-CoA or oxaloacetate). Cell pellets were resuspended in 500 µL of MeOHW-D_4S, lysed with three cycles of freezing and thawing using liquid N_2 and sonicated with three cycles of 30 s. Samples were maintained on ice for 1 min between each sonication step. Proteins were precipitated, samples centrifuged, and supernatant collected. Animal tissues (100 mg) were placed in plastic tubes containing 1 mL of MeOHW-D_4S and homogenized using a Precellys 24 system (Izasa, Barcelona, Spain). After centrifugation at 14,000 rpm 10 min at 4°C, supernatant was collected and the homogenization step was repeated. Then proteins were precipitated, samples centrifuged, and supernatant collected. The extraction of nonpolar compounds was performed adding chloroform to have a final proportion of chloroform/methanol (2/1), according to Folch protocol [27]. All supernatants were further vortexed, centrifuged, filtered using 0.22 µm filters, and freeze-dried overnight.

Derivatization

Samples were dried under N_2 and derivatized to rapidly form silyl derivatives. Briefly, in order to protect ketone groups [28], we added 30 µL of methoxylamine hydrochloride dissolved in pyridine [40 mg/mL (0.48 M)] to each sample, which was then incubated for 1.5 h at 37°C with agitation. Then, 45 µL of TMS was added and samples were agitated for 10 min and placed in the dark for 1 h and transferred into a vial before immediate analysis.

Data Analysis

Raw data were processed and compounds were detected and quantified using the Qualitative and Quantitative Analysis B.06.00 software (Agilent Technologies), respectively. Results were compared by one-way ANOVA with Dunnett's multiple pair-wise comparison tests using a significance threshold of 0.05. Other calculations including comparisons with the U of Mann–Whitney test and/or correlations were made using GraphPad Prism software 6.01 (GraphPad Software, San Diego, CA, USA).

Results and Discussion

Method Validation

Calibration curves were obtained for each metabolite by plotting the standard concentration as a function of the peak area. Because the differences in concentration of some metabolites may be highly variable, we required, in some cases, the simultaneous use of different calibration curves covering the expected concentration range for each metabolite. Recovery of each metabolite was calculated and the variation in the percentage of recovery was between 83% and 99%. Ten points of the selected range of all calibration curves were injected and showed linearity with regression coefficients higher than 0.99. The limit of detection (LOD) and quantification (LOQ) for each metabolite were calculated according to International Union of Pure and Applied Chemistry recommendations [29]. Within-day precision or repeatability was calculated injecting each standard on the same day, and between-day repeatability on 5 separate d (n = 5 replicates at three concentration levels) and expressed as relative standard deviation (RSD). Values for each metabolite were considered excellent (RSD from 0.65% to 3.68% and from 1.12 to 4.15%, respectively). Selected and relevant validation parameters are shown in Table 1, and results for other variables may be also examined in Supplemental Table 1.

Table 1. Validation method parameters: regression curve values (slope and intercept), linearity, limit of detection (LOD), limit of quantification (LOQ), intra- and interday % RSD, and recovery (see also Supplemental Table 1)

Metabolite	Slope / intercept	Linearity (R^2)	LOD (μM)	LOQ (μM)	Intraday RSD (%)	Interday RSD (%)	Recovery (%)
2-Hydroxyglutarate	330378 / –64056	0.9991	0.127	0.425	1.12	1.95	91.65
3-Hydroxybutirate	101090 / –15769	0.9976	0.010	0.032	0.65	1.15	96.74
3-Phosphoglycerate	237249 / –2135051	0.9993	0.065	0.215	2.24	3.05	85.65
6-Phospho-gluconate	526980 / –1258050	0.9987 0.9989	0.527	1.758	3.21	3.98	89.35
	87569 / –284587						
α-Ketoglutarate	128155 / 14577	0.9997	0.029	0.098	1.14	2.08	94.99
Acetyl-coenzyme A	10158 / 1785	0.9972	0.610	2.030	1.98	3.01	84.12
Aconitate	749201 / –788502	0.9990	0.010	0.032	2.98	3.65	88.68
Alanine	1987694 / –229517	0.9994	0.288	0.959	1.25	2.34	97.48
Aspartic acid	1715209/ –28378	0.9996	0.835	2.783	0.84	1.25	98.02
(Iso)citrate	1469611 / –271860	0.9996	0.039	0.130	2.54	2.96	93.58
Fructose-1,6-bisphosphate	140842 / –428131	0.9981	0.117	0.389	1.65	2.15	83.26
Fructose-6-phosphate	824733 / –956090	0.9987	0.146	0.487	1.29	1.99	88.69
Fumarate	1119413 / –117375	0.9997	0.040	0.132	0.99	1.34	91.68
Glucose	113676 / –74297	0.9997	0.009	0.029	1.54	2.03	97.35
Glucose-6-phosphate	1040659 / –2961082	0.9990	0.039	0.129	2.14	2.97	96.67
Glutamate	1371976 / –306806	0.9989	0.334	1.114	3.05	4.01	94.31
	284354 / –76489	0.9990					
Glutamine	477954 / –224408	0.9988	0.114	0.380	2.87	3.56	93.11
	957845 / –79154	0.9987					
Glyceraldehyde-3-phosphate	85106 / –44424	0.9979	0.029	0.096	1.32	1.68	87.64
Isoleucine	1652773 / 219943	0.9996	0.108	0.360	0.96	1.42	98.39
Lactate	23667 / 77898	0.9998	0.021	0.070	0.86	1.74	98.96
Leucine	1735828 / 422255	0.9993	0.102	0.340	1.33	1.89	96.84
Malate	336640 / –57888	0.9992	0.113	0.377	0.92	1.12	91.64
Malonyl-coenzyme A	16769 / –359	0.9989	0.039	0.130	2.73	3.06	85.23
Oxaloacetate	70439 / –43811	0.9991	0.590	1.966	3.68	4.15	89.34
Phosphoenolpyruvate	285046 / –222284	0.9981	0.313	1.044	2.38	3.18	92.48
Pyruvate	379309 / 156902	0.9991	0.060	0.200	1.01	1.69	94.67
Ribose-5-phosphate	553740 / –344047	0.9976	0.202	0.675	1.79	2.06	94.58
Serine	1461082 / 11922	0.9999	0.304	1.012	1.14	1.79	97.46
Succinate	176185 / 7109	0.9997	0.077	0.258	0.91	1.35	98.74
Succinyl-coenzyme A	34216 / 5480	0.9998	0.020	0.086	2.06	2.67	87.56
Valine	1836799 / 46946	0.9994	0.098	0.326	1.05	1.68	98.12

Identification and Quantification

The relevant analytical data are summarized in Supplemental Table 2. For some organic acids (3-hydroxybutyrate, fumarate, lactate, oxaloacetate, phosphoenolpyruvate, pyruvate, and succinate) and the internal standard (D_4-succinate), the ion $[M]^+$ was used as qualifier ion and the most abundant ion $[M\text{-}CH_3]^+$ resulting from the characteristic loss of a methyl group in TMS after the electron impact, was used as quantifier ion. As shown in Figure 2a, the proposed quantifier ion of acetyl-CoA was observed at *m/z* 219, which is the result of acetate moiety linked to S–C_2H_4–N–TMS from the 4'-phosphopantetheine moiety included in the CoA moiety. The subsequent loss of 15 u suggests the loss of a methyl group from the TMS resulting in an ion at *m/z* 204 that was used as qualifier. For malonyl-CoA, the loss of the TMS from the acid group in malonate moiety linked to S–C2H4–N–TMS from the CoA moiety gives a qualifier ion with *m/z* at 262. The presence of other minor ions with a consecutive loss of 16 u (*m/z* 246 and 230) suggest the loss of the TMS group linked to the acid group of the malonate moiety, which can lose two oxygen atoms consecutively. This is followed by the loss of the methoxyl group from the methoxyamine, giving an ion at *m/z* 187. To stabilize this ion, a rearrangement is made through a cyclation between the radicals CH2• in malonate moiety and the N• linked to the TMS (Figure 2b). A similar reasoning was used to explain the presence in succinyl-CoA of an ion at *m/z* 276 (qualifier) and minor ions at *m/z* 260 and 244. The N–TMS group and the methyl group from the methoxyamine are finally lost, giving a quantifier ion at *m/z* 174. In this case, to stabilize this structure, the CH_2• radical should be linked to the oxygen from the oxyamine group (Figure 2c). Special attention is required in the identification of phosphate compounds (Figure 2d) because they yield three characteristic fragments [30] and retention time is crucial. Quantifier and qualifier ions used to identify phosphate compounds are summarized in Supplemental Table 2. Of note, with this method isocitrate and citrate have the same retention time. In addition, both give a qualifier ion corresponding to the loss of a carboxyl group and the most abundant ion was $[M\text{-}COOTMS\text{-}OTMS]^+$ due to the consecutive loss of an OTMS group from the ion $([M\text{-}COOTMS]^+$ (Figure 2e). Although the signal for isocitrate using pure standards is

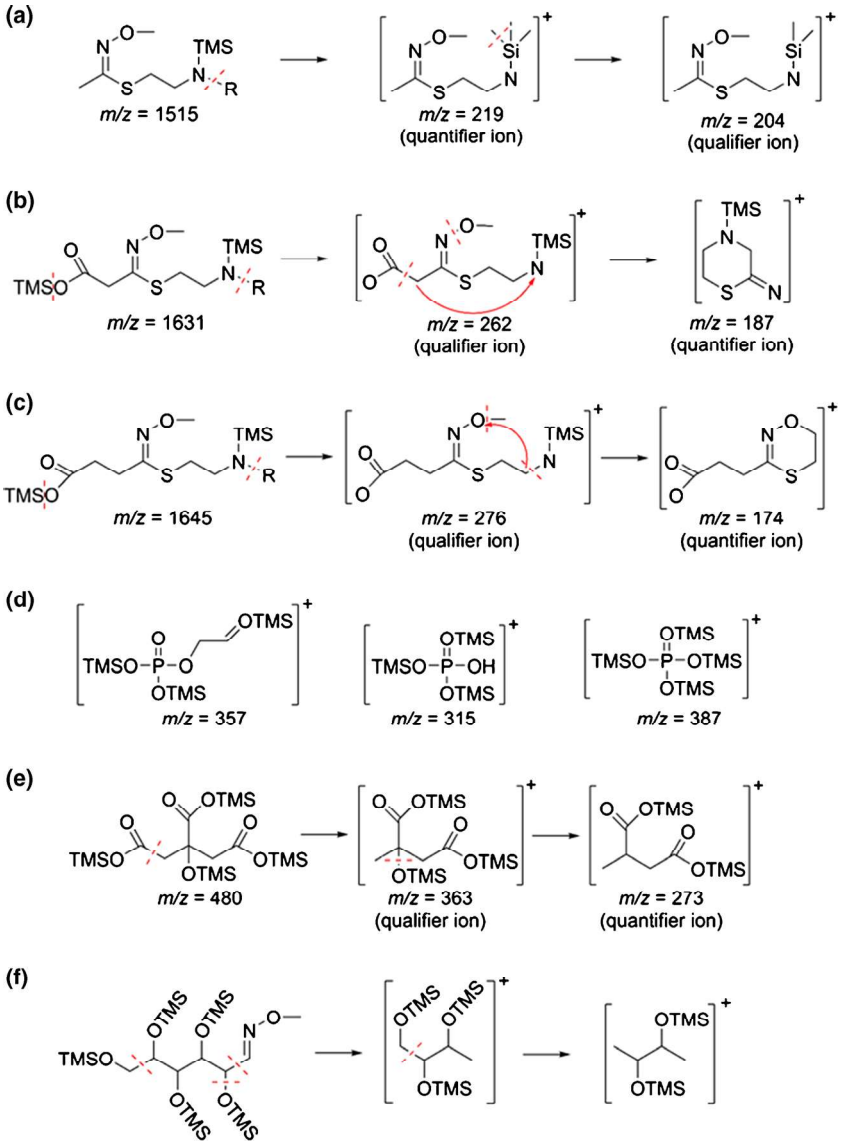

Figure 2. Fragmentation pattern of **(a)** acetyl-CoA, **(b)** malonyl-CoA, **(c)** succinyl-CoA, **(d)** phosphate group, **(e)** (iso)citrate, and **(f)** glucose

significantly less intense, results were expressed as (iso)citrate to denote the lack of chromatographic separation. The quantifier ion for glucose, which is derivatized with five TMS and one MA group (Figure 2f) is $[M\text{-}CH_2\text{-}CH\text{-}NOCH_3\text{-}2OTMS]^+$ (attributable to the loss of the methoxyamine group and the CH where it is linked, an OTMS group and a CH_2-OTMS group), and the subsequent loss of an additional CH-OTMS group results in the qualifier ion $[M\text{-}CH_2\text{-}2CH\text{-}NOCH_3\text{-}3OTMS]^+$ [31].

In contrast, the interpretation for alanine, valine, leucine, isoleucine, serine, aspartic acid, glutamic acid, malate, and glutamine is simpler because $[M\text{-}CH3]^+$ is constant (qualifier ion) and $[M\text{-}COOTMS]^+$ is identified as the quantifier ion. $[M\text{-}CH_3]^+$, however, was the qualifier ion and $[M\text{-}COOTMS]^+$ the quantifier ion for 2-hydroxyglutarate. Aconitate also shows $[M\text{-}CH_3]^+$ as qualifier ion after derivatization with three TMS groups. The loss of two TMS groups and a methyl from the third TMS group yields the quantifier ion $[M\text{-}2TMS\text{-}CH_3]^+$. Finally, $[M\text{-}OCH_3]^+$ (loss of the OCH_3 from the methoxiamine group) is the qualifier ion for α-ketoglutarate, and the additional loss of an OTMS results in the quantifier ion $[M\text{-}OCH_3\text{-}OTMS]^+$.

Applications in Biological Samples

In our previous efforts with untargeted metabolomics using LC/MS and GC/MS platforms, we found that comparisons between groups were limited by the lack of accurate quantification [32–34]. Conversely, the use of a nuclear magnetic resonance platform [25, 26] provided

Table 2. Metabolite concentrations in plasma (in μM) from selected participants and expressed as mean ± SD. Fold change and significance (*P* value) are also reported and decimals were set according to the first significant digit of the measured SD

Metabolite	Plasma control (n = 50)	Plasma PAD (n = 50)	Fold change	*P* value
2-Hydroxyglutarate	9.2 ± 0.4	9.0 ± 0.3	–1.02	N.S.
3-Hydroxybutirate	0.13 ± 0.01	0.31 ± 0.07	2.38	<0.0001
3-Phosphoglycerate	-	-	-	-
6-Phosphogluconate	-	-	-	-
α-Ketoglutarate	3.3 ± 0.2	4.6 ± 0.4	1.39	0.0091
Aconitate	0.52 ± 0.01	4.4 ± 0.9	8.46	<0.0001
Alanine	211 ± 11	203 ± 27	–1.04	N.S.
Aspartic acid	133 ± 3	199 ± 11	1.50	<0.0001
(Iso)citrate	279 ± 13	706 ± 22	2.53	<0.0001
Fructose-1,6-bisphosphate	-	-	-	-
Fructose-6-phosphate	-	-	-	-
Fumarate	0.33 ± 0.02	0.26 ± 0.03	–1.27	<0.0001
Glucose	4856 ± 305	5044 ± 346	1.04	N.S.
Glucose-6-phosphate	N.Q.	N.Q.	-	-
Glutamate	462 ± 366	5197 ± 317	11.25	<0.0001
Glutamine	1115 ± 206	3691 ± 237	3.31	<0.0001
Glyceraldehyde-3-phosphate	-	-	-	-
Isoleucine	49 ± 1	63 ± 2	1.29	<0.0001
Lactate	395 ± 8	359 ± 13	–1.10	0.0323
Leucine	73 ± 2	90 ± 3	1.23	0.0032
Malate	1.57 ± 0.08	3.0 ± 0.3	1.91	<0.0001
Malonyl-coenzyme A	N.Q.	N.Q.	-	-
Oxaloacetate	54 ± 5	N.Q.	-	-
Phosphoenolpyruvate	-	-	-	-
Pyruvate	11 ± 1	10 ± 1	–1.1	0.0270
Ribose-5-phosphate	-	-	-	-
Serine	104 ± 2	145 ± 4	1.39	<0.0001
Succinate	10.7 ± 0.1	12.2 ± 0.4	1.14	N.S.
Succinyl-coenzyme A	6.6 ± 0.9	11.9 ± 0.9	1.80	0.0014
Valine	88 ± 2	105 ± 3	1.19	N.S.

PAD: Peripheral Artery Disease
N.Q.: detected metabolite, but under limit of quantification
N.S.: not significant p-value

excellent reproducibility to quantify certain metabolites but low sensitivity to quantitatively measure the selected metabolites as indirect markers of energy metabolism and mitochondrial function, which included intermediates of glycolysis, the pentose phosphate pathway, branched chain amino acids, and the organic acids of the CAC. We therefore developed the present GC-EI-QTOF-MS analytical platform to measure, after derivatization, these selected compounds, and we found it reliable for use in different biological systems (Tables 2, 3 and 4).

In the first analysis, we compared plasma from healthy controls and patients with stage II peripheral artery disease. Samples injected in triplicate produce RSD values that were similar to those obtained in the precision study. The concentrations of these metabolites have not been previously examined in this condition but metabolites involved in the CAC have been previously suggested as biomarkers of myocardial infarction [35]. Blood was drawn from our patients when they were free of clinical signs of ischemia (i.e., after 1 h of inactivity). Controls with uncompromised circulation in the limb arteries (i.e., ABI > 0.9) had similar cardiovascular risk factors including age, hyperlipidemia, body weight, and current (not past) smoking habit (data not shown). This comparison was designed exclusively for testing analytical performance in plasma and no clinical implications were intended. Nevertheless, the high concentrations of aconitate, isocitrate, malate, α-ketoglutarate, and succinyl-coenzyme A in patients indicate that mitochondrial function is stimulated rather than inhibited (i.e., contrary to that expected in ischemic conditions) (Table 2). In addition, we found elevated levels of branched chain amino acids, which may also indicate an increased mitochondrial function via their conversion to β-hydroxybutyrate and succinyl-coenzyme A. This may seem paradoxical because elevated levels of branched chain amino acids are usually associated with poor health and cardiovascular disease. One explanation might be the increased endothelial proliferation and accumulation of immune cells resulting in a higher diffusion of these metabolites into the circulation, but may also indirectly point to increased breakdown in the leg muscles [36, 37].

The lack of circulating phosphate compounds was expected considering the hydrophobic nature of the cellular membrane, and it may similarly indicate an absence of significant cellular destruction. Under these conditions, only lactate, which is significantly decreased, may indirectly indicate normal to low glycolytic flux. Also, significant increases of glutamate and glutamine were

Table 3. Metabolite concentration in MCF10A and MCF10A-KRAS^{V12} cells (in μM/mg of protein) expressed as mean ± SD, fold change, and significance (*P* value). Decimals are reported according to the first significant digit of the measured SD

Metabolite	MCF10A (n = 12)	MCF10A-KRAS^{V12} (n = 12)	Fold change	*P* value
2-Hydroxyglutarate	-	0.22 ± 0.04	-	-
3-Hydroxybutirate	5.0 ± 0.4	1.78 ± 0.09	–2.81	0.0079
3-Phosphoglycerate	0.28 ± 0.09	36.73 ± 5.13	131.18	<0.0001
6-Phosphogluconate	8.8 ± 1	19.34 ± 2.32	2.20	0.0167
α-Ketoglutarate	0.23 ± 0.08	2.18 ± 0.23	9.48	<0.0001
Aconitate	0.21 ± 0.07	0.14 ± 0.01	–1.50	0.0387
Alanine	65 ± 6	156 ± 21	2.40	0.0067
Aspartic acid	48 ± 6	408 ± 32	8.50	<0.0001
(Iso)citrate	6.3 ± 0.9	5.3 ± 0.6	–1.19	N.S.
Fructose-1,6-bisphosphate	N.Q.	6.4 ± 0.9	-	-
Fructose-6-phosphate	-	N.Q.	-	-
Fumarate	2.4 ± 0.4	10.6 ± 0.6	4.42	<0.0001
Glucose	2.7 ± 0.2	0.22 ± 0.01	–12.27	<0.0001
Glucose-6-phosphate	0.16 ± 0.03	0.64 ± 0.07	4.00	0.0268
Glutamate	10.9 ± 0.6	289 ± 52	26.51	<0.0001
Glutamine	5.8 ± 0.7	5.9 ± 0.7	1.02	N.S.
Glyceraldehyde-3-phosphate	1.6 ± 0.4	1.3 ± 0.4	–1.23	N.S.
Isoleucine	14 ± 2	35 ± 6	2.50	0.0341
Lactate	288 ± 34	812 ± 12	2.82	<0.0001
Leucine	41 ± 8	34 ± 4	–1.21	N.S.
Malate	0.7 ± 0.2	5.0 ± 0.3	7.14	<0.0001
Malonyl-coenzyme A	88 ± 1	40.7 ± 0.6	–2.16	0.0048
Oxaloacetate	-	14 ± 2	-	-
Phosphoenolpyruvate	N.Q.	13 ± 4	-	-
Pyruvate	7 ± 1	94 ± 14	13.43	<0.0001
Ribose-5-phosphate	-	4.9 ± 0.8	-	-
Serine	47 ± 9	48 ± 3	1.02	N.S.
Succinate	12 ± 2	11 ± 2	–1.09	N.S.
Succinyl-coenzyme A	17.3 ± 0.5	31 ± 6	1.79	0.031
Valine	25 ± 2	24 ± 1	–1.04	N.S.

N.Q.: detected metabolite, but under limit of quantification
N.S.: not significant p-value

observed in patients with active atherosclerosis in the limbs, indicating a distinct use of these metabolites in this setting. Our results confirm the validity of our hypothesis with respect to the usefulness of the method to explore the energy metabolism in vivo. These findings may have implications in the search for possible biomarkers and to assess the effectiveness of therapeutic strategies.

We found that the metabolic activity of MCF10A cells engineered to overexpress oncogenic KRAS was significantly higher than MCF10A parental cells under the same culture conditions, strongly suggesting that metabolic reprogramming occurs in breast epithelial cells carrying the constitutively active KRAS^{V12} gene (Table 3). Of note, we were able to detect 2-hydroxyglutarate in MCF10A-KRAS^{V12} cells, which is a product of the mutated isocitrate dehydrogenase and is considered to be an oncometabolite [38]. Further, the increased concentration in some amino acids and indirect markers (ribose-5-phosphate) of metabolic activity in the pentose phosphate pathway were considered as an indication of a higher generation of biomass and endogenous antioxidants in MCF10A-KRAS^{V12} cells to eradicate the reactive oxygen species generated by the accelerated metabolism [39] (Table 3). The increased concentration of glucose-6-phosphate suggests both increased glucose transport and glycolysis, and indeed lactate production was significantly increased in mutated cells with respect to their isogenic controls. The overall results suggest the dependence on glycolysis for growth, indicative of the Warburg effect. Consequently, our analytical method may be used to perform experiments under different glucose environments and to explore the effect of drugs acting on either glucose uptake or mitochondrial functioning.

We next wished to determine whether this method could be used to explore energy metabolism in a relevant disease model. The simplest approach to test the functionality of the technique was to isolate tissues from mice with different mitochondrial load and importance in energy production. Thus, we compared the concentration of metabolites in adipose tissue and hepatic tissue and found significant differences in the concentration of measured metabolites (Table 4). Some were immediately expected (e.g., amino acids and CAC intermediates). We also found that oxaloacetate and phosphoenolpyruvate were barely detectable in adipose tissue, and the concentration of malonyl-CoA was similar in both tissues. No attempt was made to explore the putative metabolic pathways involved (e.g., lipogenesis), but results show that this method can be used to interrogate metabolic alterations related to excessive energy intake, obesity,

Table 4. Metabolite concentration in mouse tissue samples (in µM/100 mg of tissue) expressed as mean ± SD. Decimals are reported according to the first significant digit of the measured SDThe number of decimals varies according to the concentration

Metabolite	Liver tissue (n = 10)	Adipose tissue (n = 10)
2-Hydroxyglutarate	19 ± 1	0.87 ± 0.09
3-Hydroxybutirate	0.11 ± 0.01	0.064 ± 0.003
3-Phosphoglycerate	18 ± 3	0.24 ± 0.05
6-Phosphogluconate	38206 ± 1648	297 ± 45
α-Ketoglutarate	5.2 ± 0.6	0.15 ± 0.01
Aconitate	47 ± 3	0.061 ± 0.004
Alanine	1663± 188	63 ± 7
Aspartic acid	4259 ± 128	305 ± 59
(Iso)citrate	425 ± 46	31 ± 8
Fructose-1,6-bisphosphate	12 ± 1	1.7 ± 0.4
Fructose-6-phosphate	1323 ± 110	28 ± 3
Fumarate	26 ± 5	0.25 ± 0.04
Glucose	1802 ± 103	249 ± 21
Glucose-6-phosphate	1302 ± 147	191 ± 17
Glutamate	49043 ± 6746	1889 ± 394
Glutamine	2104 ± 273	532 ± 97
Glyceraldehyde-3-phosphate	16 ± 3	0.11 ± 0.05
Isoleucine	730 ± 74	15 ± 3
Lactate	667 ± 47	59 ± 2
Leucine	1009 ± 104	30 ± 6
Malate	319 ± 49	3.8 ± 0.8
Malonyl-coenzyme A	23 ± 2	22 ± 1
Oxaloacetate	2.3 ± 0.3	N.Q.
Phosphoenolpyruvate	12 ± 2	N.Q.
Pyruvate	5.6 ± 0.5	0.32 ± 0.03
Ribose-5-phosphate	470 ± 82	1.7 ± 0.3
Serine	5531 ± 710	182 ± 18
Succinate	138 ± 19	13.1 ± 0.8
Succinyl-coenzyme A	291 ± 7	7.0 ± 0.9
Valine	460 ± 60	22 ± 3

N.Q.: detected metabolite, but under limit of quantification

and the development of associated metabolic dysfunction in the liver (e.g., fatty liver disease).

Method Limitations

This method requires a derivatization procedure, which increases the time used for sample preparation. It should also be considered that the stability of derivatized compounds is limited to a relatively short period of time (not more than 24 h). Although most authors consider citric acid as the only compound found at its time of retention, our efforts to distinguish between isomers were unsuccessful. Finally, because of the low ionization of acetyl-CoA, the concentration in biological samples is not readily detected using GC-MS. To detect this and other possibly useful important metabolites, other analytical platforms are required. Methods using liquid chromatography-mass spectrometry [40–42] are available and provide an accurate approach.

Conclusion

We have developed a simple analytical method using GC-EI-QTOF-MS to separate, detect, and quantify numerous metabolites involved in energy metabolism, including glycolysis, the CAC, and pathways involved in metabolism of lipids, amino acids, and pentose phosphate. This method delivers an overall assessment of metabolism in biological samples used in preclinical and clinical investigation: namely, cell-culture lysates, mouse models of disease, and patient plasma. We have found that GC-EI-QTOF-MS provides better resolution and reproducibility than other available analytical platforms [43] to accurately quantify multiple metabolites. In particular, the measurement of intermediates involved in mitochondrial metabolism, in all likelihood, represents a major advance in the assessment, in vitro, of mitochondrial dysfunction in cells and tissues. The indirect measurement of these intermediates in plasma should be considered as an alternative to assess the mitochondrial dysfunction in vivo for the clinical management of common metabolic diseases.

Acknowledgments

The authors are grateful to Instituto de Salud Carlos III for the Sara Borrell grant CD12/00672 to S.F.A., Ministerio de Ciencia e Innovación (SAF2012-38914), Plan Nacional I+D+I, Agència Gestió d'Ajuts Universitaris i Recerca (2014-SGR229) to J.A.M. and Andalusian Regional Government Council of Innovation and Science (P11-CTS-7625) to A.S.C. The authors also thank Dr. Ben Ho Park for providing KRAS-transformed MCF10A cells, and Dr. Kenneth McCreath for editorial support.

References

1. Kotas, M.E., Medzhitov, R.: Homeostasis, inflammation, and disease susceptibility. Cell **160**, 816–827 (2015)
2. Chowdhury, R., Warnakula, S., Kunutsor, S., Crowe, F., Ward, H.A., Johnson, L., Franco, O.H., Butterworth, A.S., Forouhi, N.G., Thompson, S.G., Khaw, K.T., Mozaffarian, D., Danesh, J., Di Angelantonio, E.: Association of dietary, circulating, and supplement fatty acids with coronary risk: a systematic review and meta-analysis. Ann. Intern. Med. **160**, 398–406 (2014)
3. Masoodi, M., Kuda, O., Rossmeisl, M., Flachs, P., Kopecky, J.: Lipid signaling in adipose tissue: connecting inflammation and metabolism. Biochim. Biophys. Acta. **1851**, 503–518 (2015)
4. Rull, A., Camps, J., Alonso-Villaverde, C., Joven, J.: Insulin resistance, inflammation, and obesity: role of monocyte chemoattractant protein-1 (or CCL2) in the regulation of metabolism. Mediat. Inflamm. **2010**, Article ID 326580 (2010)
5. Menendez, J.A., Alarcon, T., Joven, J.: Gerometabolites: the pseudohypoxic aging side of cancer oncometabolites. Cell Cycle **13**, 699–709 (2014)
6. Menendez, J.A., Joven, J., Cufi, S., Corominas-Faja, B., Oliveras-Ferraros, C., Cuyas, E., Martin-Castillo, B., López-Bonet, E., Alarcón, T., Vazquez-Martin, A.: The Warburg effect version 2.0: metabolic reprogramming of cancer stem cells. Cell Cycle **12**, 1166–1179 (2013)
7. Patergnani, S., Pinton, P.: Mitophagy and mitochondrial balance. Methods Mol. Biol. **1241**, 181–194 (2015)
8. Peti-Peterdi, J.: Mitochondrial TCA cycle intermediates regulate body fluid and acid-base balance. J. Clin. Invest. **123**, 2788–2790 (2013)
9. Phielix, E., Meex, R., Moonen-Kornips, E., Hesselink, M.K., Schrauwen, P.: Exercise training increases mitochondrial content and ex vivo mitochondrial function similarly in patients with type 2 diabetes and in control individuals. Diabetologia **53**, 1714–1721 (2010)
10. Szeto, H.H., James, L.P., Atkinson, A.J.: Mitochondrial pharmacology: its future is now. Clin. Pharmacol. Ther. **96**, 629–633 (2014)
11. Divakaruni, A.S., Rogers, G.W., Murphy, A.N.: Measuring mitochondrial function in permeabilized cells using the Seahorse XF analyzer or a Clark-type oxygen electrode. Curr. Protoc. Toxicol. **60**, 25.22.21–25.22.16 (2014)
12. Phelan, J.J., MacCarthy, F., Feighery, R., O'Farrell, N.J., Lynam-Lennon, N., Doyle, B., O'Toole, D., Ravi, N., Reynolds, J.V., O'Sullivan, J.: Differential expression of mitochondrial energy metabolism profiles across the

metaplasia-dysplasia-adenocarcinoma disease sequence in Barrett's oesophagus. Cancer Lett. **354**, 122–131 (2014)
13. Abdurrachim, D., Ciapaite, J., Wessels, B., Nabben, M., Luiken, J.J., Nicolay, K., Prompers, J.J.: Cardiac diastolic dysfunction in high-fat diet fed mice is associated with lipotoxicity without impairment of cardiac energetics in vivo. Biochim. Biophys. Acta. **1842**, 1525–1537 (2014)
14. Prompers, J.J., Wessels, B., Kemp, G.J., Nicolay, K.: Mitochondria: investigation of in vivo muscle mitochondrial function by 31P magnetic resonance spectroscopy. Int. J. Biochem. Cell. Biol. **50**, 67–72 (2014)
15. Rodriguez-Gallego, E., Guirro, M., Riera-Borrull, M., Hernandez-Aguilera, A., Marine-Casado, R., Fernandez-Arroyo, S., Beltrán-Debón, R., Sabench, F., Hernández, M., del Castillo, D., Menendez, J.A., Camps, J., Ras, R., Arola, L., Joven, J.: Mapping of the circulating metabolome reveals alpha-ketoglutarate as a predictor of morbid obesity-associated nonalcoholic fatty liver disease. Int. J. Obes. **39**, 279–287 (2015)
16. Floegel, A., Stefan, N., Yu, Z., Muhlenbruch, K., Drogan, D., Joost, H.G., Fritsche, A., Häring, H.U., Hrabě de Angelis, M., Peters, A., Roden, M., Prehn, C., Wang-Sattler, R., Illig, T., Schulze, M.B., Adamski, J., Boeing, H., Pischon, T.: Identification of serum metabolites associated with risk of type 2 diabetes using a targeted metabolomic approach. Diabetes **62**, 639–648 (2013)
17. Inouye, M., Kettunen, J., Soininen, P., Silander, K., Ripatti, S., Kumpula, L.S., Hämäläinen, E., Jousilahti, P., Kangas, A.J., Männistö, S., Savolainen, M.J., Jula, A., Leiviskä, J., Palotie, A., Salomaa, V., Perola, M., Ala-Korpela, M., Peltonen, L.: Metabonomic, transcriptomic, and genomic variation of a population cohort. Mol. Syst. Biol. **6**, 441 (2010)
18. Shah, S.H., Kraus, W.E., Newgard, C.B.: Metabolomic profiling for the identification of novel biomarkers and mechanisms related to common cardiovascular diseases: form and function. Circulation **126**, 1110–1120 (2012)
19. Shin, S.Y., Fauman, E.B., Petersen, A.K., Krumsiek, J., Santos, R., Huang, J., Arnold, M., Erte, I., Forgetta, V., Yang, T.P., Walter, K., Menni, C., Chen, L., Vasquez, L., Valdes, A.M., Hyde, C.L., Wang, V., Ziemek, D., Roberts, P., Xi, L., Grundberg, E.: Multiple TissueHuman Expression Resource (MuTHER) Consortium, Waldenberger, M., Richards, J.B., Mohney, R.P., Milburn, M.V., John, S.L.,Trimmer, J., Theis, F.J., Overington, J.P., Suhre, K., Brosnan, M.J., Gieger, C., Kastenmüller, G., Spector, T.D., Soranzo, N.: An atlas of genetic influences on human blood metabolites. Nat. Genet. **46**, 543–550 (2014)
20. Rull, A., Hernandez-Aguilera, A., Fibla, M., Sepulveda, J., Rodriguez-Gallego, E., Riera-Borrull, M., Sirvent, J.J., Martín-Paredero, V., Menendez, J.A., Camps, J., Joven, J.: Understanding the role of circulating chemokine (C–C motif) ligand 2 in patients with chronic ischemia threatening the lower extremities. Vasc. Med. **19**, 442–451 (2014)
21. Konishi, H., Karakas, B., Abukhdeir, A.M., Lauring, J., Gustin, J.P., Garay, J.P., Konishi, Y., Gallmeier, E., Bachman, K.E., Park, B.H.: Knock-in of mutant K-ras in nontumorigenic human epithelial cells as a new model for studying K-ras mediated transformation. Cancer Res. **67**, 8460–8467 (2007)
22. Joven, J., Rull, A., Ferre, N., Escola-Gil, J.C., Marsillach, J., Coll, B., Alonso-Villaverde, C., Aragones, G., Claria, J., Camps, J.: The results in rodent models of atherosclerosis are not interchangeable: the influence of diet and strain. Atherosclerosis **195**, e85–e92 (2007)
23. Sauer, U.: Metabolic networks in motion: 13C-based flux analysis. Mol. Syst. Biol. **2**, 62 (2006)
24. Beltran, A., Suarez, M., Rodriguez, M.A., Vinaixa, M., Samino, S., Arola, L., Correig, X., Yanes, O.: Assessment of compatibility between extraction methods for NMR- and LC/MS-based metabolomics. Anal. Chem. **84**, 5838–5844 (2012)
25. Rull, A., Vinaixa, M., Angel Rodriguez, M., Beltran, R., Brezmes, J., Canellas, N., Correig, X., Joven, J.: Metabolic phenotyping of genetically modified mice: an NMR metabonomic approach. Biochimie. **91**, 1053–1057 (2009)
26. Vinaixa, M., Rodriguez, M.A., Rull, A., Beltran, R., Blade, C., Brezmes, J., Correig, X., Joven, J.: Metabolomic assessment of the effect of dietary cholesterol in the progressive development of fatty liver disease. J. Proteome. Res. **9**, 2527–2538 (2010)
27. Folch, J., Lees, M., Sloane Stanley, G.H.: A simple method for the isolation and purification of total lipides from animal tissues. J. Biol. Chem. **226**, 497–509 (1957)
28. Yang, L., Kombu, R.S., Kasumov, T., Zhu, S.H., Cendrowski, A.V., David, F.: Metabolomic and mass isotopomer analysis of liver gluconeogenesis and citric acid cycle. I. Interrelation between gluconeogenesis and cataplerosis; formation of methoxamates from aminooxyacetate and ketoacids. J. Biol. Chem. **283**, 21978–21987 (2008)
29. Currie, L.A.: Nomenclature in evaluation of analytical methods including detection and quantification capabilities (IUPAC Recommendations 1995). Anal. Chim. Acta. **391**, 105–126 (1999)
30. Wegner, A., Weindl, D., Jager, C., Sapcariu, S.C., Dong, X., Stephanopoulos, G., Hiller, K.: Fragment formula calculator (FFC): determination of chemical formulas for fragment ions in mass spectrometric data. Anal. Chem. **86**, 2221–2228 (2014)
31. Sakamoto, Y., Nakagawa, K., Miyagawa, H., Kawana, S., Fukumoto, S.: Quantitative analysis of stable isotopes of glucose in blood plasma using quadrupole GC-MS. Shimadzu Corporation, GC-MS technical repport No. 2 (2010)
32. Garcia-Heredia, A., Kensicki, E., Mohney, R.P., Rull, A., Triguero, I., Marsillach, J., Tormos, C., Mackness, B., Mackness, M., Shih, D.M., Pedro-Botet, J., Joven, J., Sáez, G., Camps, J.: Paraoxonase-1 deficiency is associated with severe liver steatosis in mice fed a high-fat high-cholesterol diet: a metabolomic approach. J. Proteome. Res. **12**, 1946–1955 (2013)
33. Holvoet, P., Rull, A., Garcia-Heredia, A., Lopez-Sanroma, S., Geeraert, B., Joven, J., Camps, J.: Stevia-derived compounds attenuate the toxic effects of ectopic lipid accumulation in the liver of obese mice: a transcriptomic and metabolomic study. Food Chem. Toxicol. **77**, 22–33 (2015)
34. Rull, A., Geeraert, B., Aragones, G., Beltran-Debon, R., Rodriguez-Gallego, E., Garcia-Heredia, A., Pedro-Botet, J., Joven, J., Holvoet, P., Camps, J.: Rosiglitazone and fenofibrate exacerbate liver steatosis in a mouse model of obesity and hyperlipidemia. A transcriptomic and metabolomic study. J. Proteome. Res. **13**, 1731–1743 (2014)
35. Yao, H., Shi, P., Zhang, L., Fan, X., Shao, Q., Cheng, Y.: Untargeted metabolic profiling reveals potential biomarkers in myocardial infarction and its application. Mol. Biosyst. **6**, 1061–1070 (2010)
36. Greenhaff, P.L., Karagounis, L.G., Peirce, N., Simpson, E.J., Hazell, M., Layfield, R., Wackerhage, H., Smith, K., Atherton, P., Selby, A., Rennie, M.J.: Disassociation between the effects of amino acids and insulin on signaling, ubiquitin ligases, and protein turnover in human muscle. Am. J. Physiol. Endocrinol. Metab. **295**, E595–E604 (2008)
37. Suhre, K., Meisinger, C., Doring, A., Altmaier, E., Belcredi, P., Gieger, C., Chang, D., Milburn, M.V., Gall, W.E., Weinberger, K.M., Mewes, H.W., Hrabé de Angelis, M., Wichmann, H.E., Kronenberg, F., Adamski, J., Illig, T.: Metabolic footprint of diabetes: a multiplatform metabolomics study in an epidemiological setting. PLoS ONE **5**, e13953 (2010)
38. Krell, D., Mulholland, P., Frampton, A.E., Krell, J., Stebbing, J., Bardella, C.: IDH mutations in tumorigenesis and their potential role as novel therapeutic targets. Future Oncol. **9**, 1923–1935 (2013)
39. Chen, X., Qian, Y., Wu, S.: The Warburg effect: evolving interpretations of an established concept. Free Radic. Biol. Med. **79**, 253–263 (2015)
40. Armando, J.W., Boghigian, B.A., Pfeifer, B.A.: LC-MS/MS quantification of short-chain acyl-CoA's in *Escherichia coli* demonstrates versatile propionyl-CoA synthetase substrate specificity. Lett. Appl. Microbiol. **54**, 140–148 (2012)
41. Gilibili, R.R., Kandaswamy, M., Sharma, K., Giri, S., Rajagopal, S., Mullangi, R.: Development and validation of a highly sensitive LC-MS/MS method for simultaneous quantitation of acetyl-CoA and malonyl-CoA in animal tissues. Biomed. Chromatogr. **25**, 1352–1359 (2011)
42. Hayashi, O., Satoh, K.: Determination of acetyl-CoA and malonyl-CoA in germinating rice seeds using the LC-MS/MS technique. Biosci. Biotechnol. Biochem. **70**, 2676–2681 (2006)
43. Lei, Z., Huhman, D.V., Sumner, L.W.: Mass spectrometry strategies in metabolomics. J. Biol. Chem. **286**, 25435–25442 (2011)

Supplemental Information

Exploring the process of energy generation in pathophysiology by targeted metabolomics: Performance of a simple and quantitative method

Exploring energy metabolism by metabolomics

Marta Riera-Borrull[1,2], Esther Rodríguez-Gallego[1,2], Anna Hernández-Aguilera[1,2], Fedra Luciano[1,2], Rosa Ras[3], Elisabet Cuyàs[4,5], Jordi Camps[1,2], Antonio Segura-Carretero[6,7], Javier A. Menéndez[4,5], Jorge Joven[1,2a*], Salvador Fernández-Arroyo[1,2a*]

[1]Unitat de Recerca Biomèdica, Hospital Universitari de Sant Joan, IISPV, Universitat Rovira i Virgili, Reus, Spain
[2]Campus of International Excellence Southern Catalonia, Tarragona, Spain
[3]Center for Omics Sciences, Reus, Spain
[4]Metabolism and Cancer Group, Translational Research Laboratory, Catalan Institute of Oncology (ICO), Girona, Spain
[5]Girona Biomedical Research Institute (IDIBGI), Girona, Spain
[6]Department of Analytical Chemistry, University of Granada, Spain.
[7]Research and Development of Functional Food Centre (CIDAF), Granada, Spain
[a]Shared senior authorship

* Corresponding authors. Address request reprints to:

Salvador Fernández-Arroyo & Jorge Joven
Unitat de Recerca Biomèdica, Institut d'Investigació Sanitària Pere Virgili,
Hospital Universitari de Sant Joan, Universitat Rovira i Virgili,
C/Sant Joan s/n, 43201 Reus, Spain
E-mail: sfernandez@fiispv.cat; jorge.joven@urv.cat
Phone number: +34 977 310 300 ext. 55409

Supplemental Table 1. Validation method parameters.

Metabolite	Concentration Range[a]	Slope ± SD / Intercept ± SD (Max. % Residual)[b]	Linearity (R^2)	LOD[a]	LOQ[a]	Intraday RSD (%)	Interday RSD (%)	Recovery (%)
2-hydroxyglutarate	0.07-3.70 (0.5-25)	330378 ± 1787 / -64056 ± 7124	0.9991	0.019 (0.127)	0.063 (0.425)	1.12	1.95	91.65
3-hydroxybutirate	0.005-1.041 (0.05-10)	101090 ± 9841 / -15769 ± 2329 (5.2%)	0.9976	0.001 (0.010)	0.003 (0.032)	0.65	1.15	96.74
3-phosphoglycerate	0.01-0.93 (0.07-5)	237249 ± 8717 / -2135051 ± 194331 (3.2%)	0.9993	0.012 (0.065)	0.040 (0.215)	2.24	3.05	85.65
6-phospho-gluconate	11.05-110.45 (40-400) 2761-13806 (10000-50000)	526980 ± 33064 / -1258050 ± 184029 (7.2%) 87569 ± 5489 / -284587 ± 65724 (6.9%)	0.9987 0.9989	0.146 (0.527)	0.485 (1.758)	3.21	3.98	89.35
α-ketoglutarate	0.015-1.460 (0.1-10)	128155 ± 512 / 14577 ± 872 (1.5%)	0.9997	0.004 (0.029)	0.014 (0.098)	1.14	2.08	94.99
Acetyl-coenzyme A	(0.7-10)	10158 ± 947 / 1785 ± 548 (4.1%)	0.9972	0.494 (0.610)	1.643 (2.030)	1.98	3.01	84.12
Aconitate	0.01-8.71 (0.05-50)	749201 ± 7421 / -788502 ± 131992 (2.8%)	0.9990	0.002 (0.010)	0.005 (0.032)	2.98	3.65	88.68
Alanine	4.46-178.18 (50-2000)	1987694 ± 49173 / -229517 ± 52490 (4.1%)	0.9994	0.026 (0.288)	0.085 (0.959)	1.25	2.34	97.48
Aspartic acid	6.66-266.20 (50-5000)	1715209 ± 7656 / -28378 ± 3102 (2.1%)	0.9996	0.111 (0.835)	0.370 (2.783)	0.84	1.25	98.02
(Iso)Citrate	0.96-96.05 (5-500)	1469611 ± 6187 / -271860 ± 35612 (1.3%)	0.9996	0.007 (0.039)	0.025 (0.130)	2.54	2.96	93.58
Fructose-1,6-bisphosphate	0.17-1.70 (0.5-5)	140842 ± 2592 / -428131 ± 64256 (3.3%)	0.9981	0.040 (0.117)	0.132 (0.389)	1.65	2.15	83.26
Fructose-6-phosphate	0.26-390.15 (1-1500)	824733 ± 9172 / -956090 ± 90237 (2.3%	0.9987	0.038 (0.146)	0.127 (0.487)	1.29	1.99	88.69
Fumarate	0.01-3.48 (0.1-30)	1119413 ± 4307 / -117375 ± 39781 (1.6%)	0.9997	0.005 (0.040)	0.015 (0.132)	0.99	1.34	91.68
Glucose	180.16-2702.40 (1000-15000)	113676 ± 806 / -74297 ± 3489 (1.6%)	0.9997	0.002 (0.009)	0.005 (0.029)	1.54	2.03	97.35
Glucose-6-phosphate	0.52-520.20 (2-2000)	1040659 ± 13926 / -2961082 ± 115348 (2.1%)	0.9990	0.010 (0.039)	0.033 (0.129)	2.14	2.97	96.67
Glutamate	2.94-735.50 (20-5000) 1471-7355 (10000-50000)	1371976 ± 10190 / -306806 ± 354189 (2.4%) 284354 ± 3789 / -76489 ± 3249 (1.9%)	0.9989 0.9990	0.049 (0.334)	0.164 (1.114)	3.05	4.01	94.31
Glutamine	0.731-146.100 (5-1000) 292 2922 (2000-20000)	477954 ± 3556 / -224408 ± 18753 (2.8%) 957845 ± 759 / -79154 ± 6788 (2.9%)	0.9988 0.9987	0.017 (0.114)	0.056 (0.380)	2.87	3.56	93.11
Glyceraldehyde-3-phosphate	0.02-3.40 (0.1-20)	85106 ± 921 / -44424 ± 3589 (4.7%)	0.9979	0.005 (0.029)	0.016 (0.096)	1.32	1.68	87.64
Isoleucine	1.31-131.20 (10-1000)	1652773 ± 13114 / 219943 ± 7893 (4.0%)	0.9996	0.014 (0.108)	0.047 (0.360)	0.96	1.42	98.39
Lactate	4.51-180.2 (50-2000)	23667 ± 414 / 77898 ± 7891 (2.2%)	0.9998	0.002 (0.021)	0.006 (0.070)	0.86	1.74	98.96
Leucine	1.31-131.20 (10-1000)	1735828 ± 25023 / 422255 ± 17342 (7.3%)	0.9993	0.013 (0.102)	0.045 (0.340)	1.33	1.89	96.84
Malate	0.13-67.05 (1-500)	336640 ± 2081 / -57888 ± 6421 (2.5%)	0.9992	0.015 (0.113)	0.051 (0.377)	0.92	1.12	91.64
Malonyl-coenzyme A	0.13-4.27 (0.15-5)	16769 ± 205 / -359 ± 41 (1.8%)	0.9989	0.033 (0.039)	0.111 (0.130)	2.73	3.06	85.23
Oxaloacetate	0.66-13.21 (5-100)	70439 ± 779 / -43811 ± 3924 (2.3%)	0.9991	0.078 (0.590)	0.260 (1.966)	3.68	4.15	89.34
Phosphoenolpyruvate	0.08-0.84 (0.5-5)	285046 ± 3772 / -222284 ± 27845 (4.5%)	0.9981	0.053 (0.313)	0.175 (1.044)	2.38	3.18	92.48
Pyruvate	0.02-4.40 (0.2-50)	379309 ± 8030 / 156902 ± 67475 (2.0%)	0.9991	0.005 (0.060)	0.018 (0.200)	1.01	1.69	94.67
Ribose-5-phosphate	0.23-115.05 (1-500)	553740 ± 5721 / -344047 ± 57894 (3.7%)	0.9976	0.047(0.202)	0.155 (0.675)	1.79	2.06	94.58
Serine	10.5-630.6 (100-6000)	1461082 ± 2239 / 11922 ± 1798 (0.6%)	0.9999	0.032 (0.304)	0.106 (1.012)	1.14	1.79	97.46
Succinate	1.18-23.62 (10-200)	176185 ± 929 / 7109 ± 621 (2.3%)	0.9997	0.009 (0.077)	0.030 (0.258)	0.91	1.35	98.74
Succinyl-coenzyme A	0.09-4.34 (0.1-5)	34216 ± 107 / 5480 ± 758 (4.6%)	0.9998	0.017 (0.020)	0.075 (0.086)	2.06	2.67	87.56
Valine	1.17-58.58 (10-500)	1836799 ± 53914 / 46946 ± 5328 (7.5%)	0.9994	0.011 (0.098)	0.038 (0.326)	1.05	1.68	98.12

[a] Data expressed in μg/mL (μM).
[b] Max. % Residual, maximum percentage of residual deviation

Supplemental Table 2. Optimized data for detection and quantification of metabolites analyzed by GC-EI-QTOF-MS.

Metabolite	Retention time (min)	Molecular formula	Molecular formula (after derivatization)	*m/z*	Qualifier ion		Quantifier ion	
					m/z	Ion	(*m/z*)	Ion
2-hydroxyglutarate	9.41	$C_5H_8O_5$	$C_5H_5O_5(TMS)_3$	364.1558	247.1112	$[M\text{-}COOTMS]^+$	349.1317	$[M\text{-}CH_3]^+$
3-hydroxybutirate	5.03	$C_4H_8O_3$	$C_4H_6O_3(TMS)_2$	248.1264	248.1258	$[M]^+$	233.1029	$[M\text{-}CH_3]^+$
3-phosphoglycerate	11.71	$C_3H_7O_7P$	$C_3H_3O_7P(TMS)_5$	547.1984	357.1133	$[PO_4CH_2CH{=}O\ +3TMS]^+$	387.1423	$[PO_4H\ +4TMS]^+$
6-phosphogluconate	14.57	$C_6H_{13}O_{10}P$	$C_6H_6O_{10}P(TMS)_8$	853.3487	357.1133	$[PO_4CH_2CH{=}O{+}3TMS]^+$	387.1423	$[PO_4{+}4TMS]^+$
α-ketoglutarate	9.47	$C_5H_6O_5$	$C_5H_4O_4(TMS)_2(MA)$	319.1271	288.1089	$[M\text{-}OCH_3]^+$	198.0581	$[M\text{-}OTMS\text{-}OCH_3]^+$
Acetyl-CoA	4.49	$C_{23}H_{38}N_7O_{17}P_3S$	$C_{23}H_{29}N_7O_{15}P_3S(TMS)_9(MA)_2$	1515.5341	204.0747	$[(C_2H_3(MA)S(C_2H_4N(TMS\text{-}CH_3))]^+$	219.0982	$[(C_2H_3(MA))S(C_2H_4N(TMS))]^+$
Aconitate	11.04	$C_6H_6O_6$	$C_6H_3O_6(TMS)_3$	390.1350	375.1115	$[M\text{-}CH_3]^+$	229.1080	$[M\text{-}2TMS\text{-}CH_3]^+$
Alanine	4.59	$C_3H_7NO_2$	$C_3H_5NO_2(TMS)_2$	233.1267	218.1033	$[M\text{-}CH_3]^+$	116.0868	$[M\text{-}COOTMS]^+$
Aspartic acid	8.94	C_4H_7NO4	$C_4H_4NO_4(TMS)_3$	349.1561	334.1326	$[M\text{-}CH_3]^+$	232.1189	$[M\text{-}COOTMS]^+$
(Iso)Citrate	11.68	$C_6H_8O_7$	$C_6H_4O_7(TMS)_4$	480.1851	363.1479	$[M\text{-}COOTMS]^+$	273.0973	$[M\text{-}OTMS\text{-}COOTMS]^+$
Fructose-1,6-bisphosphate	14.21	$C_6H_{14}O_{12}P_2$	$C_6H_7O_{11}P_2(TMS)_9(MA)$	1019.3940	357.1133	$[PO_4CH_2CH{=}O{+}3TMS]^+$	387.1423	$[PO_4{+}4TMS]^+$
Fructose-6-phosphate	13.98	$C_6H_{13}O_9P$	$C_6H_7O_8P(TMS)_7(MA)$	794.3408	357.1133	$[PO_4CH_2CH{=}O{+}3TMS]^+$	315.1028	$[PO_4H{+}3TMS]^+$
Fumarate	7.01	$C_4H_4O_4$	$C_4H_2O_4(TMS)_2$	260.0900	260.0895	$[M]^+$	245.0665	$[M\text{-}CH_3]^+$
Glucose	12.25	$C_6H_{12}O_6$	$C_6H_7O_5(TMS)_5(MA)$	569.2876	217.1080	$[M\text{-}CH_2\text{-}2CH\text{-}MA\text{-}3OTMS]^+$	319.1581	$[M\text{-}CH_2\text{-}CH\text{-}MA\text{-}2OTMS]^+$
Glucose-6-phosphate	14.09	$C_6H_{13}O_9P$	$C_6H_7O_8P(TMS)_7(MA)$	794.3408	357.1133	$[PO_4CH_2CH{=}O{+}3TMS]^+$	387.1423	$[PO_4{+}4TMS]^+$
Glutamate	9.85	$C_5H_9NO_4$	$C_5H_6NO_4(TMS)_3$	363.1717	348.1483	$[M\text{-}CH_3]^+$	246.1346	$[M\text{-}COOTMS]^+$
Glutamine	11.59	$C_5H_{10}N_2O_3$	$C_5H_7N_2O_3(TMS)_3$	362.1877	347.1642	$[M\text{-}CH_3]^+$	245.1505	$[M\text{-}COOTMS]^+$
Glyceraldehyde-3-phosphate	10.87	$C_3H_7O_6P$	$C_3H_4O_6P(TMS)_4$	459.1640	315.1028	$[PO_4H{+}3TMS]^+$	357.1133	$[PO_4CH_2CH{=}O{+}3TMS]^+$
Isoleucine	6.49	$C_6H_{13}NO_2$	$C_6H_{11}NO_2(TMS)_2$	275.1737	260.1502	$[M\text{-}CH_3]^+$	158.1365	$[M\text{-}COOTMS]^+$
Lactate	4.05	$C_3H_6O_3$	$C_3H_4O_3(TMS)_2$	234.1107	234.1102	$[M]^+$	219.0867	$[M\text{-}CH_3]^+$
Leucine	6.26	$C_6H_{13}NO_2$	$C_6H_{11}NO_2(TMS)_2$	275.1737	260.1502	$[M\text{-}CH_3]^+$	158.1365	$[M\text{-}COOTMS]^+$
Malate	8.58	$C_4H_6O_5$	$C_4H_3O_5(TMS)_3$	350.1401	335.1161	$[M\text{-}CH_3]^+$	233.1029	$[M\text{-}COOTMS]^+$
Malonyl-CoA	6.57	$C_{24}H_{38}N_7O_{19}P_3S$	$C_{24}H_{28}N_7O_{17}P_3S(TMS)_{10}(MA)_2$	1631.5634	262.0569	$[(C_3H_2O_2(MA))S(C_2H_4N(TMS))]^+$	187.0725	$[C_4H_6N_2S(TMS)]^+$
Oxaloacetate	8.38	$C_4H_4O_5$	$C_4H_2O_4(TMS)_2(MA)$	305.1115	305.1109	$[M]^+$	290.0880	$[M\text{-}CH_3]^+$
Phosphoenolpyruvate	9.75	$C_3H_5O_6P$	$C_3H_2O_6P(TMS)_3$	384.1010	384.1004	$[M]^+$	369.0755	$[M\text{-}CH_3]^+$
Pyruvate	3.96	$C_3H_4O_3$	$C_3H_3O_2(TMS)(MA)$	189.0821	189.0816	$[M]^+$	174.0586	$[M\text{-}CH_3]^+$
Ribose-5-phosphate	13.51	$C_5H_{11}O_8P$	$C_5H_6O_7P(TMS)_6(MA)$	692.2907	357.1133	$[PO_4CH_2CH{=}O{+}3TMS]^+$	315.1028	$[PO_4H{+}3TMS]^+$
Serine	7.23	$C_3H_7NO_3$	$C_3H_4NO_3(TMS)_3$	321.1612	306.1377	$[M\text{-}CH_3]^+$	204.1240	$[M\text{-}COOTMS]^+$
Succinate	6.63	$C_4H_6O_4$	$C_4H_4O_4(TMS)_2$	262.1057	262.1051	$[M]^+$	247.0822	$[M\text{-}CH_3]^+$
Succinyl-CoA	7.38	$C_{25}H_{40}N_7O_{19}P_3S$	$C_{25}H_{30}N_7O_{17}P_3S(TMS)_{10}(MA)_2$	1645.5791	276.0958	$[(C_4H_4O_2(MA))S(C_2H_4N(TMS))]^+$	174.0225	$[C_6H_8O_3NS]^+$
Valine	5.62	$C_5H_{11}NO_2$	$C_5H_9NO_2(TMS)_2$	261.1580	246.1346	$[M\text{-}CH_3]^+$	144.1209	$[M\text{-}COOTMS]^+$
D_4-Succinate	6.61	$C_4H_2D_4O_4$	$C_4D_4O_4(TMS)_2$	266.1308	266.1302	$[M]^+$	251.1073	$[M\text{-}CH_3]^+$

TMS, trimethylsilyl ($Si(CH_3)_3$); MA, methoxyamine ($NOCH_3$)

nutrients

MDPI

Article

Metformin potentiates the benefits of dietary restraint: a metabolomic study

Marta Riera-Borrull [1,2], Anabel García-Heredia [1], Salvador Fernández-Arroyo [1,3], Anna Hernández-Aguilera [1], Noemí Cabré [1], Elisabet Cuyàs [3,4], Fedra Luciano-Mateo [1], Jordi Camps [1], Javier A. Mendendez [3,4] and Jorge Joven [1,5*].

[1] Unitat de Recerca Biomèdica, Hospital Universitari Sant Joan, Institut d'Investigació Sanitària Pere Virgili, Universitat Rovira i Virgili, 43201 Reus, Spain; marta.riera.borrull@gmail.com (M.R-B.); ghanabel@gmail.com (A.G-H.); salvador.fernandezarroyo@gmail.com (S.F-A.); anna.hernandeza@gmail.com (A.H-A.); noemi.cabre@gmail.com (N.C.); fedra.luciano@gmail.com (F.L-M.); jcamps@grupsagessa.com (J.C.); jorge.joven@urv.cat (J.J.)
[2] Centro de Investigaciones Biológicas, CIB-CSIC, 28040 Madrid, Spain; marta.riera.borrull@gmail.com (M.R-B.)
[3] Molecular Oncology Group, Girona Biomedical Research Insitiute (IDIBGI), 17190 Girona, Spain; salvador.fernandezarroyo@gmail.com (S.F-A.); ecuyas@idibgi.com (E.C.); jmenendez@idibgi.com (J.A.M.)
[4] ProCURE (Program Against Cancer Therapeutic Resistance), Metabolism and Cancer Group, Catalan Institute of Oncology, 17190 Girona, Spain; ecuyas@idibgi.com (E.C.); jmenendez@idibgi.com (J.A.M.)
[5] The Campus of International Excellence Southern Catalonia, 43003 Tarragona, Spain; jorge.joven@urv.cat (J.J.)
* Correspondence to: jorge.joven@urv.cat (J.J.); Tel. +34-977-310-300 ext. 55409.

Received: date; Accepted: date; Published: date

Abstract:

Identification of therapeutic approaches to protect against the metabolic consequences of chronic energy-dense/high-fat diet (HFD) remains a public health priority because associated diseases are the leading causes of death worldwide. Here, we evaluated whether metformin could protect against HFD-induced metabolic disturbances in low-density lipoprotein receptor-knockout mice. Once rendered obese, glucose-intolerant and hyperlipidemic, mice were switched to diet reversal with or without metformin to explore how proinflammatory and metabolic changes respond. Metabolic phenotypes were evaluated by integrating biochemical, histological, and metabolomic components closely related to the multi-faceted metabolic disturbances provoked by HFD. Metformin combined with diet reversal promoted a more effective weight loss along with better glucose control, notably lowered levels of circulating cholesterol and triglycerides, and moderately reduced adipose tissue content. Moreover, mice treated with metformin showed a dramatically improved protection against HFD-induced hepatic steatosis, a beneficial effect that was accompanied by a lowering of liver-infiltrating proinflammatory macrophages and lower release of proinflammatory cytokines. The ability of metformin to target the contribution of branched chain amino acids to adipose tissue metabolism while suppressing mitochondrial-dependent biosynthesis in hepatic tissue might contribute to the additional beneficial effects elicited beyond

those of dietary restriction alone. Our findings underscore how the adipose tissue and liver crosstalk provides clinical potential for combining metformin and dietary modifications as a therapeutic maneuver to protect against the metabolic damage occurring upon excessive dietary fat intake.

Keywords: adipose tissue; caloric restriction; energy state; inflammation; liver steatosis; metabolomics.

1. Introduction

Contemporary high-energy and high-fat poor quality diets coupled with the effect of sedentary lifestyles are closely related to the convergent epidemics of obesity, insulin resistance, type 2 diabetes (T2D) and non-alcoholic fatty liver disease (NAFLD). These metabolic comorbidities foster patterns of functional decline and major chronic diseases that compromise health span and quality of life [1]. Therefore, to identify therapeutic options aimed to protect against dietary-induced, multifaceted metabolic damage is a clinical priority.

Lifestyle modification approaches are commonly indicated to manage the vicious cycle of metabolic damage triggered by energy-dense/high-fat diets (HFD) but the efficacy is seriously hampered by relatively unknown cellular metabolic strategies and compensatory pathways induced by reducing fat intake or taking regular exercise [2, 3]. The typical diets in industrialized countries and calorie (energy) restriction (CR) would be expected to exert the opposite effect by operating as extreme ends of the same disease-health metabolic spectrum. However, the adoption of a CR-like lifestyle seems impractical outside of research settings [4, 5]. An alternative strategy might combine lifestyle modification with pharmacotherapy and in this context efficacy is likely for adenosine monophosphate-activated protein kinase (AMPK) activators [6].

The biguanide metformin, a first-line diabetes drug, has been repeatedly suggested to promote long-term programming of metabolic health with little or no toxicological significance [7-10] and may take new routes (i.e., to treat patients without diabetes) to clinical usefulness [11, 12] with the potential to differentially affect medical outcomes [13-17]. Despite the growing evidence demonstrating the multiple protective effects of metformin against metabolic diseases, the combined effects of diet planning along with metformin have been scarcely investigated. For example, the combination of metformin and a 70% restriction in calories yielded superior results than either treatment alone in diabetic rats [18] and metformin alone improved liver damage without modifying adipose tissue in HFD-fed C57BL6/J mice [19]. Using a metabolomic approach, we tested the hypothesis that concomitant metformin and simple diet reversal treatment could ameliorate HFD-induced disturbances in energy metabolism. We performed an integrated analysis of the metabolic phenotypes occurring upon feeding experimental diets with or without metformin treatment in low-density lipoprotein receptor-deficient mice (*Ldlr*$^{-/-}$). We have previously shown that this is a robust model to assess the effect of nutrition in a context of subclinical chronic inflammation, which reproducibly measure objective and quantifiable metabolic characteristics, and includes hyperlipidemia without the confounding effects of diabetes [20, 21]. We provide evidence that switching to normal diet in combination with metformin can significantly alleviate the metabolic disturbances provoked by previous HFD.

2. Materials and Methods

2.1 Animals and animal care

Male *Ldlr*$^{-/-}$ mice in a C57BL/6 genetic background were obtained by breeding animals purchased from Jackson Laboratory (Bar Harbor, ME, USA) and maintained under controlled temperature (22ºC), humidity (50%) and lighting (12h-12h light-dark cycle). To prevent sex-dependent variability, female animals were not included [20]. Mice had *ad libitum* access to water and control breeder chow diet (CD; crude fat 3.1% and 71.8% available carbohydrate) prepared by Scientific Animal Food & Engineering, Augy, France, until the experiments began at 10 weeks of age. All procedures were performed by dedicated staff in accordance with current regulations and supervision by the Ethics Committee on Animal Experimentation of the Universitat Rovira i Virgili following European guidelines (Directive 2010/63/EU). Diets were chosen to examine relevant differences. In CD, calories (3.3 Kcal/g) were from protein (19%), fat (roughly 9%) and carbohydrates (72%). In the high-fat diet (HFD), Ssnif Spezialdiäten (Soest, Germany), calories (5.7 Kcal/g) were from protein (19%), fat (roughly 60%) and carbohydrates (21%).

2.2 Experimental design

We explored the metformin response in mice fed with either the original CD or HFD for 14 weeks. The animals were allocated to experimental groups using computer-generated randomization schedules and the investigators responsible for the assessment of outcomes had no knowledge of the experimental group to which the animals belonged. No animals were excluded from the analysis. First, mice were allocated into two dietary groups (n=16, each) and further divided in mice receiving metformin (Sigma, Madrid, Spain) or placebo (Monteloeder, Elche, Spain) daily (n=8, each) (Fig. 1A). Mice were sacrificed at 24 weeks using isoflurane inhalation. The route of administration and dose of metformin was designed after confirming that metformin does not accumulate in plasma after repeated administration and that the mean plasma concentration in mice was similar to that obtained in humans with a dose of 1.25 g.day-1 as described [22]. Hence, we used metformin dissolved in drinking water (5 mg·mL^{-1}) to provide 250 mg·Kg^{-1}·day^{-1} in concordance with previously published data [23, 24]. We then examined in parallel experiments the metformin response in mice with adverse inflammatory and metabolic status established through feeding animals with HFD for 6 weeks. Some animals (n=6) were sacrificed at this time for comparative analysis. Other littermates were then fed with HFD or CD for other 8 weeks. Those mice fed with CD were divided to receive metformin or placebo (n=8, each) as stated above (Fig. 1B). Mice were sacrificed at 24 weeks after a similar fasting time (4 hours with a maximum difference of 15 min).

2.3. Sample collection and analytical methods

Glucose tolerance tests (GTT) were performed in all animals one week before their sacrifice by injecting intraperitoneally glucose in saline solution (2 mg·g^{-1} of body weight) after 4 hours of fasting. Blood was drawn from the tail to measure glucose levels (Roche Diagnostics, Basel, Switzerland), 0, 15, 30, 60 and 120 min after the injection. Blood samples were also collected from anesthetized animals into EDTA-treated blood collection tubes during sacrifice and immediately centrifuged and stored at -80ºC until analysis. There were no detectable iatrogenic experimental variables. Plasma concentrations of glucose, cholesterol, triglycerides and liver enzymes were measured by standard assays in an automated analyzer Synchron LXi 725 (Beckman Coulter, IZASA, Barcelona, Spain). Plasma lipoproteins were separated by fast-performance liquid chromatography (FPLC) using a Bio-Rad Bio Logic Duo Flow 10 system (Bio-Rad, Alcobendas, Spain). Serum pooled samples from each group (200 µl) were injected into a Superose 6 /300 GL column (GE Healthcare Europe GmbH, Munich, Germany), and 500 µl fractions were collected.

Cholesterol and triglycerides concentrations were analyzed in each fraction as reported [20]. Organs were perfused in phosphate buffered saline and tissue samples removed and fixed for 24h in 10% neutral-buffered formalin for histology.

2.4. Histological analysis

Paraffin-embedded tissues were stained with hematoxylin and eosin (H&E). The extent of steatosis in the liver and adipocyte size of epididymal white adipose tissue (eWAT) were estimated by image analysis software (AnalySIS, Soft Imaging System, Munster, Germany) and the hepatic proportion of macrophages (anti F4/80, Serotec, Oxford, UK) was determined by immunohistochemistry essentially as described [25, 26].

2.5. Cytokine measurements

Liver samples were homogenized using a Precellys 24 homogenizer (Bertin Technologies, Toulouse, France) in lysis buffer containing protease inhibitors at a concentration of 250 μg/mL. The levels of interleukin (IL)-1β, IL-2, IL-6, IL-10, interferon-γ, chemokine (C-C motif) ligand 2 (CCL2), and tumor necrosis factor-α (TNFα) were measured in the homogenates following the manufacturer's instructions using Bio-plexProTM magnetic bead-based assays (Bio-Rad, Madrid, Spain) on the Luminex platform (Bio-Rad).

2.6. Targeted metabolomics

The list of metabolites of major pathways related to energy metabolism was designed with the rationale that cells must allocate nutrients toward boosting glycolysis, and to generate ATP and intermediates for macromolecule biosynthesis. Metabolites were quantitatively measured as described [21]. Briefly, metabolites in liver (50 mg) and epididymal white adipose tissue (eWAT; 100 mg) were extracted in 1 mL of methanol/water (8:2) using a Precellys 24 system (Izasa, Barcelona, Spain). After centrifugation at 14,000 rpm 10 min at 4°C, supernatants were collected and the homogenization step repeated. Nonpolar compounds were further extracted in chloroform/methanol (2:1). All supernatants were centrifuged, filtered using 0.22 μm filters, and freeze-dried overnight. Samples were dried under N2, derivatized using methoxyamine dissolved in pyridine (40 mg/mL) and N-methyl-N-(trimethylsilyl)-trifluoroacetamide and injected into a 7890A gas chromatograph coupled with an electron impact source to a 7200 quadrupole time-of-flight mass spectrometer (MS) equipped with a 7693 auto-sampler module and a J&W Scientific HP-5MS column (30 m × 0.25 mm, 0.25 μm) (Agilent Technologies, Santa Clara, CA, USA). We measured 31 metabolites in related pathways, including the pentose-phosphate, glycolysis and gluconeogenesis, citric acid cycle (CAC) and metabolism of amino acids (see Figures). Values in eWAT homogenates were lower than in liver and malonyl-CoA and succinyl-CoA were not considered because, although detected, they were under the limit of quantification using these conditions.

2.7. Statistical analysis

All results are shown as the mean ± SD unless otherwise stated. Differences between groups were assessed with the Mann-Withney *U* test (nonparametric) and considered statistically significant when $P < 0.05$. Some comparisons required one-way ANOVA. All statistical analyses were carried out using the GraphPad Prism 6.0 Software, Inc (USA). For the metabolomic analysis, the obtained raw data were processed and compounds were detected and quantified using the Qualitative and Quantitative Analysis B.06.00 software (Agilent Technologies). Results were compared by one-way ANOVA with Dunnett's multiple pair-wise comparison tests using a significance threshold of 0.05. MetaboAnalyst 3.0, available on the web (http://www.metaboanalyst.ca/) was used to generate meaningful scores/loading plots [27].

3. Results

3.1. Effects on the regulation of body weight and food intake

Predictably, mice in the HFD group gained weight quicker than CD littermates. Whereas metformin treatment had no effect on body weight regulation in mice challenged with HFD, it led to a significant reduction in body weight gain in mice on CD from the fourth week until the end of the follow-up (24 weeks) (Fig. 1A). Body weight gain of HFD-fed mice decreased immediately after switching to CD. Remarkably, administration of metformin was significantly more effective than CD alone in reducing body weight gain, particularly after 6–7 weeks of diet reversal when mice fed CD alone began to regain lost body weight (Fig. 1B).

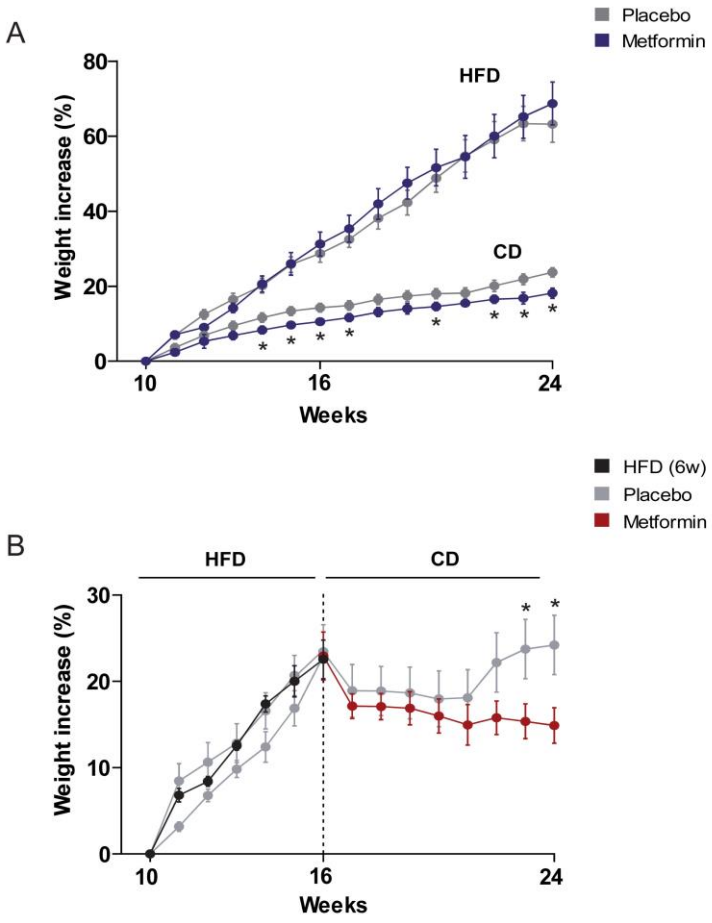

Figure 1. Dietary-induced changes and the effect of metformin on weight control. Overall design in experimental animals. (A) Values obtained in mice upon feeding with experimental diets for 14 weeks. CD, chow diet; HFD, high-fat diet. (B) Values obtained after a 6 weeks period of HFD feeding and shift to CD. Asterisks denote significant ($P < 0.05$) changes compared to the respective group.

Mice on HFD exhibited decreased food intake relative to CD-fed mice; however, the total caloric intake by body weight was similar in both groups when considering the food energy density in the diets. Metformin treatment had no effect on food consumption between groups (Fig. 2A, B).

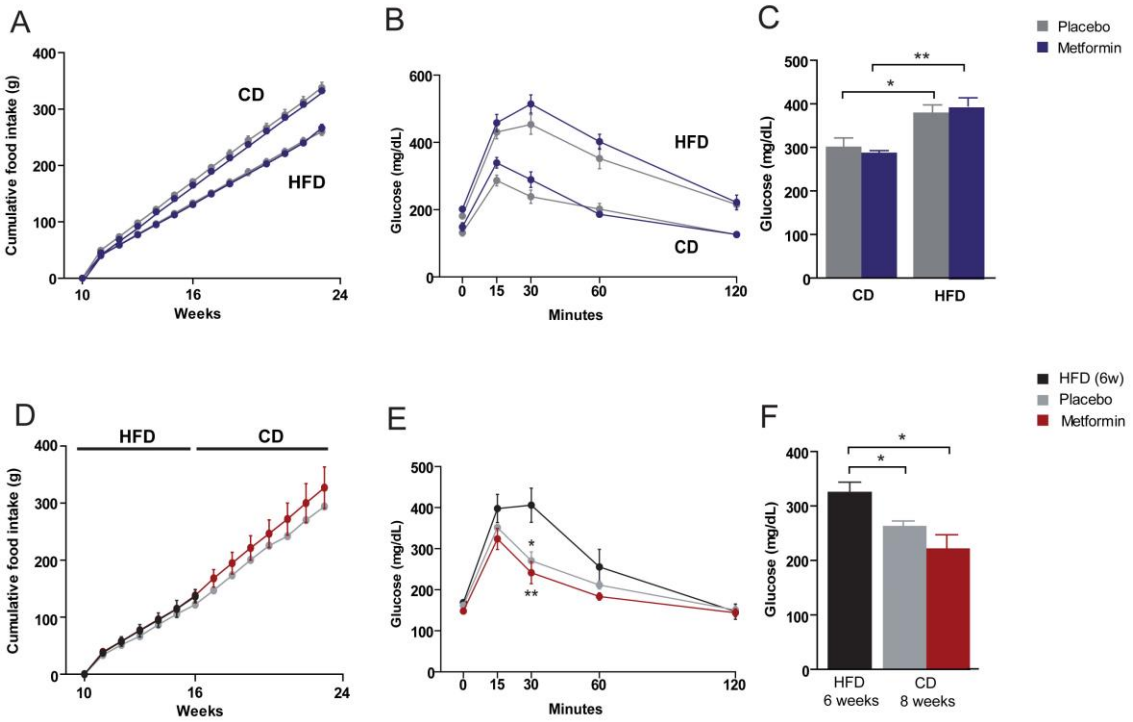

Figure 2. Dietary-induced changes and the effect of metformin on food intake and glucose homeostasis. (A, B) Cumulative food intake, (C, D) glucose tolerance tests, and (E, F) plasma glucose levels segregated by the type of dietary experiment and use of metformin as indicated. Asterisks denote significant (*P < 0.05; **P < 0.01) changes.

3.2. Effects on glucose homeostasis

Fasting serum glucose levels were significantly higher in the HFD group than in the CD group. To assess in more detail the impact of chronic HFD exposure on glucose homeostasis, both groups were subjected to a glucose tolerance test (GTT). Intraperitoneally injected glucose resulted in a more rapid increase of blood glucose in the HFD group than in the CD group, indicating the development of HFD-induced systemic glucose intolerance. The effect of metformin administration on plasma glucose levels and glucose tolerance was negligible in CD and HFD groups. We then re-evaluated glucose homeostasis in HFD-fed mice subjected to diet reversal with or without metformin treatment. Diet reversal and metformin were similarly effective in reducing the HFD-provoked increase in plasma glucose. Of note, although peak values of blood glucose levels were similar for diet reversal alone and with metformin in the GTT, animals treated with metformin exhibited faster glucose clearance (Fig. 2 C-F).

3.3. Effects on hyperlipidemia

Plasma levels of cholesterol and triglycerides were significantly higher in the HFD group than in the CD group (Fig. 3A). Metformin treatment resulted in a significant reduction in the concentration of total serum cholesterol and of dense LDL-cholesterol in CD-fed animals (Fig. 3 A, B). Metformin-induced changes to LDL levels in CD-fed mice were accompanied by a significant decrease in serum triglyceride concentrations and of triglycerides in the LDL

fraction (Fig. 3 A, B). Diet reversal to CD abolished the increase in circulating cholesterol promoted by HFD feeding (Fig. 3C). Indeed, lipoprotein distribution in mice subjected to diet reversal with or without metformin largely resembled that commonly observed in wild-type animals (i.e., almost all cholesterol in the HDL fraction) (Fig. 3D). Remarkably, administration of metformin promoted a further reduction in the circulating levels of cholesterol in diet-switched mice and also a statistically significant reduction in serum triglyceride concentration (Fig. 3C).

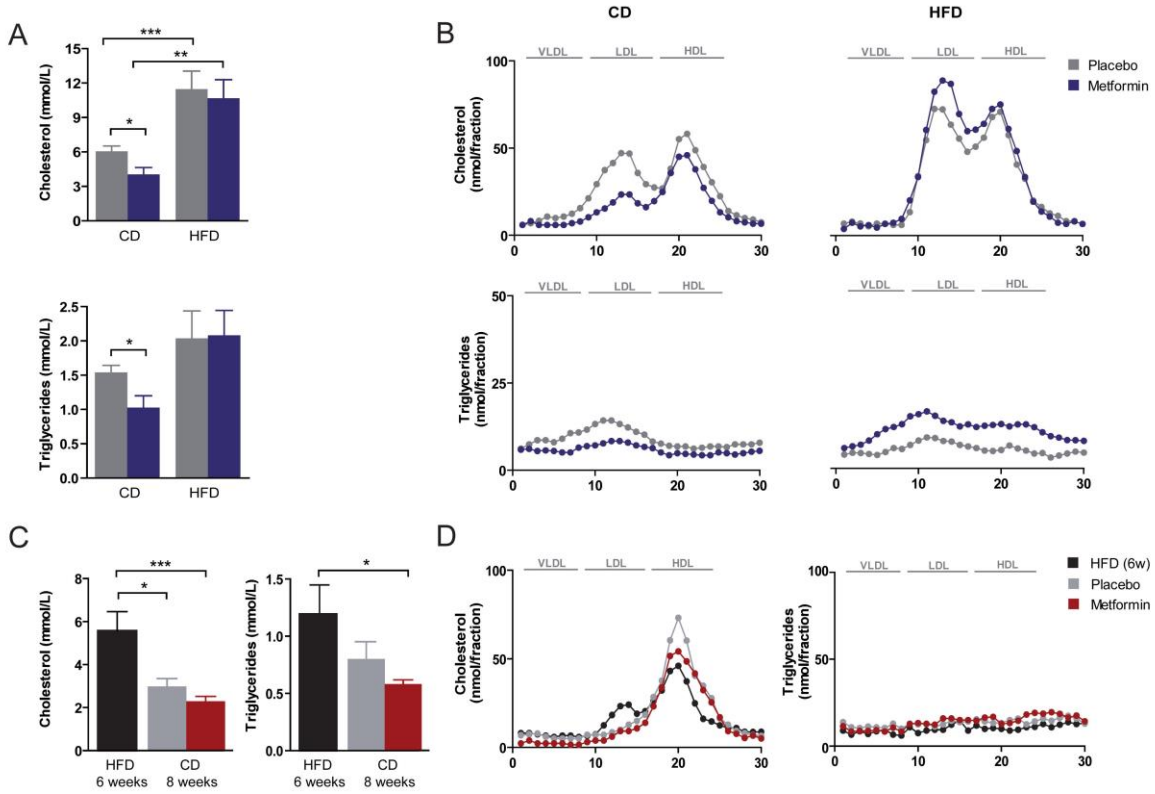

Figure 3. Dietary-induced changes and the effect of metformin on plasma lipids and lipoprotein distribution. (A) Plasma lipids and (B) lipoprotein distribution as measured with fast-performance liquid chromatography in mice upon feeding with experimental diets for 14 weeks. CD, chow diet; HFD, high-fat diet. (C, D) Same measurements in mice after diet reversal with or without metformin. Asterisks denote significant (*P < 0.05; **P < 0.01; ***P<0.001) changes as indicated.

3.4. Effects on white adipose tissue

Given the changes to triglyceride levels between CD and HFD groups, we next questioned how metformin might impact eWAT content. Morphometric analysis of visceral/eWAT depots revealed that average adipocyte size in HFD-fed mice was significantly greater than that found in CD-fed mice (Fig. 4 A, B). Metformin administration significantly decreased adipocyte size and also the relative weight of the eWAT depot in CD-fed mice (Fig. 4 A, B). By contrast, metformin treatment further increased adipocyte size and also the relative weight of WAT in HFD-fed animals (Fig. 4 A, B). Whereas metformin treatment augmented the loss of the WAT depot in animals subjected to diet reversal and led to a significant decrease in adipocyte size, the average size of adipocytes remained larger than in those from animals treated with diet reversal alone (Fig. 4 C, D).

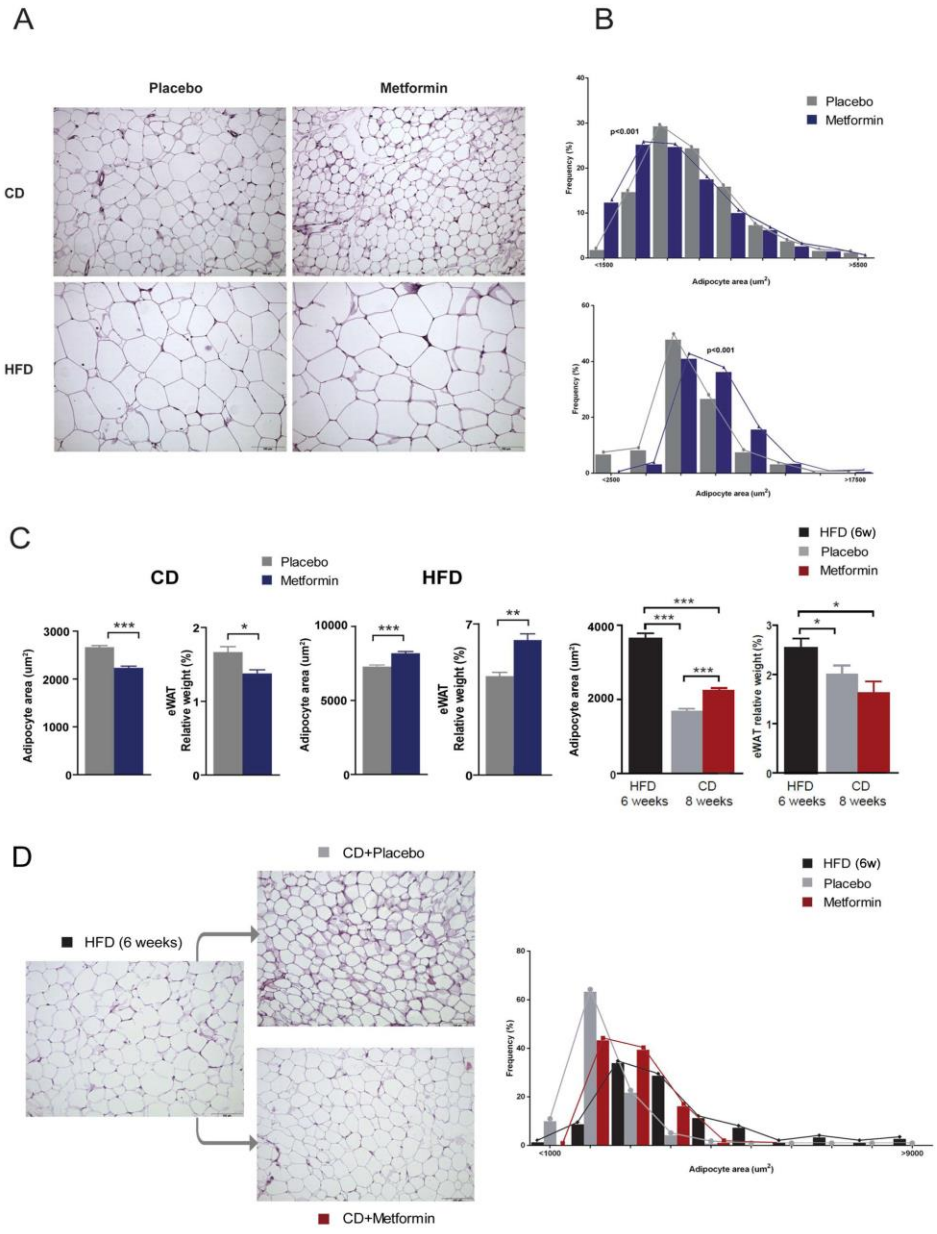

Figure 4. Dietary-induced changes and the effect of metformin on the epididymal WAT phenotype. (A): Representative microphotographs (200x) showing the differential effects of diet and metformin in epididymal white adipose tissue (eWAT) and (B) frequency distribution of adipocyte size. (C) Mean values for adipocyte area and relative weight with respect to body weight in experiments. (C, D) Phenotypic changes and frequency distribution of adipocyte size combining shift in diets and metformin. Legends as in Fig. 1 and asterisks denote significant (*P < 0.05; **P < 0.01; ***P<0.001) changes as indicated.

3.5. Effects on hepatic steatosis

Chronic HFD exposure is known to cause lipid accumulation in the liver, a process that ultimately leads to NAFLD and eventually to nonalcoholic steatohepatitis. As expected, HFD-fed animals presented with severe fatty liver disease. No significant differences in hepatic steatosis were found in the CD and HFD groups following metformin administration (Fig. 5A). Remarkably, whereas diet reversal alone failed to ameliorate HFD-induced hepatic steatosis,

the combination of diet reversal and metformin treatment significantly reduced the occurrence of steatosis (Fig. 5B).

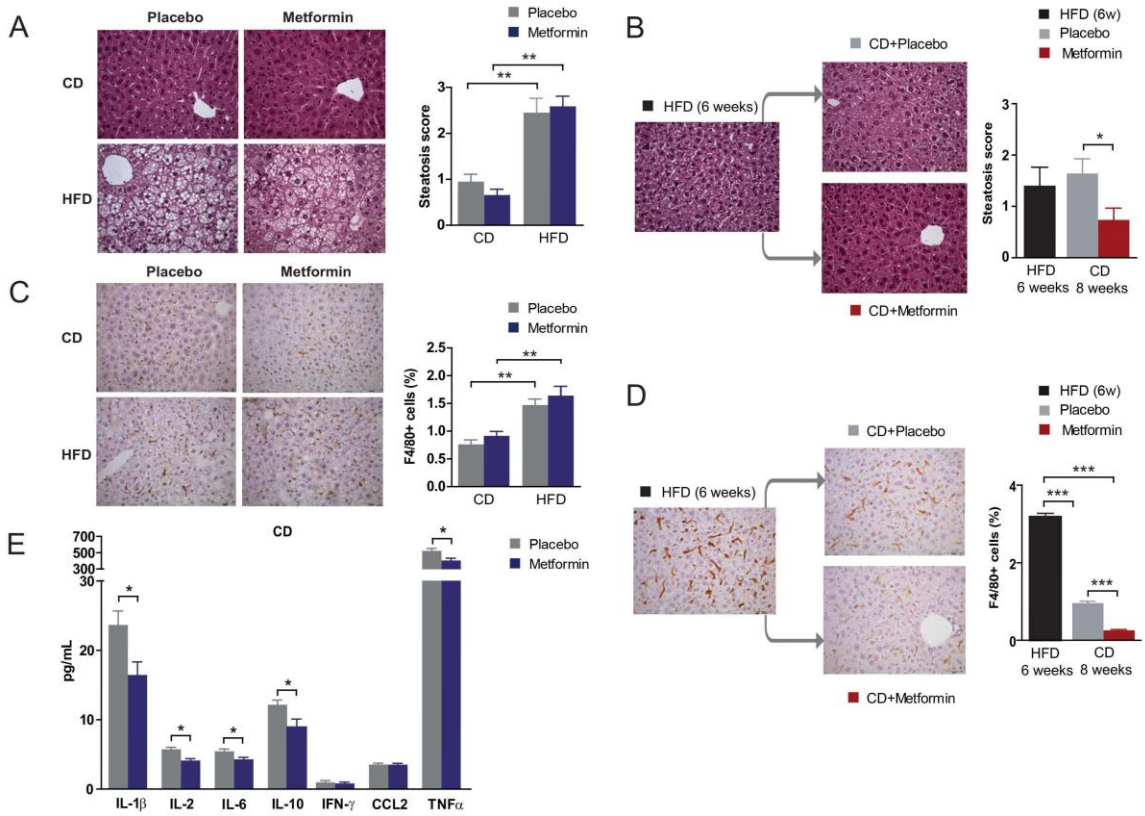

Figure 5. Dietary-induced changes and the effect of metformin on the liver phenotype. Effects of diet and metformin at indicated times during nutritional variations. Representative microphotographs (100x) of liver sections stained with H&E (A, B) and F4/80 immunochemistry (C, D) showing the effects of diet and metformin in steatosis score and proportion of macrophages. (E) The effect of metformin in the hepatic concentration of selected cytokines. Legends as in Fig 1 and asterisks denote significant (*P < 0.05; **P < 0.01; ***P<0.001) changes as indicated.

3.6. Effects on hepatic inflammation

There were no signs of ballooning or fibrosis and liver enzymes were not differentially affected by diet but we detected a significantly increased number of macrophages in liver of HFD-fed animals when compared with CD-fed animals, as revealed by immunohistochemistry for F4/80, a pan-marker for murine tissue macrophages (Fig. 5C). Diet reversal ameliorated liver inflammation in the HFD group, as demonstrated by the significant decrease in the number of F4/80+ inflammatory cells (Fig. 5D). Of note, metformin treatment of diet-reversed animals almost completely eliminated the presence of F4/80⁺ macrophages (Fig. 5D), which also appeared to be enlarged; a morphology that might be suggestive of an activated state following HFD. The ability of metformin to reduce HFD-induced chronic inflammation might involve the reduced production of prototypical pro-inflammatory cytokines including interleukin (IL)-1◎ and tumor necrosis factor-◎ (TNF◎), as levels of these cytokines were significantly reduced in metformin-treated mice. Quantitative and qualitative changes were similar in both CD and HFD regimens and values obtained in CD fed mice with or without metformin are shown in Fig. 5E.

3.7. Effects on the levels of energy metabolites in hepatic and adipose tissue

The exposure of mice to HFD has an impact on levels of energy metabolites, which is different in WAT and liver. In WAT, HFD led to a decrease in the levels of glycolytic

intermediates proximal to glucose-6-phosphate, while increasing the TCA cycle intermediates citrate/isocitrate and α-ketoglutarate. Conversely, HFD promoted in liver the accumulation of glycolytic intermediates proximal to glucose-6-phosphate, that is, those intermediates involved in glucose transport and phosphorylation, while significantly decreasing branched-chain amino acids (BCAAs) (Fig. 6).

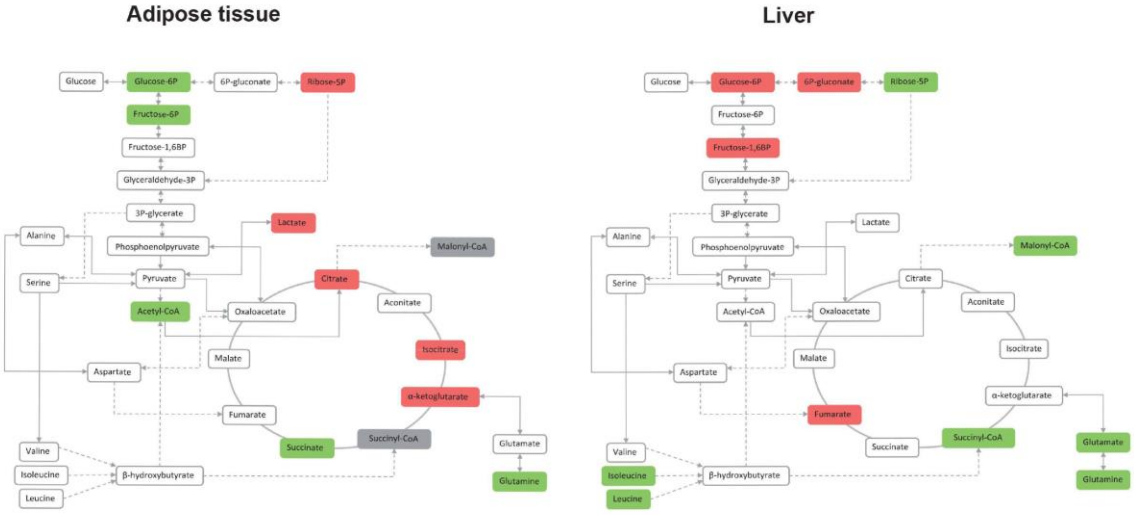

Figure 6. The relative impact of dietary fat on the levels of metabolites associated with energy metabolism in adipose tissue and liver. Metabolites are marked in green or red if they were significantly decreased or increased respectively according to the impact of HFD alone.

We then evaluated the tissue-specific (WAT versus liver) nature of the impact of metformin for energy metabolites. Metformin treatment led to a significant decrease in the levels of the BCAAs valine, leucine, and isoleucine in WAT of mice fed CD, and additionally increased glycolytic intermediates distal to glucose-6-phosphate (phosphoenolpyruvate, pyruvate, and lactate) and most of the TCA cycle intermediates (Fig. 7A). Whereas the decrease in the glycolytic intermediates proximal to glucose-6-phosphate remained unaltered by metformin treatment, neither glycolytic intermediates distal to glucose-6-phosphate nor TCA intermediates were significantly altered by metformin in WAT of mice on HFD. Metabolite-based clustering in WAT obtained by the partial least squares-discriminant analysis (PLS-DA) model revealed a clear and significant separation between CD and HFD regimens in the absence or presence of metformin treatment in two-dimensional score plots (Fig. 7B). When the criteria of variable importance in the projection (VIP scores ≥1) in the PLS-DA model were used to maximize the difference of metabolic profiles between the different diet groups, the subset of metabolites majorly impacted were early glycolytic intermediates and BCAAs (Fig. 7C). Heatmap visualization, commonly used for unsupervised clustering, revealed a similar segregation of metformin-impacted glycolytic and amino acids metabolites in WAT from CD and HFD groups (Fig. 7D).

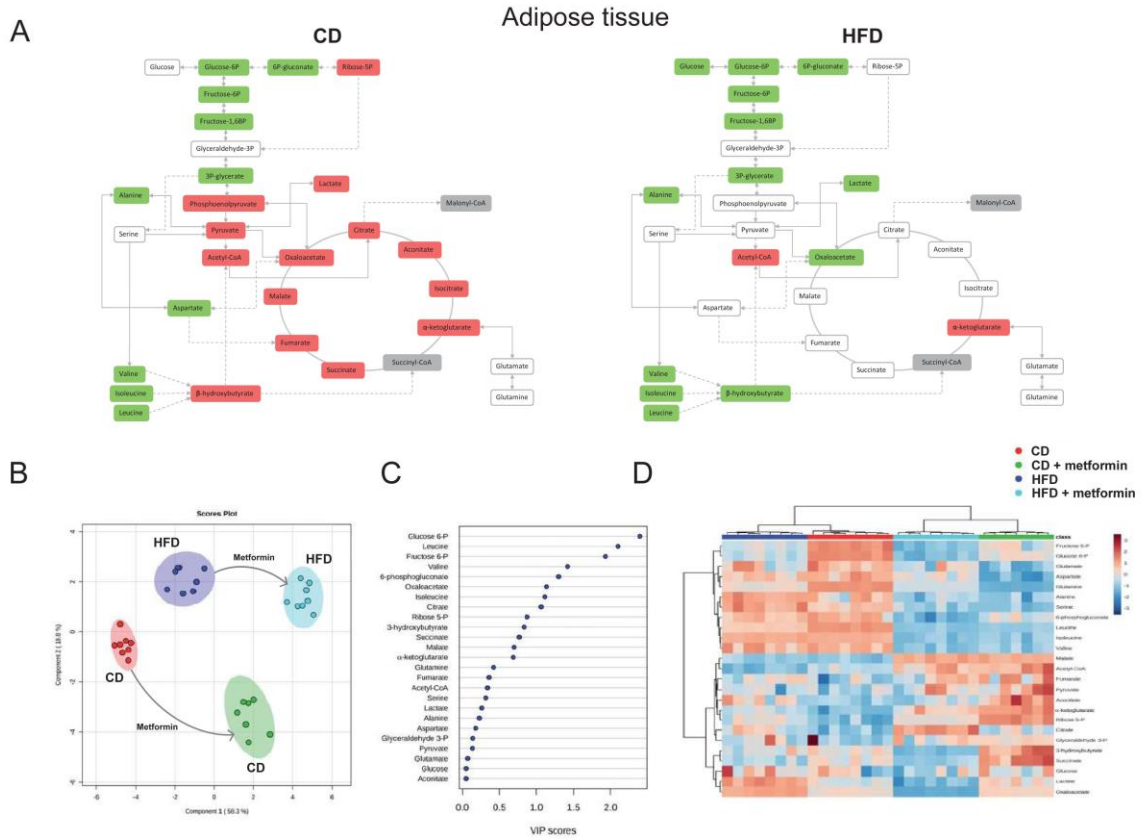

Figure 7. Dietary-induced changes and the effect of metformin on WAT energy metabolites. (A) The effect of both diets is segregated to highlight specific changes in metformin response; metabolites are marked in green or red if they were significantly decreased or increased respectively. (B) Partial least square discriminant analysis indicates visually the role of the measured metabolites in discriminating among the different experimental groups. (C) Random forests were used to rank without supervision the importance of metabolites to explain the differential effect of metformin. (D) Standardized metabolite concentrations represented as a heatmap. Mice populations with different diets and metformin treatment are reported as a color code in the upper part of the graph, while metabolite names have been assigned to rows.

A completely different picture emerged when assessing metformin-driven metabolomic shifts in liver from CD and HFD groups. The significant reduction of phosphoenolpyruvate and acetyl-CoA, accompanied by an increase in the levels of glycolytic intermediates proximal to glucose-6-phosphate, including glucose-6-phosphate itself, 6-phosphogluconate, and fructose 1,6-bisphosphate, suggested a reduced entry of glucose carbon into mitochondrial biosynthetic metabolism in mice fed CD together with metformin treatment (Fig. 8A). Mitochondria from liver of mice fed HFD apparently exhibited an increased dependency in reductive glutamine metabolism capable of replenishing the high levels of lipogenic acetyl-CoA/malonyl-CoA as an adaptive response to metformin (Fig. 8A). Metabolite-based clustering in liver obtained by the PLS-DA model confirmed a clear and significant separation of animals fed a CD alone and with metformin (Fig. 8B). Conversely, a small overlap occurred in animals fed HFD alone and with metformin (Fig. 8B). When the distinct metabolites between hepatic groups were selected with the criteria of VIP ≥1 in the PLS-DA model, the subset of metabolites majorly impacted were glycolytic intermediates and those metabolites related to the biosynthetic fates of glutamine metabolism (Fig. 8C). Unlike the scenario observed with the similar impact of metformin for WAT metabolites in CD- and HFD-fed mice, the segregation of the selected metabolites

obtained by using heatmap visualization confirmed a completely distinct segregation of metformin-impacted metabolites in liver of CD- and HFD-fed mice (Fig. 8D).

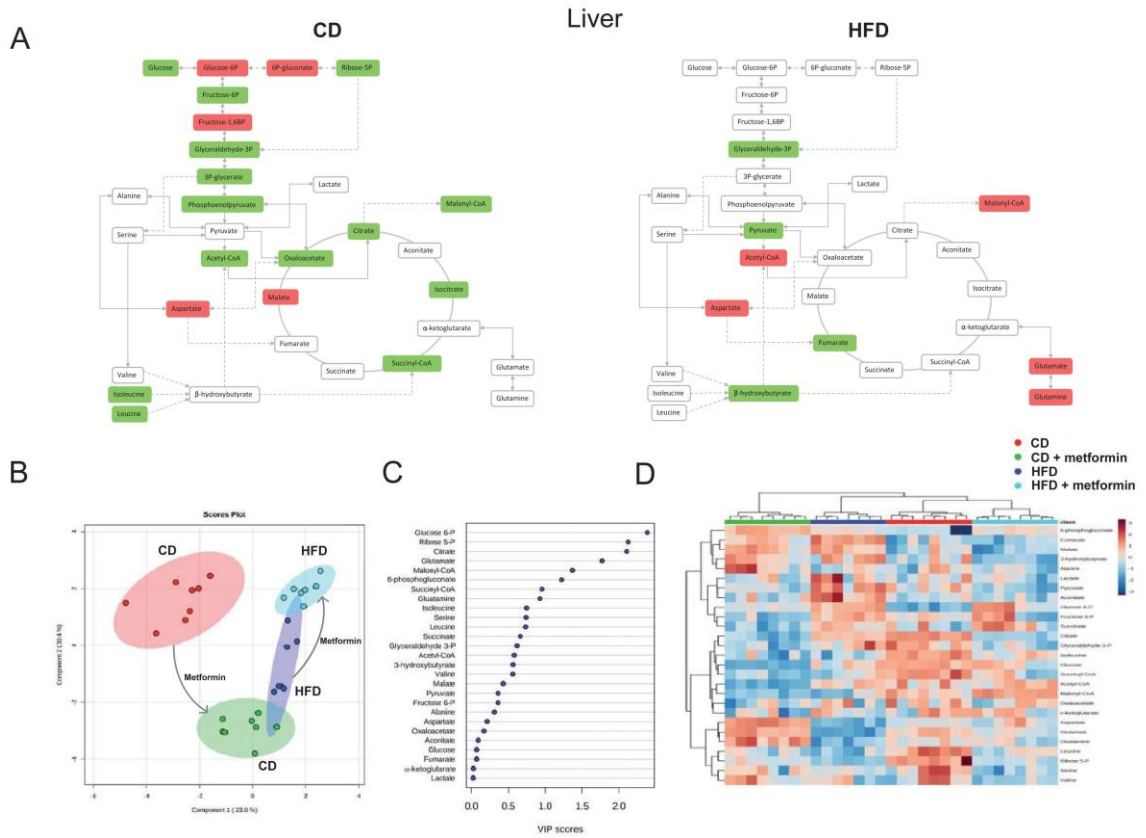

Figure 8. Dietary-induced changes and the effect of metformin on hepatic energy metabolites. Descriptive details are conserved as in Fig. 7.

4. Discussion

Our major finding is that metformin treatment might play a major role in preventing the metabolic disturbances caused by earlier exposure to HFD in both adipose and liver tissues. Metformin also enlarges the benefits of simple dietary restrain as a stand-alone intervention. Feeding *Ldlr*$^{-/-}$ mice with HFD promoted the appearance of classical metabolic derangements occurring after excessive intake of dietary lipids (i.e., weight gain, glucose intolerance, hyperlipidemia, hepatic steatosis and liver inflammation). When HFD-fed animals were subjected to diet reversal alone and also to metformin for a short duration, it became apparent that switching to regular feeding alone (which mimics patients guided towards a healthier overall pattern of eating) could not fully reverse the full spectrum of metabolic abnormalities provoked by the initial exposure to HFD. However, the addition of metformin treatment to diet reversal remarkably ameliorated the metabolic status associated with the previous HFD pattern.

Animals started to regain body weight 6 weeks after switching to normal diet but the trend towards lower weight gain remained unaltered in the presence of metformin, likely indicating that the effect of metformin in weight loss maintenance could prevent the long-term consequences of HFD-associated overweight. Similarly, feeding mice HFD induced an insulin resistance phenotype. Although the reduction of energy intake by switching the diet from HFD to CD significantly improved the hyperglycemia induced by HFD, it was noteworthy that metformin treatment elicited additional glycemic control. The significantly better-preserved glucose tolerance of mice on metformin was accompanied by an improved attenuation of the circulating levels of cholesterol and triglycerides, thus revealing its capacity to protect from the long-term effects of HFD-imposed

periods of metabolic hyperlipidemia. These effects are attributable to metformin [28] and our data suggest that can reverse an HFD-established obese and insulin-resistant phenotype.

Exposure to HFD causes chronic inflammation in the liver, a critical factor for the development of obesity-related glucose intolerance and insulin resistance [29]. Glucose intolerance and hepatic insulin resistance, in turn, can promote the development and progression of NAFLD [30, 31], thereby driving a harmful cycle of metabolic disturbances. This key mechanistic component of the lifelong risk for developing metabolic complications in response to energy overload appears to be the one most profoundly affected by metformin. Metformin treated mice exhibited a dramatically improved protection against HFD-induced hepatic steatosis, which was accompanied by a significant lowering of liver-infiltrating pro-inflammatory macrophages as well as lower levels of major proinflammatory cytokines. The ability of metformin to modulate the polarization or migration of these cells has been recently demonstrated in tumor-associated macrophages [32, 33]. Future studies should examine whether the ability of metformin to restore impaired glucose and hepatic lipid metabolism may have aided in the reduction of hepatic tissue inflammation by preventing either the recruitment or pro-inflammatory activation of macrophages (or both).

Liver and WAT from HFD-fed *Ldlr*$^{-/-}$ mice appear to have a significantly different metformin-induced response to the inability of HFD-damaged tissues to benefit from the expected response to diet reversal [34-37]. On the one hand, diet reversal failed to restore HFD-induced hepatic damage unless combined with metformin. Metformin decreased the flow of glucose- and glutamine-derived metabolic intermediates into the TCA cycle and appears to overcome the hepatic ability to store and metabolize carbohydrates, thereby better preventing HFD-induced hepatic damage when switching to normal diet occurs. This metformin effect has already been appreciated in proliferating cells, suppressing the mitochondrial-dependent biosynthetic activity and de novo lipogenesis [38,39]. Hence, our findings support the notion that elevated mitochondrial TCA function and increased flow through anabolic pathways plays a crucial role in the pathology of fatty liver and insulin resistance induced by an obesogenic diet [40]. This is in accordance with recent data indicating that metformin might alleviate oxidative stress and inflammation [41]. Mitochondrial adaptations might therefore be explored as mechanisms of HFD-induced hepatic complications. On the other hand, it appears that adipocyte hypertrophy in WAT of *Ldlr*$^{-/-}$ mice, a hallmark of WAT enlargement in obesity, is clearly corrected upon diet reversal. The frequency distribution of adipocyte sizes across the WAT depot suggests an apparently limited capacity of metformin to remodel WAT tissue architecture, likely indicating a specific protection from hepatic insulin resistance rather than a protection from systemic insulin resistance. We now know that, in contrast to the usage of glucose and glutamine for mitochondrial generation of lipogenic pools of acetyl-CoA in proliferating cells, differentiated adipocytes exhibit an increased catabolic flux of BCCAs such as leucine and isoleucine that account for a significant amount of lipogenic acetyl-CoA pools [42, 43]. In this regard, it is noteworthy that the capacity of metformin to target the contribution of BCAAs to WAT metabolism, likely by up-regulating the BCAA degradation pathway [44], might contribute to the additional beneficial effects elicited by metformin beyond those of diet reversal alone by altering the functional integrity of this tissue. Future research should include the effect of metformin and other drugs apparently converging in mechanisms involving BCAAs.

The health-promoting effects of metformin are largely viewed as the consequence of its ability to simultaneously target the core nutrient-sensing networks insulin/IGF-1, at the non-cell autonomous level, and AMPK/mTOR, at the cell-autonomous level [7, 24, 45, 46]. Alternatively, they might reflect downstream consequences of a primary action on a single master mechanism that has not yet been identified. Along this line, very recent reports are providing evidence for epigenetic targets potentially contributing to the protective effects of metformin against several diseases [47-49]. Because the pathogenesis of HFD- induced metabolic disturbances causally involves the long-term persistence of epigenetic alterations [34-36, 50-52], there is an urgent need to elucidate the mechanism of metformin to mediate global epigenetic programming in multiple host tissues [48, 53]. We have found robust patterns indicating the potential of metformin to serve as a model compound for preventing HFD-driven progression of metabolic complications despite attainment of changes in

dietary habits. The clinical combination of metformin-based pharmacotherapy with dietary modification might herald the development of much-needed therapeutic and preventive strategies against metabolic consequences of excessive dietary fat intake.

Acknowledgments:

Current work in our laboratories is supported by grants from the Plan Nacional de I+D+I, Spain, Instituto de Salud Carlos III (Grant PI15/00285 co-founded by the European Regional Development Fund [FEDER]) to JJ, and the Ministerio de Ciencia e Innovación (Grant SAF2012-38914) to JM. We also acknowledge the support by the Agència de Gestió d'Ajuts Universitaris i de Recerca (AGAUR) (Grants 2014 SGR1227 and 2014 SGR229), and the Fundació La Marató de TV3. The funders had no role in study design, data collection and analysis, decision to publish, or preparation of the manuscript.

Author Contributions:

J.J. and J.A.M. conceived and designed the study. M.R-B., A.G-H., S.F-A., A.H-A. and N.C performed experiments and molecular assays. A.G-H., E.C. and F.L-M. performed immunohistochemical assays. M.R-B. and S.F-A. performed metabolomics assays. J.C. and J.A.M. contributed important reagents. M.R-B., J.C. and J.J. performed data interpretation. J.C., J.A.M. and J.J. prepared the manuscript, which was revised and finally approved by all authors.

Conflicts of Interest:

The authors declare no conflict of interest

References

1. Hernández-Aguilera, A.; Fernández-Arroyo, S.; Cuyàs, E.; Luciano-Mateo, F.; Cabre, N.; Camps, J.; et al. Epigenetics and nutrition-related epidemics of metabolic diseases: Current perspectives and challenges. *Food Chem Toxicol*. **2016**, *96*, 191-204, doi: 10.1016/j.fct.2016.08.006. PMID: 27503834.
2. Hardie, D.G.; Schaffer, B.E.; Brunet, A. AMPK: An Energy-Sensing Pathway with Multiple Inputs and Outputs. *Trends Cell Biol*. **2016**, *26*, 190-201, doi: 10.1016/j.tcb.2015.10.013. PMID: 26616193.
3. Massucci, F.A.; Wheeler, J.; Beltrán-Debón, R.; Joven, J.; Sales-Pardo, M.; Guimerà, R. Inferring propagation paths for sparsely observed perturbations on complex networks. *Sci Adv*. **2016**, *2*, e1501638, PMID: 27819038.
4. Mattison, J.A.; Roth, G.S.; Beasley, T.M.; Tilmont, E.M.; Handy, A.M.; Herbert, R.L.; et al. Impact of caloric restriction on health and survival in rhesus monkeys from the NIA study. *Nature*. **2012**, *489*, 318-321, doi: 10.1038/nature11432. PMID: 22932268.
5. Roth, G.S.; Ingram, D.K. Manipulation of health span and function by dietary caloric restriction mimetics. *Ann N Y Acad Sci.* **2016**, *1363*, 5-10, doi: 10.1111/nyas.12834. PMID: 26214681.
6. Smith, B.K.; Marcinko, K.; Desjardins, E.M.; Lally, J.S.; Ford, R.J.; Steinberg, G.R. Treatment of nonalcoholic fatty liver disease: role of AMPK. *Am J Physiol Endocrinol Metab*. **2016**, *311,* E730-E740, doi: 10.1152/ajpendo. 00225.2016. PMID: 27577854.
7. Barzilai, N.; Crandall, J.P.; Kritchevsky, S.B.; Espeland, M.A. Metformin as a Tool to Target Aging. *Cell Metab*. **2016**, *23*, 1060-1065, doi: 10.1016/j.cmet.2016.05.011. PMID: 27304507.
8. Menendez, J.A.; Joven, J. One-carbon metabolism: an aging-cancer crossroad for the gerosuppressant metformin. *Aging (Albany NY)*. **2012**, *4*, 894-898, PMID: 23525940.
9. Corominas-Faja, B.; Quirantes-Piné, R.; Oliveras-Ferraros, C.; Vazquez-Martin, A.; Cufí, S.; Martin-Castillo, B.; et al. Metabolomic fingerprint reveals that metformin impairs one-carbon metabolism in a manner similar to the antifolate class of chemotherapy drugs. *Aging (Albany NY)*. **2012**, *4*, 480-498, PMID: 22837425

10. Viollet, B.; Guigas, B.; Sanz Garcia, N.; Leclerc, J.; Foretz, M.; Andreelli, F. Cellular and molecular mechanisms of metformin: an overview. *Clin Sci (Lond)*. **2012**, *122*, 253-270, doi: 10.1042/CS20110386.
11. Foretz, M.; Viollet, B. Metformin takes a new route to clinical efficacy. *Nat Rev Endocrinol*. **2015**, *11*, 390-392, doi: 10.1038/nrendo.2015.85. PMID: 26032104.
12. Pernicova, I.; Korbonits, M. Metformin--mode of action and clinical implications for diabetes and cancer. *Nat Rev Endocrinol*. **2014**, *10*, 143-156, doi: 10.1038/nrendo.2013.256.
13. Saisho, Y. Metformin and Inflammation: Its Potential Beyond Glucose-lowering Effect. *Endocr Metab Immune Disord Drug Targets*. **2015**, *15*, 196-205, PMID: 25772174.
14. Song, Y.M.; Lee, Y.H.; Kim, J.W.; Ham, D.S.; Kang, E.S.; Cha, B.S.; Lee, H.C.; Lee, B.W. Metformin alleviates hepatosteatosis by restoring SIRT1-mediated autophagy induction via an AMP-activated protein kinase-independent pathway. *Autophagy*. **2015**, *11*, 46-59, doi: 10.4161/15548627. PMID: 25484077.
15. Jadhav, K.S.; Dungan, C.M.; Williamson, D.L. Metformin limits ceramide-induced senescence in C2C12 myoblasts. *Mech Ageing Dev*. **2013**, *134*, 548-559, doi: 10.1016/j.mad.2013.11.002. PMID: 24269881.
16. Domecq, J.P.; Prutsky, G.; Leppin, A.; Sonbol, M.B.; Altayar, O.; Undavalli, C.; et al. Clinical review: Drugs commonly associated with weight change: a systematic review and meta-analysis. *J Clin Endocrinol Metab.* **2015**, *100*, 363-70, doi: 10.1210/jc.2014-3421.
17. Foretz, M.; Hébrard, S.; Leclerc, J.; Zarrinpashneh, E.; Soty, M.; Mithieux, G.; et al. Metformin inhibits hepatic gluconeogenesis in mice independently of the LKB1/AMPK pathway via a decrease in hepatic energy state. *J Clin Invest.* **2010**; *120*, 2355-2369, doi: 10.1172/JCI40671. PMID: 20577053.
18. Linden, M.A.; Lopez, K.T.; Fletcher; J.A.; Morris, E.M.; Meers, G.M.; Siddique, S.; et al. Combining metformin therapy with caloric restriction for the management of type 2 diabetes and nonalcoholic fatty liver disease in obese rats. *Appl Physiol Nutr Metab*. **2015**, *40*, 1038-47, doi: 10.1139/apnm-2015-0236. PMID: 26394261.
19. Woo, S.L.; Xu, H.; Li, H.; Zhao, Y.; Hu, X.; Zhao, J.; et al. Metformin ameliorates hepatic steatosis and inflammation without altering adipose phenotype in diet-induced obesity. *PLoS One*. **2014**, *9*, e91111, doi:10.1371/ journal. pone. 0091111. PMID: 24638078.
20. Joven, J.; Rull, A.; Ferré, N.; Escolà-Gil, J.C.; Marsillach, J.; Coll, B.; et al. The results in rodent models of atherosclerosis are not interchangeable: the influence of diet and strain. *Atherosclerosis*. **2007**, *195*, e85-92, PMID: 17651742.
21. Riera-Borrull, M.; Rodríguez-Gallego, E.; Hernández-Aguilera, A.; Luciano, F.; Ras, R.; Cuyàs, E.; et al. Exploring the Process of Energy Generation in Pathophysiology by Targeted Metabolomics: Performance of a Simple and Quantitative Method. *J Am Soc Mass Spectrom.* **2016**; *27*, 168-77, doi: 10.1007/s13361-015-1262-3. PMID: 26383735.
22. Cufí, S.; Corominas-Faja, B.; Lopez-Bonet, E.; Bonavia, R.; Pernas, S.; López, I.Á.; et al. Dietary restriction-resistant human tumors harboring the PIK3CA-activating mutation H1047R are sensitive to metformin. *Oncotarget*. **2013**, *4*, 1484-1495, PMID: 23986086.
23. García-Heredia, A.; Riera-Borrull, M.; Fort-Gallifa, I.; Luciano-Mateo, F.; Cabré, N.; Hernández-Aguilera, A.; Joven, J.; Camps, J. Metformin administration induces hepatotoxic effects in paraoxonase-1-deficient mice. *Chem Biol Interact.* **2016**, *249*, 56-63, doi: 10.1016/j.cbi.2016.03.004. PMID: 26945512.
24. Anisimov, V.N. Metformin for Prevention and Treatment of Colon Cancer: A Reappraisal of Experimental and Clinical Data. *Curr Drug Targets.* **2016**, *17*, 439-46, PMID: 25738299.
25. García-Heredia, A.; Kensicki, E.; Mohney, R.P.; Rull, A.; Triguero, I.; Marsillach, J.; et al. Paraoxonase-1 deficiency is associated with severe liver steatosis in mice fed a high-fat high-cholesterol diet: a metabolomic approach. *J Proteome Res.* **2013**, *12*, 1946-1955, doi: 10.1021/pr400050u. PMID: 23448543.
26. Joven, J.; Espinel, E.; Rull, A.; Aragonès, G.; Rodríguez-Gallego, E.; Camps, J.; et al. Plant-derived polyphenols regulate expression of miRNA paralogs miR-103/107 and miR-122 and prevent diet-induced fatty liver disease in hyperlipidemic mice. *Biochim Biophys Acta.* **2012**; *1820*, 894-899, doi: 10.1016/j.bbagen.2012.03.020. PMID: 22503922.
27. Xia, J.; Sinelnikov, I.V.; Han, B.; Wishart, D.S. MetaboAnalyst 3.0--making metabolomics more meaningful. *Nucleic Acids Res.* **2015**, *43*, W251-257, doi: 10.1093/nar/gkv380.
28. Menendez, J.A.; Martin-Castillo, B.; Joven, J. Metformin and cancer: Quo vadis et cui bono? *Oncotarget*. **2016**, doi: 10.18632/oncotarget.10262. PMID: 27356748.
29. Shoelson, S.E.; Herrero, L.; Naaz, A. Obesity, inflammation, and insulin resistance. *Gastroenterology*. **2007**, *132*, 2169-2180, doi: 10.1053/j.gastro.2007.03.059 PMID: 17498510.

30. Ota, T.; Takamura, T.; Kurita, S.; Matsuzawa, N.; Kita, Y.; Uno, M.; et al. Insulin resistance accelerates a dietary rat model of nonalcoholic steatohepatitis. *Gastroenterology*. **2007**, *132*, 282-293, PMID: 17241878.
31. Pfluger, P.T.; Herranz, D.; Velasco-Miguel, S.; Serrano, M.; Tschöp, M.H. Sirt1 protects against high-fat diet-induced metabolic damage. *Proc Natl Acad Sci U S A.* **2008**, *105*, 9793-9798, doi: 10.1073/pnas.0802917105. PMID: 18599449.
32. Ding, L.; Liang, G.; Yao, Z.; Zhang, J.; Liu, R.; Chen, H.; et al. Metformin prevents cancer metastasis by inhibiting M2-like polarization of tumor associated macrophages. *Oncotarget*. **2015**, *6*, 36441-36455, doi: 10.18632/oncotarget.5541. PMID: 26497364.
33. Incio, J.; Suboj, P.; Chin, S.M.; Vardam-Kaur, T.; Liu, H.; Hato, T.; Babykutty, S.; et al. Metformin Reduces Desmoplasia in Pancreatic Cancer by Reprogramming Stellate Cells and Tumor-Associated Macrophages. *PLoS One*. **2015**, *10*, e0141392, doi: 10.1371/journal.pone.0141392. PMID: 26641266.
34. Tonna, S.; El-Osta, A.; Cooper, M.E.; Tikellis, C. Metabolic memory and diabetic nephropathy: potential role for epigenetic mechanisms. *Nat Rev Nephrol*. **2010**, *6*, 332-341, doi: 10.1038/nrneph.2010.55. PMID: 20421885.
35. Villeneuve, L.M.; Natarajan, R. The role of epigenetics in the pathology of diabetic complications. *Am J Physiol Renal Physiol*. **2010**, *299*, F14-25, doi: 10.1152/ajprenal.00200.2010. PMID: 20462972.
36. Kumar, S.; Pamulapati, H.; Tikoo, K. Fatty acid induced metabolic memory involves alterations in renal histone H3K36me2 and H3K27me3. *Mol Cell Endocrinol*. **2016**, *422*, 233-242, doi: 10.1016/j.mce.2015.12.019. PMID: 26747726.
37. Tikoo, K.; Sharma, E.; Amara, V.R.; Pamulapati, H.; Dhawale, V.S. Metformin improves metabolic memory in high fat diet (HFD)-induced renal dysfunction. *J Biol Chem.* **2016**, pii: jbc.C116.732990, doi: 10.1074/jbc.C116.732990. PMID: 27551045.
38. Griss, T.; Vincent, E.E.; Egnatchik, R.; Chen, J.; Ma, E.H.; Faubert, B.; et al. Metformin Antagonizes Cancer Cell Proliferation by Suppressing Mitochondrial-Dependent Biosynthesis. *PLoS Biol.* **2015**, 13:e1002309, doi: 10.1371/journal.pbio.1002309. PMID: 26625127.
39. Cuyàs, E.; Fernández-Arroyo, S.; Alarcón, T.; Lupu, R.; Joven, J.; Menendez, J.A. Germline BRCA1 mutation reprograms breast epithelial cell metabolism towards mitochondrial-dependent biosynthesis: evidence for metformin-based "starvation" strategies in BRCA1 carriers. *Oncotarget*. **2016**, *7*, 52974-52992, doi: 10.18632/oncotarget.9732. PMID: 27259235.
40. Satapati, S.; Sunny, N.E.; Kucejova, B.; Fu, X.; He, T.T.; Méndez-Lucas, A.; Shelton, J.M.; Perales, J.C.; Browning, J.D.; Burgess, S.C. Elevated TCA cycle function in the pathology of diet-induced hepatic insulin resistance and fatty liver. *J Lipid Res*. **2012**, *53*, 1080-1092, doi: 10.1194/jlr.M023382. PMID: 22493093.
41. Satapati, S.; Kucejova, B.; Duarte, J.A.; Fletcher, J.A.; Reynolds, L.; Sunny, N.E.; et al. Mitochondrial metabolism mediates oxidative stress and inflammation in fatty liver. *J Clin Invest*. **2015**, *125*, 4447-4462, doi: 10.1172/JCI82204. PMID: 26571396.
42. Herman, M.A.; She, P.; Peroni, O.D.; Lynch, C.J.; Kahn, B.B. Adipose tissue branched chain amino acid (BCAA) metabolism modulates circulating BCAA levels. *J Biol Chem*. **2010**, *285*, 11348-11356, doi: 10.1074/jbc.M109.075184. PMID: 20093359.
43. Green, C.R.; Wallace, M.; Divakaruni, A.S.; Phillips, S.A.; Murphy, A.N.; Ciaraldi, T.P.; Metallo, C.M. Branched-chain amino acid catabolism fuels adipocyte differentiation and lipogenesis. *Nat Chem Biol.* **2016**, *12*, 15-21, doi: 10.1038/nchembio.1961. PMID: 26571352.
44. De Haes, W.; Frooninckx, L.; Van Assche, R.; Smolders, A.; Depuydt, G.; Billen, J.; et al. Metformin promotes lifespan through mitohormesis via the peroxiredoxin PRDX-2. *Proc Natl Acad Sci U S A.* **2014**, *111*, E2501-2509, doi: 10.1073/pnas.1321776111. PMID: 24889636.
45. López-Otín, C.; Galluzzi, L.; Freije, J.M.; Madeo, F.; Kroemer, G. Metabolic Control of Longevity. *Cell*. **2016**, *166*, 802-821, doi: 10.1016/j.cell.2016.07.031. PMID: 27518560.
46. Anisimov, V.N. Metformin: do we finally have an anti-aging drug? *Cell Cycle*. **2013**, *12*, 3483-3489, PMID: 24189526.
47. de Kreutzenberg, S.V.; Ceolotto, G.; Cattelan, A.; Pagnin, E.; Mazzucato, M.; Garagnani, P.; et al. Metformin improves putative longevity effectors in peripheral mononuclear cells from subjects with prediabetes. A randomized controlled trial. *Nutr Metab Cardiovasc Dis.* **2015**, *25*, 686-693, doi: 10.1016/j.numecd.2015.03.007. PMID: 25921843.

48. Cuyàs, E.; Fernández-Arroyo, S.; Joven, J.; Menendez, J.A. Metformin targets histone acetylation in cancer-prone epithelial cells. *Cell Cycle*. **2016**, *15*, 3355-3361, doi: 10.1080/15384101.2016.1249547. PMID: 27792453.
49. Niu, N.; Liu, T.; Cairns, J.; Ly, R.C.; Tan, X.; Deng, M.; et al. Metformin pharmacogenomics: a genome-wide association study to identify genetic and epigenetic biomarkers involved in metformin anticancer response using human lymphoblastoid cell lines. *Hum Mol Genet.* **2016**, pii: ddw301, doi: 10.1093/hmg/ddw301. PMID: 27616566.
50. Zhong, T.; Men, Y.; Lu, L.; Geng, T.; Zhou, J.; Mitsuhashi, A.; et al. Metformin alters DNA methylation genome-wide via the H19/SAHH axis. *Oncogene*. **2016**, *36*, 2345-2354, doi: 10.1038/onc.2016.391. PMID: 27775072.
51. Reddy, M.A.; Tak Park, J.; Natarajan, R. Epigenetic modifications in the pathogenesis of diabetic nephropathy. *Semin Nephrol*. **2013**, *33*, 341-353, doi: 10.1016/j.semnephrol.2013.05.006. PMID: 24011576.
52. Reddy, M.A.; Zhang, E.; Natarajan, R. Epigenetic mechanisms in diabetic complications and metabolic memory. *Diabetologia*. **2015**, *58*, 443-455, doi: 10.1007/s00125-014-3462-y. PMID: 25481708.
53. Krautkramer, K.A.; Kreznar, J.H.; Romano, K.A.; Viva,s E.I.; Barrett-Wilt, G.A.; Rabaglia, M.E.; et al. Diet-Microbiota Interactions Mediate Global Epigenetic Programming in Multiple Host Tissues. *Mol Cell.* **2016**, *64*, 982-992, doi: 10.1016/j.molcel.2016.10.025. PMID: 27889451.

Palmitate conditions macrophages for enhanced responses towards pro-inflammatory stimuli via JNK activation.

Running title: **Palmitate primes macrophage pro-inflammatory responses**

Marta Riera-Borrull [1,2,*], Víctor D. Cuevas [1,*], Bárbara Alonso [1], Miguel A. Vega [1], Jorge Joven [2], Elena Izquierdo [1,] and Ángel L. Corbí [1,**]**

[1] Centro de Investigaciones Biológicas, CSIC, Madrid, Spain.

[2] Unitat de Recerca Biomèdica, Hospital Universitari Sant Joan, Institut d'Investigació Sanitària Pere Virgili, Universitat Rovira i Virgili, Reus, Spain

* MRB and VDC contributed equally to this work, and the order of authors is arbitrary

** ALC and EI contributed equally to this work, and the order of authors is arbitrary

Corresponding author: Dr. Ángel L. Corbí (acorbi@cib.csic.es). Centro de Investigaciones Biológicas, CSIC. Ramiro de Maeztu, 9. 28040 Madrid, SPAIN. Phone: 34-918373112; FAX: 34-915627518.

ABSTRACT

Obesity is associated with low-grade inflammation and elevated levels of circulating saturated fatty acids (SFA), which trigger inflammatory responses by engaging pattern recognition receptors in macrophages. Since tissue homeostasis is maintained through an adequate balance of pro- and anti-inflammatory macrophages, we assessed the transcriptional and functional profile of M-CSF-dependent monocyte-derived human macrophages (M-MØ) exposed to concentrations of SFA found in obese individuals. We report that palmitate (C16:0, 200 μM) lowers the expression of transcription factors that positively regulate IL-10 expression (MAFB, AhR), modulates significantly the macrophage gene signature, and promotes a pro-inflammatory state whose acquisition requires JNK activation. Unlike LPS, palmitate exposure does not activate STAT1, and its transcriptional effects can be distinguished from those triggered by LPS as both agents oppositely regulate the expression of CCL19 and *TRIB3*. Besides, palmitate conditions macrophages for exacerbated pro-inflammatory responses (lower IL-10 and CCL2, higher TNFα, IL-6 and IL1β) towards pathogenic stimuli, a process also mediated by JNK activation. All these effects of palmitate are fatty acid-specific since oleate (C18:1, 200 μM) does not modify the macrophage transcriptional and functional profiles. Therefore, pathologic palmitate concentrations promote the acquisition of a specific polarization state in human macrophages and condition macrophages for enhanced responses towards inflammatory stimuli, what provides a further insight on the macrophage contribution to obesity-associated inflammation.

INTRODUCTION

Obesity has become a major worldwide health problem due to its association with the development of metabolic diseases (type 2 diabetes, metabolic syndrome, non-alcoholic fatty liver disease), and its correlation with several types of cancer [1, 2]. Numerous studies have demonstrated that inflammation underlies the link between obesity and metabolic diseases. So, an excessive nutrient intake results in the accumulation of saturated fatty acids (SFA, like palmitate), which correlates with an increase in pro-inflammatory cytokines [3]. Moreover, adipose and liver tissues from obese individuals exhibit infiltration by immune cells, primarily macrophages, an event proposed as a primary trigger for obesity-induced inflammation [4]. Chronic obesity produces a low-grade activation of the innate immune system that affects homeostasis over time [5]. A key role for macrophages in the pathogenesis of metabolic disorders has been demonstrated in mouse models of obesity, where defective CCR2-dependent monocyte/macrophage recruitment towards adipose tissue protects from obesity-induced inflammation and insulin resistance [6]. Likewise, depletion of CD11c-positive cells in mice reduces adipose tissue inflammation [7], and myeloid cell-specific deletion of IKKβ or JNK1 also protects mice from high-fat diet induced insulin resistance [8, 9]. *In vitro* and *in vivo* studies have suggested that SFA activate macrophage inflammatory signaling pathways leading to adipose tissue inflammation and systemic insulin resistance in a TLR4-dependent manner [10]. However, recent reports suggest that the link between SFA and insulin resistance might not be a direct consequence of a canonical TLR4 activation [11-13] because MyD88 KO mice display a more severe metabolic disease in response to a high fat diet [12] and TLR4 deficiency exacerbates diet-induced obesity,

steatosis, and insulin resistance on the C57BL/10 genetic background [13]. Palmitate may also induce TLR-independent actions through epigenetic modifications [14, 15]. Chronic palmitate exposure reprograms gene expression of human pancreatic islets by altering DNA methylation level [14]. Likewise, palmitate treatment increases DNA methylation levels at PPARγ1 promoter in mouse macrophages [15]. Therefore, whereas the role of macrophages in obesity-induced diseases in mice is well established, the triggers for the inflammatory activation of macrophages by SFA and the underlying molecular mechanisms have not been completely elucidated.

Inflamed tissues contain heterogeneous populations of resident and newly recruited macrophages that display a continuum of functional (activation/polarization) states whose appropriate balance allows elimination of tissue injuries and recovery and maintenance of tissue homeostasis. The huge macrophage functional and phenotypic heterogeneity derives from their ability to integrate information from the surrounding environment [16]. Our group and others have functionally and transcriptionally characterized human monocyte-derived macrophages generated in the presence of either GM-CSF (GM-MØ) or M-CSF (M-MØ), and shown that they resemble macrophages found in vivo under inflammatory conditions (GM-MØ) or in homeostatic/anti-inflammatory settings (M-MØ) [17-20]. Accordingly, TLR-mediated activation of GM-MØ results in the production of large levels of pro-inflammatory cytokines, whereas M-MØ activation primarily leads to release of the anti-inflammatory cytokine IL-10 [20]. Moreover, LPS activation of GM-MØ and M-MØ has allowed the identification of novel gene sets whose expression is regulated by LPS in a macrophage subtype-specific manner (*Cuevas et al.*,

unpublished). Since palmitate exerts its activation, at least partly, via TLR4, the analysis of the transcriptional and functional responses of GM-MØ and M-MØ to palmitate should help clarify the mechanisms behind macrophage activation by SFA. Besides, since identified mouse macrophage polarization-specific genes cannot be extrapolated to the case of human macrophages [21, 22], it is mandatory to identify genes whose expression correlates with SFA activation in human macrophages as a primary step to determine the polarization state of adipose tissue macrophages under homeostatic and pathological conditions. We have now analyzed the effects of palmitate on human macrophages at the transcriptomic and functional levels, and found that palmitate triggers a JNK-dependent pro-inflammatory shift in human macrophages and primes macrophages for exacerbated pro-inflammatory response towards other pathogenic stimuli. Our results illustrate the existence of a palmitate-specific polarization state in human macrophages and demonstrate that palmitate, but not oleate, primes macrophages for exacerbated responses towards inflammatory stimuli.

MATERIALS AND METHODS

Generation of human monocyte-derived macrophages. Human Peripheral Blood Mononuclear Cells (PBMC) were isolated from buffy coats from normal donors over Lymphoprep (Nycomed Pharma, Oslo, Norway) gradient according to standard procedures. Monocytes were purified from PBMC by magnetic cell sorting using anti-CD14 microbeads (Miltenyi Biotec, Bergisch Gladbach, Germany) (>95% CD14+ cells). Monocytes (0.5×10^6 cells/ml, >95% CD14+ cells) were cultured in RPMI 1640 supplemented with 10% fetal bovine serum (FBS) for 7 d in the presence of 1000 U/ml GM-CSF or 10 ng/ml M-CSF (ImmunoTools, Friesoythe, Germany) to generate GM-CSF-polarized macrophages (hereafter termed GM-MØ) or M-CSF-polarized macrophages (hereafter termed M-MØ), respectively [23]. Cytokines were added every two days. Where indicated, macrophages were treated with 10 ng/ml E. coli 055:B5 LPS (Sigma-Aldrich, MO, USA), palmitate (C16:0, 200 µM) or BSA for the indicated periods of time. Cells were cultured in 21% O_2 and 5% CO_2. For intracellular signaling inhibition, macrophages were exposed to JNK inhibitor SP600125 (30 µM) or the GSK3β inhibitor LiCl (30 mM) during 1 hour before treatment with BSA or palmitate (C16:0).

Fatty acid preparation. Sodium palmitate (P9767, Sigma-Aldrich, Steinheim, Germany) and sodium oleate (O7501, Sigma-Aldrich) were prepared by diluting a 200 mM stock solution in 70% ethanol into 10% fatty acid-free, low endotoxin BSA (A-8806, Sigma-Aldrich; adjusted to pH 7.4) to obtain a 5 mM palmitate-BSA stock solution that was filtered using a 0.22 µm low protein binding filter (Millipore, Billerica, MA, USA).

Palmitate and oleate were added at 200 µM, and BSA/ethanol was used in control treatments.

Fatty acid uptake. Macrophage fatty acid uptake was evaluated using an Oil Red O staining protocol [24]. Briefly, macrophages were fixed with 10% phosphate buffered formalin for 10 min, rinsed with PBS once and then rinsed with 60% isopropanol, after that, macrophages were stained with Oil Red O (Sigma) at 37ºC for 1 minute in darkness. Finally, macrophages were destained with 60% isopropanol, washed with PBS for three times, and samples counterstained with hematoxylin for 5 minutes before examination by light microscopy.

Quantitative real-time RT-PCR. Total RNA was extracted using the NucleoSpin RNA/Protein kit (Macherey-Nagel, Düren, Germany), retrotranscribed, and amplified using the Universal Human Probe library (Roche Diagnostics, Mannheim, Germany). Oligonucleotides for selected genes were designed according to the Roche software for quantitative real-time PCR (Roche Diagnostics, Mannheim, Germany). Assays were made in triplicate and results normalized according to the expression levels of TBP (TATA box-binding protein) mRNA. Results were expressed using the ΔΔCT method for quantification. Analyzed genes included the "Pro-inflammatory gene set" and the "Anti-inflammatory gene set" that have been previously defined [18, 25]. Where indicated, microfluidic gene cards were custom-made (Roche Diagnostics) and designed to analyze the expression of a set of genes whose expression is variably modulated by LPS (10 ng/ml E. coli 055:B5, 4h) in either GM-MØ and/or M-MØ [26] (*Delgado-Cuevas et al.*,

unpublished). Specifically, the gene cards included 10 genes upregulated by LPS in both GM-MØ and M-MØ, 9 genes upregulated by LPS exclusively in GM-MØ, 3 genes downregulated by LPS exclusively in GM-MØ, 28 genes upregulated by LPS exclusively in M-MØ, 20 genes downregulated by LPS exclusively in M-MØ, 7 genes upregulated by LPS in GM-MØ but downregulated in M-MØ, and 9 genes downregulated by LPS in GM-MØ but upregulated in M-MØ. Assays were made in triplicate on two independent samples of each type, and the results normalized according to the mean of the expression level of endogenous reference genes *HPRT1*, *TBP* and *RPLP0*. In all cases (quantitative real-time PCR or gene cards), the results were expressed using the ΔΔCT method for quantitation. Non-supervised hierarchical clustering was done on the mean expression level of each gene in BSA- or palmitate-treated LPS-activated M-MØ, and using Genesis software (http://genome.tugraz.at/genesisclient/genesisclient_description.shtml) [27].

ELISA. Macrophage supernatants were assayed for the presence of cytokines using commercial ELISA kits for TNFα, CCL2 (BD Biosciences, CA, USA), IL-10, IL-6, IL-1β (Biolegend, CA, USA) and CCL19 (Sigma-Aldrich) according to the protocols supplied by the manufacturers.

Western blot. Cell lysates were obtained in 10 mM Tris-HCl (pH 8), 150 mM NaCl, 1% Nonidet P-40 lysis buffer containing 2 mM Pefabloc, 2 mg/ml aprotinin/ antipain/leupeptin/pepstatin, 10 mM NaF, and 1 mM Na3VO4. 10-15 µg of cell lysate was subjected to SDS-PAGE and transferred onto an Immobilon polyvinylidene difluoride membrane (Millipore). Protein detection was carried out using antibodies

against MAFB (sc-10022, Santa Cruz, CA, USA), AHR (sc-8087, Santa Cruz) and CEBP/β (sc-150, Santa Cruz), phospho-ERK1/2, phospho-JNK, phospho-p38, phospho-p65, phospho-IKK, total IKK, ERK 1/2 and IKBα (all from Cell Signaling), total and phosphorylated STAT1 and STAT 3 (BD Bioscences), phospho-IRF3 (Cell Signaling) and total IRF3 (Santa Cruz). Protein loading was normalized using a monoclonal antibody against GAPDH (Santa Cruz) or an antibody against human Vinculin (Sigma-Aldrich).

Phosphoarrays. Intracellular signaling in response to palmitate was assessed with lysates from macrophages exposed to palmitate for 4 hours and using the Human Phospho-Kinase Antibody Array (R&D Systems), which detects the relative phosphorylation levels of 46 intracellular serine/threonine/tyrosine kinases, and following the manufacturer recommendations.

Statistical analysis. Statistical analysis was performed using Student's t-test, and $p<0.05$ was considered significant (*$p<0.05$; **$p<0.01$; ***$p<0.001$).

RESULTS

Palmitate modifies the functional, transcriptomic and protein profile of human anti-inflammatory M-MØ. Numerous evidences indicate that macrophage dysfunction in states of lipid excess contribute to the development of obesity-related diseases [6-9]. To determine to what extent fatty acid exposure modifies the functional properties of human macrophages, GM-MØ and M-MØ were exposed to palmitate (200 μM, 24 h) and the production of pro- and anti-inflammatory cytokines was assessed. Palmitate was efficiently captured by both macrophage subtypes (Supplementary Figure 1A) and significantly increased the production of TNFα and IL-1β, while diminished the basal production of CCL2, in M-MØ (Figure 1A). Palmitate stimulation also modified macrophage polarization at the transcriptomic level, as it drastically down-regulated all the M-MØ-specific genes assayed ("Anti-inflammatory gene set", *HTR2B, HTR7, FOLR2, IL10, IGF1, CCL2, FABP4, MAFB*) [18, 25] (Figure 1B), while increased the mRNA expression of GM-MØ-associated *INHBA, EGLN3, PPARG1, TNF*, *IL6* and *IDO* genes ("Pro-inflammatory gene set") (Figure 1B). Kinetics analysis revealed that the expression of prototypical genes within "Anti-inflammatory gene set" (*CCL2, IL10, HTR2B, HTR7*) was already decreased 4h after palmitate treatment (Figure 1C) whereas upregulation of genes of the "Pro-inflammatory gene set" (*INHBA, EGLN3, TNF, IDO, IL6*) was only seen at later time points after palmitate exposure (Figure 1C). In the case of GM-MØ, palmitate significantly enhanced the basal production of TNFα, IL-6 and IL-1β (Figure 1A), enhanced the mRNA levels of *TNF*, *IL1B, IL6* and *IDO*, and reduced the expression of various GM-MØ- and M-MØ-specific genes (Supplementary Figure 1B). The ability of palmitate to down-regulate M-MØ-specific gene expression prompted us to

determine its effects on the expression of transcription factors that control macrophage polarization (AhR, MAFB, C/EBPβ) [18, 25, 26, 28, 29]. M-MØ exhibited considerably higher levels of MAFB and AhR than GM-MØ, whereas the latter exhibit a higher content of C/EBPβ (Figure 1D). Palmitate treatment significantly reduced MAFB and AhR protein levels, and increased C/EBPβ, in M-MØ (Figure 1D), and these changes in transcription factor levels were evident 4-10 hours after palmitate treatment (Figure 1E). Therefore, palmitate promotes M-MØ to acquire a GM-MØ-like pro-inflammatory signature at the transcriptional and cytokine levels, and also induces M-MØ to gain a transcription factor profile that resembles that of GM-MØ. The palmitate-induced downregulation of MAFB protein expression is especially significant given the involvement of MAFB in the acquisition of an anti-inflammatory profile by human macrophages [26].

Palmitate and LPS induce distinct transcriptional profiles in human macrophages. Innate immune cells sense palmitate as a danger signal via TLR4 [30, 31] and additional receptors [30, 32-34]. Numerous studies have already defined the LPS-induced transcriptional changes in mouse and human macrophages [35], and we have previously determined the global transcriptional profile of LPS-treated GM-MØ and M-MØ, and identified gene sets whose LPS responsiveness is distinct in GM-MØ and M-MØ (*Cuevas et al., unpublished*). Given the ability of TLR4 to recognize LPS or palmitate, we next compared the transcriptomic changes elicited by palmitate (200 μM) or LPS (10 ng/ml) for 4 h and 24 h on M-MØ. LPS and palmitate exhibited distinct transcriptional effects on genes of the "Pro-inflammatory gene set" and "Anti-inflammatory gene set"

(Supplementary Figure 2A,B), including opposite actions on the expression of *MMP12*, *PPARG1*, *CCR2B*, *IL10* and *CCL2* after 24 hours in M-MØ (Figure 2A). The differences in the transcriptional responses of M-MØ to LPS and palmitate were also observed upon analysis of a large set of LPS-regulated genes (Supplementary Figure 3) as *IDO*, *CXCL10*, *MAOA*, *TNFRSF1B*, *EMR2*, *CCL19*, *LAMB3* and *TRIB3* expression was oppositely modified upon exposure to LPS or palmitate for 4h (Figure 2B) and 24h (Figure 2C). The differential regulation of IFN-regulated genes (*IDO*, *CXCL10*) by LPS and palmitate was in agreement with the effect of either stimulus on STAT1, whose activation was exclusively promoted by LPS (Figure 2D). Altogether, this set of experiments indicate that palmitate induces a unique and specific transcriptional response in human macrophages, and that the palmitate-induced macrophage pro-inflammatory shift is only partly reminiscent of that triggered by LPS.

JNK activation mediates the transcriptional changes triggered by palmitate on human macrophages. Screening of the phosphorylation state of intracellular signalling molecules after palmitate treatment identified JNK as the kinase with the higher level of palmitate-induced activation (Figure 3A,B). Correspondingly, c-Jun was also found to be phosphorylated in M-MØ exposed to palmitate for 4h (Figure 3A). The contribution of the palmitate-induced JNK activation to the transcriptional changes promoted by the fatty acid was next assessed using the selective JNK inhibitor SP600125 (Figure 3C). JNK inhibition significantly impaired the palmitate effect on the expression of *INHBA*, *TNF*, *IL10*, *IGF1*, *MAFB* and *TRIB3* (Figure 3D). In addition, the JNK inhibitor also diminished the palmitate-induced downregulation of MAFB protein expression (Figure

3E). Therefore, JNK activation mediates the palmitate-dependent modification of the transcriptional profile of human macrophages and also contributes to the palmitate-induced loss of MAFB, whose expression is required for the acquisition of the macrophage anti-inflammatory profile [26].

Palmitate conditions the LPS-induced cytokine profile of M-MØ. Macrophages are extremely sensitive to the surrounding extracellular milieu and their exposure to an initial stimulus determines their subsequent functional responses to additional stimuli [36-39]. Since palmitate levels are enhanced in obesity-related pathologies, whose comorbidities include altered inflammatory responses, we hypothesized that palmitate exposure might also condition human macrophages for altered responses to additional stimuli. Thus, we initially assessed whether palmitate influences LPS-initiated intracellular signaling in M-MØ. Palmitate alone caused only a very low NFκB activation (as illustrated by a weak phosphorylation of p65) (Figure 4A) and a weak reduction in basal STAT3 phosphorylation levels (Figure 4B). However, palmitate had a remarkable effect on the intracellular signaling pathways activated by LPS. Specifically, palmitate pre-treatment (24h) led to more potent LPS-induced activation of NFκB (as evidenced by increased phosphorylation of IKKαβ and p65 and a more profound loss of IkBα, Figure 4A), lower LPS-induced STAT1 and STAT3 phosphorylation, and higher LPS-induced activation of IRF3, p38MAPK and JNK (Figure 4A,B). Therefore, the presence of palmitate conditions the intracellular signaling triggered by a pathogenic stimulus in macrophages.

Next, we evaluated whether palmitate also modulates the transcriptional responses initiated by LPS in M-MØ. To that end, macrophages were exposed to palmitate (24 h) before stimulation with LPS (4 h), and the expression of the gene sets whose LPS responsiveness is distinct in GM-MØ and M-MØ (*Cuevas et al., unpublished*) was determined. Palmitate pre-treatment greatly altered the LPS-induced transcriptional response, with a profound effect on the expression of genes upregulated by LPS exclusively in M-MØ (Figure 5A, Supplementary Figure 4). Specifically, palmitate significantly impaired the LPS-induced upregulation of 25% of the genes whose expression in enhanced by LPS only in M-MØ (Figure 5B, Supplementary Figure 4), an effect that was most pronounced on genes with the highest M-MØ-specific upregulation by LPS (*CCL19, ARNT2, RGS16, ADIRF, MAOA*) (*Cuevas et al., unpublished*) (Supplementary Figure 4). Regarding the gene set whose expression in diminished by LPS only in M-MØ (Supplementary Figure 4), palmitate impaired the LPS-induced downregulation of 25% of them (5 out of 26), and concomitantly potentiated the LPS-induced downregulation of six genes (Figure 5B, Supplementary Figure 4). Therefore, exposure to palmitate significantly affects the LPS-regulated gene expression in human macrophages.

Finally, we evaluated whether pre-exposure to palmitate affected the production of LPS-induced cytokines of human macrophages. To that end, M-MØ were exposed to palmitate for 24 h and then stimulated with LPS (Figure 6A). Palmitate pre-treatment significantly enhanced the LPS-induction of the pro-inflammatory cytokines TNFα, IL-6 and IL-1β, while inhibited LPS-induced IL-10 and CCL2 production, by M-MØ (Figure 6B).

Therefore, palmitate not only limits the differentiation of anti-inflammatory (M-CSF-dependent) M-MØ but primes M-MØ for increased production of pro-inflammatory cytokines, and reduced production of anti-inflammatory cytokines, in response to a pathogenic stimulus like LPS. Importantly, these effects of palmitate are fatty-acid-specific since the unsaturated free fatty acid oleate (C18:1) was efficiently taken up by human macrophages (Supplementary Figure 5A) but neither modified the basal level of expression of MAFB, AhR and C/EBPβ in M-MØ (Supplementary Figure 5B) nor altered the LPS-induced production of TNFα, IL-6 and CCL2 (Supplementary Figure 5C). Besides, and lending further relevance to its transcriptional effects, palmitate pre-treatment completely blocked the LPS-induced production of the CCL19 chemokine by M-MØ (Figure 6B).

JNK activation mediates the ability of palmitate to condition macrophage responses to LPS. The ability of palmitate to modify the LPS-induced cytokine profile of M-MØ correlates with its capacity to modulate LPS-initiated intracellular signaling (shown in Figure 4). Such a correlation is especially relevant in the case of JNK, which play a central role in the development of inflammation in adipose tissue and insulin resistance in animal models [40]. Given the ability of palmitate to activate JNK, we analyzed whether the palmitate-induced JNK activation contributes to its macrophage-conditioning effect. Inhibition of JNK activation by SP600125 reduced the palmitate-dependent inhibition in the production of LPS-induced IL-10 (Figure 6D). Therefore, the palmitate-induced JNK activation modifies the macrophage transcriptome and also mediates the ability of palmitate to alter macrophage responses towards pathogenic stimuli like LPS.

Lithium chloride impairs the palmitate-induced loss of MAFB and abrogates the ability of palmitate to inhibit LPS-induced IL-10 production. We have previously shown that MAFB regulates the expression of the "Anti-inflammatory gene set", and that MAFB protein levels correlate with IL-10 production in human macrophages [26]. Interestingly, MAFB regulates human adipose tissue inflammation [41] and its deficiency in hematopoietic cells accelerates obesity [42]. MAFB protein stability is regulated by the JNK and ubiquitin–proteasome pathway [43], what agrees with the JNK-dependent ability of palmitate to downregulate MAFB protein levels (Figure 3). However, MAFB degradation is also controlled by a GSK3β-mediated phosphorylation of the transcriptional activation domain [44]. Since palmitate activates GSK3β [45, 46] and GSK3β inhibition suppresses palmitate-induced JNK phosphorylation in human liver cells [45], we hypothesized that GSK3β inhibition might alter palmitate effects on the macrophage cytokine profile. To determine whether the GSK3β/MAFB axis contributes to the inhibitory action of palmitate on the LPS-induced IL-10 production, we exposed macrophages to palmitate in the presence of Lithium Chloride (LiCl, 30 mM), a well-known GSK3β inhibitor [47, 48]. As shown in Figure 7A, LiCl inhibited the palmitate-induced MAFB downregulation, an effect not observed in the presence of NaCl. LiCl also significantly reduced the inhibitory effect of palmitate on the expression of MAFB-regulated genes like *SLC40A1*, *IL10* and *CCL2* (Figure 7B). More importantly, the presence of LiCl, but not NaCl, completely abrogated the inhibitory effect of palmitate on the LPS-induced IL-10 production in human macrophages (Figure 7C). Therefore, Lithium chloride impairs two relevant palmitate-dependent effects (MAFB

downregulation and loss of LPS-induced IL-10 expression), thus suggesting that modulation of the GSK3β/MAFB axis also contributes to the pro-inflammatory activity of palmitate.

DISCUSSION

Macrophages are critically involved in the initiation and resolution of inflammatory processes, and their deregulated activation contributes to chronic inflammatory diseases [4]. In the case of chronic inflammation associated to metabolic syndromes, the production of pro-inflammatory cytokines by macrophages correlates with the serum concentration of SFA [49], whose increased levels modify macrophage effector functions either by itself (e.g., palmitate) [10] or in combination with high levels of glucose and insulin [50]. Taking advantage of the previous identification of gene sets that specifically define the pro-inflammatory and anti-inflammatory state of human macrophage [18, 25], we now report that palmitate promotes the acquisition of a pro-inflammatory state that depends on JNK and differs from the LPS-induced pro-inflammatory activation at the transcriptional and functional levels. Further supporting the specificity of the palmitate-induced macrophage activation, we also provide evidences that, unlike LPS, palmitate conditions ("trains") human macrophages for stronger pro-inflammatory responses towards pathogenic stimuli.

Since metabolic diseases are driven by a low-grade inflammation and elevated levels of pro-inflammatory cytokines [51], the ability of palmitate to condition macrophage responses to other inflammatory stimuli (e.g., LPS) has very relevant pathological implications. It is now well established that metabolic endotoxemia initiates obesity and insulin resistance and, in fact, lowering plasma LPS concentration has been proposed as a strategy to tackle metabolic diseases [52]. Consequently, the palmitate pro-inflammatory

conditioning that we now report might exacerbate the pro-inflammatory responses of monocyte/macrophage towards pathogen-associated molecular patterns (PAMP) (e.g., LPS) derived from bacteria translocating from the gut, thus enhancing the production of PAMP-induced inflammatory cytokines. In agreement with the palmitate-induced increased LPS-responsiveness, palmitate conditions macrophages for stronger LPS-induced NFκB, IRF3, p38, ERK and JNK signaling. Since NFκB and JNK are chronically activated in adipose tissue from obese and insulin resistance subjects [53] and JNK activation in mouse macrophages is required for obesity-induced insulin resistance and inflammation [40], the macrophage-conditioning ability of palmitate that we now report might contribute to the known association between bacterial DNA translocation and increased insulin resistance [54].

The macrophage-conditioning ability of palmitate also resembles the effect of PAMPs like β-glucan, which render macrophages more responsive to a subsequent stimulation by LPS [38, 39]. This "boosting" effect has led to the concept of "trained immunity" and allowed the demonstration that innate immunity cells like macrophages produce much higher levels of pro-inflammatory cytokines if previously exposed to certain "training" stimuli [38, 39]. From this point of view, the changes that we have detected in palmitate-treated macrophages (loss of AhR and MAFB expression, reduced expression of the anti-inflammatory gene set) are compatible with the acquisition of a "palmitate-trained state" that would confer palmitate-conditioned macrophages with the ability to produce higher levels of pro-inflammatory cytokines upon exposure to a second stimulus.

The capacity of palmitate to downregulate MAFB protein expression in macrophages is especially relevant for the whole set of transcriptional and functional changes triggered by this SFA. Palmitate exerts rapid transcriptional effects and upregulates the expression of the macrophage "pro-inflammatory gene set" (*INHBA, EGLN3*) [18, 25] in less than 24 hours, a time at which palmitate has also provoked the loss of the transcription factors that drive "anti-inflammatory gene set" expression (AhR, MAFB) [18, 25]. The loss of MAFB expression appears to critically underlie the pro-inflammatory ability of palmitate because MAFB is a major positive regulator for the expression of a significant number of genes that characterize anti-inflammatory IL-10-producing macrophages (e.g., *IL10, IGF1, CCL2*) [26]. Importantly, the palmitate-induced loss of MAFB expression is partly mediated by JNK, an effect that is in line with the ability of JNK to promote MAFB ubiquitination [43] and agrees with the known pro-inflammatory nature of JNK *in vivo* [40]. Besides, MAFB protein levels are also controlled by other kinases like GSK3β [44], whose activation state might be also affected by palmitate [46]. In this regard, it is worth noting that the diminished LPS-induced production of IL-10 seen in palmitate-treated macrophages can be prevented by lithium chloride, a well-known GSK3β inhibitor [55] (*Riera-Borrull and Corbí, data not shown*). Whereas this effect of lithium chloride (enhanced levels of IL-10 after macrophage re-stimulation) would fit with the potential ability of GSK3 inhibitors to overcome insulin resistance, the involvement of the GSK3β kinase in the human macrophage "palmitate training" is also counterintuitive since GSK3β mediates TNFα-induced cross-tolerance [56].

Previous studies have assumed that palmitate activation of macrophages mostly resembles LPS-induced mechanisms because palmitate is recognized by TLR4 and activates pro-inflammatory signaling pathways *in vitro* and *in vivo* [10]. However, and in line with previous reports [11-13], our results indicate that palmitate and LPS differ in their respective transcriptional and functional effects on human macrophages. Thus, palmitate and LPS oppositely modulate the expression of genes like *IDO1, MAOA, EMR2* and *LAMB3*. Palmitate and LPS also differ in terms of the intracellular signaling triggered in human macrophages. Palmitate leads to JNK activation at late time points, but causes a very weak NF-κB activation and has not effect on STAT1/STAT3 or IRF3 phosphorylation (Figure 4). In fact, palmitate pre-treatment even reduces the LPS-induced activation of STAT1 and STAT3. This differential signaling ability of palmitate and LPS correlates with their distinct effect on the expression of IFN-regulated genes like *IDO1*, and strongly suggests that the palmitate-initiated intracellular signaling originates from TLR4 and additional PAMP/DAMP receptors.

Especially relevant is the fact that palmitate and LPS differentially regulate the expression of *CCL19* and *TRIB3*. Contrarily to the effect of LPS, which greatly enhances *CCL19* mRNA (*Cuevas and Corbí, data not shown*), palmitate significantly downregulates CCL19 at the mRNA and protein level (Figure 2) and even abrogates the LPS-induced upregulation of CCL19 production (Figure 6). Together with CCL21, the chemokine CCL19 is a ligand of CCR7, whose expression critically determines lymph node homing of T cells and dendritic cells [57]. Interestingly, CCL19, but not CCL21, promotes CCR7 phosphorylation, internalization and desensitization towards CCL21

[57]. Therefore, the ability of 200 μM palmitate to ablate the basal and LPS-mediated CCL19 expression implies that stronger CCR7-dependent responses (dendritic cell homing and maturation, and antigen-presentation) [58] must take place in the presence of the palmitate concentrations found in obese individuals. This prediction would be in line with the ability of palmitate to foster the acquisition of the cytokine and transcriptional profile of pro-inflammatory (and immunogenic) macrophages that we now report.

Regarding the palmitate-mediated upregulation of *TRIB3* gene expression, our results agree with the ability of palmitate to induce TRIB3 expression in human liver cells [59] and podocytes [60]. TRIB3 is a pseudokinase that modulates many signaling cascades associated with ER stress, nutrient deficiency and insulin resistance [61], and that acts as a negative regulator of NFκB-dependent transcription [62]. Since TRIB3 negatively regulates CCL2 expression in podocytes [60], it is tempting to speculate that palmitate-induce TRIB3 upregulation might underlie the negative effect that palmitate has on the basal and LPS-induced expression of CCL2 in human macrophages.

REFERENCES

1. Gallagher, E.J. and D. LeRoith, *Epidemiology and molecular mechanisms tying obesity, diabetes, and the metabolic syndrome with cancer.* Diabetes Care, 2013. **36 Suppl 2**: p. S233-9.
2. Hopkins, B.D., M.D. Goncalves, and L.C. Cantley, *Obesity and Cancer Mechanisms: Cancer Metabolism.* J Clin Oncol, 2016. **34**(35): p. 4277-4283.
3. Das, U.N., *Is obesity an inflammatory condition?* Nutrition, 2001. **17**(11-12): p. 953-66.
4. Chawla, A., K.D. Nguyen, and Y.P. Goh, *Macrophage-mediated inflammation in metabolic disease.* Nat Rev Immunol, 2011. **11**(11): p. 738-49.
5. Lumeng, C.N. and A.R. Saltiel, *Inflammatory links between obesity and metabolic disease.* J Clin Invest, 2011. **121**(6): p. 2111-7.
6. Weisberg, S.P., et al., *CCR2 modulates inflammatory and metabolic effects of high-fat feeding.* J Clin Invest, 2006. **116**(1): p. 115-24.
7. Patsouris, D., et al., *Ablation of CD11c-positive cells normalizes insulin sensitivity in obese insulin resistant animals.* Cell Metab, 2008. **8**(4): p. 301-9.
8. Arkan, M.C., et al., *IKK-beta links inflammation to obesity-induced insulin resistance.* Nat Med, 2005. **11**(2): p. 191-8.
9. Solinas, G., et al., *JNK1 in hematopoietically derived cells contributes to diet-induced inflammation and insulin resistance without affecting obesity.* Cell Metab, 2007. **6**(5): p. 386-97.
10. Shi, H., et al., *TLR4 links innate immunity and fatty acid-induced insulin resistance.* J Clin Invest, 2006. **116**(11): p. 3015-25.
11. Erridge, C. and N.J. Samani, *Saturated fatty acids do not directly stimulate Toll-like receptor signaling.* Arterioscler Thromb Vasc Biol, 2009. **29**(11): p. 1944-9.
12. Hosoi, T., et al., *Myeloid differentiation factor 88 (MyD88)-deficiency increases risk of diabetes in mice.* PLoS One, 2010. **5**(9).
13. Vijay-Kumar, M., et al., *Loss of function mutation in toll-like receptor-4 does not offer protection against obesity and insulin resistance induced by a diet high in trans fat in mice.* J Inflamm (Lond), 2011. **8**(1): p. 2.
14. Hall, E., et al., *Effects of palmitate on genome-wide mRNA expression and DNA methylation patterns in human pancreatic islets.* BMC Med, 2014. **12**: p. 103.
15. Wang, X., et al., *Epigenetic regulation of macrophage polarization and inflammation by DNA methylation in obesity.* JCI Insight, 2016. **1**(19): p. e87748.
16. Gordon, S. and P.R. Taylor, *Monocyte and macrophage heterogeneity.* Nat Rev Immunol, 2005. **5**(12): p. 953-64.
17. Escribese, M.M., et al., *The prolyl hydroxylase PHD3 identifies proinflammatory macrophages and its expression is regulated by activin A.* J Immunol, 2012. **189**(4): p. 1946-54.
18. Sierra-Filardi, E., et al., *Activin A skews macrophage polarization by promoting a proinflammatory phenotype and inhibiting the acquisition of anti-inflammatory macrophage markers.* Blood, 2011. **117**(19): p. 5092-101.
19. Soler Palacios, B., et al., *Macrophages from the synovium of active rheumatoid arthritis exhibit an activin A-dependent pro-inflammatory profile.* J Pathol, 2015. **235**(3): p. 515-26.
20. Verreck, F.A., et al., *Human IL-23-producing type 1 macrophages promote but IL-10-producing type 2 macrophages subvert immunity to (myco)bacteria.* Proc Natl Acad Sci U S A, 2004. **101**(13): p. 4560-5.
21. Lacey, D.C., et al., *Defining GM-CSF- and Macrophage-CSF-Dependent Macrophage Responses by In Vitro Models.* J Immunol, 2012. **188**(11): p. 5752-65.
22. Raes, G., et al., *Arginase-1 and Ym1 are markers for murine, but not human, alternatively activated myeloid cells.* J Immunol, 2005. **174**(11): p. 6561; author reply 6561-2.
23. Izquierdo, E., et al., *Reshaping of Human Macrophage Polarization through Modulation of Glucose Catabolic Pathways.* J Immunol, 2015. **195**(5): p. 2442-51.
24. Xu, S., et al., *Evaluation of foam cell formation in cultured macrophages: an improved method with Oil Red O staining and DiI-oxLDL uptake.* Cytotechnology, 2010. **62**(5): p. 473-81.
25. Gonzalez-Dominguez, E., et al., *Atypical Activin A and IL-10 Production Impairs Human CD16+ Monocyte Differentiation into Anti-Inflammatory Macrophages.* J Immunol, 2016. **196**(3): p. 1327-37.

26. Cuevas, V.D., et al., *MAFB Determines Human Macrophage Anti-Inflammatory Polarization: Relevance for the Pathogenic Mechanisms Operating in Multicentric Carpotarsal Osteolysis.* J Immunol, 2017.
27. Sturn, A., J. Quackenbush, and Z. Trajanoski, *Genesis: cluster analysis of microarray data.* Bioinformatics, 2002. **18**(1): p. 207-8.
28. Kimura, A., et al., *Aryl hydrocarbon receptor in combination with Stat1 regulates LPS-induced inflammatory responses.* J Exp Med, 2009. **206**(9): p. 2027-35.
29. Ruffell, D., et al., *A CREB-C/EBPbeta cascade induces M2 macrophage-specific gene expression and promotes muscle injury repair.* Proc Natl Acad Sci U S A, 2009. **106**(41): p. 17475-80.
30. Huang, S., et al., *Saturated fatty acids activate TLR-mediated proinflammatory signaling pathways.* J Lipid Res, 2012. **53**(9): p. 2002-13.
31. Pal, D., et al., *Fetuin-A acts as an endogenous ligand of TLR4 to promote lipid-induced insulin resistance.* Nat Med, 2012. **18**(8): p. 1279-85.
32. Ibrahimi, A., et al., *Expression of the CD36 homolog (FAT) in fibroblast cells: effects on fatty acid transport.* Proc Natl Acad Sci U S A, 1996. **93**(7): p. 2646-51.
33. Senn, J.J., *Toll-like receptor-2 is essential for the development of palmitate-induced insulin resistance in myotubes.* J Biol Chem, 2006. **281**(37): p. 26865-75.
34. Nguyen, M.T., et al., *A subpopulation of macrophages infiltrates hypertrophic adipose tissue and is activated by free fatty acids via Toll-like receptors 2 and 4 and JNK-dependent pathways.* J Biol Chem, 2007. **282**(48): p. 35279-92.
35. Xue, J., et al., *Transcriptome-based network analysis reveals a spectrum model of human macrophage activation.* Immunity, 2014. **40**(2): p. 274-88.
36. Erwig, L.P., et al., *Initial cytokine exposure determines function of macrophages and renders them unresponsive to other cytokines.* J Immunol, 1998. **161**(4): p. 1983-8.
37. Cheng, S.C., et al., *mTOR- and HIF-1alpha-mediated aerobic glycolysis as metabolic basis for trained immunity.* Science, 2014. **345**(6204): p. 1250684.
38. Netea, M.G., et al., *Trained immunity: A program of innate immune memory in health and disease.* Science, 2016. **352**(6284): p. aaf1098.
39. Saeed, S., et al., *Epigenetic programming of monocyte-to-macrophage differentiation and trained innate immunity.* Science, 2014. **345**(6204): p. 1251086.
40. Han, M.S., et al., *JNK expression by macrophages promotes obesity-induced insulin resistance and inflammation.* Science, 2013. **339**(6116): p. 218-22.
41. Pettersson, A.M., et al., *MAFB as a novel regulator of human adipose tissue inflammation.* Diabetologia, 2015. **58**(9): p. 2115-23.
42. Tran, M.T., et al., *MafB deficiency accelerates the development of obesity in mice.* FEBS Open Bio, 2016. **6**(6): p. 540-7.
43. Tanahashi, H., et al., *MafB protein stability is regulated by the JNK and ubiquitin-proteasome pathways.* Arch Biochem Biophys, 2010. **494**(1): p. 94-100.
44. Herath, N.I., et al., *GSK3-mediated MAF phosphorylation in multiple myeloma as a potential therapeutic target.* Blood Cancer J, 2014. **4**: p. e175.
45. Cao, J., et al., *Saturated free fatty acid sodium palmitate-induced lipoapoptosis by targeting glycogen synthase kinase-3beta activation in human liver cells.* Dig Dis Sci, 2014. **59**(2): p. 346-57.
46. Choi, S.E., et al., *Involvement of glycogen synthase kinase-3beta in palmitate-induced human umbilical vein endothelial cell apoptosis.* J Vasc Res, 2007. **44**(5): p. 365-74.
47. Eldar-Finkelman, H. and A. Martinez, *GSK-3 Inhibitors: Preclinical and Clinical Focus on CNS*. Front Mol Neurosci, 2011. **4**: p. 32.
48. Freland, L. and J.M. Beaulieu, *Inhibition of GSK3 by lithium, from single molecules to signaling networks.* Front Mol Neurosci, 2012. **5**: p. 14.
49. Ray, I., S.K. Mahata, and R.K. De, *Obesity: An Immunometabolic Perspective.* Front Endocrinol (Lausanne), 2016. **7**: p. 157.
50. Kratz, M., et al., *Metabolic dysfunction drives a mechanistically distinct proinflammatory phenotype in adipose tissue macrophages.* Cell Metab, 2014. **20**(4): p. 614-25.
51. Johnson, A.R., J.J. Milner, and L. Makowski, *The inflammation highway: metabolism accelerates inflammatory traffic in obesity.* Immunol Rev, 2012. **249**(1): p. 218-38.

52. Cani, P.D., et al., *Metabolic endotoxemia initiates obesity and insulin resistance.* Diabetes, 2007. **56**(7): p. 1761-72.
53. Odegaard, J.I. and A. Chawla, *Alternative macrophage activation and metabolism.* Annu Rev Pathol, 2011. **6**: p. 275-97.
54. Ortiz, S., et al., *Bacterial DNA translocation holds increased insulin resistance and systemic inflammatory levels in morbid obese patients.* J Clin Endocrinol Metab, 2014. **99**(7): p. 2575-83.
55. Phiel, C.J. and P.S. Klein, *Molecular targets of lithium action.* Annu Rev Pharmacol Toxicol, 2001. **41**: p. 789-813.
56. Park, S.H., et al., *Tumor necrosis factor induces GSK3 kinase-mediated cross-tolerance to endotoxin in macrophages.* Nat Immunol, 2011. **12**(7): p. 607-15.
57. Forster, R., A.C. Davalos-Misslitz, and A. Rot, *CCR7 and its ligands: balancing immunity and tolerance.* Nat Rev Immunol, 2008. **8**(5): p. 362-71.
58. Sanchez-Sanchez, N., L. Riol-Blanco, and J.L. Rodriguez-Fernandez, *The multiple personalities of the chemokine receptor CCR7 in dendritic cells.* J Immunol, 2006. **176**(9): p. 5153-9.
59. Yan, W., et al., *Palmitate induces TRB3 expression and promotes apoptosis in human liver cells.* Cell Physiol Biochem, 2014. **33**(3): p. 823-34.
60. Morse, E., et al., *TRB3 is stimulated in diabetic kidneys, regulated by the ER stress marker CHOP, and is a suppressor of podocyte MCP-1.* Am J Physiol Renal Physiol, 2010. **299**(5): p. F965-72.
61. Mondal, D., A. Mathur, and P.K. Chandra, *Tripping on TRIB3 at the junction of health, metabolic dysfunction and cancer.* Biochimie, 2016. **124**: p. 34-52.
62. Wu, M., et al., *SINK is a p65-interacting negative regulator of NF-kappaB-dependent transcription.* J Biol Chem, 2003. **278**(29): p. 27072-9.

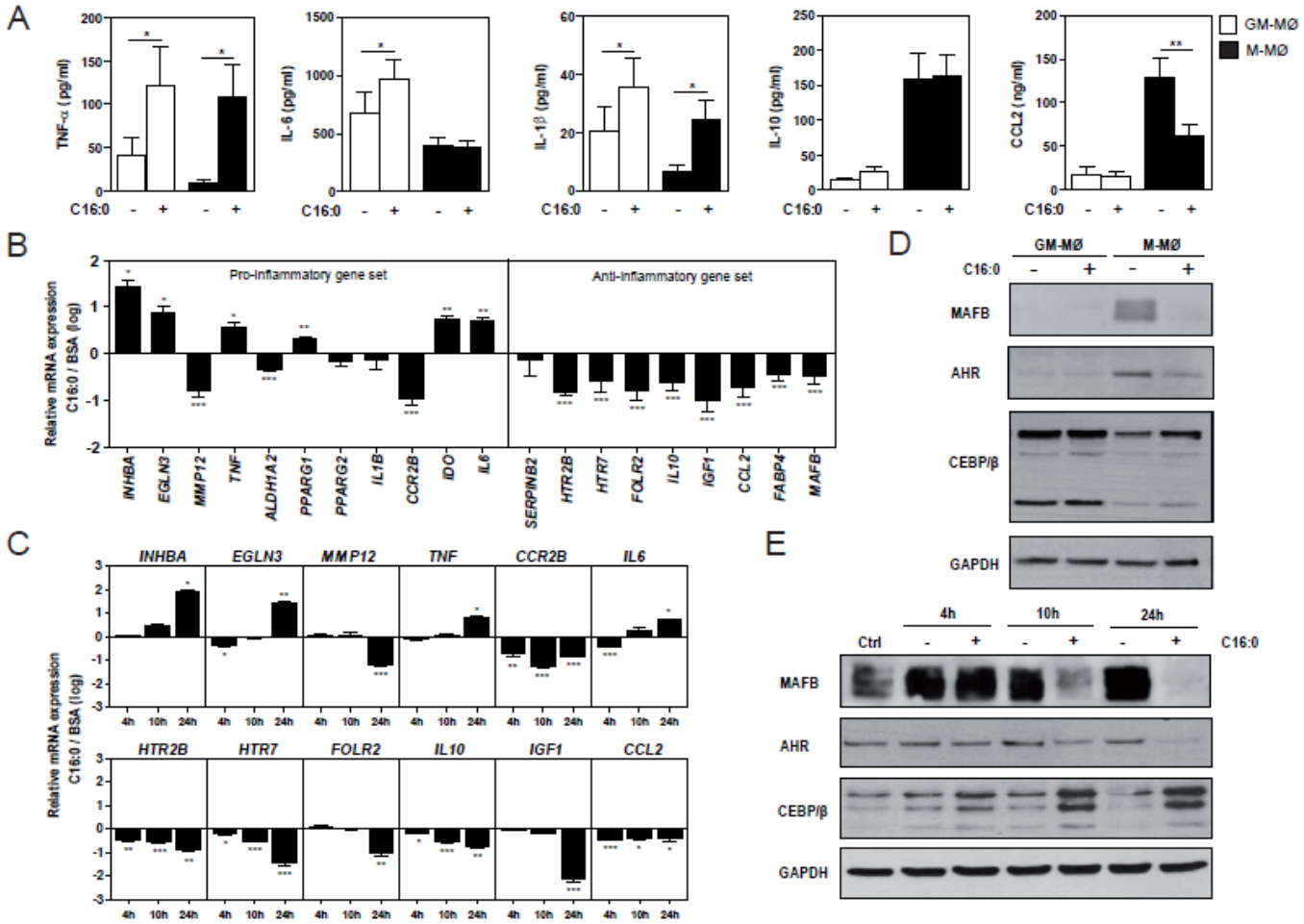

Figure 1. Functional, transcriptomic and transcription factor profile of palmitate-treated human macrophages. (A) Levels of the indicated cytokines in the culture media of macrophages (GM-MØ and M-MØ) exposed to 200 µM palmitate (C16:0) or BSA for 24h, as determined ELISA. Shown is the mean ± SEM of ten independent experiments. **(B)** Relative mRNA expression of the indicated genes in M-MØ exposed to 200 µM palmitate (C16:0) or BSA for 24h, as determined by qRT-PCR using *TBP* as a reference. The expression of each gene after palmitate treatment and relative to its expression after BSA treatment in indicated. Shown is the mean ± SEM of ten independent experiments. **(C)** Relative mRNA expression of the indicated genes in M-MØ exposed to 200 µM palmitate (C16:0) or BSA for 4h, 10h or 24h, as determined by qRT-PCR using *TBP* as a reference. The expression of each gene after palmitate treatment and relative to its expression after BSA treatment is indicated. Shown is the mean ± SEM of three independent experiments (*, $p<0.05$; **, $p<0.01$; ***, $p<0.001$). **(D)** Expression of MAFB, AhR and CEBP/β in macrophages (GM-MØ and M-MØ) treated with 200 µM palmitate (C16:0) or BSA (-) for 24h, as determined by Western blot. **(E)** Expression of MAFB, AhR and CEBP/β in M-MØ non-treated (Ctrl) or treated with 200 µM palmitate or BSA (-) for 4h, 10h or 24h, as determined by Western blot. In (**D-E**), three independent experiments were done and one of them is shown, and GAPDH protein levels were determined in parallel as a protein loading control.

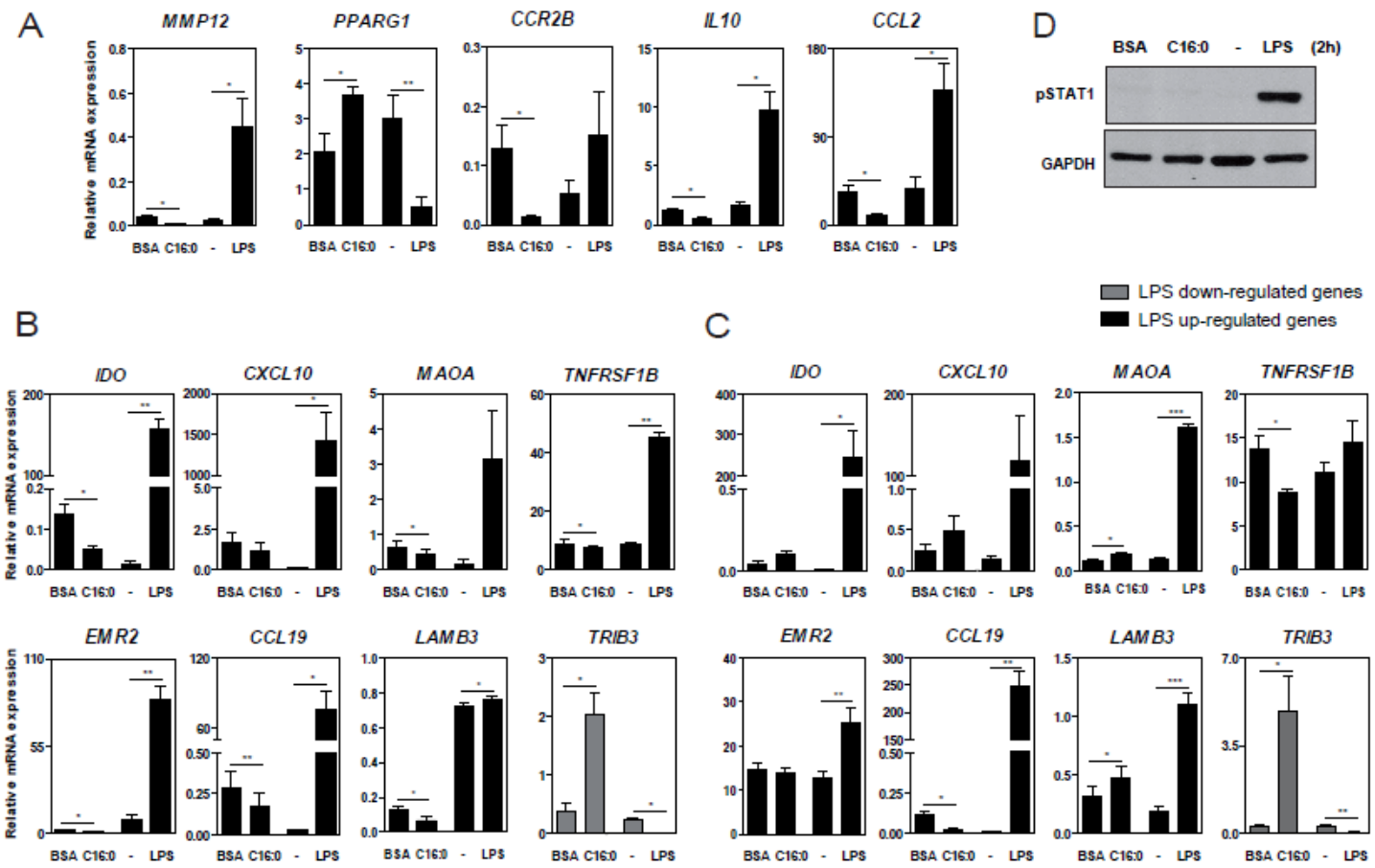

Figure 2. Comparison of the transcriptomic changes elicited by palmitate or LPS on human macrophages. (A) Relative mRNA expression of the indicated polarization-specific genes in M-MØ untreated (-) or exposed to 10 ng/ml LPS, 200 µM palmitate (C16:0) or BSA for 24h, as determined by qRT-PCR using *TBP* as a reference. **(B,C)** Relative mRNA expression of the indicated LPS-regulated genes in M-MØ untreated (-) or exposed to 10 ng/ml LPS, 200 µM palmitate or BSA for **(B)** 4h or **(C)** 24h, as determined by qRT-PCR using *TBP* as a reference. In **(A-C)**, results are shown as mean ± SEM of five independent experiments (*, $p<0.05$; **, $p<0.01$; ***, $p<0.001$). **(D)** Expression of activated STAT1 in M-MØ non-treated (-) or treated with 10 ng/ml LPS, 200 µM palmitate or BSA for 2h, as determined by Western blot. GAPDH protein levels were determined in parallel as a protein loading control.

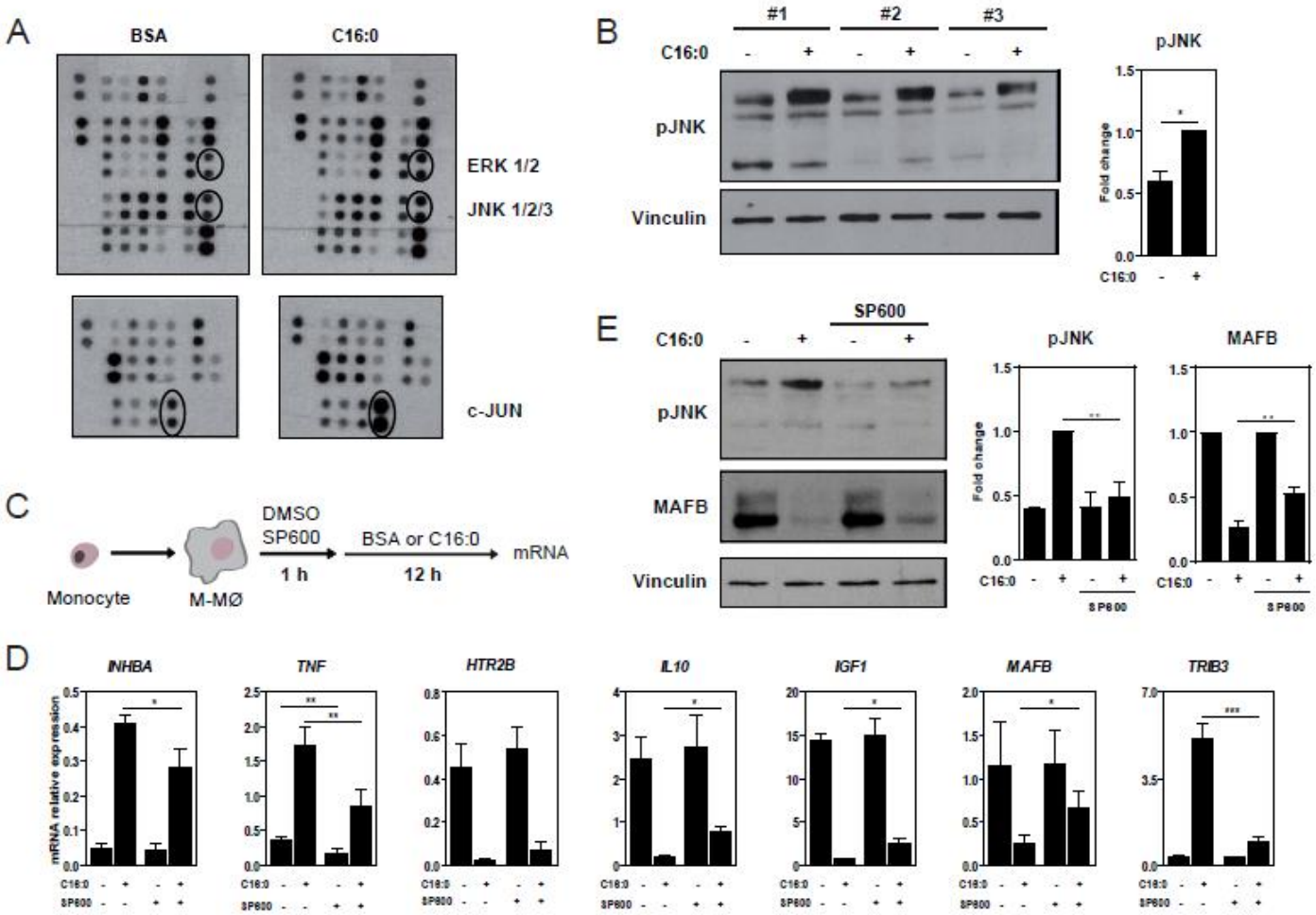

Figure 3. Effect of JNK activation on the palmitate-induced transcriptional changes in human macrophages. (A) M-MØ were left untreated (BSA) or exposed to 200 µM palmitate (C16:0) for 4h, and the phosphorylation state of representative signaling molecules was determined using the Proteome Profiler® protein array (R&D Systems, USA). The kinases specifically mentioned in the text are indicated. **(B)** M-MØ from three independent donors (#1-3) were left treated with BSA (-) or exposed to 200 µM palmitate (C16:0) for 4h, and the phosphorylation state of JNK was determined by Western blot using specific antibodies. The level of vinculin was determined in parallel as a protein loading control. Right panels show the mean ± SEM of the densitometric analysis of the three experiments (*, $p<0.05$). **(C)** Schematic representation of the experimental procedure. **(D)** Relative mRNA expression of the indicated genes in M-MØ exposed to SP600125 (SP600) or DMSO (-) for 1 hour and exposed to BSA (-) or 200 µM palmitate (C16:0) for 12h, as determined by qRT-PCR using *TBP* as a reference. Results are shown as mean ± SEM of five independent experiments (*, $p<0.05$; **, $p<0.01$; ***, $p<0.001$). **(E)** JNK activation and MAFB protein levels in M-MØ untreated or exposed to SP600125 (SP600) for 1 hour and then exposed to BSA (-) or 200 µM palmitate (C16:0) for 12h, as determined by determined by Western blot using specific antibodies. The level of vinculin was determined in parallel as a protein loading control. The experiment was performed on four independent M-MØ preparations, and one of them is shown. Right panels show the mean ± SEM of the densitometric analysis of the four experiments (**, $p<0.01$).

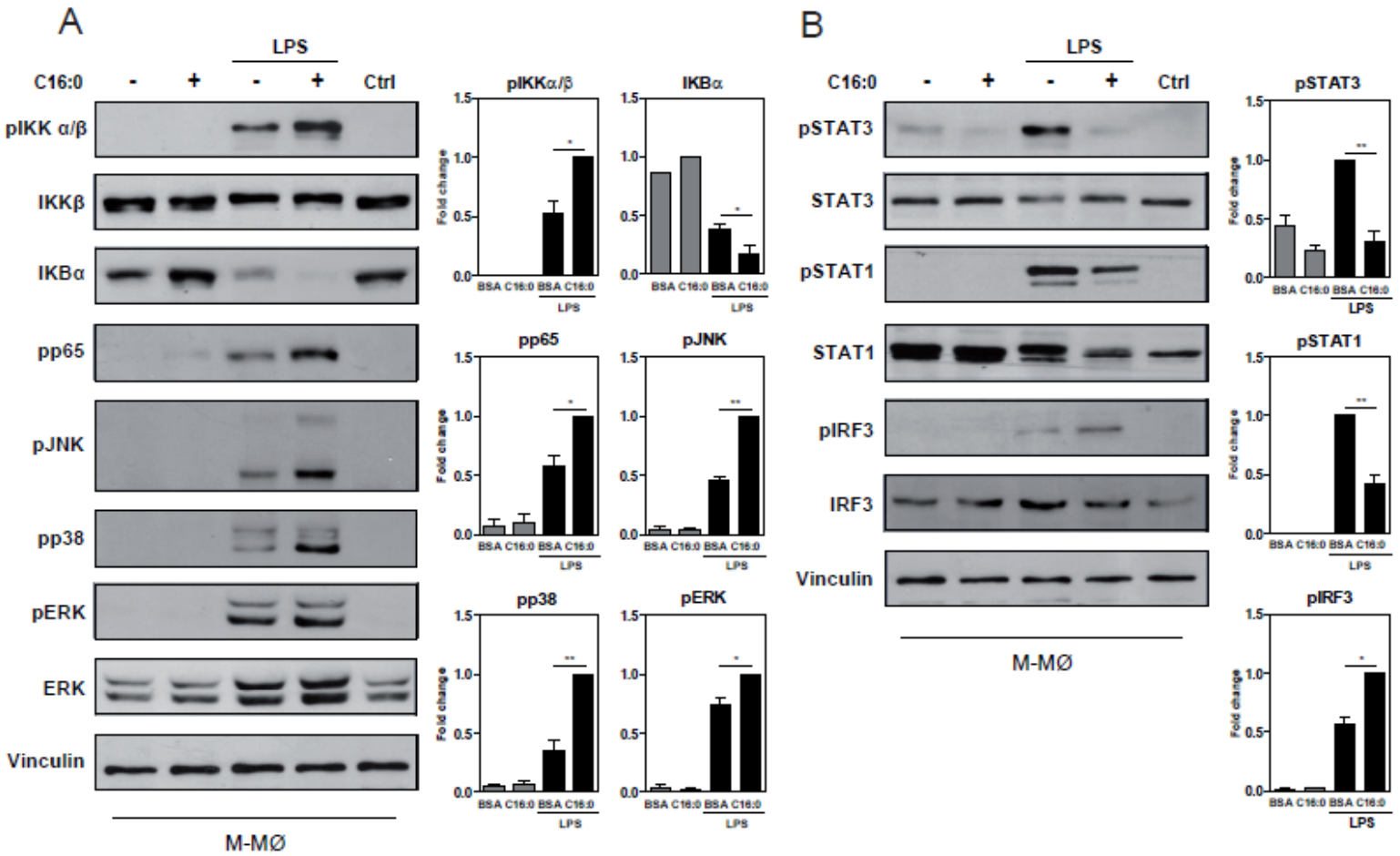

Figure 4. Palmitate exposure modulates LPS-initiated intracellular signalling in human macrophages. (A,B) Determination of the phosphorylation state of (**A**) IKKα/β, IκBα, NFκB p65, ERK1/2, JNK, p38 MAPK, STAT3, STAT1 and IRF3 in M-MØ exposed to BSA (-) or palmitate (C16:0) for 24 h and then stimulated with LPS (10 ng/ml) for 15-30 min **(A)** or 120 min **(B)**. The total levels of IKKα/β, ERK1/2, STAT3, STAT1 and IRF3 were determined in parallel. The levels of vinculin were determined as a protein loading control. The levels of each protein were also determined in untreated cells (Ctrl). In all cases, four independent experiments were performed, and one of them is shown. Right panels show the mean ± SEM of the densitometric analysis of the four experiments (*, $p<0.05$; **, $p<0.01$).

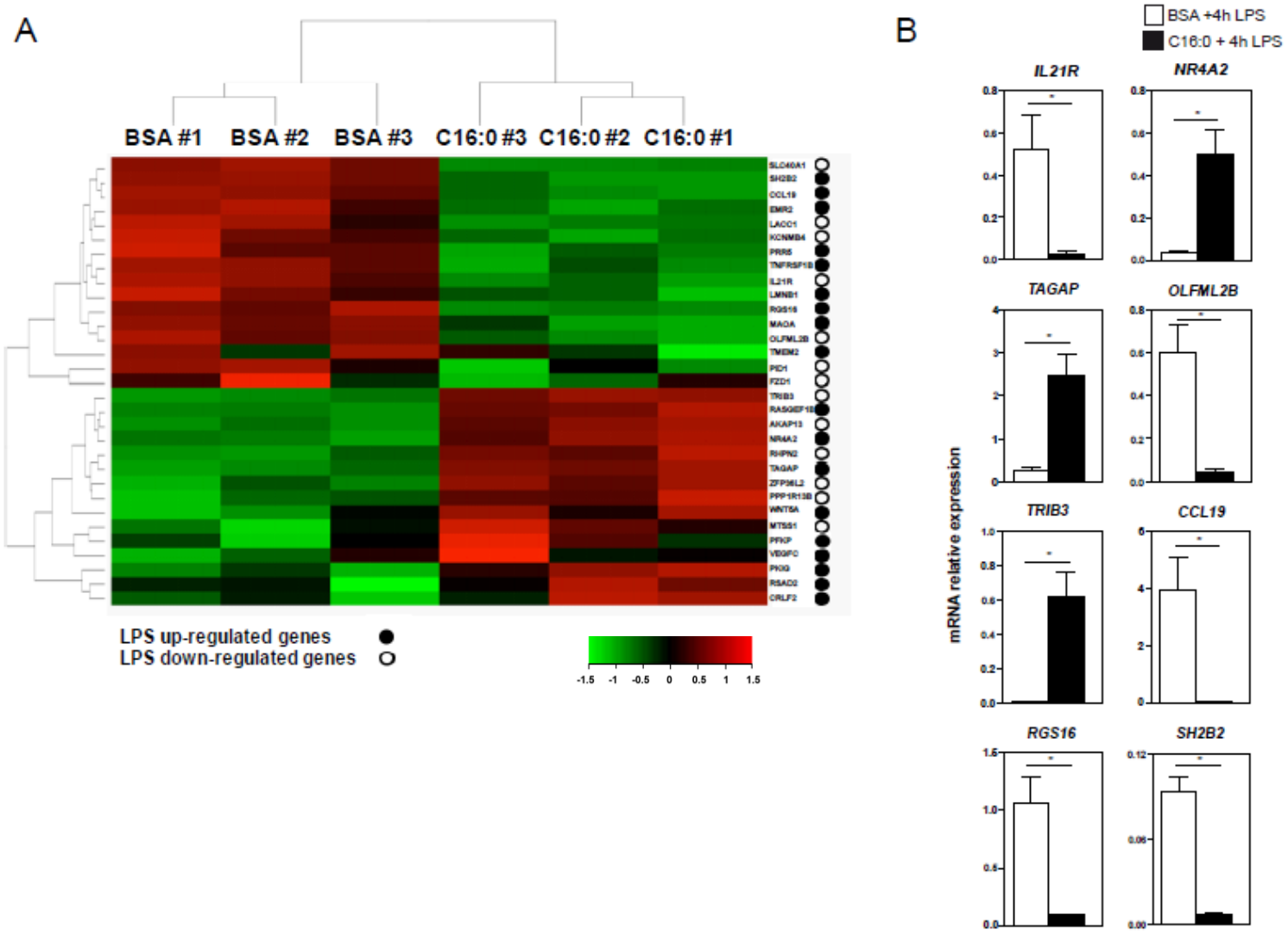

Figure 5. Palmitate pre-treatment alters the LPS-induced transcriptomic response in human macrophages. (A) Heat map representation of the mRNA expression of the LPS-regulated genes whose expression is significantly different ($p < 0.05$) in M-MØ exposed to either BSA or 200µM palmitate (C16:0) (24 h) before stimulation with LPS (10ng/ml) for 4 hours. The effect of LPS on the expression of the analysed genes is shown. **(B)** Relative mRNA expression of the indicated genes in M-MØ exposed to either BSA or 200µM palmitate (C16:0) (24 h) before stimulation with LPS (10ng/ml) for 4 hours, as determined by qRT-PCR using *TBP* as a reference. Shown is the mean ± SEM of three independent experiments (*, $p<0.05$).

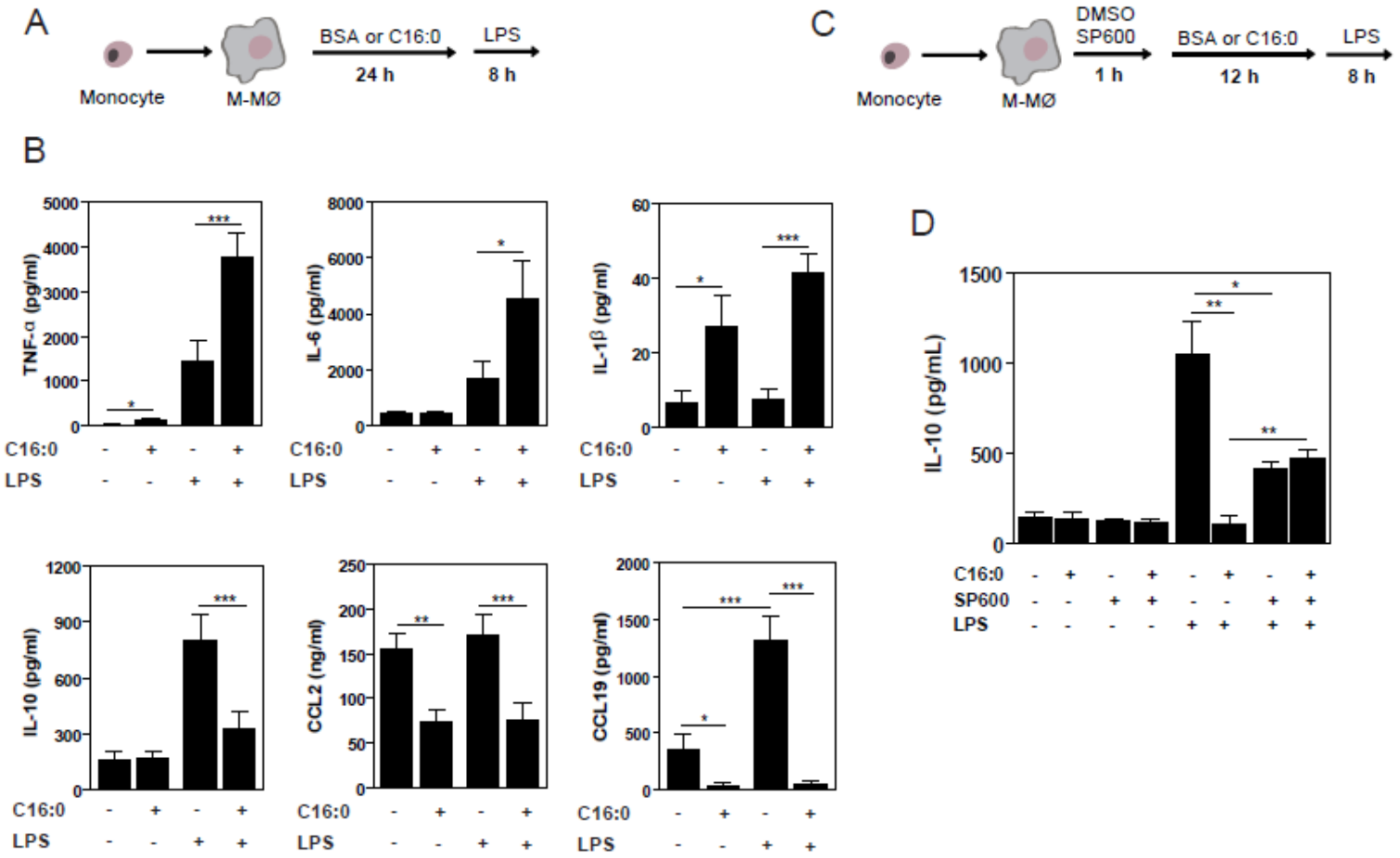

Figure 6. Effect of palmitate treatment on the LPS-induced cytokine profile in human macrophages. (A) Schematic representation of the experimental procedure. **(B)** Levels of the indicated cytokines in the culture supernatants of macrophages (M-MØ) exposed to 200 µM palmitate (C16:0) or BSA (-) for 24h before stimulation with 10 ng/ml LPS for 8 hours. Shown is the mean ± SEM of eight independent experiments (*, $p<0.05$; **, $p<0.01$; ***, $p<0.001$). **(C)** Schematic representation of the experimental procedure. **(D)** Levels of IL-10 in the culture media of macrophages (M-MØ) not treated o treated with SP600125 (SP600), and then exposed to 200 µM palmitate (C16:0) or BSA (-) (24h) before stimulation with 10 ng/ml LPS (8h). Shown is the mean ± SEM of four independent experiments (*, $p<0.05$; **, $p<0.01$).

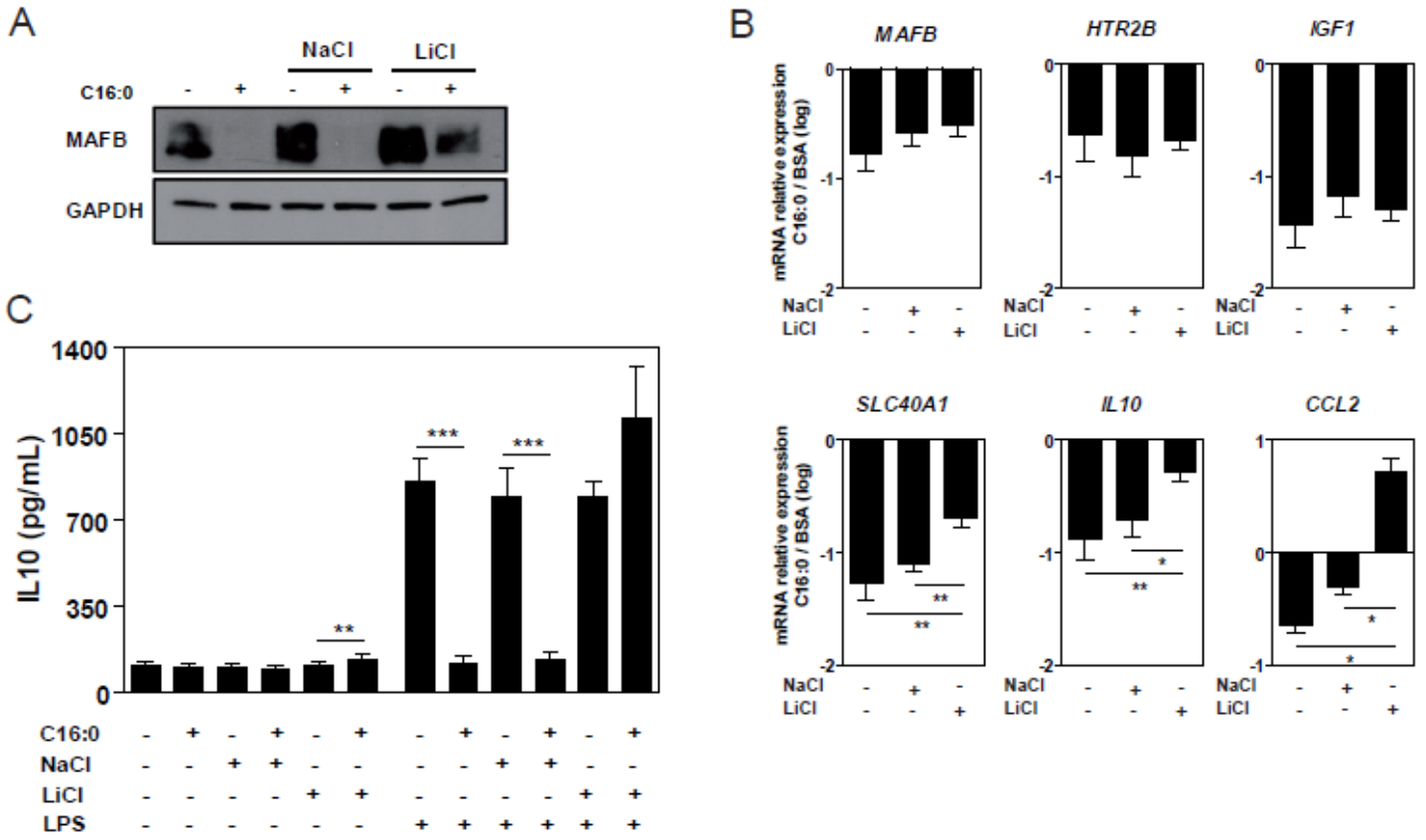

Figure 7.- Lithium chloride inhibits palmitate-dependent effects in human macrophages. (A) Expression of MAFB in macrophages (M-MØ) treated with LiCl or NaCl before exposure to 200 µM palmitate (C16:0) or BSA (-) for 24h, as determined by Western blot. **(B)** Relative mRNA expression of the indicated genes in M-MØ treated with LiCl or NaCl before exposure to 200 µM palmitate (C16:0) or BSA for 24h, as determined by qRT-PCR using *TBP* as a reference. The expression of each gene after palmitate treatment and relative to its expression after BSA treatment is indicated. Shown is the mean ± SEM of six independent experiments (*, $p<0.05$; **, $p<0.01$). **(C)** Levels of IL-10 in the culture media of macrophages (M-MØ) not treated o treated with LiCl or NaCl, and then exposed to 200 µM palmitate (C16:0) or BSA (-) (24h) before stimulation with 10 ng/ml LPS (8h). Shown is the mean ± SEM of six independent experiments (**, $p<0.01$; ***, $p<0.001$).

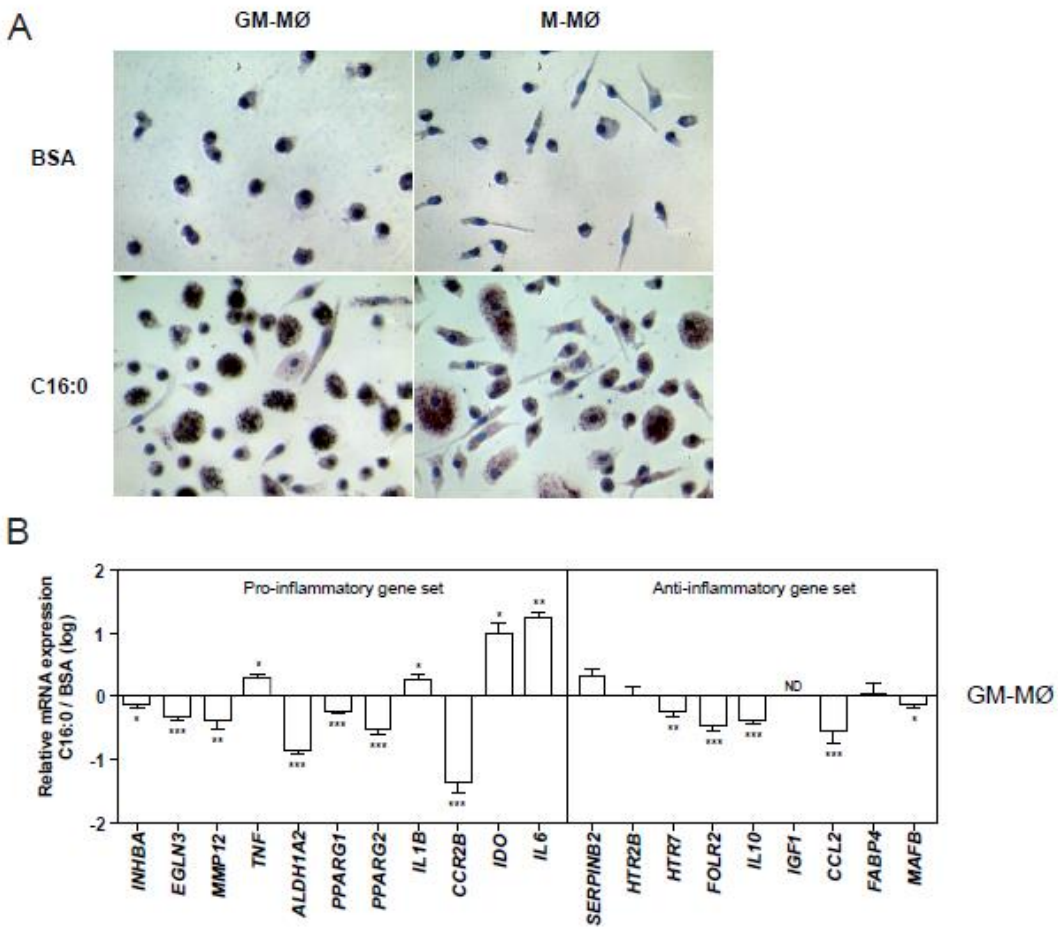

Supplementary Figure 1. Uptake of palmitate by human macrophages and transcriptomic effect of palmitate in GM-MØ. (A) Palmitate (C16:0) uptake by human macrophages (GM-MØ and M-MØ), as determined by Oil Red staining after 24 hours. For comparative purposes, macrophages were exposed in parallel to BSA (upper panels). **(B)** Relative mRNA expression of the indicated genes in GM-MØ exposed to 200 µM palmitate or BSA for 24h, as determined by qRT-PCR using *TBP* as a reference. Shown is the expression of each gene after palmitate treatment and relative to its expression after BSA treatment. Shown is the mean ± SEM of ten independent experiments (*, $p<0.05$; **, $p<0.01$; ***, $p<0.001$).

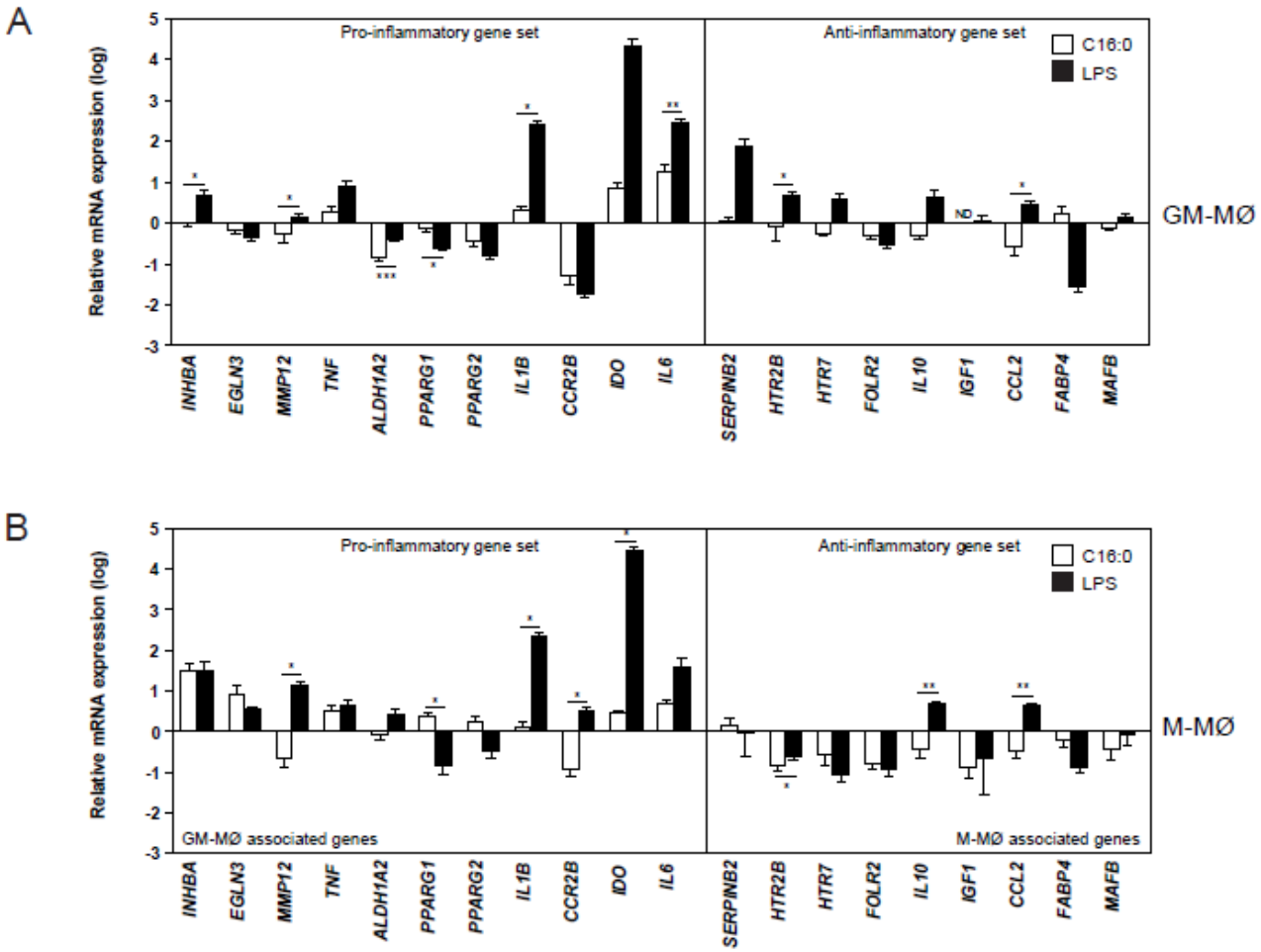

Supplementary Figure 2. Modulation of the expression of macrophage polarization-specific genes by LPS or palmitate. Relative mRNA expression of the "Pro-inflammatory gene set" and "Anti-inflammatory gene set" in GM-MØ **(A)** and M-MØ **(B)** exposed to either 200 µM palmitate (C16:0) or 10 ng/ml LPS for 24 hours. Results are presented as the mRNA expression of each gene after palmitate or LPS treatment and relative to the mRNA expression of the same gene after treatment with either BSA (control for palmitate treatment) or no treatment (control for LPS stimulation). Shown is the mean ± SEM of five independent experiments (*, $p<0.05$; **, $p<0.01$; ***, $p<0.001$).

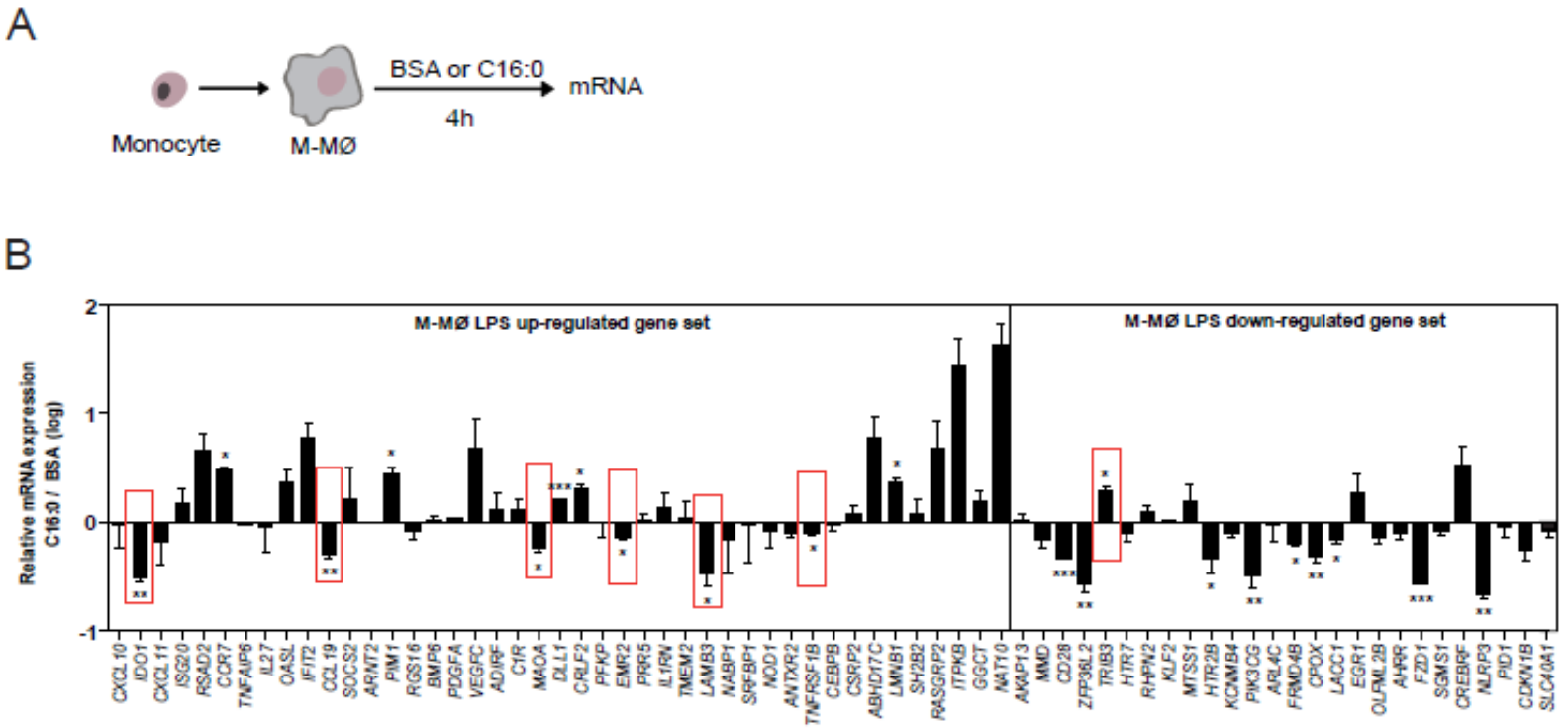

Supplementary Figure 3. Palmitate treatment modulates the expression of LPS-regulated genes in human macrophages. (A) Experimental design of the experiment. **(B)** Relative mRNA expression of the indicated LPS-responsive genes in M-MØ exposed to either 200 µM palmitate (C16:0) or BSA for 4 hours. Results are presented as the mRNA expression of each gene after palmitate treatment and relative to the mRNA expression of the same gene after treatment with BSA. Shown is the mean ± SEM of three independent experiments (#, $p<0.06$; *, $p<0.05$; **, $p<0.01$; ***, $p<0.001$).

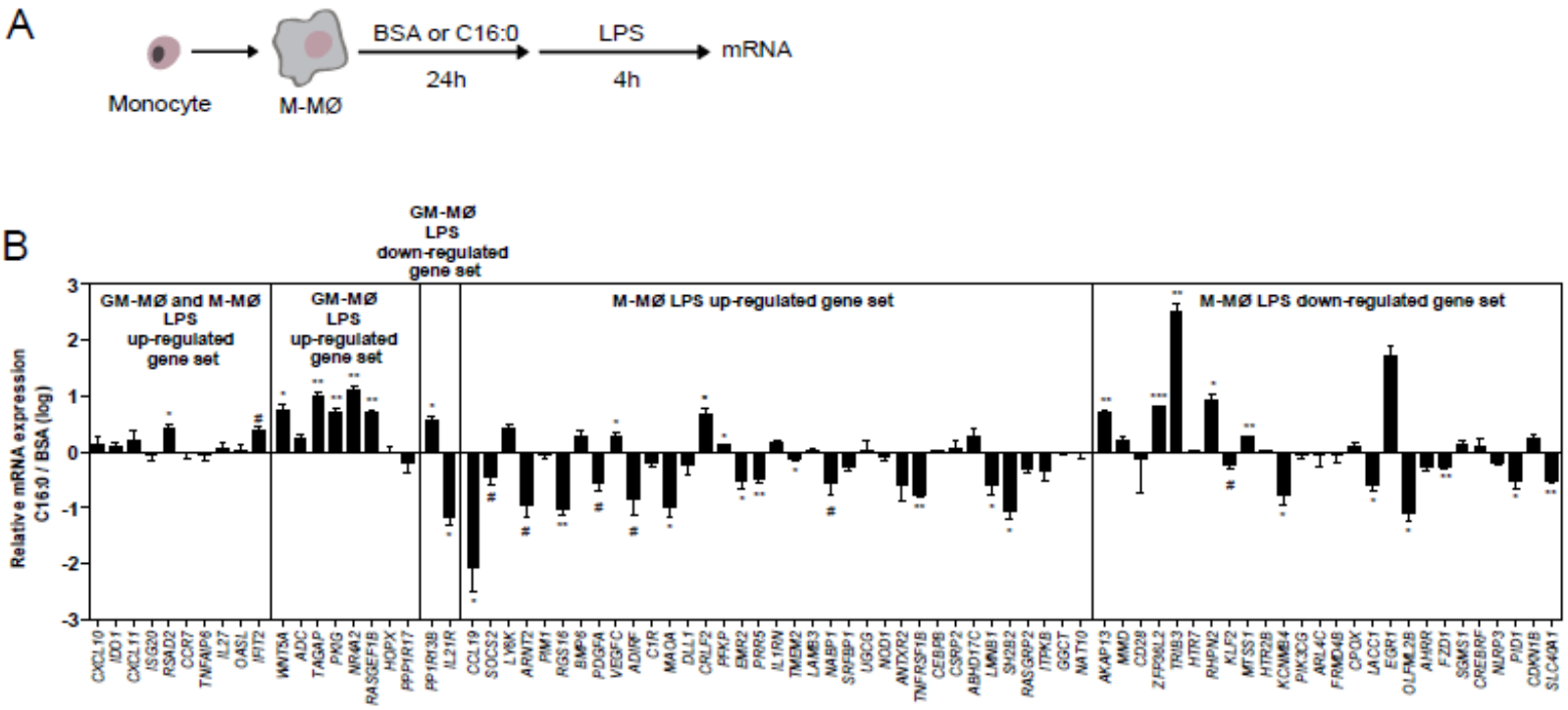

Supplementary Figure 4. Palmitate pre-treatment alters the LPS-induced transcriptional response in human macrophages. (A) Experimental design of the experiment. **(B)** Relative mRNA expression of the indicated LPS-responsive genes in M-MØ exposed to either 200 µM palmitate (C16:0) or BSA for 24 h and later stimulated with 10 ng/ml LPS for 4 hours. Results represent the LPS-induced changes in the mRNA expression of each gene in cells pre-treated with palmitate and relative to the expression of the same gene in cells pre-treated with BSA. Shown is the mean ± SEM of three independent experiments (#, $p<0.06$; *, $p<0.05$; **, $p<0.01$; ***, $p<0.001$).

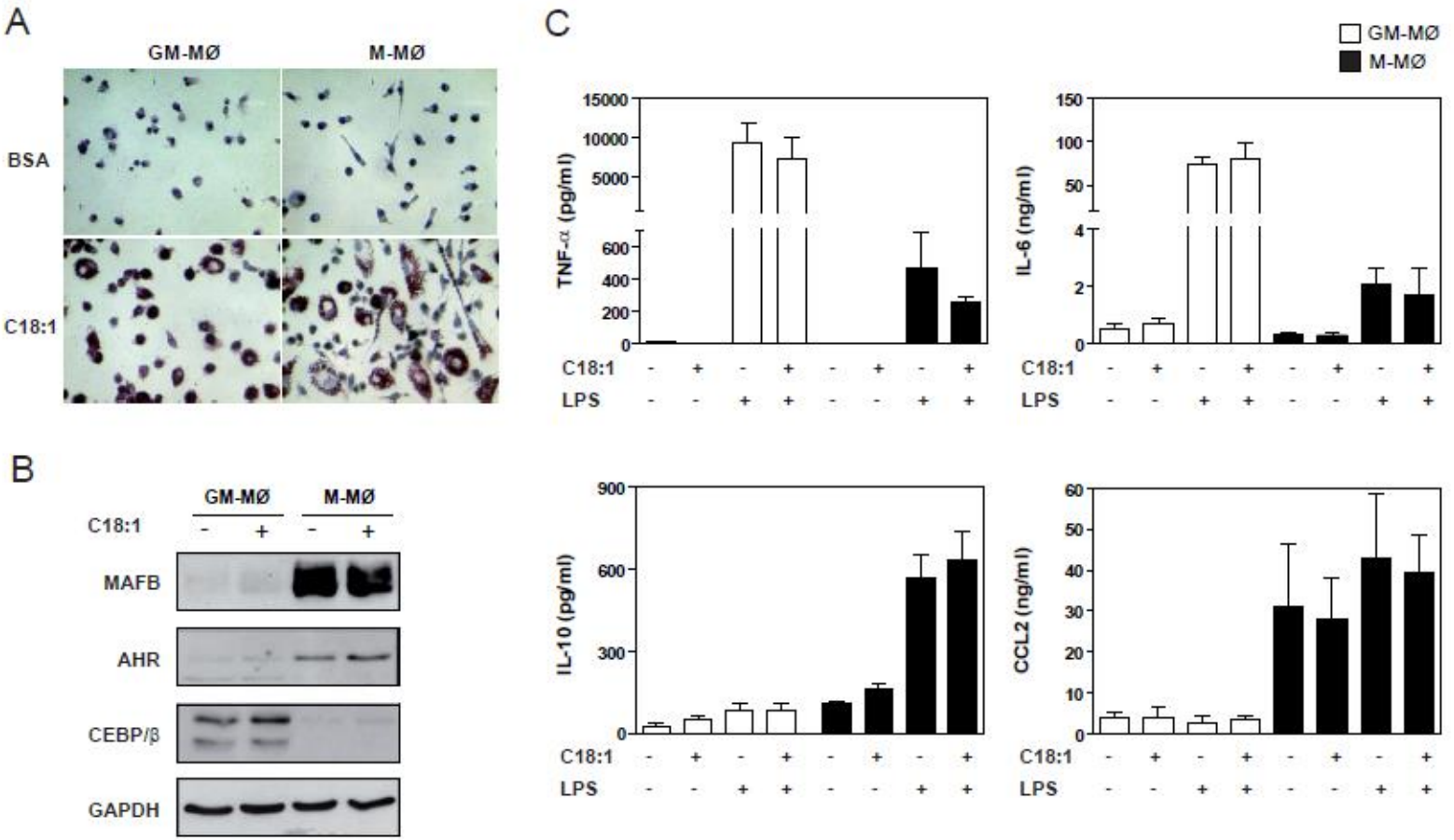

Supplementary Figure 5. Functional and transcription factor profile of oleate-treated human macrophages. (A) Oleate uptake by human macrophages (GM-MØ and M-MØ), as determined by Oil Red staining. For comparative purposes, macrophages were exposed in parallel to BSA (upper panels). **(B)** Expression of MAFB, AhR and CEBP/β in macrophages (GM-MØ and M-MØ) treated with 200 µM oleate (C18:1) or BSA (-) for 24h, as determined by Western blot. GAPDH protein levels were determined in parallel as a protein loading control. **(C)** Levels of the indicated cytokines in the culture media of macrophages (GM-MØ and M-MØ) exposed to 200 µM oleate (C18:1) or BSA (-) for 24h before stimulation with 10 ng/ml LPS for 8 hours. Shown is the mean ± SEM of three independent experiments (*, $p<0.05$).

UNIVERSITAT ROVIRA I VIRGILI
ASSESSMENT OF PATHOPHYSIOLOGICAL MECHANISMS IN OBESITY-RELATED DISEASES THROUGH METABOLOMICS, TRANSCRIPTOMICS AND MOUSE MODELS OF DISEASE
Marta Riera Borrull

UNIVERSITAT ROVIRA I VIRGILI
ASSESSMENT OF PATHOPHYSIOLOGICAL MECHANISMS IN OBESITY-RELATED DISEASES THROUGH METABOLOMICS, TRANSCRIPTOMICS AND MOUSE MODELS OF DISEASE
Marta Riera Borrull

UNIVERSITAT
ROVIRA i VIRGILI